



Space engineering

Threaded fasteners handbook

**ECSS Secretariat
ESA-ESTEC
Requirements & Standards Section
Noordwijk, The Netherlands**

Foreword

This Handbook is one document of the series of ECSS Documents intended to be used as supporting material for ECSS Standards in space projects and applications. ECSS is a cooperative effort of the European Space Agency, national space agencies and European industry associations for the purpose of developing and maintaining common standards.

This handbook has been prepared by the ECSS-E-HB-32-23 Working Group, reviewed by the ECSS Executive Secretariat and approved by the ECSS Technical Authority.

Disclaimer

ECSS does not provide any warranty whatsoever, whether expressed, implied, or statutory, including, but not limited to, any warranty of merchantability or fitness for a particular purpose or any warranty that the contents of the item are error-free. In no respect shall ECSS incur any liability for any damages, including, but not limited to, direct, indirect, special, or consequential damages arising out of, resulting from, or in any way connected to the use of this document, whether or not based upon warranty, business agreement, tort, or otherwise; whether or not injury was sustained by persons or property or otherwise; and whether or not loss was sustained from, or arose out of, the results of, the item, or any services that may be provided by ECSS.

Published by: ESA Requirements and Standards Section
ESTEC, P.O. Box 299,
2200 AG Noordwijk
The Netherlands

Copyright: 2023© by the European Space Agency for the members of ECSS

Change log

ECSS-E-HB-32-23A 16 April 2010	First issue
ECSS-E-HB-32-23A Rev.1 6 February 2023	<p>First issue, Revision 1.</p> <p>The main changes with respect to the previous version ECSS-E-HB-32-23A (16 April 2010) are:</p> <ul style="list-style-type: none">• Implementation of Change Requests• Correction of formulas and references• Addition of clause 5.5.3 “Planarity of Flanges”• Shortened 10.2.3 and removed 10.5.3 as the topic of thermal conductance is covered by ECSS-E-HB-31-01 Part 4A Section 5• Section 11 significantly reworked• Update of Table D-5 to provide Material 17-7PH properties instead of 13-PH

a

Table of contents

Change log	3
Introduction	17
1 Scope	18
2 References	19
3 Terms, definitions and abbreviated terms	20
3.1 Terms from other documents	20
3.2 Terms specific to the present document	20
3.3 Abbreviated terms	22
3.4 Variables	23
3.4.1 Uppercase variables.....	23
3.4.2 Lowercase variables.....	25
3.4.3 Symbols.....	26
3.4.4 Subscripts.....	28
4 How to use the guidelines	30
4.1 Introduction.....	30
4.2 Procedure.....	30
4.2.1 Stage I	30
4.2.2 Stage II	31
4.2.3 Stage III	31
4.2.4 Stage IV.....	32
4.3 Annexes	32
5 General Fastener Analysis Guidelines	33
5.1 Introduction.....	33
5.2 Main Joint Categories.....	33
5.2.1 Overview.....	33
5.2.2 Concentric Axially Loaded Joints.....	34
5.2.3 Eccentric Axially Loaded Joints	34
5.2.4 Shear Loaded Joints.....	34
5.2.5 Combined Loaded Joints.....	34
5.2.6 Low Duty Joints	35
5.3 Joint Analysis Procedure	38

5.3.1	Overview.....	38
5.3.2	Margins of Safety.....	38
5.4	Joint Geometry	40
5.4.1	Fastener Geometry.....	40
5.4.2	Thread Geometry	41
5.5	Safety Factors	44
5.5.1	Overview.....	44
5.5.2	The Joint Fitting Factor.....	45
5.5.3	Planarity of Flanges.....	45
5.6	References	45
6	The Preload	46
6.1	Overview	46
6.2	Coefficient of Utilisation.....	46
6.3	Theoretical Aspects.....	47
6.3.1	The Relation between Torque and Preload.....	47
6.3.2	Determining the Design Torque Level	50
6.3.3	Locking Devices and Prevailing Torque	52
6.3.4	Sources of Error	53
6.3.5	Forces Induced by Thermal Fluctuation	54
6.4	Mechanisms of Preload Loss	56
6.4.1	Overview.....	56
6.4.2	Embedding	56
6.4.3	Fastener Group Interaction.....	61
6.4.4	Gaskets	63
6.4.5	Metallic Creep.....	63
6.4.6	Washers	63
6.4.7	Torsional Relaxation.....	64
6.5	Margin of Safety on Tightening	65
6.6	Worked Example	66
6.7	References	66
7	Concentric Axially Loaded Joints	67
7.1	Overview	67
7.2	Joint Stiffness	67
7.3	The Joint Diagram	68
7.3.1	Overview.....	68
7.3.2	Compressive Loading.....	71
7.4	The Force Ratio.....	72

7.5	The Compliance of the Fastener	73
7.6	The Compliance of the Clamped Parts	74
7.6.1	Overview.....	74
7.6.2	Compression Zone Configurations	75
7.6.3	Determining the Compression Zone Configuration	78
7.6.4	The Compression Zone Compliance	79
7.6.5	Gasket Compliance	80
7.7	Calculation of the Loading Plane Factor	82
7.7.1	Introduction.....	82
7.7.2	Simple Calculation of the Loading Plane Factor.....	85
7.7.3	Analytical Calculation of the Loading Plane Factor	87
7.8	Joint Separation	90
7.8.1	Introduction.....	90
7.8.2	The Margin of Safety for Joint Separation	90
7.9	Fastener Tensile Failure.....	91
7.9.1	External Vs Overall Load.....	91
7.9.2	Margin of Safety on Fastener Failure	91
7.10	Thread Failure by Shear Pull-Out.....	93
7.10.1	Introduction.....	93
7.10.2	Failure of the Female Thread	93
7.10.3	Failure of the Male Thread	94
7.10.4	Margin of Safety on Thread Pull-Out.....	95
7.11	Crushing of Flanges	95
7.12	Repeated Loading to a Point above Yield	96
7.13	Dynamic Loading.....	97
7.14	Worked Examples	99
7.14.1	Preload in a Concentric Axially Loaded Joint	99
7.14.2	Thread Shear Pull-Out Example.....	104
7.15	References	106
8	Eccentric Axially Loaded Joints.....	107
8.1	Effects of Eccentricity	107
8.1.1	Overview.....	107
8.1.2	Prying	110
8.2	Joints with Large Areas of Contact.....	111
8.2.1	Compliance of the Clamped Parts.....	111
8.2.2	The Joint Diagram	115
8.2.3	The Force Ratio.....	116

8.2.4	Loading Plane Factor	116
8.2.5	The Interface Opening Limit	117
8.2.6	Preload Considerations	118
8.3	Cantilevered Flange Joints	119
8.3.1	Overview	119
8.3.2	Compliance of Circular Flanges	119
8.3.3	Force Ratio for Circular Cantilever Flanges	123
8.3.4	Simplified Joint Diagram for Eccentric Joints	124
8.3.5	Joint Diagram for Eccentric Nonlinear Joints.....	124
8.4	Fastener Loads in Eccentric Joints	126
8.4.1	Bending Moments.....	126
8.5	References	128
9	Shear Loaded Joints	129
9.1	Introduction.....	129
9.1.1	Overview.....	129
9.1.2	Analysis Approach.....	130
9.2	Friction Grip Joints	131
9.2.1	Design Principles.....	131
9.2.2	Slip Resistance.....	133
9.2.3	Friction Grip Strength Analysis	136
9.3	Bearing Joints.....	136
9.3.1	Design Principles.....	136
9.3.2	Fastener Shear Failure.....	138
9.3.3	Net Tension Section Failure of Flanges	142
9.3.4	Hole Bearing Failure.....	144
9.3.5	Shear-Out or Tear-Out Failure	146
9.4	Eccentrically Loaded Shear Joints	148
9.4.1	Overview.....	148
9.4.2	Fastener Group Centroid.....	149
9.4.3	Bearing Design of Eccentric Shear Joints	149
9.4.4	Friction Grip Design of Eccentric Shear Joints	150
9.5	Worked Examples	152
9.5.1	Shear Loaded Joint Example	152
9.5.2	Net Tension Section Failure Example	155
9.5.3	Eccentric Shear Bearing Joint Example	156
9.6	References	158
10	Low Duty Joints.....	159

10.1	Introduction.....	159
10.2	Low Duty Joint Design Guidelines.....	159
10.2.1	Overview.....	159
10.2.2	Insert Pull out Strength.....	159
10.2.3	Joint Thermal Conductance.....	161
10.2.4	Joint Electrical Conductivity.....	161
10.2.5	Handling Size.....	162
10.2.6	Stiffness.....	162
10.2.7	Tolerances.....	162
10.2.8	Redundancy.....	162
10.3	Non-Metallic Joints.....	162
10.4	Low Duty Threshold.....	163
10.5	Example: Low Duty Thermal Joint.....	163
10.5.1	Overview.....	163
10.5.2	Initial Assumptions.....	164
10.5.3	<<deleted>>.....	165
10.6	References.....	165
11	Fatigue and Fracture Control of Fasteners.....	166
11.1	Introduction.....	166
11.2	Fastener Fatigue.....	166
11.2.1	Fundamentals.....	166
11.2.2	Palmgren – Miner rule.....	175
11.2.3	Fatigue Design Principles.....	176
11.3	Fundamentals of Fracture Control and Fracture Mechanics.....	178
11.3.1	Fracture Control.....	178
11.3.2	The Stress Intensity Factor.....	184
11.3.3	The Stress Intensity Correction Factor.....	184
11.3.4	Crack Growth Calculations.....	188
11.3.5	Corrosion Considerations.....	189
11.4	Worked Examples.....	189
11.4.1	Fatigue of a Threaded Fastener Example.....	189
11.4.2	Threaded Fastener Fracture Mechanics Example.....	190
11.5	References.....	192
12	Preloaded Fastener Installation.....	194
12.1	Overview.....	194
12.2	Torque Controlled Tightening.....	194
12.3	Yield Load Controlled Tightening.....	194

12.3.1	Introduction.....	194
12.3.2	Method of Operation.....	195
12.3.3	Preload Developed in Fastener.....	196
12.4	Angle of Rotation Controlled Tightening.....	198
12.4.1	Introduction.....	198
12.4.2	Elastic Range Tightening.....	198
12.5	Ultrasonic Methods.....	200
12.5.1	Introduction.....	200
12.5.2	Ultrasonic Extensometers.....	200
12.6	Direct Measurement.....	204
12.6.1	Overview.....	204
12.6.2	Method of Application and Practical Considerations.....	204
12.7	Reuse of Fasteners.....	204
12.7.1	Overview.....	204
12.7.2	Effects on Friction Coefficients.....	204
12.7.3	Effects on Prevailing Torques.....	206
12.7.4	Recommended Practice for Fastener Reuse.....	207
12.8	References.....	207
13	Corrosion.....	209
13.1	Overview.....	209
13.2	Galvanic Corrosion.....	211
13.2.1	Introduction.....	211
13.2.2	Factors Which Affect the Rate of Corrosion.....	211
13.2.3	Prevention of Bimetallic Corrosion.....	212
13.3	Stress Corrosion Cracking.....	214
13.3.1	Introduction.....	214
13.3.2	Factors Affecting Stress Corrosion Cracking.....	215
13.4	Crevice Corrosion.....	219
13.4.1	Introduction.....	219
13.4.2	Methods of Avoiding Crevice Corrosion.....	219
13.5	Pitting corrosion.....	219
13.5.1	Introduction.....	219
13.5.2	Alloy Susceptibility.....	220
13.5.3	Prevention of Pitting Corrosion.....	220
13.6	References.....	220
14	Lubricants for Space Use.....	221
14.1	Introduction.....	221

14.2	Lubricant Selection	221
14.3	Plating and Coatings for Fasteners	222
14.4	Liquid Lubricants	222
14.5	Dry Lubricants	223
14.6	Codification of Space Lubricant Systems and Processes	223
14.7	References	223
15	Manufacturing Quality Control	225
15.1	Introduction.....	225
15.2	Manufacturing and Quality Assurance	225
15.3	Quality of Threaded Fastener Joints	226
15.3.1	Overview.....	226
15.3.2	Process Variations.....	226
15.3.3	Material Variations.....	226
15.3.4	Tolerancing.....	227
15.4	References	227
16	Joint Validation by Testing	228
16.1	Introduction.....	228
16.2	Types of Testing	228
16.3	Development Testing	228
16.3.1	Overview.....	228
16.3.2	The Test Factor	229
16.3.3	Specific Development Tests	230
16.4	Production Testing	231
Annex A	Recommended Starting Values for Seating Torque.....	232
A.1	Recommended values.....	232
A.2	References	233
Annex B	Measured Friction Coefficients of Fasteners.....	234
Annex C	Typical Friction Coefficients for Joint Materials	235
Annex D	Material Data of Fasteners Typically Used in Aerospace Industry	237
D.1	Overview	237
D.2	Stainless Steel.....	237
D.3	Nickel and Nickel/Cobalt Based Alloys.....	241
D.4	Titanium Alloys	242
D.5	References	243

Other Useful References..... 244

Figures

Figure 5-1 - Joint Categories (1 to 6)35

Figure 5-2 - Joint Categories (7 to 12)36

Figure 5-3 - Joint Categories (13 to 17)37

Figure 5-4 - Definitions of Forces and Moments Acting on a Joint.....38

Figure 5-5 – Fastener Dimensions40

Figure 5-6 – Definition of the under-head bearing angle40

Figure 5-7 – Thread Geometry42

Figure 5-8 - Illustration of bending on the screw45

Figure 6-1 – Forces Present During Tightening (the Wedge Model).....47

Figure 6-2 - Typical Preload vs. Applied Torque Graph54

Figure 6-3 - Fastener Faying Surfaces.....56

Figure 6-4 - Microscopic View of Surface Asperities Initially in Contact.....57

Figure 6-5 - Embedding Preload Decay57

Figure 6-6 - Joint with Conical Mating Surfaces.....59

Figure 6-7 - Effect of Fastener Stiffness on Preload Loss Due to Embedding.....60

Figure 6-8 - Increasing Joint Compliance Using Belleville Washers60

Figure 6-9 - Initial and Final Preload of a Typical Flange Joint for the First Tightening Pass.....62

Figure 6-10 - Initial and Final Preload Levels after Four Tightening Passes.....62

Figure 6-11 - Self Tightening by Torsional Relaxation64

Figure 7-1 - Typical Joint Components68

Figure 7-2– Fastener Stiffness68

Figure 7-3 – Clamped Parts Stiffness68

Figure 7-4 - Growth of the Joint Diagram Illustrating the Tightening Process69

Figure 7-5 – Application of external axial load70

Figure 7-6 - Joint Diagram Showing the Effect of an External Axial Load.....70

Figure 7-7 – External Load Causing Gapping71

Figure 7-8 – Joint Diagram for Compressive Loading.....71

Figure 7-9 – Dimensioning of the Fastener for Compliance Calculations73

Figure 7-10 - Compression zones in cylindrical clamped parts.....75

Figure 7-11 - The compression zone when multiple edge distances are present76

Figure 7-12- Approximation of the Compression Zone for Insert Joints.....77

Figure 7-13 - The compression zone with multiple interacting fasteners77

Figure 7-14 - Typical Gasket Deflection81

Figure 7-15 – Gasket Showing Hysteresis	81
Figure 7-16- Joint Diagram for a Gasket Joint Showing Gasket Creep	81
Figure 7-17 - Tension Joint Loading Planes and the Forces Acting within the Joint.....	82
Figure 7-18 - Joint Diagram for Loading Planes within the Joint ($n < 1$)	82
Figure 7-19 - Geometry for Determination of Loading Plane Factor	83
Figure 7-20 – Extraction of the Joint from its Environment	84
Figure 7-21 - The Basic and Connector Bodies	85
Figure 7-22 – Joint Types According to the Points of Force Introduction.....	86
Figure 7-23 – Basic and Connector Bodies of a Flange.....	87
Figure 7-24- Moment Conduction Factor Variation with the Connector Body Position .	88
Figure 7-25 - Joint Diagram at Onset of Separation Failure.....	90
Figure 7-26 – Joint Diagram Showing Repeated Loading into the Plastic Region.....	96
Figure 7-27 – Preload Loss with Repeated Loading into Yield	96
Figure 7-28 – Joint Diagram Showing a Dynamic External Load	97
Figure 7-29 – Typical S-N Curve (For a Given Mean Stress)	98
Figure 7-30 - Example problem of concentric axially loaded joint	99
Figure 8-1 - A Typical Eccentric Joint.....	107
Figure 8-2 - Interface Pressure Distribution after Preloading	108
Figure 8-3 - Typical Joint Eccentrically Loaded.....	108
Figure 8-4 - Redistribution of interface pressure (with force F_{A1} not sufficient to cause gapping).....	109
Figure 8-5 - An Eccentrically Loaded Joint with Gapping.....	109
Figure 8-6 - Redistribution of Interface Pressure (Force F_{A2} Causes Gapping).....	110
Figure 8-7 - Limitations of the Eccentric Joint Analysis Method	112
Figure 8-8 - The Interface Area for Multiple Fastener Joints.....	112
Figure 8-9 - An Eccentrically Loaded Joint where $s = a$	113
Figure 8-10 - The General Eccentrically Loaded Joint	114
Figure 8-11 - The Joint Diagram for Eccentrically Loaded Joints showing the Non-Linearity of the Clamped Parts	115
Figure 8-12 - Joint Diagram with a Higher Preload	116
Figure 8-13 - An Eccentrically Joint Loaded to the Interface Opening Limit with the Loading Plane Inside the Joint.....	117
Figure 8-14 - Definition of Flange Compliance due to Bending Loads at Different Points	120
Figure 8-15 - Dimensions of a Fixed Circular Flange (with a Weldneck)	121
Figure 8-16 - Bending Deformation of Circular Loose Flange	122
Figure 8-17 - Simplified Joint Diagram for Cantilevered Flanged Joints	124
Figure 8-18 - The Joint Diagram for Non-Linear Gasket Joints.....	125

Figure 8-19 - Idealised Linear Pressure Distribution across an Eccentrically Loaded Joint's Interface.....	127
Figure 9-1 - Typical Double Lap Shear Joint.....	129
Figure 9-2 - Load Deformation Curve for a Fastener in Direct Shear	130
Figure 9-3 - A Symmetrical Shear Joint	131
Figure 9-4 - The Joint Diagram for Each Fastener in Figure 9-3.....	132
Figure 9-5 - Typical Unsymmetrical Friction Grip Shear Joint.....	132
Figure 9-6 - Fastener Bending and Tension in an Unsymmetrical Shear Joint.....	132
Figure 9-7 - Simple Friction Grip Joint with Added Tension Loading	134
Figure 9-8 - Reduction of Shear Capacity with Increasing External Axial Load	134
Figure 9-9 - Joint Design Features that Increase Slip Resistance	135
Figure 9-10 - Shear Joint in Bearing	136
Figure 9-11 - Long Bearing Shear Stress Distribution.....	137
Figure 9-12 - Graphical Determination of the Margin of Safety on Combined Loads..	140
Figure 9-13 - Fastener Group with hole clearance.....	140
Figure 9-14 - Shear load parameter versus hole clearance	141
Figure 9-15 - Nomenclature for Net Tension Section Calculation	142
Figure 9-16 - Ultimate Strength Reduction Factors for Net Tension Section Failure ..	143
Figure 9-17 - Initial Bearing Contact Elastic Stresses and Deformations.....	144
Figure 9-18 - Elastic / Plastic Stresses and Deformations After Increased Loading ...	145
Figure 9-19 - Idealised Bearing Stresses	145
Figure 9-20 - Shear-Out Failure	146
Figure 9-21 - Tear-Out Failure	146
Figure 9-22 - Nomenclature for Plate Shear Out Calculation.....	147
Figure 9-23 - A Typical Eccentric Loaded Shear Joint.....	148
Figure 9-24 - Load v Rotation Curve for a Typical Eccentric Loaded Shear Joint	148
Figure 9-25 - Shear Resistance Relative to the Centre of Rotation	150
Figure 9-26 - Shear loaded joint example	152
Figure 9-27 - Shear Joint Example to Show the Method of Net Tension Section Calculation	155
Figure 9-28 - Offset Loads on Fastener Groups	156
Figure 9-29 - Vector addition of the fastener loads	158
Figure 10-1 - Types of Inserts Used in Honeycomb Panels.....	160
Figure 10-2 - Typical Earthing Arrangements	161
Figure 10-3 - Typical Low Duty Clamp Connections	162
Figure 10-4 - Equipment Mounting Box Geometry.....	163
Figure 11-1 - Typical Fatigue Curve at Constant Mean Stress	167
Figure 11-2 - Typical Constant Amplitude Loading	167

Figure 11-3 - Typical Stress Ratio – Mean Stress Diagram	168
Figure 11-4 - Typical Preload Effects on Fatigue Life of Fasteners (taken from reference 11.6)	169
Figure 11-5 – ESALOAD S-N curves for A286 steel bolts (UTS=1100MPa)	170
Figure 11-6 – ESALOAD S-N curves for A286 steel bolts (UTS=960MPa)	171
Figure 11-7 – ESALOAD S-N curves for A2-80 stainless steel bolts (UTS=800MPa)	172
Figure 11-8 – ESALOAD S-N curves for Ti6Al4V bolts (UTS=1100MPa).....	173
Figure 11-9 – Fatigue test results for M5 DIN 912 stainless steel screws, A2-70	174
Figure 11-10 – Tensile test results for M5 DIN 912 stainless steel screws, A2-70	174
Figure 11-11 - Joint Diagram Comparing Steel and Titanium Fasteners	176
Figure 11-12 - Typical Fatigue Comparison, Ref. 11.8	177
Figure 11-13 – Residual bolt strength under sustained loads, Ti6Al4V STA	181
Figure 11-14 – Residual bolt strength under sustained loads, Ti6Al4V annealed.....	181
Figure 11-15 – Residual bolt strength under sustained loads, A286 steel	182
Figure 11-16 – Residual bolt strength under sustained loads, Inconel 718	182
Figure 11-17 – Residual bolt strength under sustained loads, AISI 316 stainless steel	183
Figure 11-18 – Residual bolt strength under sustained loads, MP35N STA	183
Figure 11-19 - ESACRACK Model of a Circumferential Crack.....	185
Figure 11-20 - ESACRACK Model of a Thumbnail Crack.....	186
Figure 11-21 - ESACRACK Model of a Fillet Crack under a Fastener Head	187
Figure 12-1 - Yield Load Controlled Tightening.....	195
Figure 12-2 - Torque and Gradient Values as a Function of e	196
Figure 12-3 - Variation of Strain along Fastener	198
Figure 12-4 - Prevailing torques during a series of loosening and retightening cycles of a LN 29949 M6 fastener and with Helicoil LN9499 made of CuSn6.....	206
Figure 13-1 - Forms of Corrosion	210
Figure 13-2 - Grain Orientations in Standard Wrought Forms	216
Figure 13-3 - Assembly Stress Resulting from Mismatch	217
Figure 13-4 - High Assembly Stresses in Short Transverse Direction	217
Figure 13-5 - Examples of Tensile Stresses in Short Transverse Direction Resulting from Assembly	218

Tables

Table 5-1 - Margins of Safety to be analysed for a threaded fastener	39
Table 5-2 - Physical Dimensions of Fasteners.....	41
Table 5-3 - Derived Dimensions for Metric Fasteners.....	42
Table 5-4 - Factors of safety for joints, inserts and connections	44

Table 6-1 - Uncertainty factors of tightening methods (from reference 5.1).....	51
Table 6-2 - Prevailing Torques of Locking Devices on Unlubricated Fasteners.....	52
Table 6-3 - Approximate values for plastic deformation caused by embedding.....	58
Table 7-1 - Typical Substitution Lengths for Commonly Used Fasteners (data from Reference 7.3).....	74
Table 7-2 - Loading Plane Factors for Simplified Method	86
Table 7-3 - Criteria for Axial Load Analysis	91
Table 7-4 - <<deleted>>	94
Table 7-5: Preload in a Concentric Axially Loaded Joint, fastener material properties	99
Table 7-6: Preload in a Concentric Axially Loaded Joint, Thread parameters	100
Table 7-7: Preload in a Concentric Axially Loaded Joint, flange material properties ..	100
Table 9-1 - Failure Modes of Shear Joint Types	130
Table 11-1 - Stress Intensity Factors for Thumbnail Crack in a Fastener Thread.....	186
Table 11-2 - Stress Concentration Factors at a Fastener Minor Diameter.....	187
Table 11-3 - Analysis of cycles to failure.....	190
Table 12-1 - σ_y/σ_V for a Range of Fastener Sizes and Typical Friction Conditions...	197
Table 12-2 - Typical Scatter of Ultrasonic Extensometer Preload Readings Using a Direct Load Method of Calibration	203
Table 12-3 - Friction Coefficients of Unlubricated Reused Fasteners.....	205
Table 12-4 - Prevailing Torques of Locking Devices after Several Loosening and Retightening Cycles for Unlubricated Fasteners	207
Table 13-1 - Galvanic Series of Metals in an Aqueous Environment	213
Table 14-1 - Recommended Lubricants for Space Applications	221
Table 16-1 - Test Factors to be used for Given Probability of Failure	229
Table A-1 - Recommended torques for unlubricated fasteners.....	232
Table B-1 - Friction Coefficients of Fasteners used in European Space Industry - Unlubricated Fasteners.....	234
Table C-1 - Typical thread and Underhead Friction Coefficients	235
Table C-2 - Friction Coefficients for Common Joint Materials (from Reference 8.3)...	236
Table D-1 - Stainless steel A 286.....	237
Table D-2 - Stainless steel A2-70 and A2-80	238
Table D-3 Stainless steel custom 450.....	238
Table D-4 - Stainless steel custom 455.....	239
Table D-5 - Stainless steel PH 13-817-7 Mo.....	239
Table D-6 - Stainless steel PH 15-7 Mo.....	240
Table D-7 - Stainless steel 15-5 PH.....	240
Table D-8 - Inconel 718.....	241
Table D-9 - MP35N	241

Table D-10 – MP159	242
Table D-11 - Ti6Al4V	242

Introduction

- ABSTRACT

The aim of the present handbook is to assist the structural design engineers by presenting them in a single document with all the information relevant to the use of threaded fasteners in jointed spacecraft components. This document provides additional information for the application of standards ECSS-E-ST-32 (Structural general requirements), ECSS-E-ST-32-01 (Fracture control) and ECSS-E-ST-32-10 (Structural factors of safety for spaceflight hardware).

- BACKGROUND

Threaded fastener joints represent critical areas within structures and it is evident that a standardised methodology is needed for their design.

Thus, the aims of this document are:

- to bring together into one document a reliable and systematic design procedure to aid the designer and improve the efficiency of the design process, and
- to provide an approved and reliable design procedure that can reduce the possibility of design errors and subsequent structural failure.

This document addresses these aims with particular reference to Space Structures and related hardware. This constraint is reflected in the range of joint geometries covered and structural applications, and also the range of fastener types and materials for which data is presented.

- PURPOSE OF THIS ISSUE

ESA PSS-03-208 (December 1989) “Guidelines for threaded fasteners”, on which this document is based, provided a number of methodologies for analysis of threaded fastener joints in spacecraft structures. This document is Revision 1 of ECSS-E-HB-32-23A which was based on the ESA PSS document taking into account more recent developments in the field. It is intended to standardise the analysis approach and corresponding documentation for threaded fastener joints developed in ECSS projects. Therefore, this document presents a “Margin of Safety” for each mode of failure that are good practice to be considered. It is important that all relevant margins of safety are presented in the verification documentation.

- GUIDELINE LIMITATION AND IDENTIFIED PROBLEM AREA

This handbook does not provide theory for the following types of analysis:

- Compliance of cantilevered flange joints with non-circular flanges
- Friction grip of eccentric shear loaded joints
- No failure criteria are provided for fastener bending, which sometimes are important to consider (see Section 9.3.2)

- GUIDELINES FOR THE USE OF TERMS AND DEFINITIONS

Due to the extensive used of threaded fasteners in a multitude of countries and industries, there is a wide variety of terminology in use today. For the purposes of making a clear and coherent handbook it was necessary to adopt a single consistent set of terminology. The terminology that was chosen is presented in 3.2. To avoid confusion, it is recommended to refer to this section frequently when reading the document.

1 Scope

The users of this document are engineers involved in design, analysis or verification of joints on structures used for space missions. It is a guidelines document; therefore it includes advisory information rather than requirements.

This document is intended to be **used for** any type of joint that is mechanically connected by threaded fasteners (e.g. bolts, screws, etc.). It is written for joints made from metallic materials. However, subject to the engineering judgement of the user, many of the procedures presented herein **can** be applicable to joints made from composite materials.

2 References

References are provided at the end of each section.

Terms, definitions and abbreviated terms

3.1 Terms from other documents

For the purpose of this document, the terms and definitions from ECSS-S-ST-00-01 apply.

3.2 Terms specific to the present document

3.2.1 applied torque

final tightening torque applied by the torque wrench to the fastener or nut

NOTE It is also called the “installation torque”.

3.2.2 clamped parts

regions of the joint that are compressed by the fastener

NOTE Among the clamped parts in a joint, there **are** always at least two **flanges**. Other clamped parts that have specialised functions include: washers, spacers, gaskets, etc.

3.2.3 female threaded part

threaded part into which the male threaded part is inserted during fastener installation

NOTE This is normally equivalent to either a **nut** or a **threaded hole flange**.

3.2.4 flange

clamped part that transmits loads from a threaded fastener to other regions of the structure

3.2.5 insert

part with a threaded hole, which is embedded in a weaker material in order to increase the loads that can be transmitted through the joint

NOTE It is normally a metallic part.

3.2.6 joint

region of the structure in the vicinity of the threaded fastener

NOTE The dimensional extents of the joint depend on the engineering issues under consideration.

3.2.7 locking device

physical means by which the fastener is held in tension during service and that avoids loosening of the fastener

NOTE Locking devices provide the so called “prevailing torque or self-locking torque or running torque”.

3.2.8 male threaded part

threaded part that is designed to fit within a threaded hole

NOTE This is normally equivalent to the **threaded fastener**.

3.2.9 nut

device with an internally threaded hole with the primary functions being the application of tension to the shaft of a **threaded fastener** and compression to the **clamped parts**.

3.2.10 nut-tightened joint

joint with a **threaded fastener** that is tightened by a **nut**

3.2.11 prevailing torque

torque provided by the **locking device**

NOTE This torque needs to be overcome before the threaded fastener can loosen (also called “running torque or self-locking torque”).

3.2.12 prying

change in a fastener’s loading caused by a levering action in flexible flanges

NOTE It occurs in eccentrically loaded joints, see Section 8.

3.2.13 running torque

See **prevailing torque**

3.2.14 seating torque

torque that, when applied, produces the compression of the flanges and the preload on the fastener.

NOTE When added to the prevailing torque the resulting torque is called the installation torque.

3.2.15 thread

helical groove on the external surface of a shaft (male thread) or the internal surface of a hole (female thread)

3.2.16 threaded hole flange

flange with a threaded hole into which a **threaded fastener** is inserted and tightened

3.2.17 threaded hole joint

joint in which the **threaded fastener** screws into a **threaded hole flange**

3.2.18 threaded interface

pair of internal and external **threads** that are designed to fit together allowing relative rotation, and thereby variation of the length of the **threaded fastener** system

3.2.19 threaded fastener

device that joins multiple parts together by compression of their flanges, where the compression is achieved by rotation of a threaded shaft into a threaded hole

NOTE This definition includes all commonly types of threaded fasteners such as; bolt, screw, threaded pin, etc. Throughout this document, the term **threaded fastener** is frequently simplified to the word **fastener**.

3.3 Abbreviated terms

For the purpose of this document, the abbreviated terms from ECSS-S-ST-00-01 and the following apply:

Abbreviation	Meaning
ASME	American Society of Mechanical Engineers
BS	British Standard
CNES	Centre National d'Etudes spatiales (French space agency)
DIN	Deutsches Institut für Normung (German institute for standardization)
ECSS	European Cooperation on Space Standardization
EDM	Electron Discharge Machining
ESA	European Space Agency
HB	Brinell Hardness
ISO	International Standards Organization
IVD	Ion Vapour Deposited
LEFM	Linear Elastic Fracture Mechanics
LN	Luftfahrt Norm (German aviation standard)
M	Metric type thread
MGSE	Mechanical Ground Support Equipment
MJ	Metric J-type thread (for improved fatigue performance)
MoS	Margin of Safety
NASA	National Aeronautics and Space Administration
PSS	Procedures, Standards and Specifications
PTFE	Poly Tetra Fluoro Ethylene
SCC	Stress Corrosion Cracking
UN	Unified thread
UNC	Unified C-type thread
UNJ	Unified J-type thread (for improved fatigue performance)

3.4 Variables

3.4.1 Uppercase variables

For the purpose of this document, the following uppercaser variables apply:

Variable	Meaning
A	Cross-section area of a joint part (in the plane perpendicular to the fastener axis)
A_s	Effective cross-sectional area of a fastener for stress analysis
A_{sm}	Effective cross-sectional area of a fastener for stiffness calculations
A_{th}	Area of the (cylindrical) surface assumed to fail during thread pull-out
A_0	Minimum cross-sectional area of a fastener shank
A_3	Cross-sectional area of a fastener based on the thread root diameter, d_3
C	Transverse width of an eccentric joint (see Figure 8-7)
D_1	Minor diameter of the female thread
D_{avail}	Available diameter for compression zone spreading (see Section 7.7)
D_h	Nominal diameter of a hole
D_{lim}	Maximum cone diameter of compression zone spreading (see Section 7.7)
$D_{uh,brg}$	Outer diameter of the under-head or under-nut bearing surface (see Section 7.7)
E	Young's modulus
F	Force
F_A	Axial force transmitted by joint
F_Q	Shear force transmitted by joint
$F_{V,max}$	Maximum preload
$F_{V,nom}$	Nominal preload
$F_{V,min}$	Minimum preload
F_Z	Maximum loss of preload due to relaxation (includes all sources, e.g. embedding, creep, etc)
F_b	Tensile force transmitted by a fastener
F_c	Compression force transmitted by the clamped parts
F_{CL}	Shear force capable to move fastener shank by a distance equal to the hole clearance
$\Delta F_{b,A}$	Increment in fastener tension caused by the application of the external axial load, F_A

Variable	Meaning
$\Delta F_{c,A}$	Increment in clamped parts compression caused by the application of the external axial load, F_A (negative for increased compression)
F_K	Clamping force acting at the interstice between two flanges
F_{th}	Axial force transmitted by the thread
$F_{\Delta T^+}$	Maximum (most positive) increment in a fastener's axial load due to thermo-elastic effects
$F_{\Delta T^-}$	Minimum (most negative) increment in a fastener's axial load due to thermo-elastic effects
G_c	Radius of gyration of the effective interface area between clamped parts
I_c	Second moment of area of the clamped parts interface area
K	Stiffness of a joint part (N/m)
K_C	Critical stress intensity factor
K_{ISCC}	Critical stress intensity factor for stress corrosion cracking
L	Length
L_j	The joint length. The combined thickness of all clamped parts (measured without any externally preload or applied load).
ΔL_b	Change in length of the fastener
ΔL_c	Change in length of the clamped parts
M	Moment / Torque
M_{app}	Peak torque applied to the fastener or nut during tightening (includes the prevailing torque, M_P) (M_{app} is also called 'installation torque')
M_B	Bending moment transmitted by joint (see Figure 5-4)
M_P	Prevailing torque (also called 'running torque')
M_T	Torsional moment transmitted by joint (see Figure 5-4)
M_{th}	Torsional moment transmitted by the thread (does not include prevailing torque, M_P)
M_{uh}	Torsional moment transmitted by frictional forces at the under-head or under-nut interface
R_s	Shear strength ratio
R_z	Average surface roughness
P	Probability
S_{mt}	Mean strength
S_{req}	Required strength
S_r	Slip resistance of a joint

Variable	Meaning
$T_{working}$	The working temperature of the joint (specified with upper and lower bounds)
$T_{reference}$	The reference temperature (generally taken as the assembly temperature)
ΔT	Change in temperature
W_p	Polar section modulus
W_p'	Yield-corrected polar section modulus

3.4.2 Lowercase variables

For the purpose of this document, the following lowercase variables apply:

Variable	Meaning
a	Load eccentricity (distance from joint axis to axis of applied load)
a_k	Distance between the edge of the under-head bearing surface and the point of load introduction (used for eccentric joints, see Section 6.6)
a_R	Shortest distance between the edge of the bearing surface and the edge of the clamped part
a_l	Edge distance (measured from hole axis to edge of flange)
b	Effective longitudinal width of the joint (see Figure 8-8)
c	Empirical coefficient
d	Nominal diameter of a fastener
d_{min}	Minimum thread diameter = d_3
d_s	Effective diameter of a fastener for stress calculations
d_{head}	Diameter of fastener head
d_{sha}	Diameter of a shank segment
d_{sm}	Effective diameter of fastener used for stiffness calculations
d_{uh}	Effective diameter at which under-head or under-nut frictional forces act
$d_{uh,brg}$	Outer diameter of the under-head or under-nut bearing surface
d_0	Minimum diameter of a fastener shank
d_2	Pitch diameter of a fastener thread (assumed diameter at which torsion forces are introduced within a thread)
d_3	Diameter of a fastener's thread root = d_{min}
f_l	Deflection of points of action of the external load
f_z	Plastic deformation of the joint due to embedding
$f_{\Delta T}$	Thermal elongation of an item

Variable	Meaning
$f_{b,v}$	Elongation of fastener due to preload
h	Thickness of a flange (referred to as a 'length' for compliance calculations), or: Height of thread
h_k	The distance between the point of load introduction and the interstice (used for eccentric joints, see Section 6.6)
k_{ar}	Parameter for describing the effect of the component height on the load introduction factor
k_{dh}	Parameter for describing the effect of the hole on the load introduction factor
k_{dw}	Parameter for describing the effect of the bearing area diameter on the load introduction factor
m	Number of fasteners in a joint
n	Loading plane factor
n_G	Loading plane factor of the basic body
n_{G^*}	Loading plane factor of the basic body whose parameter a_k/h is reduced
n_M	Moment conduction factor
n_{2D}	2D loading plane factor
p	Pitch of a thread
p_i	Horizontal distance between holes
S	Clamping eccentricity (distance from joint axis to fastener axis)
s_i	Vertical distance between holes
sf	Safety factor
s_w	Size of wrench (measured 'across the flats' of a head or nut)
x	Number of faying surfaces that resist the shear load

3.4.3 Symbols

For the purpose of this document, the following symbols apply:

Symbol	Meaning
α	Coefficient of thermal expansion for a material
β	Bending compliance
ε	Uncertainty factor used in the typical coefficient method (not applicable to the experimental coefficient method)
γ	Coefficient of utilization (ratio of preload stress to yield stress)

Symbol	Meaning
λ	Under-head bearing angle (see Figure 5-6)
ω	Torque wrench accuracy used in the experimental coefficient method (expressed at a \pm value)
ϕ	Compression cone half angle (see Section 6.6)
φ	Thread helix angle (see Figure 6-1)
ρ	Local friction angle at thread interface
θ	Half angle of thread grooves (see Figure 6-1)
δ_b	Compliance of the fastener (see Section 6.5)
δ_c	Compliance of the clamped parts (see Section 6.6)
σ_V	Axial stress in fastener due to nominal preload, $F_{V,nom}$
$\sigma_{V,max}$	Axial stress in fastener due to maximum preload, $F_{V,max}$
$\sigma_{V,min}$	Axial stress in fastener due to minimum preload, $F_{V,min}$
σ_y	Yield stress
μ_{th}	Friction coefficient at the thread interface
μ_{uh}	Friction coefficient at the under-head or under-nut interface
μ_s	Friction coefficient at the slipping interface (the interstice between the loaded flanges)
σ_{br}	Bearing stress
$\sigma_{v.m.}$	Von mises stress
τ	Shear stress
Φ	Basic force ratio (assumes $n=1$ and a concentric joint)
Φ_n	Force ratio of a concentric joint including the loading plane factor effect
$\Phi_{e,n}$	Force ratio of an eccentric joint including the loading plane factor effect
Φ_C	Force ratio of a joint with cantilever flanges
Ω	Fatigue damage
Ψ	Inversion compliance (used for circular flange compliance, see Section 7.3.1)

3.4.4 Subscripts

For the purpose of this document, the following subscripts apply:

Subscript	Meaning
<i>A</i>	Axial stress
<i>apex</i>	Peak
<i>av</i>	Average
<i>avail</i>	Available
<i>b</i>	Fastener (or bolt, screw, etc.)
<i>ben</i>	Bending
<i>br</i>	bearing
<i>brg</i>	Bearing strength
<i>c</i>	Clamped parts (refers to the net elastic properties of all the clamped parts in a joint)
<i>comb</i>	Combined (loads)
<i>con</i>	Concentric
<i>crit</i>	Critical
<i>crush</i>	Crushing
<i>e</i>	Eccentric
<i>eff</i>	Effective
<i>eng</i>	Engaged
<i>free</i>	Used for fastener or clamped parts lengths to indicate that the measure is in the absence of applied loading
<i>g</i>	Gasket
<i>h</i>	Head
<i>lim</i>	limiting
<i>n</i>	Nut
<i>nom</i>	Nominal
<i>net</i>	Net tension
<i>max</i>	Maximum
<i>min</i>	Minimum
<i>Q</i>	Shear
<i>req</i>	Required
<i>S</i>	Shear
<i>sha</i>	Shank
<i>slip</i>	Slipping
<i>sep</i>	Separation
<i>SO</i>	Shear out
<i>sub</i>	Substitutional
<i>T₀</i>	Reference temperature
<i>T_w</i>	Working temperature

Subscript	Meaning
<i>ti</i>	Tightening
<i>th</i>	Thread
<i>tot</i>	Total (or overall)
<i>uh</i>	Under head
<i>ult</i>	Ultimate
<i>V</i>	Preload
<i>y</i>	yield

How to use the guidelines

4.1 Introduction

This guidelines document contains a number of self-contained sections covering specific joint configurations and joint loading situations. Additionally, it contains a number of sections on ancillary subjects related to joint design.

In general, **it is expected that** the user of this document **is** experienced in structural design and **is able to** make use of the various sections as needed. However, to assist the first time user and to provide a 'check list' of essential features to be considered when designing joints, this section includes a procedure guiding the user to the relevant sections of this document.

The various steps are discussed **in sections** 4.2.1 to 4.2.4 and then summarised in a flow chart. Since the purpose of **Section 4** of the **Handbook** is to direct the user through the document, in general, the logic criteria on which the decisions (accept/reject, yes/no) are made are not stated, rather these are included in each of the relevant sections (referenced as appropriate).

4.2 Procedure

4.2.1 Stage I

4.2.1.1 Defining Joint & Loads

The precept on which the guideline is based is that the joint being analysed can be isolated from the surrounding structure. The joint can then be represented by one of five main joint categories, which depend on its configuration and applied forces. Therefore, the first task is to define the physical extent of the joint within the structure, and identify its category (see Section 5). It is assumed that an analysis of the structural system in which joint exists has been carried out in sufficient detail to specify the loads transmitted via the joint.

4.2.1.2 Combined Loading

The case of combined axial and bending loading is treated as an eccentric axially loaded joint, and dealt with in **Section 8**. A method is given in **Section 9** to deal with combined axial and shear loading which is assumed to be the most frequently encountered.

4.2.1.3 Dynamic Loading

In all but exceptional cases the working load on the joint **is** dynamic. This is dealt with in more detail in each section, as appropriate. However, it is recommended that the engineer, at an early stage in the design process, is aware of the influence of varying external joint loads on the loads transmitted by the fastener and at the clamped interface. Reference is therefore made to Section 7.4, which discusses the force ratio.

4.2.1.4 Thermal Loading

Analysis of preloaded joints operating in a varying temperature environment is needed to ensure that they meet functional requirements across the full temperature range. Section 6.3.5 covers the effects of temperature change on the preload. Furthermore, certain joints have requirements for thermal conductivity to be either above or below certain limits. Section 10 covers the analysis of thermal conductivity.

4.2.2 Stage II

4.2.2.1 Joint Analysis & Design Procedures

Depending on the category of joint, the user is directed to the appropriate section, which details the equations needed to calculate Margins of Safety (MoS) for all relevant failure modes. Worked examples are provided to illustrate the application of the proposed design procedures.

4.2.2.2 Embedding & Relaxation

For many joint designs the effects of embedding and relaxation are important. These effects are covered in Section 6.4.2.

4.2.2.3 Fatigue & Fracture Mechanics Aspects

For a more detailed analysis of either fatigue or fracture mechanics, the user is referred to Section 11, which treats these subjects in more detail.

If, within the general design constraints, the joint meets neither the basic nor the detailed fatigue criteria, it **can** be necessary to reconsider the initial joint design concept.

4.2.3 Stage III

4.2.3.1 Corrosion

Environmental effects are identified as an important design parameter. Section 13 discusses a number of corrosion mechanisms relevant to joint components and provides a checklist against which the proposed design can be assessed and possible problem areas identified. Where a severe or intractable corrosion problem is predicted it **can** be necessary to review the initial structural concept, which **can** lead to a change in the joint's materials or detailed design.

4.2.3.2 Methods of Preloading & Lubrication

It is expected that at some stage the fastener assembly method is specified, together with the use or not of a lubricant. The method of preloading can be critical as this determines the accuracy with which the fastener preload can be achieved.

Section 12 covers a number of different methods of installing preloaded fasteners. Design data and estimates of achievable accuracy for the preload are given where appropriate.

Section 14 contains advice on lubrication aspects and contains details of the characteristics of a selected range of fastener lubricants.

4.2.3.3 Preloading Method

The calculation procedures need that a particular preloading method is specified at the start of the design process. It is necessary to check later that the specified preloading method is capable of ensuring the preload accuracy to be achieved, and also that it is compatible with joint location and access constraints.

4.2.4 Stage IV

4.2.4.1 Manufacturing Quality Control Procedures

Section 15 provides the engineer with a guide to the factors that need to be controlled during production to guarantee adequate joint performance.

4.2.4.2 Joint Validation by Testing

Consideration needs to be given to demonstrating that the joint design is adequate. This [can](#) be achieved either by testing the complete structure or by isolating and testing individual joints. These aspects are covered in Section 16.

4.3 Annexes

The following Annexes of the document contain additional technical data that [can](#) assist the engineer undertaking design of threaded fastener joints:

- [Annex A](#): Recommended starting values for seating torque
- [Annex B](#): Measured Friction coefficients of fasteners
- [Annex C](#): Typical friction coefficients for joint materials
- [Annex D](#): Material data of fasteners typically used in the aerospace industry

General Fastener Analysis Guidelines

5.1 Introduction

For the purposes of this guidelines document the different types of joints have been divided into the following five main categories;

- a. Concentric Axially Loaded Joints,
- b. Eccentric Axially Loaded Joint,
- c. Shear Loaded Joints,
- d. Combined Loaded Joints, and
- e. Low Duty Joints.

These are defined by the geometry and system of loading. Due to the different verification procedures “Shear Loaded Joints” and the “Combined Loaded Joints” are further subdivided in to;

- Bearing Joints, and
- Friction Grip Joints.

The categorisation of joints in this manner is reflected in the structure and format of the document. Within each of the main categories, sub-categories can be identified depending on specific geometrical or loading attributes. Details of the main categories together with examples of typical sub-categories are given in this section. It is intended that this indicates the range of joint types covered in the guideline and operates as an index to direct the user to the relevant parts of the document.

5.2 Main Joint Categories

5.2.1 Overview

The definition for a particular joint configuration depends on the geometry of the clamped parts and fasteners, and the effective loading applied at the fastener (or fastener group). As stated in Section 1 it is assumed that the user has knowledge of the system of loads acting on the joint in the vicinity of the fastener(s); these being derived by analysis of the overall structure prior to detailed consideration of joint design. Adequate definition of the applied loading system is essential as this can determine the particular category to which a joint belongs and hence the method of analysis adopted. This is particularly critical when distinguishing between concentric and eccentric axially loaded joints. The selection of the appropriate analysis for the combined loading case is also dependent on adequate specification of the loading system. More complex situations arise where combined loading occurs, typically axial, shear and bending. However, where a single load is dominant in a combined loading case and other load(s) are small it can be possible to assume the joint falls into one of the first three categories outlined in 5.2.2, 5.2.3 or 5.2.4, thereby simplifying the analysis without significant reduction in accuracy. Criteria are included to determine when such an assumption is applicable.

5.2.2 Concentric Axially Loaded Joints

The distinguishing feature of this joint category is that the line of action of the applied loading on the joint is parallel to and coincident with the longitudinal axis of the fastener. Therefore, any combination of joint geometry and system of applied loads which conform to this definition can be analysed by the methods and procedures specified for this category.

Examples of joints for this category are illustrated in Figure 5-1 to Figure 5-3. For clarity a single fastener is shown, although in many cases the same analysis can be applied to a group of fastener if they are in a symmetric pattern. However, it is important to note that the effect of flange flexibility can lead to eccentric fastener loads in joints that with symmetric fastener pattern (see Figure 5-3, Joint 17).

5.2.3 Eccentric Axially Loaded Joints

For this joint category the line of action of the applied loading on the joint, whilst being parallel to the fastener longitudinal axis, is not coincident, but offset. The result of this is that a “prying” (or “prising”) action occurs between the clamped parts of the joint such that bending loads are introduced under the bolt head and in the shank. Three fundamental loading case variants can be identified depending on the relative position of the bolt axis, line of action of the applied load, and the joint centroid.

This category of joint and its variants represent a large proportion of the joints encountered in practice. The main examples of these are illustrated in Figure 5-1 to Figure 5-3. For clarity a single fastener is shown, although in practice this can be a group.

5.2.4 Shear Loaded Joints

The principle feature of this joint category is that the line of action of the applied loading on the joints is in the plane of the clamped parts immediately adjacent to the fastener, and therefore normal to the fastener longitudinal axis. The forces need not be coplanar if the joint is of the non-symmetrical or single lap shear type. Joints of this type can be further subdivided into friction grip or bearing categories, depending on whether load is transferred through the joint by friction at the faying surfaces or by transverse shear in the fastener(s). Examples of joints in this category are illustrated in Figure 5-1 to Figure 5-3. For clarity a single fastener is shown, although in practice this can be a group if the joint has multiple fasteners.

5.2.5 Combined Loaded Joints

The essential feature of this joint category is that more than one system of loads act on the joint relative to the fastener axis. In the most general case features of all the preceding categories are combined. Examples of joints for this category are illustrated in Figure 5-1 to Figure 5-3. For simplicity a single fastener can often be considered, although in practice the same can be a group if the joint has multiple fasteners.

During the design process, joints initially being placed in the (most general) category of combined loaded joints can be reclassified into a sub-category, for the purpose of analysis. This guideline does not provide specific criteria for determining when this simplification can be assumed. Rather, the appropriate analysis method is determined using engineering judgment considering the relative magnitudes of the shear and axial loads, the configuration of the joint and any other relevant attributes of the design.

5.2.6 Low Duty Joints

Joints in this category have loadings and configurations that fit into one of the preceding categories, however they form a unique category since they have small external loading with respect to the fastener strength. In many cases this is readily apparent due to the particular application, e.g. hold-downs, access panel attachments, etc. Some example diagrams of joints that frequently fall into this category are shown in Figure 5-1 to Figure 5-3.

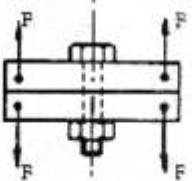
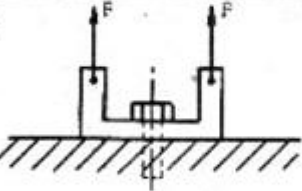
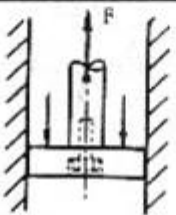
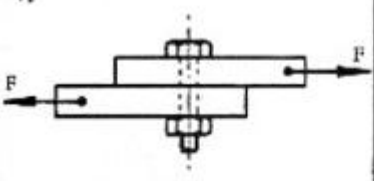
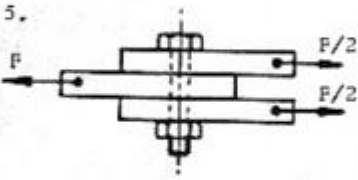
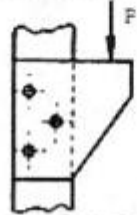
GEOMETRY	NOTES	JOINT CATEGORY
1. 	1. SINGLE OR MULTIBOLTED	CONCENTRIC AXIAL
2. 	1. SINGLE OR MULTIBOLTED	CONCENTRIC AXIAL
3. 	1. SINGLE OR MULTIBOLTED	CONCENTRIC AXIAL
4. 	1. SINGLE OR MULTIBOLTED 2. BEARING LOAD TRANSFER 3. FRICTION GRIP LOAD TRANSFER	SYMMETRIC SHEAR
5. 	1. SINGLE OR MULTIBOLTED 2. BEARING LOAD TRANSFER 3. FRICTION GRIP LOAD TRANSFER	SYMMETRIC SHEAR
6. 	1. BEARING LOAD TRANSFER 2. FRICTION GRIP LOAD TRANSFER	ECCENTRIC SHEAR

Figure 5-1 - Joint Categories (1 to 6)

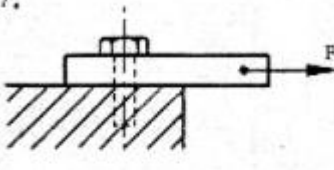
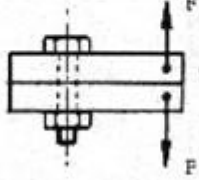
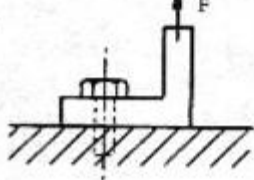
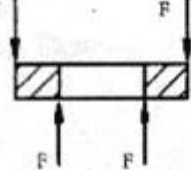
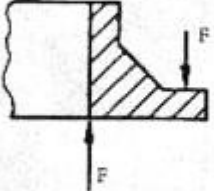
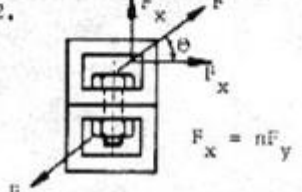
GEOMETRY	NOTES	JOINT CATEGORY
7. 	1. SINGLE OR MULTIBOLTED 2. BEARING LOAD TRANSFER 3. FRICTION GRIP LOAD TRANSFER	SHEAR PLATE
8. 	1. SINGLE OR MULTIBOLTED	ECCENTRIC
9. 	1. SINGLE OR MULTIBOLTED	ECCENTRIC
10. 	1. PLAIN FLANGE	ECCENTRIC
11. 	1. WELDNECK FLANGE	ECCENTRIC
12. 	1. SINGLE OR MULTIBOLTED 2. LOAD RATIOS	a) CONCENTRIC AXIAL b) UNSYMMETRIC SHEAR c) COMBINED LOADING

Figure 5-2 - Joint Categories (7 to 12)

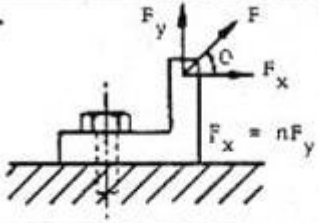
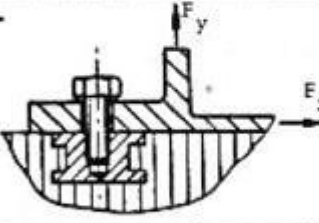
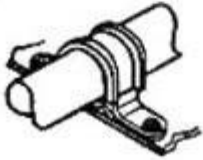
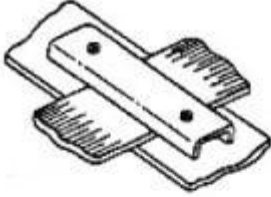
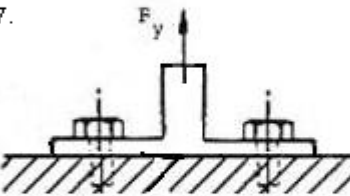
GEOMETRY	NOTES	JOINT CATEGORY
13. 	1. SINGLE OR MULTIBOLTED 2. LOAD RATIOS IF:- a) $0 < n < 0.1$ b) $9 < n < \infty$ c) $0.1 < n < 9$	a) ECCENTRIC b) SHEAR PLATE c) COMBINED LOADING MAY BE LOW DUTY
14. 	1. SINGLE OR MULTIBOLTED 2. MOUNT TO SANDWICH PANEL WITH POTTED INSERT 3. MAY BE PART OF HEAT CONDUCTION PATH	LOW DUTY
15. 	1. NORMALLY SINGLE BOLTED	LOW DUTY
16. 	1. NORMALLY MULTIBOLTED	LOW DUTY
17. 	1. THIN FLANGES CAN DEFORM INDEPENDENTLY 2. PRYING MUST BE CONSIDERED	ANALYSE AS INDEPENDENT ECCENTRIC JOINTS

Figure 5-3 - Joint Categories (13 to 17)

5.3 Joint Analysis Procedure

5.3.1 Overview

The calculation of a mechanically fastened joint begins with the definition of the external operational loading environment, which includes the axial load F_A , the shear load F_Q , the bending moment M_B and the torsional moment M_T (if present). For the fastener analysis it is assumed, that these external forces and moments are known. Figure 5-4 shows a joint with the dimensions indicated.

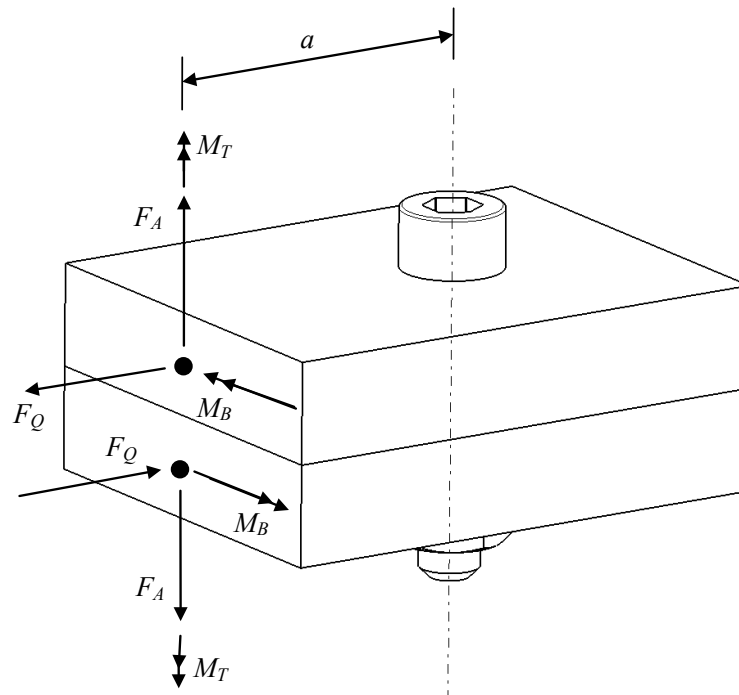


Figure 5-4 - Definitions of Forces and Moments Acting on a Joint

Based on the applied loads and expected operating environment the joint's configuration can be determined including details such as the preload in the fastener, flange dimensions and the materials used. Following this, **it is important to verify** the functionality and strength of the joint system by calculating all relevant Margins of Safety (MoS) according the Equations presented in this document (see 5.3.2 below).

5.3.2 Margins of Safety

It is important to demonstrate positive values for all MoS that are applicable to the specific type of joint.

The generic equation for a Margin of Safety is,

$$MoS = \frac{\text{Allowable Load}}{\text{Limit Load} \times sf} - 1 \quad [5.3.1]$$

where the *Allowable Load* is the load at which a mode of failure is predicted to occur and the *Limit Load* is the determined by analysis of the service loads expected during the joint's lifetime. The *sf* is the safety factor corresponding to the specific mode of failure being considered.

For each of the joint modes of failure covered in this document, equations derived for the MoS are provided. Table 5-1 shows where each of the MoS derivations is given in this handbook.

Table 5-1 - Margins of Safety to be analysed for a threaded fastener

MoS variable name	Relevant failure mode Description	Relevant joint categories		Refer to handbook section
		Friction grip	bearing	
MoS _{ti,y} & MoS _{ti,ult}	Combined stresses in fastener during tightening (yield and ultimate)	Yes	Yes	6.5
MoS _{sep}	Separation (or gapping) of flanges	Yes	Yes	7.8
MoS _{A,y} & MoS _{A,ult}	Axial stress in fastener for external load only (yield and ultimate)	Yes	Yes	7.9
MoS _{tot,y} & MoS _{tot,ult}	Axial stress in fastener due to preload and external load (yield and ultimate)	Yes	Yes	7.9
MoS _{th}	Shear pull-out of thread (either nut or insert)	Yes	Yes	7.10
MoS _{crush}	Crushing of flanges	Yes	Yes	7.11
MoS _{slip}	Slipping of joint flanges	Yes	No	9.2
MoS _{Q,y} & MoS _{Q,ult}	Shear load in fastener (yield and ultimate)	No	Yes	9.3.2
MoS _{comb,y} & MoS _{comb,ult}	Combined loads on fastener (yield and ultimate)	No	Yes	9.3.2
MoS _{Q,net}	Net tension section failure of flange	No	Yes	9.3.3
MoS _{br,y} & MoS _{br,ult}	Bearing stress on flange hole (yield and ultimate)	No	Yes	9.3.4
MoS _{so}	Shear-out of flange	No	Yes	9.3.5
MoS _{ben}	Bending load on fastener	No	Yes	[1]

NOTE 1. Not included in this version of the handbook, however [it is important to assess this failure mode](#)

5.4 Joint Geometry

5.4.1 Fastener Geometry

For a fastener analysis several dimensions are important. These are depicted in Figure 5-5 and Figure 5-6.

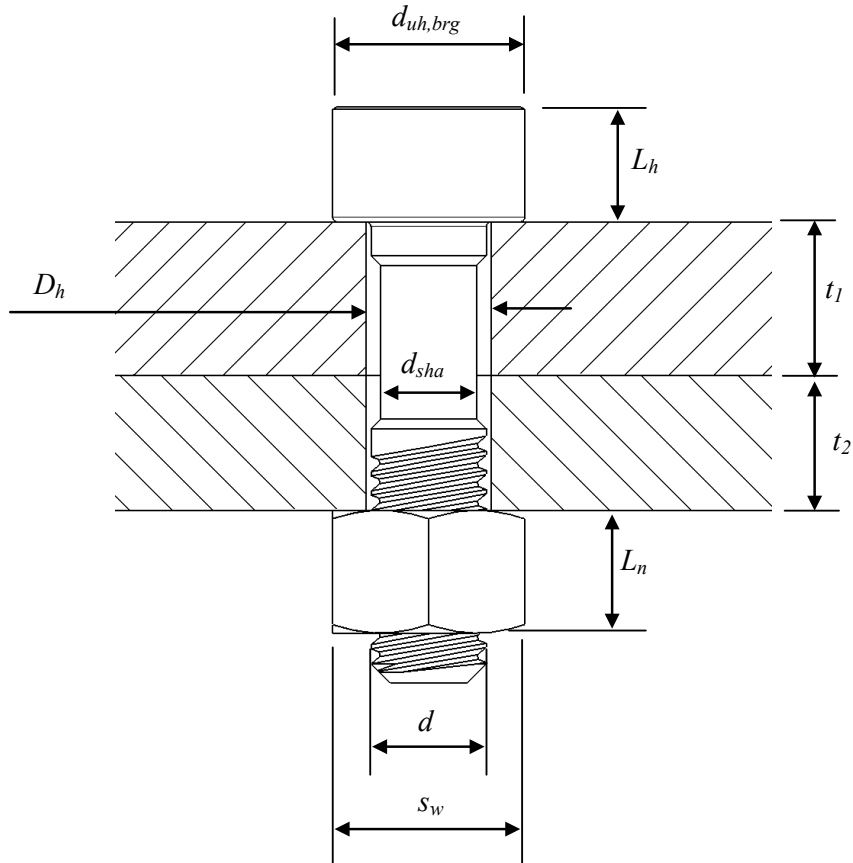


Figure 5-5 – Fastener Dimensions

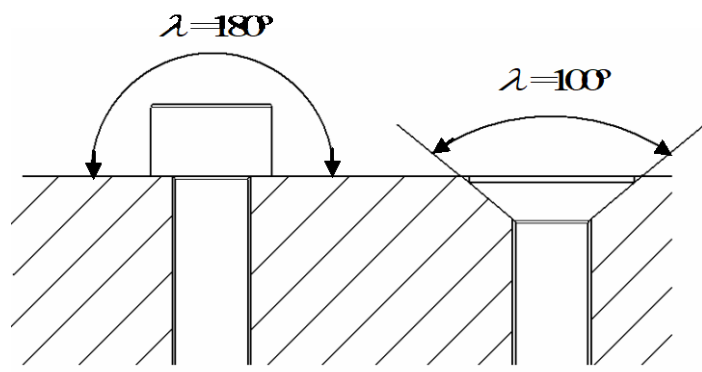


Figure 5-6 – Definition of the under-head bearing angle

Table 5-2 shows the definitions of the physically measurable fastener variables used in this handbook. Some of these are omitted from Figure 5-5 for clarity.

Table 5-2 - Physical Dimensions of Fasteners

Variable	Definition	Notes
p	Pitch of thread	
h	Height of the basic thread	
d	Nominal fastener diameter	Outside diameter of thread
d_0	Diameter at smallest cross-section of fastener shank	
d_3	Minor diameter of thread	For the true thread, not the basic profile
d_{sha}	Shank diameter	For necked-down fasteners
$d_{uh,brg}$	Outer diameter of bearing area	Either under a head or under a nut
D_h	Nominal diameter of hole in flange	
A_0	Smallest cross-section of fastener shank	
A_3	Cross-sectional area at minor diameter of fastener thread	
λ	Under-head bearing angle	Always 100° for countersunk aerospace standard fasteners (right side of Figure 5-6)
S_w	Size of wrench	Across flats dimension of either a head or a nut

5.4.2 Thread Geometry

Figure 5-7 shows the geometric definition of the metric (M and MJ) threads. Both the male and female threads are based on the “Base Profile” shown in the left of the figure. The base profile defines the maximum spatial envelope of the male threaded part (normally the fastener itself), and the minimum spatial envelop of the female threaded part (normally the nut or threaded hole). The exact thread

profiles are defined in the relevant standards. The only difference between M and MJ type threads is the thread root radius, which is larger (to give improved fatigue performance) in the MJ type thread.

Table 5-3 shows the definitions of the derived fastener variables used in this handbook.

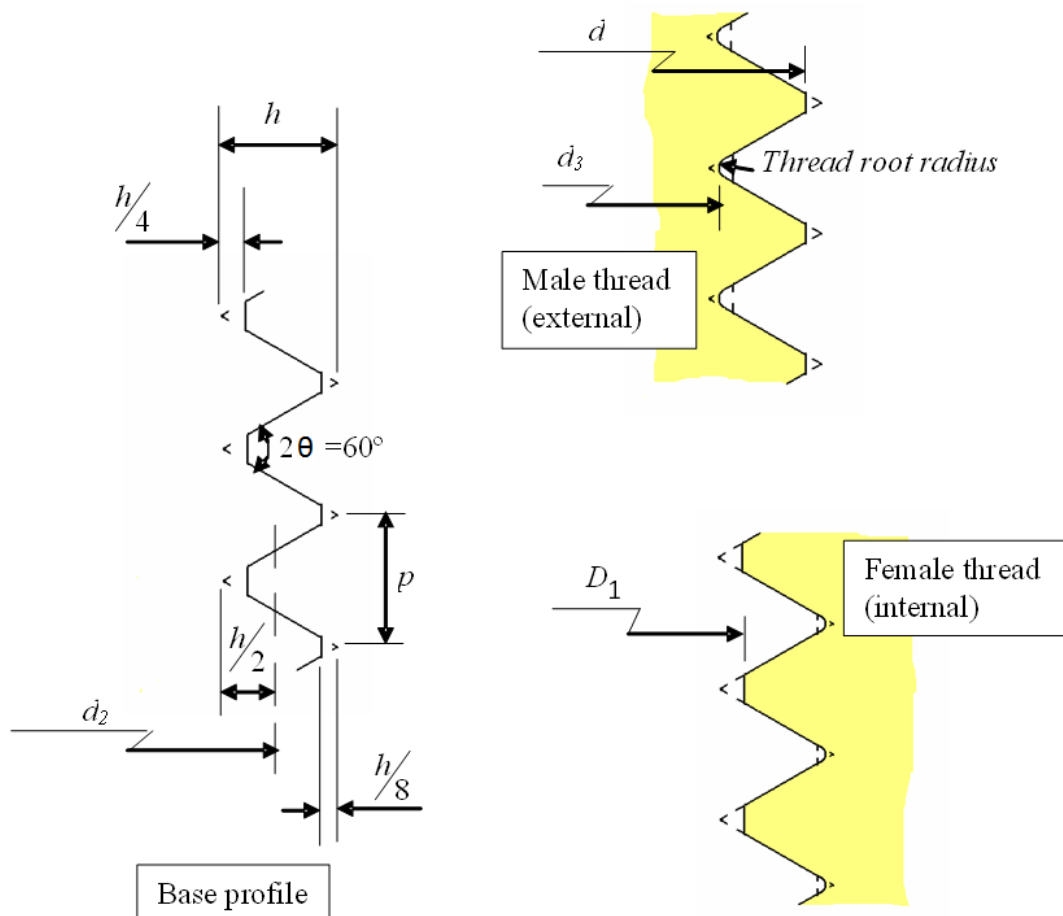


Figure 5-7 – Thread Geometry

Table 5-3 - Derived Dimensions for Metric Fasteners

Variable	Notation	Equation	
Pitch diameter	d_2	$= d - 0,64952 p$	[5.4.1]
Minor diameter	d_3	$= d - 1,22687 p$	[5.4.2]
Diameter used for stress calculation	d_s	$= 0,5 (d_2 + d_3)$ (for M type thread)	[5.4.3]
		$= \text{see stress area below}$ (for MJ type thread)	[5.4.4]
Diameter used for stiffness calculation	d_{sm}	$= d_3$	[5.4.5]
Effective diameter of friction under head or nut	d_{uh}	$= 0,5 (D_{head} + D_h)$	[5.4.6]
Stress area	A_s	$= 0,25 \pi d_s^2$ (for standard fasteners, M type thread)	[5.4.7]

Variable	Notation	Equation	
		$0,25\pi(d_3)^2 [2-(d_3/d_2)^2]$ (for standard fasteners, MJ type thread)	
		$= 0,25 \pi d_0^2$ (for reduced shank fasteners)	[5.4.8]
Stiffness area	A_{sm}	$= 0,25 \pi d_{sm}^2$	[5.4.9]
Smallest cross-section of fastener shank	A_0	$= 0,25 \pi d_0^2$	[5.4.10]
Minor diameter of the female thread	D_1	$= d - 1,0285 p$	[5.4.11]

In general, [it is important to find](#) the correct equation in the relevant fastener technical specification, e.g. ISO 9152 for Titanium fasteners (Reference 5.1).

For unified threads (UNC, UNF, etc) the same equations apply except that the pitch, p , is not normally given in the fastener specification. In order to use the above equations provided in Table 5-3, it is necessary to calculate first the pitch by inverting the ‘threads per inch’ specification, which is given in the thread designation.

[It is also important to take into account](#) tolerance information in determining some or all of the dimensions used for stress calculations.

ISO 5855 (Reference 5.2) specifies the MJ-type thread, which is specially suited for aerospace applications and has a larger diameter at the thread root to improve the fastener’s fatigue life. The UNJ thread is the analogous modification for unified threads.

5.5 Safety Factors

5.5.1 Overview

Table 5-4, extracted from ECSS-E-ST-32-10C Rev. 2 Corrigendum 1, shows the recommended safety factors for the analysis of threaded fasteners in European space projects (e.g. on behalf of ESA). Ultimate responsibility for the definition of safety factors for a space project rests with the project management. Since safety factors depend strongly on the type of load, the stated safety factors are to be regarded as minimum values.

The safety factors can be decreased significantly if a test with the appropriate test factor is performed either on dedicated test structure identical to the flight structure (a proto-type test) or on the flight hardware (a proto-flight test).

Table 5-4 - Factors of safety for joints, inserts and connections

Structure type	Vehicle	Requirements			
		FOSY	FOSU	FOSY verification by analysis only	FOSU verification by analysis only
Joints and inserts: ^a - Failure - Gapping/Sliding (Safety Critical) ^d - Gapping/Sliding (other)	Satellite	1,1	1,25	1,25	2,0
		N/A		N/A	
		1,1		2,0	
	Launch vehicle ^e	1,1	1,25	N/A	N/A
		N/A		2,0	
		1,1		2,0	
	Man-rated S/C	See Note ^c	1,4	See Note ^c	See Note ^c
		1,4		2,0	
		1,25		2,0	
Elastomer system and elastomer to structure connection ^b	Satellite	See Note ^c	2,0	See Note ^c	See Note ^c
	Launch vehicle	See Note ^c	2,0	See Note ^c	See Note ^c
a These factors are not applied on the bolts preload b Analysis and test are performed to show that the possible non linear dynamic behaviour of the elastomer does not jeopardize the satellite strength and alignment. c No commonly agreed value within the space community can be provided. d For Safety Critical Structures definition applicable to man rated s/c see NASA SSP 52005 e See requirement 4.3.2.2b of ECSS-E-ST-32-10C Rev.2 Corrigendum 1: "For expendable launch vehicles, FOSU and FOSY to failure, gapping and sliding, associated with thermally induced loads shall be 1,0."					

5.5.2 The Joint Fitting Factor

In cases where the joint load distribution is difficult to accurately predict, it is important to apply an extra joint fitting factor of 1,15 in addition to the safety factors provided in Table 5-4. This factor is used on yield and ultimate loads in the structural analysis of all fittings with threaded fasteners, whose strength is not proven by limit and ultimate load test in which the actual stress conditions are simulated and measured in the joint and surrounding structure. It is important to apply this factor to all portions of the fitting, the means of fastening, and the bearing on the members joined.

The fitting factor is not used with limit and ultimate loads where the specific type of joint is strength-verified by comprehensive limit and ultimate tests. This commonly is the case for joints such as continuous row of fasteners in sheet or plate.

5.5.3 Planarity of Flanges

The absence of planarity between flanges can generate bending on the screw (see Figure 5-8).

In most cases this angle is so small with regard to the stiffness of the screw that the induced constraint is negligible, but in some specific designs (e.g. long screws) this has to be considered with different possible solutions:

- Spherical washers to suppress this imposed angle
- Or decrease of the torque/tension to maintain an acceptable safety margin on the screw.

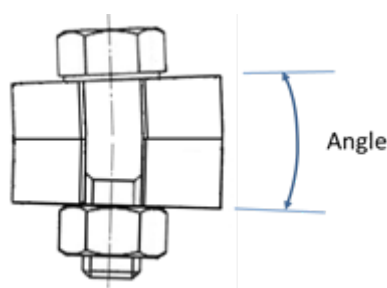


Figure 5-8 - Illustration of bending on the screw

5.6 References

5.1	ISO 9152:1998	Procurement specification – Aerospace - Bolts, with MJ threads, in titanium alloys, strength class 1 100 MPa
5.2	ISO 5855-2:1999	Aerospace - MJ Threads - Part 2: Limit dimensions for bolts and nuts
5.3	ISO 724:1993	ISO general-purpose metric screwthreads - Basic dimensions

6

The Preload

6.1 Overview

The integrity of a threaded fastener joint, either shear or tension, is maintained by the preload in the fastener. It has been shown that the optimum joint has as high a preload as possible. However, equally important is the need to accurately control the preload to a specified value. In many instances the reason for failure of bolted joints is incorrect initial preload, loss of the preload due to loosening, or relaxation of the preload due to a variety of mechanisms.

The fundamental problem, however, is to assemble the joint and accurately achieve the required initial preload in the fastener. A number of methods are available for controlling or achieving the preload during assembly. These are discussed in this section.

The methods described are generally amenable to theoretical analysis, and where relevant this is included. It is **important to note** that, although apparently simple, the bolted joint is extremely complex. Simple theoretically "correct" methods suffer from inaccuracies, some quite subtle. The accuracy of the analysis depends on the specification of materials and geometrical parameters, which in practice are impossible to specify without resorting to empirical data derived from tests on actual or representative joints. Friction data for some common joint materials are given in [Annex C](#).

This section relates to the method of torque tightening, which is the most common method of tightening threaded fasteners. Other methods intended for obtaining more precise preload during tightening are presented in Section 12.

The torque tightening method utilises the relationship between applied torque and preload induced in the fastener. The relationship is dependent on both geometry and effective coefficients of friction at the "under head" bearing region and in the threads.

6.2 Coefficient of Utilisation

The size and strength class of fasteners is chosen taking into account the coefficient of utilization γ . This is the maximum pretension stress divided by the yield stress of the fastener material,

$$\gamma = \frac{\sigma_{v,max}}{\sigma_y} \quad [6.2.1]$$

where $\sigma_{v,max}$ is the **maximum** pretension stress, and σ_y is the yield stress of the fastener material.

The value of γ can be varied in order to fine-tune the performance of the joint however it is **important that the value** typically lies in the range from 0,5 to 0,8. The recommended value to start the design process is 0,8.

Once the desired coefficient of utilization is selected, the related **maximum** preload $F_{v,max}$, can then be calculated by,

$$F_{v,max} = \gamma \sigma_y A_S \quad [6.2.2]$$

In practice, the preload achieved in service varies around this value due to effects such as friction, inaccuracies in applied torque measurement, embedding and thermal loads. The remainder of this section explains effects such as friction, inaccuracies in applied torque measurement, embedding and thermal loads on the preload and provides theory for quantifying the statistical scatter in the preload.

6.3 Theoretical Aspects

6.3.1 The Relation between Torque and Preload

The idealised model used to describe the system of forces in action during tightening assumes the developed shape of the nut thread helix as a “wedge” driven between the ‘wedge’ of the fasteners thread and surface of the clamped material. The axial result force transmitted by the engaged thread is assumed to act normal to the ideal thread surface at the pitch radius ($d_2/2$). The forces present during tightening are shown in the left of Figure 6-1, and the corresponding wedge model with forces are resolved into a plane is shown on the right of the figure.

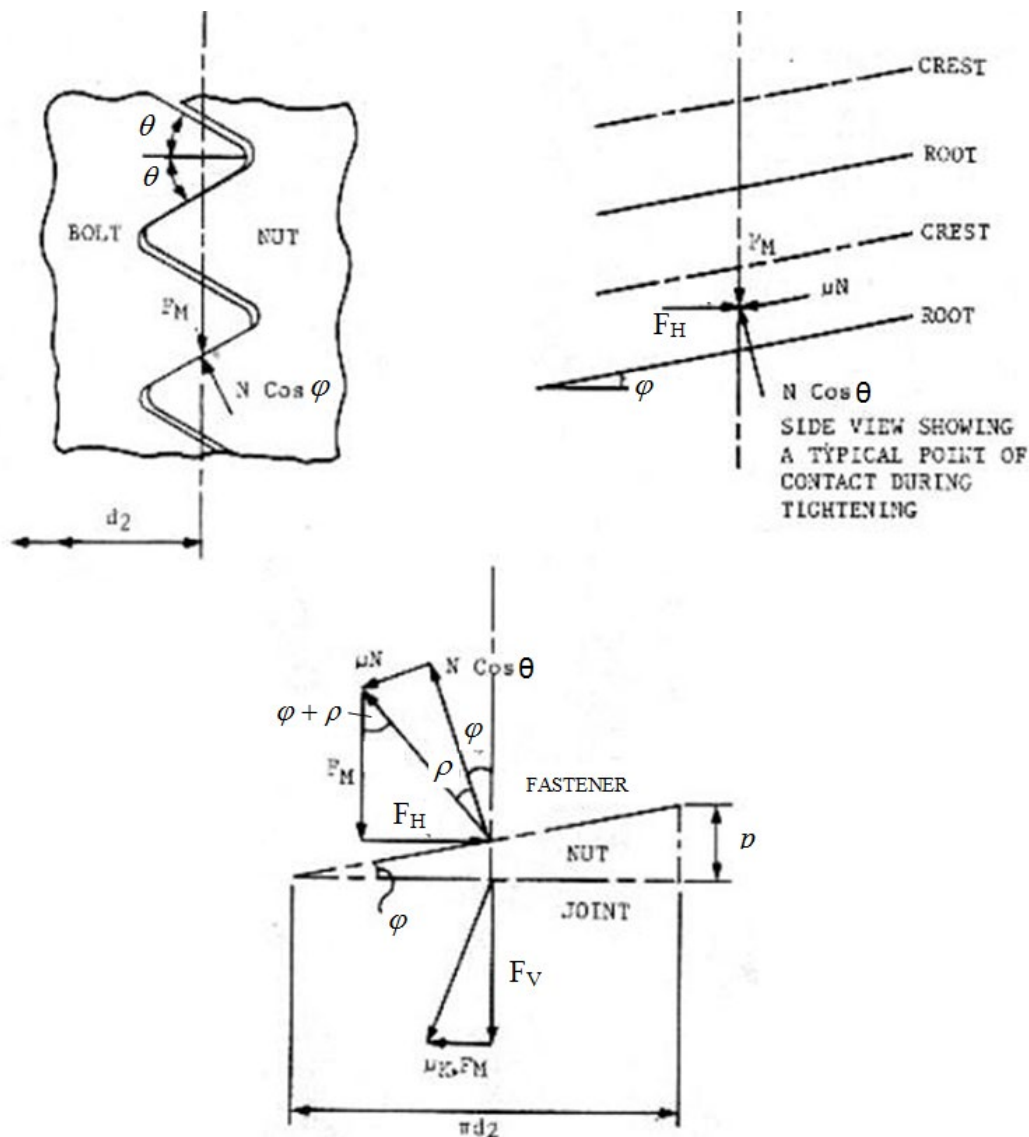


Figure 6-1 – Forces Present During Tightening (the Wedge Model)

From the lower diagram in Figure 6-1 the applied force acting to “slip the wedge” (analogous to rotating the thread) is,

$$F_H = F_V \tan(\varphi + \rho) \quad [6.3.1]$$

where φ is the helix angle of the thread and ρ is given by the relation,

$$\tan \rho = \frac{\mu_{th}}{\cos \theta} \quad [6.3.2]$$

where μ_{th} is the coefficient of friction of the thread interface, and θ is the half angle of the thread grooves.

The torque present at the thread interface is therefore given by,

$$M_{th} = F_V \tan(\varphi + \rho) \frac{d_2}{2} \quad [6.3.3]$$

The ‘under-head’ torque due to friction at the bearing surface between nut or fastener head and the adjacent clamped part is assumed to act at the mean bearing radius of the head (or nut). Therefore, it is given by,

$$M_{uh} = F_V \frac{\mu_{uh} d_{uh}}{2} \frac{1}{\sin(\lambda/2)} \quad [6.3.4]$$

where μ_{uh} is the coefficient of friction between the nut (or fastener head) and the adjacent clamped part, d_{uh} is the effective diameter of the under-head friction torque as defined by equation [5.4.6], and λ is the under-head bearing angle (see Figure 5-6).

Thus, the total installation torque applied (to either the head or nut) during tightening in order to produce the preload F_V is,

$$M_{app} = M_{th} + M_{uh} + M_P = F_V \left[\frac{d_2}{2} \tan(\varphi + \rho) + \mu_{uh} \frac{d_{uh}}{2 \sin(\lambda/2)} \right] + M_P \quad [6.3.5]$$

where M_P is the prevailing torque (self-locking torque) of the locking device (see Section 6.3.3). In case of highly preloaded joints, M_P can be ignored; however in such a case, a demonstration that M_P does not contribute to preload reduction shall be provided.

M_P is subject to scatter so, in addition to quoting mean values, an indication of its expected variation is given by either the range or coefficient of variation. M_P is likely to vary with fastener size. Section 6.3.3 contains more information about locking devices and Table 6-2 provides some experimental data.

A second approach in industry applied to critical joints is to measure the prevailing torque of each self locking insert, wire thread insert, nut, add the value to the established seating torque and install the fastener with the combined torque. It is important that the measured prevailing torque is within the range given by the insert, wire thread insert, nut manufacturer.

The geometric relation,

$$\tan(\varphi + \rho) = \frac{\tan \varphi + \tan \rho}{1 - \tan \varphi \tan \rho} \quad [6.3.6]$$

with the approximation $\tan \varphi \tan \rho \ll 1$, gives,

$$\tan(\varphi + \rho) \approx \tan \varphi + \tan \rho \quad [6.3.7]$$

Hence, [6.3.5] can be rewritten as,

$$M_{app} = F_V \left[\frac{d_2}{2} \left\{ \tan \varphi + \frac{\mu_{th}}{\cos \theta} \right\} + \mu_{uh} \frac{d_{uh}}{2 \sin(\lambda/2)} \right] + M_P \quad [6.3.8]$$

or using the geometric relation

$$\tan \varphi = \frac{p}{\pi d_2} \quad [6.3.9]$$

$$M_{app} = F_V \left[\frac{p}{2\pi} + d_2 \frac{\mu_{th}}{2 \cos \theta} + \mu_{uh} \frac{d_{uh}}{2 \sin(\lambda/2)} \right] + M_P \quad [6.3.10]$$

The applied torque Equation [6.3.10] can be separated into the following terms:

$$F_V \left[\frac{p}{2\pi} \right] \text{ representing the torque absorbed in stretching the fastener,}$$

$$F_V \left[\frac{d_2 \mu_{th}}{2 \cos \theta} \right] \text{ representing the torque due to friction in the threaded interface,}$$

$$F_V \left[\frac{\mu_{uh} d_{uh}}{2 \sin(\lambda/2)} \right] \text{ representing the torque due friction under the nut (or head), and}$$

$$M_P \text{ representing the prevailing torque due to the locking device}$$

A typical distribution of the torque between these components is as follows:

- 10% Stretching bolt
- 30% Absorbed by friction in threads
- 50% Absorbed by friction under head of bolt or nut
- 10% Prevailing torque of a self-locking thread

The following simplified expression for M_{app} can be used for the common case of Unified or Metric threads (where $\theta = 30^\circ$) and standard heads (where $\lambda = 180^\circ$),

$$M_{app} = F_V \left[0.16p + 0.58\mu_{th}d_2 + \mu_{uh} \frac{d_{uh}}{2} \right] + M_P \quad [6.3.11]$$

In practice manufacturing variations in p , d_2 and d_{uh} are negligible. Thus, for a geometrically similar fastener system, M_{app} depends primarily on variations in μ_{th} and μ_{uh} . If, for a given joint, the friction coefficients are fixed, the torque to preload relationship is linear.

6.3.2 Determining the Design Torque Level

6.3.2.1 Overview

Excessive fastener torque can lead to tensile failure of the fastener. On the other hand, insufficient torque can lead to inadequate compression of the clamped parts, leading to failure by gapping or to slipping (when slipping is not allowed).

The specified torque range is normally found by an iterative design process whereby the margins of safety are calculated for each relevant failure mode.

It is important to first calculate the maximum and minimum applied torques, $M_{app,max}$ and $M_{app,min}$, taking into account the torque measurement accuracy. The most common way to specify these torque levels is to calculate them relative to a nominal applied torque, M_{nom} . Annex A recommends starting values of nominal torque, $M_{app,nom}$, for some of the most commonly used fasteners.

Two methods are presented in sections 6.3.2.2 and 6.3.2.3 for calculating the preload range based on the torque range:

- a. Experimental Coefficient Method, and
- b. Typical Coefficient Method.

It is important to apply the Experimental Coefficient Method whenever the preload in the joint is critical (e.g. for friction grip joints) since it considers independently the uncertainties of the fastener friction coefficients and torque wrench accuracy.

The Typical Coefficient Method is mostly used in cases where control of the preload is non-critical. This occurs most often for bearing joints or low-duty joints.

6.3.2.2 The Experimental Coefficient Method

This method takes into account all sources of preload uncertainty, namely the prevailing torque, preload loss due to embedding, thermo-elastic effects, and the torque wrench accuracy.

Firstly, the maximum and minimum bounds of the applied torque, $M_{app,max}$ and $M_{app,min}$ are determined by,

$$M_{app,max} = (1 + \omega)M_{nom} \quad [6.3.12]$$

$$M_{app,min} = (1 - \omega)M_{nom} \quad [6.3.13]$$

where M_{nom} is the nominal applied torque (normally determined by an iterative process) and ω is the torque wrench accuracy, which is typically in the range $\pm 5\%$ to $\pm 15\%$.

It is important to guarantee the torque wrench accuracy by certificates obtained during periodic calibrations.

Next, the maximum and minimum preloads are found by the following equations, which are derived from Equation [6.3.10], and modified to include thermal and embedding effects:

$$F_{V,max} = \frac{(M_{app,max} - M_{P,min})}{\frac{1}{2}d_2 \left(\tan \varphi + \frac{\mu_{th,min}}{\cos \theta} \right) + \frac{1}{2}d_{uh}\mu_{uh,min}} + F_{\Delta T^+} \quad [6.3.14]$$

$$F_{V,min} = \frac{(M_{app,min} - M_{P,max})}{\frac{1}{2}d_2 \left(\tan \varphi + \frac{\mu_{th,max}}{\cos \theta} \right) + \frac{1}{2}d_{uh}\mu_{uh,max}} + F_{\Delta T^-} - F_Z \quad [6.3.15]$$

$$F_{V,nom} = \frac{M_{app,nom} - M_{P,max}}{\frac{1}{2}d_2 \left(\tan \phi + \frac{\mu_{th,nom}}{\cos \theta} \right) + \frac{1}{2}d_{uh}\mu_{uh,nom}} + F_{\Delta T^-} - F_Z \quad [6.3.16]$$

where $F_{\Delta T^+}$ and $F_{\Delta T^-}$ are the maximum (most positive) and minimum (most negative) increments in the fastener load due to thermo-elastic effects (see Section 6.3.5), and F_Z is the maximum preload loss due to relaxation (see Section 6.4).

The term $M_{P,min}$ in Equation [6.3.14] is relatively insignificant and, as a conservative simplification, is often excluded from the calculation.

The minimum preload calculated by Equation [6.3.15], includes the preload loss due to relaxation, F_Z . This term does not appear in the maximum preload equation [6.3.14] since embedding can only loosen a fastener, and therefore cannot increase the maximum preload.

6.3.2.3 The Typical Coefficient Method

In this method an uncertainty factor ε is introduced to account for all sources of scatter observed during the tightening process. The friction coefficients used are nominal (or average) values.

$$F_{V,max} = \frac{(1 + \varepsilon)M_{app,max}}{\frac{1}{2}d_2 \left(\tan \phi + \frac{\mu_{th,nom}}{\cos \theta} \right) + \frac{1}{2}d_{uh}\mu_{uh,nom}} + F_{\Delta T^+} \quad [6.3.17]$$

$$F_{V,min} = \frac{(1 - \varepsilon)(M_{app,min} - M_{p,max})}{\frac{1}{2}d_2 \left(\tan \phi + \frac{\mu_{th,nom}}{\cos \theta} \right) + \frac{1}{2}d_{uh}\mu_{uh,nom}} + F_{\Delta T^-} - F_Z \quad [6.3.18]$$

The Equations [6.3.17] and [6.3.18] separate the applied torque into its minimum and maximum values, $M_{app,max}$ and $M_{app,min}$. However, since the preload scatter is dominated by friction variability, in many cases it is equally conservative to use the nominal applied torque, $M_{app,nom}$, in both of these equations.

Table 6-1 gives typical values of ε for a range of tightening.

Table 6-1 - Uncertainty factors of tightening methods (from reference 5.1)

Method of preload application	Uncertainty factor (ε)
Torque measurement of unlubricated bolts	± 0,35
Torque measurement of cadmium-plated bolts (*)	± 0,30
Torque measurement of lubricated bolts	± 0,25
Hydraulic fasteners	± 0,15
Preload indicating washers	± 0,10
Ultrasonic measurement devices	± 0,10
Bolt elongation measurement	± 0,05
Instrumented bolts	± 0,05
NOTE(*) This information is provided for reference only, since the use of cadmium-plated fasteners is not allowed	

The uncertainty factor can be reduced when the preload is measured by more accurate methods such as those discussed in Section 12, or sometimes also by increasing the accuracy of the torque wrench.

6.3.3 Locking Devices and Prevailing Torque

A joint in a spacecraft is exposed to extensive vibration loads during the launch phase of its mission. Therefore, **it is important that** all joints with threaded fasteners have locking devices to avoid vibration loosening. Locking can be realised by either self-locking threads (applicable to both nuts and helicoils or inserts) or by other means such as adhesives, lock wire **or highly preloaded bolted junctions**.

Self-locking thread devices commonly used in spacecraft can be put in three categories:

- Helicoil (screwlock) or insert: The locking is achieved by one or several deformed threads located in the threaded hole.
- Self-locking nuts: The nuts cross section is deformed to an elliptical shape and has to be reshaped to a circle when screwing through it.
- Self-locking anchor nuts: The locking mechanism is the same as self-locking nuts but the nut is anchored to the flange.

A variety of other self-locking thread devices exist for terrestrial applications; plastic thread inserts, etc.

To rely on the high preload as locking mechanism it is very important, that the desired preload is applied to the bolted junction, which is usually done by dedicated Quality Assurance measures.

Before the fastener can rotate it is necessary to overcome a certain torque, named the prevailing torque. This is measured by turning the threaded parts while there is neither under-head nor under-nut contact. This practice is recommended for every safety-critical fastener, which has a self-locking device.

The prevailing torque of some commonly manufactured devices meeting LN norms are listed in Table 6-2. If an adhesive is used to guarantee locking of the threaded parts, **it is important that tests are performed to determine its prevailing torque.** It is important to note that liquid adhesives are known to act as a lubricant prior to curing, so a lower friction coefficient **is** used when determining the preload torque. Also, the use of liquid adhesives as locking mean is not recommended since its effect **cannot** be verified during the installation of the fastener (the inferred locking torque **cannot** be measured).

Table 6-2 - Prevailing Torques of Locking Devices on Unlubricated Fasteners

Fastener Type	Type of Nut or Insert	Size	$M_{p,min}$ [Nm]	$M_{p,max}$ [Nm]	$M_{p,av}$ [Nm]
Cylinder-head fastener, LN 29949	Helicoil (screwlock) bronze (not cadmium plated), LN 9499 [1]	M4	-[2]	-	-
		M5	1,10	1,60	1,28
		M6	2,60	4,60	3,36
		M8	4,40	5,60	4,91
	Anchornut, LN 29693	M4	-	-	-
		M5	-	-	-
		M6	0,40	2,00	1,47
		M8	-	-	-
	Nut, LN 9161-M	M4	-	-	-
		M5	1,10	2,00	1,56
		M6	0,50	1,00	0,66
	NOTE [1] LN 9499 is only applicable for CRES helicoils. DIN 65536-1 is the correct standard for bronze helicoils.				
NOTE [2] In many cases data can be requested from the insert, wire thread insert, nut manufacturer.					

When using Table 6-2 some additional information **need to** be considered. Generally, helicoils (screwlock) as defined in LN 29949 show the largest statistical spread of self-locking torque with the most and largest outlier values. These outliers are not taken into account in the table. Uncommonly high values for the prevailing torque normally indicate a failure of the helicoil.

Table 6-2 is given as reference only. The reader is addressed to look into the data sheets published by the manufacturers of self-locking **wire thread inserts**, inserts and nuts. They usually provide the minimum and maximum values of the self-locking torque for each thread size. It is necessary to measure the actual value of the self-locking torque during the fastener installation process, and to check that it is within the limits provided by the manufacturer.

To avoid galling, it is recommended that the helicoils **are** made from bronze CuSn6 material number 2.1020.34.

For additional best practise guidelines for various locking features refer to Annex B of reference 6.1.

6.3.4 Sources of Error

Referring to Equation [6.3.10], the dominant factor contributing to scatter in the torque vs. preload relationship is the variability in the friction conditions.

Variations in fastener geometry that influence the friction radii **can** also contribute to scatter but to a lesser extent. Of these, variations in the under-head and under-nut radii are most dominant.

In addition, variation in the applied assembly torque **can** also contribute to scatter.

Prevailing torque scatter also **contributes** to the variation in the effective assembly torque seen by the fastener. To minimise this effect **it is important that** the torque applied to each fastener **is** adjusted by its (measured) prevailing torque, which is measured while turning the threaded parts prior to contact at the under-head or under-nut interfaces.

The effect of these factors on the possible scatter in the fastener preload is shown in Figure 6-2. This illustrates the dominant effect of friction and demonstrates the high scatter possible if friction conditions are not controlled by the careful specification and application of lubrication.

Figure 6-2 shows an example of the preload as a function of the applied torque. The relationship is linear and the slope depends on the friction coefficients. The graph shows contours of the fastener stress ratio, $\sigma_{v.m.} / \sigma_y$, which indicate the strength utilisation.

The maximum preload, 90% of the fastener yield load, is found at the point X, where the maximum thread torque $M_{th,max}$ and minimum friction μ_{min} occur. The minimum preload load $F_{V,min}$ is found at the point Y where the minimum thread torque $M_{th,min}$ and maximum friction coefficient μ_{max} occur.

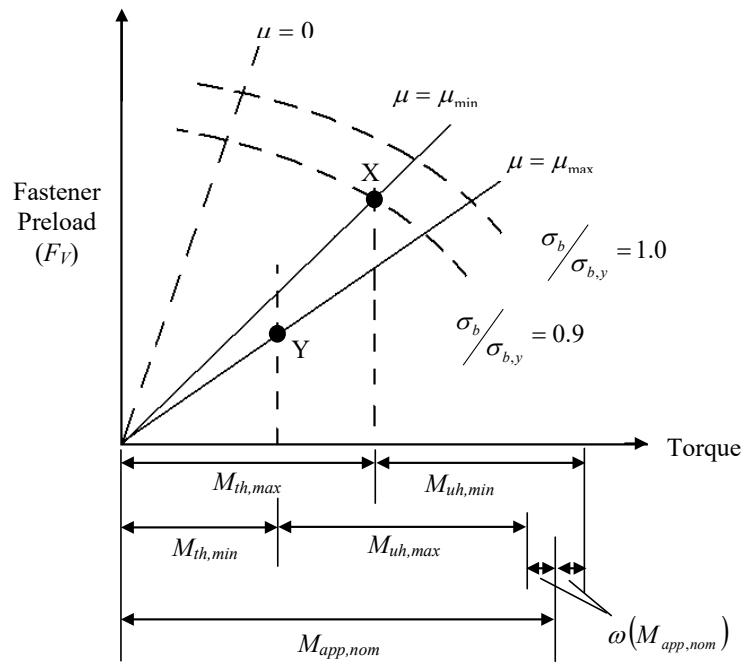


Figure 6-2 - Typical Preload vs. Applied Torque Graph

Regarding Figure 6-2 it is **important to note** that the applied torque is deterministic, i.e. the frictional torques acting on the fastener always add up to the externally applied torque, M_{app} . This means that the extreme preload conditions occur under the following conditions:

- Maximum preload - minimum thread friction and minimum under-head friction
- Minimum preload – maximum thread friction and maximum under-head friction

The joint in Figure 6-2 has no prevailing torque device. This is evidenced by the fact that the torque is zero when the preload is zero. Including a prevailing torque element shifts the curves to the right of this graph.

6.3.5 Forces Induced by Thermal Fluctuation

6.3.5.1 Overview

During thermal fluctuations the preload changes due to differing thermal expansion coefficients of the fastener and flange material. Also, the modulus of elasticity of the materials can be temperature sensitive.

The thermal expansion coefficient relates the elongation $f_{\Delta T}$ of an individual item with the length L , to a temperature difference ΔT according to,

$$f_{\Delta T} = \alpha L \Delta T \quad [6.3.19]$$

where α is the item's coefficient of thermal expansion and $\Delta T = T_{working} - T_{reference}$.

Assuming clamped parts made from a single material type, the respective elongations of the fastener and clamped parts are,

$$f_{\Delta T,b} = \alpha_b L_j \Delta T, \text{ and} \quad [6.3.20]$$

$$f_{\Delta T,c} = \alpha_c L_j \Delta T \quad [6.3.21]$$

where L_j is the joint length (equal to the combined thickness of all clamped parts), and α_b α_c are the coefficients of thermal expansion of the fastener and clamped parts respectively.

Based on the above equations, it can be shown that the thermally induced load (in the fastener) is given by,

$$F_{\Delta T,b} = \frac{L_j (\alpha_c - \alpha_b) \Delta T}{\delta_b + \delta_c} \quad [6.3.22]$$

Note that this formula assumes that the Young modulus is not varying with temperature and dT for bolt and parts are identical.

The extreme values of the thermally induced force are denoted $F_{\Delta T^+}$ and $F_{\Delta T^-}$, and these are given by the higher and lower results of,

$$F_{\Delta T^+,b} = \frac{L_j (\alpha_c - \alpha_b) \Delta T_{max}}{\delta_b + \delta_c} \text{ and} \quad [6.3.23]$$

$$F_{\Delta T^-,b} = \frac{L_j (\alpha_c - \alpha_b) \Delta T_{min}}{\delta_b + \delta_c} \quad [6.3.24]$$

where the temperature differentials are given by,

$$\Delta T_{min} = T_{working,min} - T_{reference} \quad [6.3.25]$$

$$\Delta T_{max} = T_{working,max} - T_{reference} \quad [6.3.26]$$

6.3.5.2 Clamped Parts made from Multiple Material Types

If the clamped parts have multiple material types, it is important to use a more general form of Equation [6.3.23] to account for the differing thermal expansion coefficients,

$$f_{\Delta T,c} = \left(\sum_{i=1}^m \alpha_{c,i} L_{c,i} \right) \Delta T \quad [6.3.27]$$

where $\alpha_{c,i}$ is the thermal expansion coefficient of the i 'th clamped part, $L_{c,i}$ is the length of the i 'th clamped part and m is the total number of clamped parts.

It can be shown that this equation leads to the following equation for the thermally induced load in the fastener,

$$F_{\Delta T} = \frac{\alpha_b L_j - (\sum_{i=1}^m \alpha_{c,i} L_{c,i})}{\delta_b + \delta_c} \Delta T \quad [6.3.28]$$

6.3.5.3 Temperature Dependent Modulus of Elasticity

In some cases it can be necessary to consider the variation of the modulus of elasticity with changes in temperature. When it is important to take into account this dependency, the thermally induced load can be calculated by the following equation that assumes a linear variation of E with temperature:

$$F_{\Delta T} = F_{V,T_0} \left(\frac{\delta_b - \delta_c}{\delta_b \frac{E_{b,T_0}}{E_{b,T_W}} + \delta_c \frac{E_{c,T_0}}{E_{c,T_W}}} - 1 \right) + \frac{L_j (\alpha_c \Delta T_c - \alpha_b \Delta T_b)}{\left(\delta_b \frac{E_{b,T_0}}{E_{b,T_W}} + \delta_c \frac{E_{c,T_0}}{E_{c,T_W}} \right)} \quad [6.3.29]$$

where; E_{b,T_0} and E_{b,T_W} are the moduli of elasticity of the fastener at the reference temperature and working temperature respectively, and E_{c,T_0} and E_{c,T_W} are the moduli of elasticity of the clamped parts at the reference temperature and working temperature respectively, and δ_b and δ_c are the compliances of the fastener and clamped parts respectively (see Section 7).

6.4 Mechanisms of Preload Loss

6.4.1 Overview

There are five mechanisms that cause relaxation preload loss in bolted joints:

- a. Embedding
- b. Fastener Group Interactions
- c. Gasket Creep
- d. Metallic Creep
- e. Tensional Relaxation

It is important that the user is aware of the possibilities of such preload reductions and estimations of their magnitude are considered in the design calculations. It is also important to note that vibration loosening, which can cause relaxation, is outside of the scope of this section and stress relaxation, usually due to a combination of stress and high temperature, is not applicable.

Creep is a significant factor when the temperature exceeds approximately 50% of the recrystallisation temperature of the respective material.

In addition to the five mechanisms listed above, preload loss can also occur due to localised plastic deformations in the fastener, if it is subjected to repeated loadings above material yield. This effect is further explained in Section 7.13.

6.4.2 Embedding

6.4.2.1 Overview

When new fasteners are first tightened, see Figure 6-3, the male and female threads, the under-head and under-nut surfaces and the clamped parts interfaces contact each other only on microscopically small high spots, where the surface "asperities" touch, as illustrated in Figure 6-4. The material at these high spots is overloaded, well past their yield point, during initial tightening and subsequently creeps until a large enough area of the available contact surface has been engaged to stabilize the process.

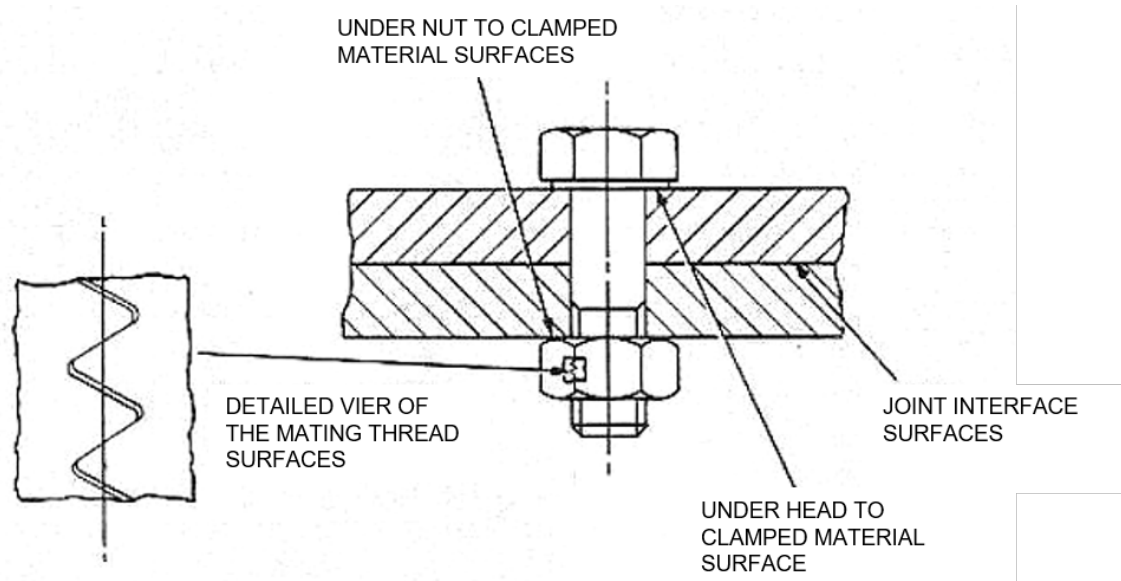


Figure 6-3 - Fastener Faying Surfaces

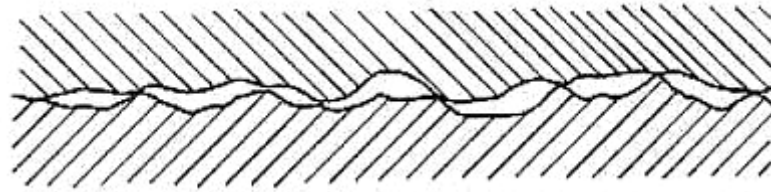


Figure 6-4 - Microscopic View of Surface Asperities Initially in Contact

In addition, plastic flow often occurs at the highest stressed points such as in thread roots, at the first engaged thread in the nut, or at other stress concentrations caused by imperfect manufacture (e.g. errors in squareness, flatness, concentricity, etc.).

These relatively short-term relaxation effects are known as "embedding". After tightening the rate of relaxation is a maximum, reducing exponentially, usually over the first minutes, to a constant very low rate of creep as illustrated in Figure 6-5. Typically embedding accounts for only a few percent loss of initial preload, however 5 to 10% preload loss is not uncommon, and maximums of 25% for torque tightening and 40% for hydraulic tensioning have been recorded.

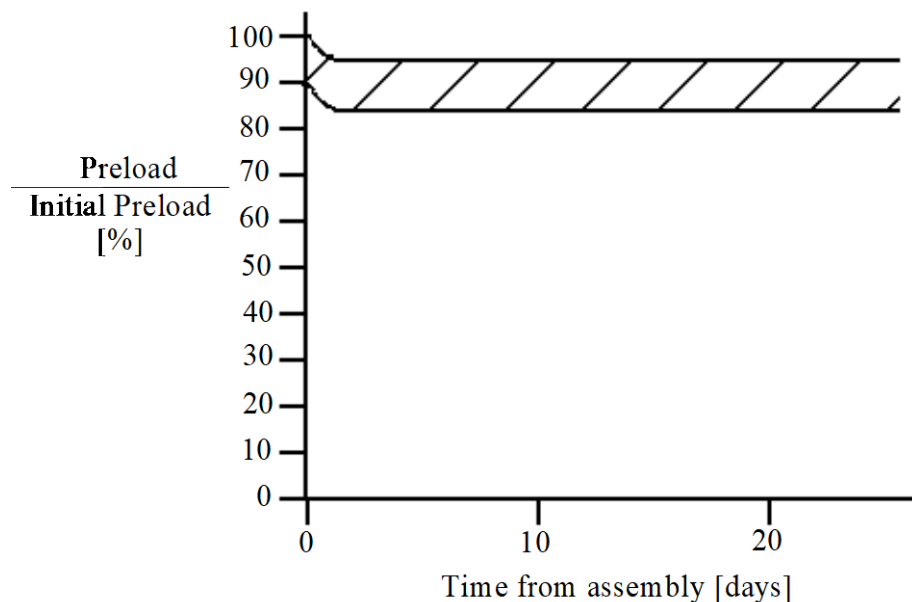


Figure 6-5 - Embedding Preload Decay

The preload loss F_Z to be put in Equation [6.3.15] depends on the plastic deformation f_Z of the joint caused by embedding. The following relationships apply,

$$\frac{F_Z}{F_V} = \frac{f_Z}{f_V} = \frac{f_Z}{f_{b,V} + f_{c,V}} = \frac{f_Z}{(\delta_b + \delta_c)F_V} \quad [6.4.1]$$

where; $f_{b,V}$ is the elongation of the fastener due to the preload and $f_{c,V}$ is the elongation of the flanges under preload, and δ_b and δ_c are the compliances of the fasteners and the clamped parts respectively (see Sections 7.4 and 7.7).

Thus it follows that,

$$F_Z = \frac{f_Z}{(\delta_b + \delta_c)} \quad [6.4.2]$$

The value of f_z depends on the surface roughness, the number of interstices in the joint and the material type. For example, using aluminium for the female thread can double the value of f_z compared with that of steel.

For uncritical cases a value of 5% of the preload can be used for calculation purposes, i.e.:

$$F_z = 0.05F_v \quad [6.4.3]$$

Otherwise it is important that the appropriate preload loss is determined by experiment. If no experimental data can be gained, Table 6-3 can be used to find approximate values. This table can only be used if the temperatures are below 50% of the recrystallisation temperatures.

Table 6-3 - Approximate values for plastic deformation caused by embedding

Average Surface Roughness, Rz (as per Ref. 7.3)	Type of External Load Applied to Joint	Standard Values for Embedding [μm]		
		In the thread	Per under-head or under-nut interface	Per inter-flange interstice
< 10 μm	Axial	3	2,5	1,5
	Shear	3	3	2
10 μm < x < 40 μm	Axial	3	3	2
	Shear	3	4,5	2,5
40 μm < x < 160 μm	Axial	3	4	3
	Shear	3	6,5	3,5

6.4.2.2 Tightening Methods

The asperities of surfaces subjected to frictional sliding during assembly, such as during conventional torque tightening, tend to shear and flatten thereby producing more embedding during assembly and leaving less to take place after tightening. In cases where embedding becomes critical (e.g. galling due to excessive friction resulting in localized welding), it is recommended to consider tightening methods that do not induce frictional sliding (e.g. hydraulic tensioning).

6.4.2.3 Retightening

The magnitude of embedding preload loss can be greatly reduced in critical cases by torque tightening, loosening and retightening several times. However, it is important to give attention to the reduction of self-locking torque due to multiple tightening cycles (see Section 12.7.3).

6.4.2.4 Hard Clamped Material

It is also an advantage, where possible, to use flanges made from harder materials or washers that resist embedding.

6.4.2.5 Controlled Thread Dimensions

To minimise preload loss in the thread, it is important to use bolts with the tightest tolerance class of thread that is available. For example Class 3 is preferred to Class 2 as are root radius controlled "J" class threads to standard threads, and it is important to use rolled threads in preference to cut threads. The use of fasteners with cut machined threads is normally subject to approval.

6.4.2.6 Conical Components

It is important to avoid conical joint mating surfaces as illustrated in Figure 6-6. For these joint configurations relaxation perpendicular to the conical surface (due to embedding) results in a far greater relaxation in the direction of the fastener axis.

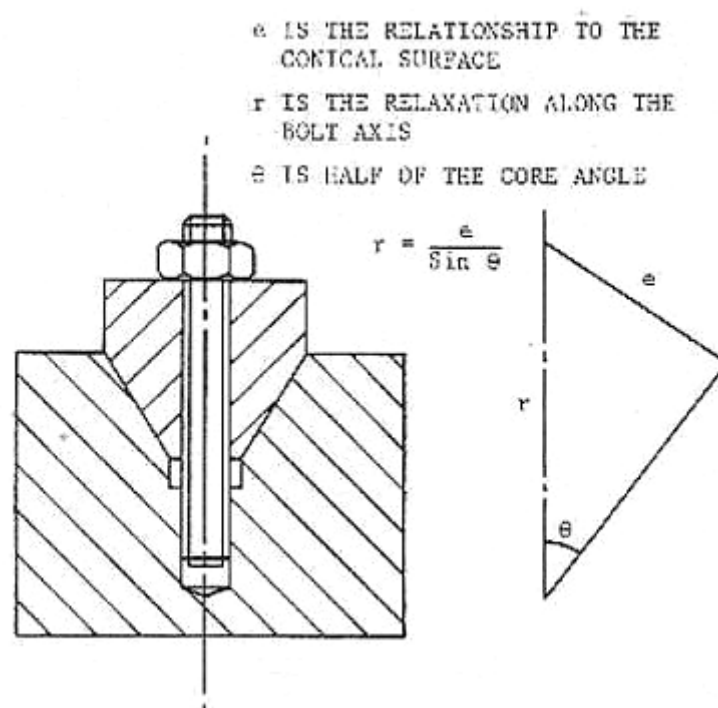


Figure 6-6 - Joint with Conical Mating Surfaces

6.4.2.7 Component Stiffness

It is important that long thin compliant fasteners are used in preference to short, stubby stiff fasteners. The total amount of embedding is the same for both for a given preload but for the compliant fastener the stiffness is less and hence a smaller preload loss occurs (see Figure 6-7). Similarly Belleville washers (conical spring washers as shown in Figure 6-8) can be used to increase the compliance of the clamped parts and hence reduce the effect of embedding.

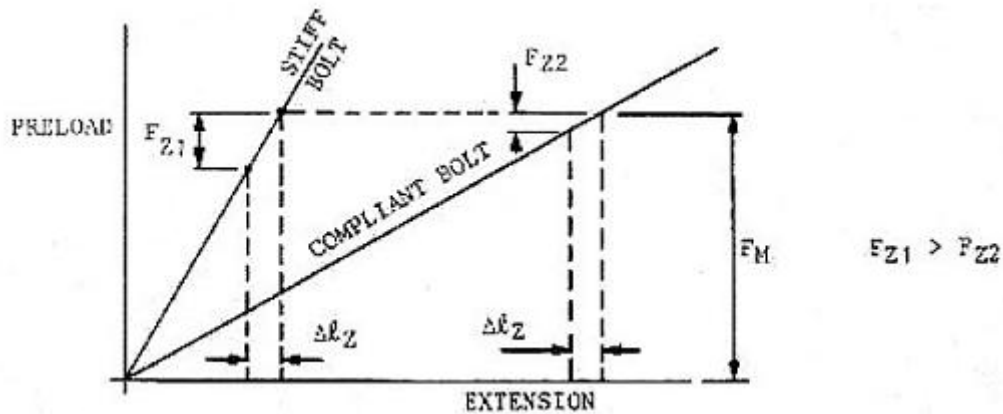


Figure 6-7 - Effect of Fastener Stiffness on Preload Loss Due to Embedding

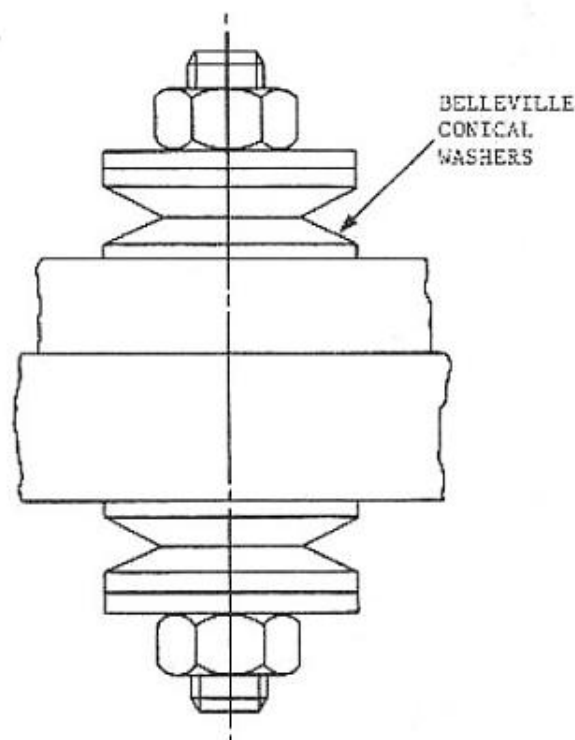


Figure 6-8 - Increasing Joint Compliance Using Belleville Washers

6.4.2.8 Bearing Strength

Relaxation occurs by major material plastic flow if the bearing surfaces are not large enough or the applied stresses are not distributed properly.

It is important to ensure in the design, manufacture and quality control checking that:

- The under head radius does not foul the edge of the clamped parts chamfer, which can result in a very small contact area leading to exaggerated embedding with a corresponding preload loss.
- Conversely, the chamfer is not so great that too small an under head bearing area results and the bolt head embeds into the clamped material.
- Slotted holes, which can greatly reduce the bearing area under the head or nut, are avoided.

6.4.2.9 Thread Engagement

The minimum acceptable thread engagement of high strength steel or titanium fastener is 0,8 times the nominal diameter of the fastener. It is important to use at least $1,5d$ thread engagement for such fastener used in aluminium tapped holes, even if wire thread inserts (e.g. helicoils) are used.

6.4.2.10 Lubrication Migration

Some lubricants can gradually migrate from the fastener and joint contacting surfaces causing a small amount of relaxation preload loss.

6.4.2.11 Surface Roughness

From the initial discussion of this section it is evident that if surface roughness is minimised by grinding or polishing the relaxation effects of embedding can be reduced, but not eliminated.

Another obvious point is that the total amount of embedding is related to the number of joint interfaces.

6.4.3 Fastener Group Interaction

6.4.3.1 Overview

Some short-term relaxation problems evolve due to interactions between fasteners in groups.

6.4.3.2 Elastic Interaction

When the first fastener in a group is tightened, it is elongated and the joint in its vicinity is compressed. When an adjacent fastener is tightened, the joint in the vicinity of the first fastener can be further compressed causing relaxation of that fastener. The amount of interaction depends on such factors as clamped parts stiffness, the spacing of fasteners and whether a gasket is used. Preload losses in the order of 50% to 100% have been recorded (see Reference 6.3). An example of this problem is given in Figure 6-9 and Figure 6-10 in which eight fasteners on the same flange are tightened in sequence. Figure 6-9 shows the "saw-tooth" effect of one tightening pass as the last fastener tightened in a particular quadrant end up with a greater preload than those immediately adjacent to it. However, after four passes Figure 6-10 illustrates that the final relaxation pattern is not a regular saw tooth. At each pass the joint is tightened by successively higher, but uniform, torques to the fasteners.

This problem can be partly overcome by giving higher initial preloads to those fasteners expected to relax the most, thus producing a more uniform fastener load after relaxation. The highest accuracy is achieved by monitoring preload tests, using a technique such as ultrasonic, and applying small amounts of extra torque to the fasteners with insufficient preload.

6.4.3.3 Bent Flanges

If flanges are soft, warped or bent, tightening one fastener can cause relaxation (or additional stress) in other fasteners. A precautionary final torque pass is always made when assembling joints with multiple fasteners.

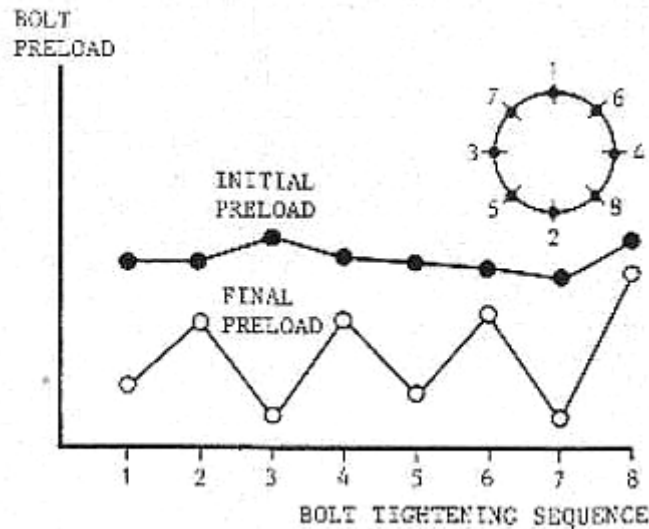


Figure 6-9 - Initial and Final Preload of a Typical Flange Joint for the First Tightening Pass.

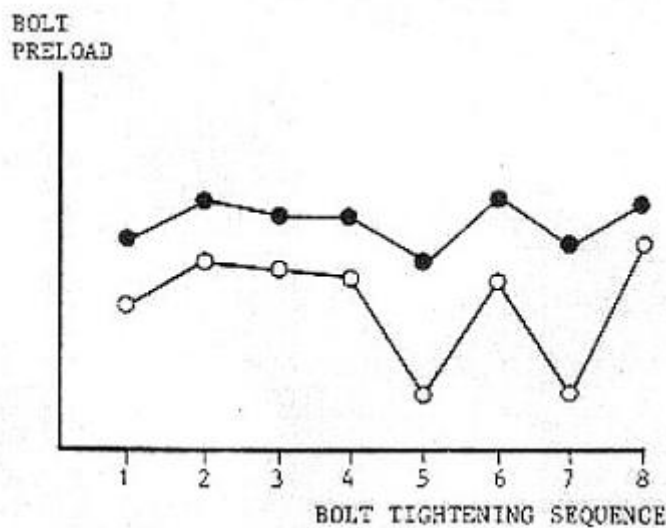


Figure 6-10 - Initial and Final Preload Levels after Four Tightening Passes.

6.4.3.4 Motorized Tightening Speed and Interaction Effects

If flanges with a large number of fasteners are tightened simultaneously using a motorized technique there is a great danger of high preload loss due to embedding. A fastener tightened alone can see higher stress than if tightened in a group, where all the bolts share the load evenly as it develops. Also this tightening process is usually carried out at relatively high speeds. It is therefore recommended that the torque is applied in a series of increments and that time is allowed between each pass for embedding to take place. This recommendation is particularly relevant where gaskets are used.

6.4.4 Gaskets

Outgassing constraints restrict the selection of gasket materials that are suitable for space applications. It is usually preferred, where possible, to eliminate gaskets and rely on metal-to-metal sealing of flanges. Where this cannot be achieved a preformed gasket from fully cured silicone rubber or a soft metal such as lead or a soft aluminium alloy is used to form the seal.

Gasket creep is another form of relatively short-term relaxation. Having a gasket in a joint ensures large amounts of relaxation compared to that expected with normal embedding. In fact, a gasket is deliberately designed to deform plastically to some extent in order to plug the paths through which the contained fluid or gas otherwise escape. Like any plastic material it **can** creep when first subjected to high surface pressures. The amount of creep is difficult to predict since it is dependent on many factors including the level of compressive load generated by the fasteners.

The following recommendations are given for design gasket joints:

- To obtain the most uniform pull down, tighten flange bolts in a cross star pattern or, if the cost is justified, tighten several bolts simultaneously.
- Use the most accurate method of tightening available.
- Use the highest design aim preload possible without damaging the gasket or joint member.
- If designing pressure vessels or pipe connections follow the relevant design codes of practices such as ASME VIII division 1 and BS 5500.

The non-linear characteristics of gaskets can significantly influence the clamped parts compliance. Section 7.6.5 contains an explanation of the compliance calculations for joints with gaskets.

6.4.5 Metallic Creep

Very high temperatures, which **can** cause relaxation due to a reduction of material strength, do not normally occur in space applications. However, differential thermal expansion **can** directly give preload loss and can also cause relaxation due to over stressing. Such thermo-elastic effects are discussed in Section 6.3.5.

6.4.6 Washers

Washers are used for a variety of reasons. Plain washers are used to spread the load into the clamped parts, to allow the use of oversized holes (**making sure to use thick washers to avoid excessive bending**), to prevent the fastener head or nut damaging the surface of the clamped parts, or to give controlled surface conditions at the under-head or under-nut interfaces. Many other types of special purpose washers exist such as insulating washers for thermal or electrical reasons, conical spring washers to minimise the effect of embedding, the dimpled or two piece crushable washers for preload detection, the straining face washer for use as a miniature load cell, shakeproof washers to prevent rotary loosening and toothed shear washers for slip prevention, etc. It is important to consider the compliance and relaxation properties of the particular washer type.

It is important that the analysis of clamped parts compliance (Section 7.7) takes into account compliance of the washers. Generally, the washer compliance can be calculated assuming that it behaves like a flange. If the washer is soft, the analysis can be done using the non-linear theory for gaskets (see Section 7.6.5).

Whenever washers are used, embedding (Section 6.4.2) is increased since there is at least one more interstice region with crushable surface asperities. For this reason, it is recommended to use hard washers whenever possible to minimise the embedding losses.

6.4.7 Torsional Relaxation

During the torque tightening process torsional stress is developed in the fastener in addition to the axial stress, which is necessary for the preload. The torsional stress is subject to varying amounts of relaxation, and it is generally believed to be the first stress to be relieved by relaxation. In most instances it disappears immediately when the wrench is removed. Also, it has been shown that the relaxation of torsional stress can induce extra tensile stress (see Reference 6.4). This self-tightening phenomenon, illustrated in Figure 6-11 is invariably masked by the greater axial embedding relaxation (see Reference 6.3). The amount of torsional stress primarily depends on the magnitude of the thread friction torque and the amount of relaxation. Whether relaxation is by head rotation or self-tightening depends largely on the under head friction conditions compared with those of the thread friction conditions.

Note that, despite this handbook recommends to consider total relaxation of the shear stress induced during installation, in special cases (i.e. large torque and high friction coefficients) a remaining torsional stress (typical value 50 %) needs to be considered.

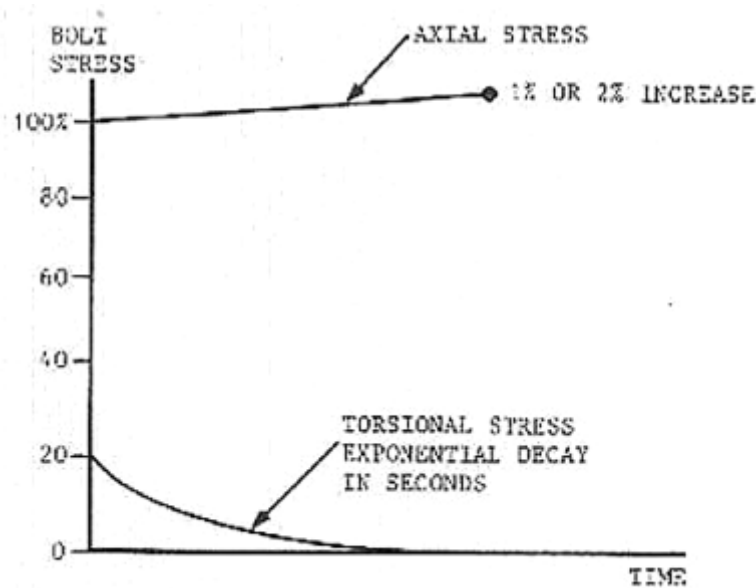


Figure 6-11 - Self Tightening by Torsional Relaxation

6.5 Margin of Safety on Tightening

When specifying the torque tightening method for fastening, it is important to check the ability of the fastener to sustain the torquing. The stress occurring during the tightening process is composed by a tension caused by the increasing preload and a shear stress caused by the application of the torque. These two stresses are combined by the shape deformation energy hypothesis according to the Von Mises equation,

$$\sigma_{v.m.} = \sqrt{\sigma_{V,max}^2 + 3\tau_{max}^2} \quad [6.5.1]$$

where $\sigma_{V,max}$ is the maximum axial stress in the fastener due to preloading, and τ_{max} is the maximum shear stress due to remaining torsion in the fastener.

The total torque applied to the fastener during torque application M_{app} is reacted by two moments; the moment of friction forces in the thread, and the moment of friction forces under the bolt head or nut

Due to equilibrium of moments, the maximum shear stress within the fastener's shank (or the adjacent non-engaged thread) is related to the moments due to under-head friction and the externally applied torque by,

$$\tau_{max} = \frac{M_{app,max} - M_{uh,min}}{W_p} \quad [6.5.2]$$

where the minimum under-head frictional torque is given by,

$$M_{uh,min} = \frac{d_{uh}}{2} (F_{V,max} - F_{\Delta T^+}) \mu_{uh,min} \frac{1}{\sin(\lambda/2)} \quad [6.5.3]$$

and the polar section modulus is,

$$W_p = \frac{\pi d_0^3}{16} \quad [6.5.4]$$

It is important to note that the prevailing torque makes a significant contribution to the torsional stress in the fastener shank. Equation [6.5.2] includes this effect via the $M_{app,max}$ term. To minimise preload scatter it is recommended to measure (and compensate for) the prevailing torque each time a fastener is tightened.

After the shear stress in the fastener exceeds its yield point a state of total plastic deformation is reached, whereby the torsional stresses through the cross section are constant. To include this effect, the polar section modulus is corrected to,

$$W_p' = \frac{\pi d_0^3}{12} \quad [6.5.5]$$

From Equations [6.3.5] and [6.3.22] the maximum pretension stress is given by,

$$\sigma_{V,max} = \frac{F_{V,max} - F_{\Delta T^+}}{A_0} \quad [6.5.6]$$

The Margins of Safety on tightening are:

$$\text{Yield:} \quad MoS_{ii,y} = \frac{\sigma_y}{\sigma_{v.m.}} - 1 \quad [6.5.7]$$

$$\text{Ultimate:} \quad MoS_{ii,ult} = \frac{\sigma_{ult}}{\sigma_{v.m.}} - 1 \quad [6.5.8]$$

No factors of safety are used in Equations [6.5.7] and [6.5.8] since all uncertainty sources are already included in $F_{V,max}$.

If the MoS for yield is positive, the MoS for the ultimate is always positive. Therefore, the ultimate MoS in Equation [6.5.8] is not normally needed. One possible exception to this is yield controlled tightening methods (see Section 12.3).

6.6 Worked Example

No example exists specifically for the theory of this section. However, the example in the Section 7 does involve preload calculations.

6.7 References

6.1	NASA-STD-5020, December 2, 2012	Requirements for Threaded Fastening systems in Spaceflight Hardware
6.2	DIN 4768:1990	Determination of values of surface roughness parameters RA, RZ, RMAX using Electrical Contact (Stylus) Instruments Concepts and Measuring Conditions.
6.3	J.H. Bickford	An Introduction to the Design and Behaviour of Bolted Joints, Marcel Dekker, 1981.
6.4	FISHER. J, STRUIK. J.H.A.	Guide to Design Criteria for Bolted and Riveted Joints, John Wiley & Sons, 1974.

Concentric Axially Loaded Joints

7.1 Overview

This section describes the recommended analysis procedure joints in which the threaded fastener/s are subjected to a pure axial load. The analysis methods presented in this section are appropriate for joints if all the following criteria are met:

- The axis of the applied loads passes through the fastener axis (or fastener group centroid)
- The flanges are symmetric about the axis of the applied load.
- The flanges are stiff enough to not develop a “prying” effect (see Section 8.1.2)

If any of the above criteria are not met, **it is important to apply** the more general analysis methods for eccentrically axially loaded joints presented in Section 8.

7.2 Joint Stiffness

Consider the joint illustrated in Figure 7-1. This comprises a fastener, nut and two flanges. In the absence of externally applied loads the fastener preload is equal and opposite to the clamping load (the compression force acting between the clamped parts). During service the joint’s dimensions **can** vary due to the applied load and the preload. For a given combination of these loads, the joint’s instantaneous length, L_j , is related to its constituent parts according to,

$$L_{b,free} + \Delta L_b = L_j \quad [7.2.1]$$

$$L_{c,free} - \Delta L_c = L_j \quad [7.2.2]$$

where; ΔL_b and ΔL_c are the extension of the fastener and the compression of the clamped parts respectively under the action of the applied loads, and $L_{b,free}$ and $L_{c,free}$ are the free (i.e. unloaded) lengths of the fastener and clamped parts respectively.

For a preloaded joint the free length of the fastener is less than that of the flanges since the fastener stretches while the flanges compress.

Combining and rearranging [7.2.1] and [7.2.2] gives,

$$L_{b,free} = L_{c,free} - \Delta L_c - \Delta L_b \quad [7.2.3]$$

However, since ΔL_b and ΔL_c are functions of the preload, the use of this relationship needs an iterative solution. Therefore, it is usual to use the approximation,

$$L_{b,free} \approx L_{c,free} \quad [7.2.4]$$

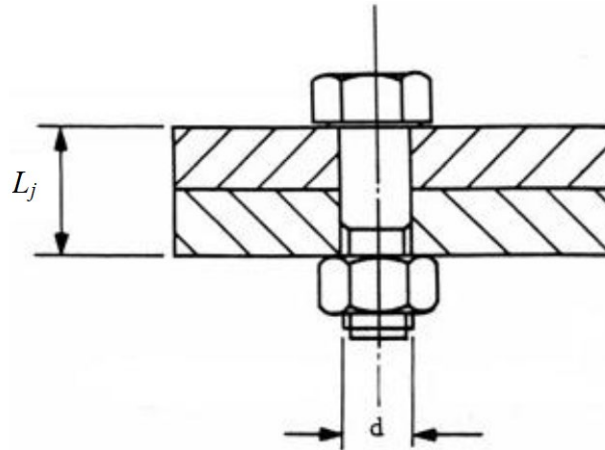


Figure 7-1 - Typical Joint Components

which leads to a simple relation between the elongations of the fastener and clamped parts,

$$\Delta L_c = -\Delta L_b \quad [7.2.5]$$

7.3 The Joint Diagram

7.3.1 Overview

The deformations within a joint can be shown in the joint diagram. Figure 7-2 shows the elongation of the fastener, $\Delta L_{b,V}$, due to the preload, F_V , and Figure 7-3 shows the corresponding deflection of the clamped parts.

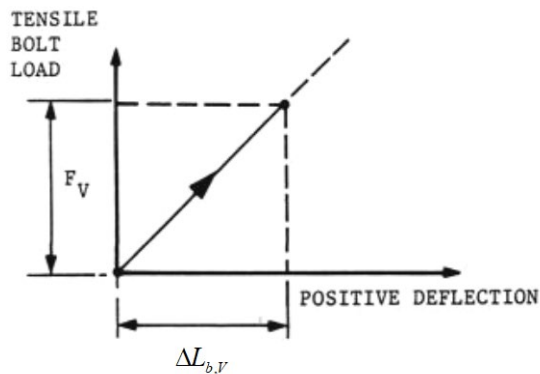


Figure 7-2- Fastener Stiffness

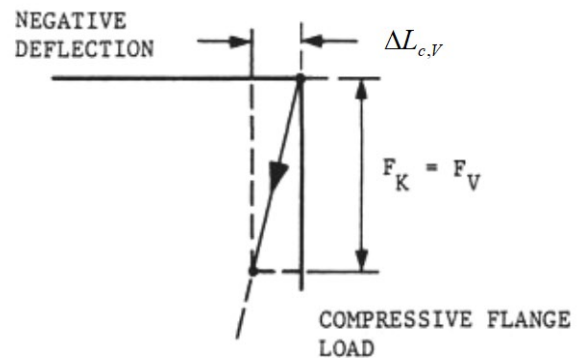


Figure 7-3 - Clamped Parts Stiffness

In the joint diagram classical analysis the stiffness plots for the two components (fastener and flanges) are combined by inverting Figure 7-3 (in the horizontal axis) and moving its origin such that the preload point is common to both curves until the final preload F_V is reached (Reference 7.2).

Figure 7-4 [6.2.3a, b & c)] show the preload F_V increasing during the tightening process.

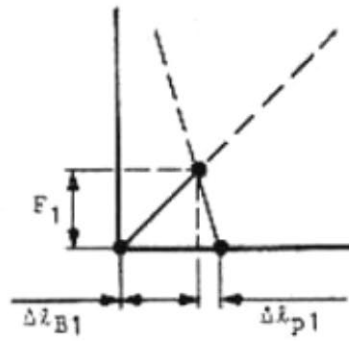


Figure 6.2.3a

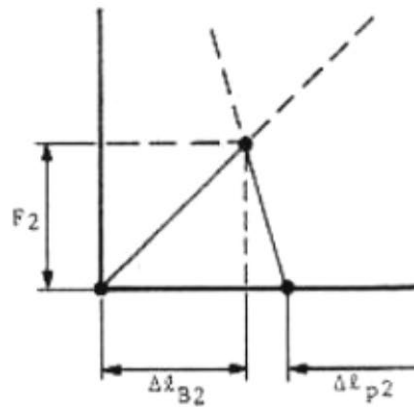


Figure 6.2.3b

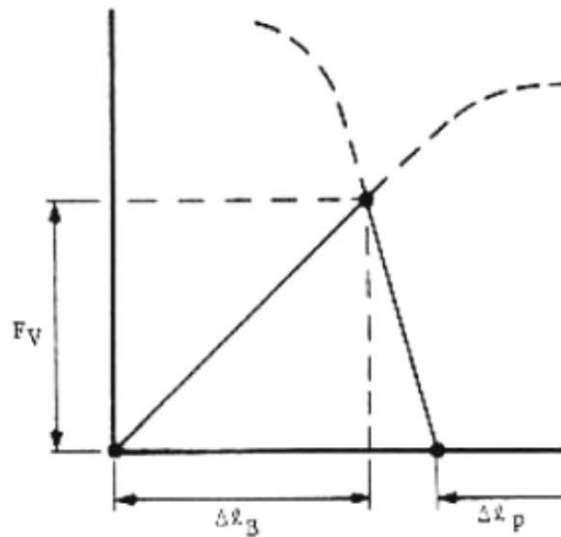


Figure 6.2.3c

Figure 7-4 - Growth of the Joint Diagram Illustrating the Tightening Process

Applying an external axial load, F_A , on the outer surfaces of the joint's flanges, as shown in Figure 7-5, increases the fastener's tension and reduces the clamped parts' compressive loading. This is reflected by the joint diagram in Figure 7-6 with the external force F_A represented by a vertical line. The load increments experienced by the fastener and clamped parts when the joint is subjected to F_A are given by $\Delta F_{b,A}$ and $\Delta F_{c,A}$ respectively.

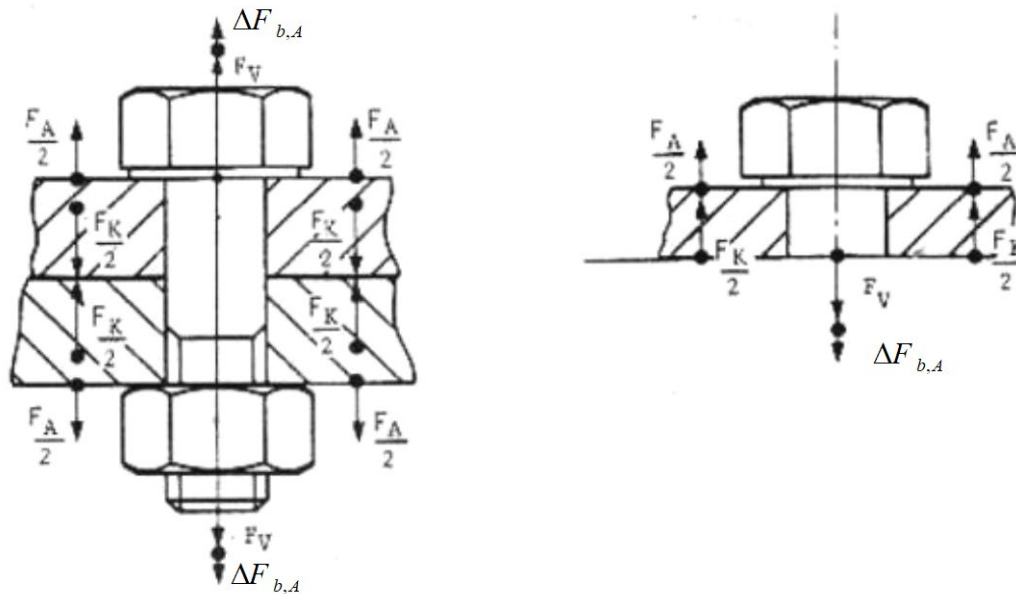


Figure 7-5 – Application of external axial load

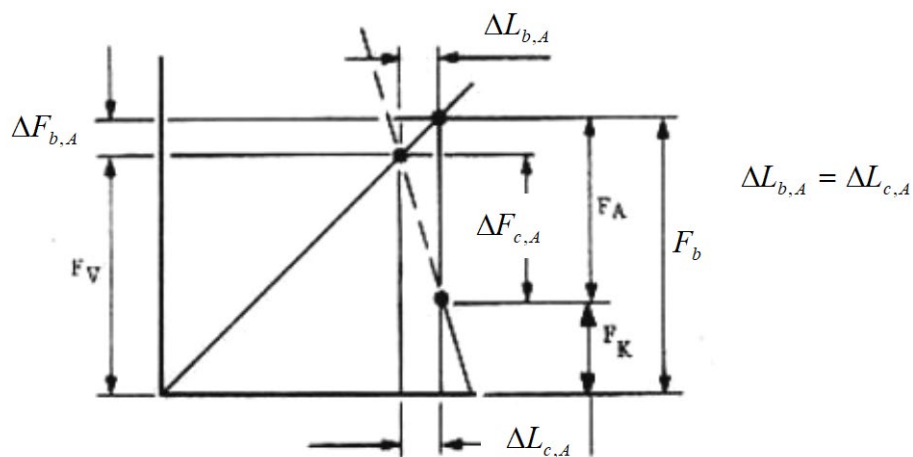


Figure 7-6 - Joint Diagram Showing the Effect of an External Axial Load

Figure 7-6 shows that if F_A is increased beyond a certain point, $F_K = 0$. This corresponds to the point at which the clamped parts are completely relieved of their preload and gapping at the interface between the flanges occurs, as illustrated in Figure 7-7.

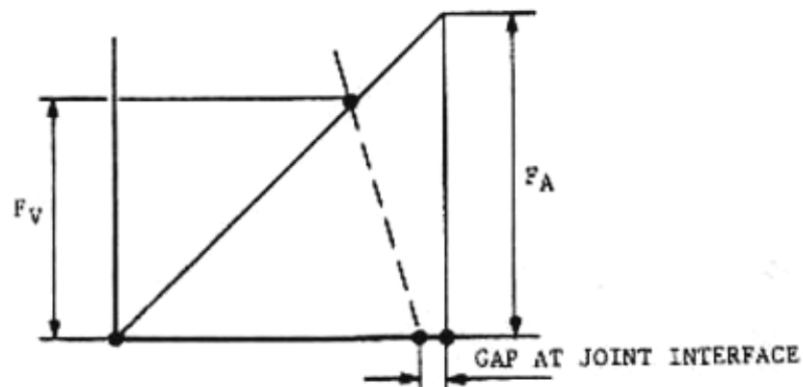


Figure 7-7 – External Load Causing Gapping

7.3.2 Compressive Loading

If the externally applied axial load on a preloaded joint is compressive, the resulting compression of the flanges and the reduction in bolt tension can be represented on a joint diagram as shown in Figure 7-8. All the equations that were derived for externally applied tensile loads are directly applicable for compressive loads, subject to the correct use of negative signs, (see Reference 7.3).

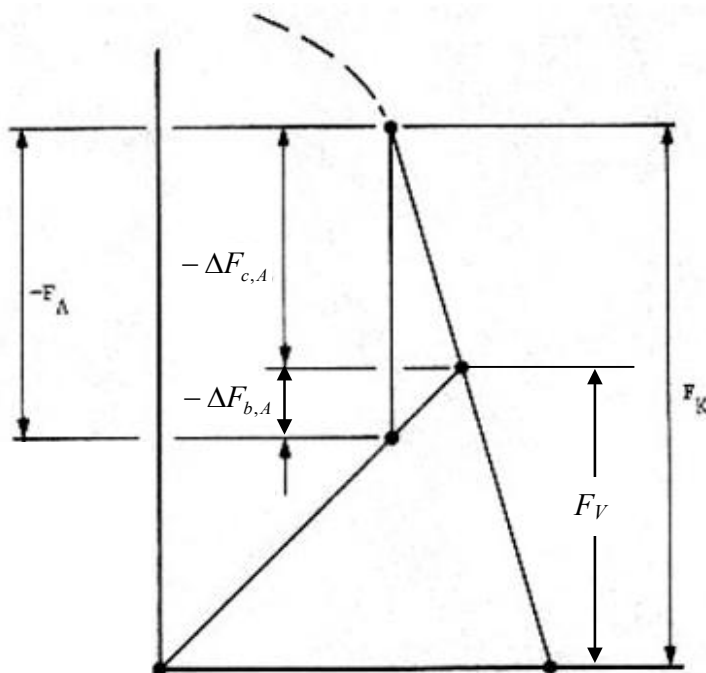


Figure 7-8 – Joint Diagram for Compressive Loading

7.4 The Force Ratio

The force ratio Φ is defined as the ratio of external load to the induced load increment seen by the fastener, and is given by,

$$\Phi = \frac{\Delta F_{b,A}}{F_A} \quad [7.4.1]$$

For certain joint configurations (such as joint type 2 in Figure 5-1) the external load's effective point of action is at the outer surface of the flanges. This is the situation that is shown in Figure 7-5. For such joints, the force ratio can be shown to depend on the relative stiffnesses (or compliances) of the fastener and the clamped parts,

$$\Phi = \frac{\Delta F_{b,A}}{F_A} = \frac{K_b}{K_c + K_b} = \frac{\delta_c}{\delta_c + \delta_b} \quad [7.4.2]$$

where K_b & K_c are the respective stiffnesses of the fastener and clamped parts, and δ_b & δ_c are the respective compliances of the fastener and clamped parts.

From Figure 7-6 it can be seen that,

$$F_A = \Delta F_{b,A} + \Delta F_{c,A} \quad [7.4.3]$$

therefore, using Equation [7.4.2],

$$F_A = \Phi F_A + \Delta F_{c,A} \quad [7.4.4]$$

Rearranging, the load reduction felt by the clamped parts due to the external load F_A is given by,

$$\Delta F_{c,A} = (1 - \Phi)F_A \quad [7.4.5]$$

Equations [7.4.2], [7.4.3], [7.4.4] and [7.4.5] are only valid for joints where the point of application of the external load is the outer surface of the flanges. In general, the external load is effectively applied at points located within the flanges. Therefore, the loading plane factor, n , is introduced into equation [7.4.2] resulting in,

$$\Phi_n = n \Phi = n \left(\frac{\delta_c}{\delta_c + \delta_b} \right) \quad [7.4.6]$$

Methods are presented in the following Sections for calculating the various parameters in Equation [7.4.6].

7.5 The Compliance of the Fastener

The fastener's load deflection relationship is given by,

$$F_b = K_b \Delta L_b = \frac{1}{\delta_b} \Delta L_b \quad [7.5.1]$$

where; F_b is the tensile load in the fastener shank, K_b is its stiffness, ΔL_b is its elongation and δ_b is its compliance.

In the general case of a fastener with varying shank diameters, such as Figure 7-9, the total elongation of the fastener is the sum of the elongations of its constituent segments (i.e. head, nut, and shank). In general, the different parts of the fastener have different local stiffness properties. Thus the total elongation can be written,

$$\Delta L_b = \sum \Delta L_i \quad [7.5.2]$$

where ΔL_i are the elongations of the constituent segments.

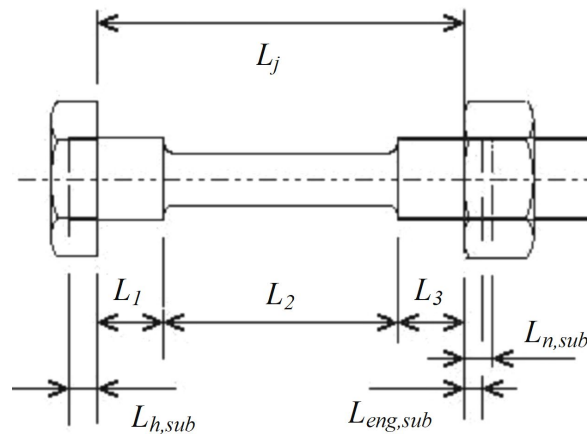


Figure 7-9 – Dimensioning of the Fastener for Compliance Calculations

Applying Hooke's law to each segment,

$$\Delta L_i = \frac{L_i F_b}{E_b A_i} \quad [7.5.3]$$

where; E_b is the Young's modulus of the fastener material and A_i is the local cross section of the segment.

Combining the above equations [7.5.2] and [7.5.3], the compliance of the fastener is then,

$$\delta_b = \frac{1}{K_b} = \frac{\Delta L_b}{F_b} = \frac{1}{E_b} \sum \frac{L_i}{A_i} \quad [7.5.4]$$

Expanding [7.5.4] and introducing substitution lengths for deformations in the head, the fastener's engaged region and the nut's engaged region gives,

$$\delta_b = \frac{1}{E_b} \left[\frac{L_{h,sub}}{A_{nom}} + \frac{L_{eng,sub}}{A_3} + \left(\frac{L_{sha,1}}{A_{sha,1}} + \frac{L_{sha,2}}{A_{sha,2}} + \dots + \frac{L_{sha,i}}{A_{sha,i}} \right) \right] + \frac{L_{n,sub}}{E_n A_{nom}} \quad [7.5.5]$$

where; $L_{h,sub}$, $L_{eng,sub}$ and $L_{n,sub}$ are the substitution lengths for deformations within the head, engaged shank and engaged nut or insert (see Table 7-1), A_{nom} is the fastener's nominal cross-sectional area, A_3 is the fasteners minor diameter area (see Figure 5-5), $A_{sha,i}$ is the effective cross-sectional area at the i 'th segment of the fastener's shank and $L_{sha,i}$ is the length of the i 'th segment of the fastener's shank.

In many cases when using Equation [7.5.5] only one segment of fastener's shank needs to be considered. However, if the fastener has varying shank diameters, **it is important to include** the length and effective stiffness area of each segment.

Table 7-1 shows typical substitution lengths for standardised fasteners, which can be used in Equation [7.5.5]. The table only includes values for typical hexagon heads, cylindrical heads and nuts. The same analysis method can be applied to other fastener heads and nuts, and **it is important to determine** the appropriate substitution lengths by experiment or analysis.

Table 7-1 - Typical Substitution Lengths for Commonly Used Fasteners
(data from Reference 7.3)

Part of Fastener	Parameter	Fastener/Joint Configuration	Typical Substitution Length
Head	$L_{h,sub}$	Hexagon head	$0,5 d$
		Cylindrical head	$0,4 d$
Locking device (nut or insert)	$L_{n,sub}$	Nut-Tightened	$0,4 d$
		Threaded hole	$0,33 d$
Engaged shank	$L_{eng,sub}$	Any	$0,5 d$

7.6 The Compliance of the Clamped Parts

7.6.1 Overview

The calculation of the compliance of the clamped parts, δ_c , is more complicated than that of the fastener due to the 3-dimensional state of stress state in the joint that is induced by the preload. The method presented here (based on Reference 7.3) neglects the compliance of the interstices, and therefore it is most accurate for joints with a small number of clamped parts. If needed (e.g. when many plates are clamped together), the compliance of the clamped parts can be determined by experiment or finite element analysis.

The compliance of the camped parts is calculated by the integral,

$$\delta_c = \frac{1}{E_c} \int_{z=0}^{z=L_c} \frac{dz}{A(z)} \quad [7.6.1]$$

where; $A(z)$ is the cross-sectional area of the assumed compression zone within the clamped parts (explained in Sections 7.6.2 to 7.6.4), z is the distance through the clamped parts, L_c is the length of the clamped parts, and E_c is the modulus of elasticity of the clamped parts.

When multiple materials are used in the clamped parts, **it is important to use** the more general form of Equation [7.6.1],

$$\delta_c = \int_{z=0}^{z=L_c} \frac{dz}{E_c(z) A(z)} \quad [7.6.2]$$

7.6.2 Compression Zone Configurations

7.6.2.1 Overview

The configuration of the compression zone depends on the geometry of the clamped parts. The following sections explain the possible configurations. Equations for calculating the compliance of the various configurations are given in Section 7.6.4.

7.6.2.2 Cylindrical Clamped Parts

Figure 7-10 shows the three possible compression zones (hatched) for cylindrical clamped parts. For clarity, the figure assumes that the flanges are compressed between infinitely stiff washers with under-head bearing diameter $D_{uh,brg}$. When the flanges are wider than the under-head bearing diameter, the compression zone spreads out. For the theory presented here, it is assumed that the compression zone spreads within a conical surface. In many cases the compliance of the washers is also significant. If so, it is important that are also treated as clamped parts.

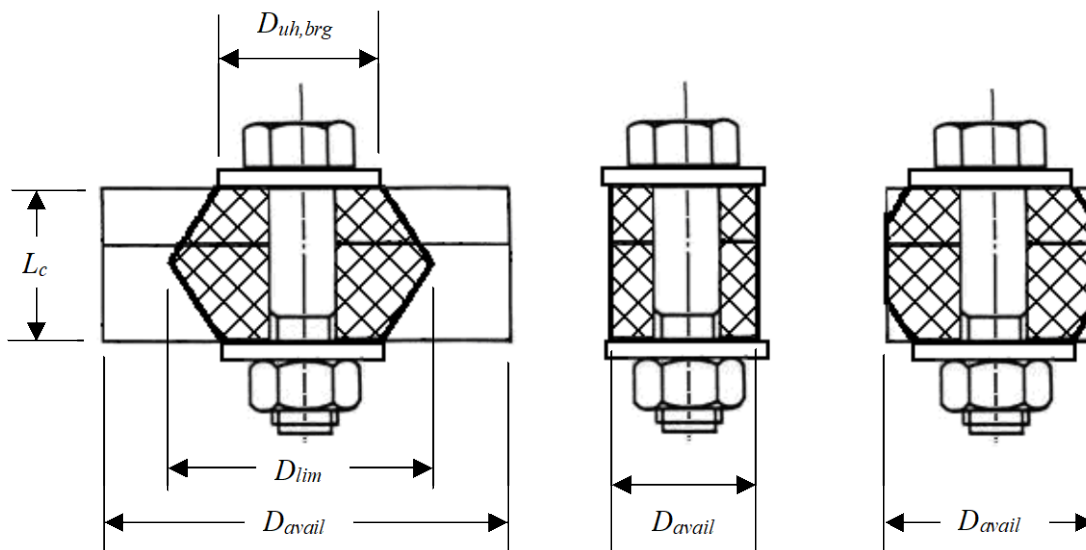


Figure 7-10 - Compression zones in cylindrical clamped parts

7.6.2.3 Fully Developed Compression Zone

The configuration on the left of Figure 7-10 has flanges that are sufficiently wide to allow full spreading of the compression zone to the limiting diameter, D_{lim} . In reality, the shape of the 3-dimensional zone of compression in an isotropic material is a paraboloid. However, the method approximates the compression zone as a pair of compression cones. The two cones are symmetric about the mid-point of the clamped parts length, L_c , (which does not necessarily correspond to the interstice between the flanges).

7.6.2.4 Compression Sleeve

The middle configuration of Figure 7-10 has narrow flanges that fit entirely within the underhead bearing diameter, i.e. $D_{avail} < D_{uh,brg}$. In this case, the compression zone is a 'sleeve' (a uniform compression cylinder).

7.6.2.5 Partially Developed Compression Zone

The configuration to the right of Figure 7-10 has flanges of intermediate edge clearances so a partial length sleeve of diameter D_{avail} approximates the compression zone, and two deformation cones are formed above and below the sleeve.

7.6.2.6 General Case of Non-Cylindrical Clamped Parts

In the general case with clamped parts that are not axially symmetric about the fastener's axis multiple edge distances are present (see Figure 7-11). For this type of joint, it is important to determine the configuration of the deformation zone by the minimum edge distance according to,

$$a_{i,min} = D_{avail,min} / 2. \quad [7.6.3]$$

Equation [7.6.3] results in a value of clamped parts compliance that is higher than reality, which can introduce significant (non-conservative) inaccuracies in the MoS. Section 7.6.2.9 discusses this issue in more detail.

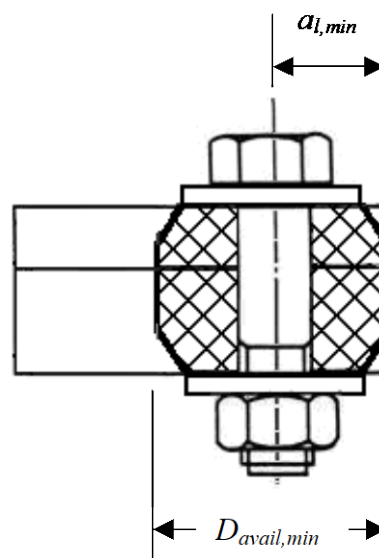


Figure 7-11 - The compression zone when multiple edge distances are present

7.6.2.7 The Compression Zone in Threaded Hole Joints

Unlike nut-tightened joints, threaded hole joints develop only one compression cone. This cone develops fully if the flange has an available diameter large enough to allow the cone to extend to the interstice of the threaded hole flange (see left of Figure 7-12).

When the compressed flange has insufficient diameter, the compression cone stops at the flange edge and a compression sleeve forms between the base of the compression cone and the interstice of the insert flange (see right of Figure 7-12).

The threaded hole flange does not contribute to the clamped parts compliance, although it is important to include in the calculation of the fastener compliance according to Table 7-1.

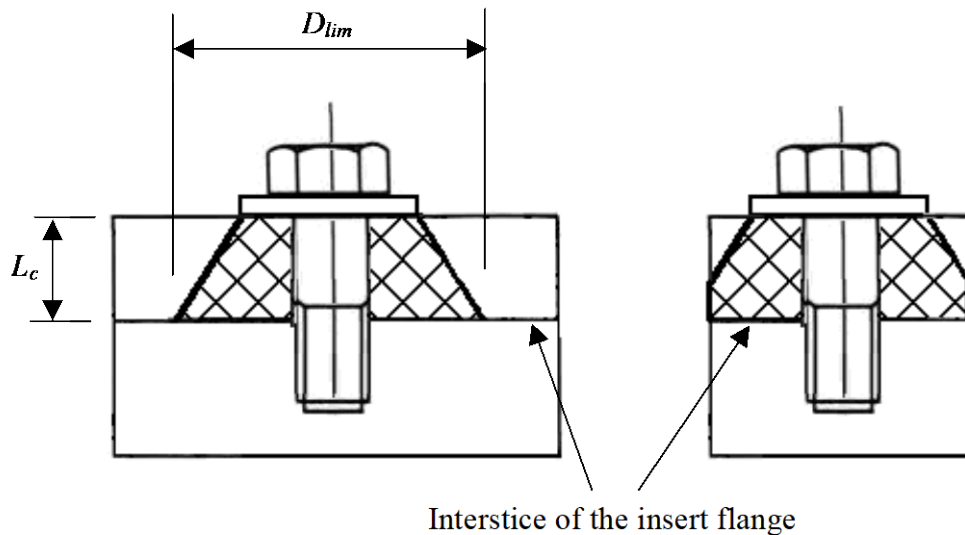


Figure 7-12- Approximation of the Compression Zone for Insert Joints

7.6.2.8 Interfering Compression Zones

When a joint has multiple fasteners, the available diameter of the deformation zone around each fastener is affected by the interference effect with its neighbour/s (see Figure 7-13). The result of this interference is a decreased compliance, relative to a similar joint without overlapping compression zones. This leads to a conservative estimate of the fasteners tensile loading, but a non-conservative estimate of the flange compression (see Section 7.6.2.9 below).

When calculating margins of safety that depend on flange compression (e.g. gapping, and slipping), it is conservative to neglect the overlapping compression zones when calculating the compliance of the clamped parts.

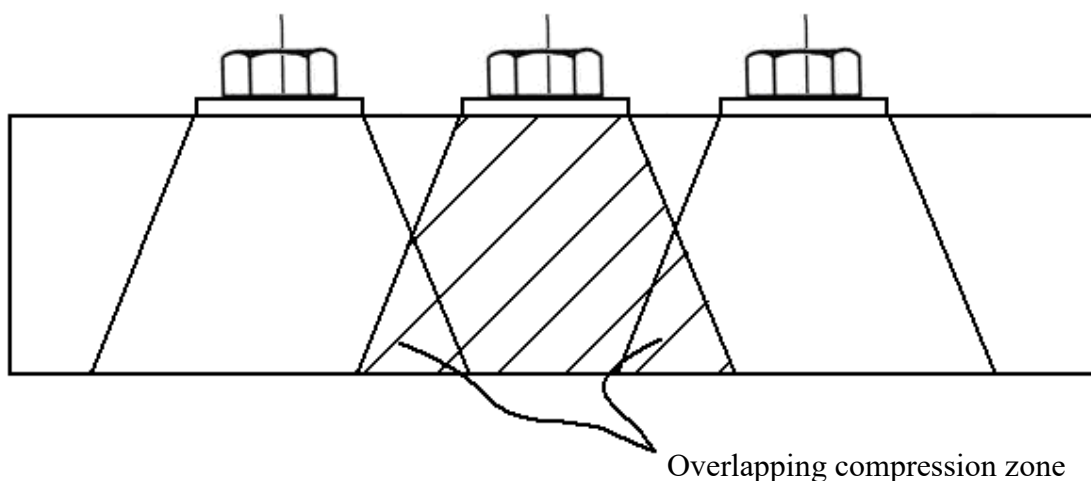


Figure 7-13 - The compression zone with multiple interacting fasteners

7.6.2.9 Influence of the Clamped Parts Compliance

Since the methods presented in this section for calculating the compliance of the clamped parts are subject to some approximations, it is worthwhile examining the effects of overestimating and underestimating this compliance.

Referring to Equation [7.4.6], overestimating the clamped parts compliance gives rise to an artificially high force ratio, Φ . This leads to an overestimate of the force increment experienced by the fastener, which is therefore conservative for the calculation of fastener tensile failure modes such as fastener shank failure or thread pull-out. However, it also leads to an underestimate for force the increment experienced by the clamped parts, which gives non-conservative for the flange performances related to separation, sealing, friction grip, crushing, etc.

In the opposite case of the clamped parts compliance being underestimated, the force ratio is artificially low. This leads to non-conservative values for the fastener and thread strengths.

Accordingly, it is recommended that more detailed analysis or testing is undertaken in cases where the clamped parts compliance might be a critical factor in the justification of the joint's design.

7.6.3 Determining the Compression Zone Configuration

7.6.3.1 Overview

It is important to determine the appropriate configuration of the compression zone for each fastener in the joint. The following sections present the equations necessary to determine which compression zone configuration is applicable.

7.6.3.2 Diameter of the Compression Zone

First, the edge distance of the flanges, a_i , is used to calculate the available diameter for the compression zone,

$$D_{\text{avail}} = 2 a_i \quad [7.6.4]$$

Then, this is compared with the limit diameter of the compression cone as given by,

$$D_{\text{lim}} = D_{uh,brg} + w L_c \tan \phi \quad [7.6.5]$$

where; $D_{uh,brg}$ is the fastener's under-head bearing diameter, L_c is the compression length, and ϕ is the compression cone half angle (see Section 7.6.3.3 below), and $w=1$ for a nut-tightened joint and $w=2$ for a threaded hole joint.

7.6.3.3 The Compression Cone Half Angle

The compression cone's half angle, ϕ , depends strongly on the available area of the flanges. It is also influenced by the fastener's under-head diameter, the hole diameter and the distribution of the compression load. Reference 7.2 proves empirically derived equations for calculating ϕ .

For nut-tightened joints $\tan(\phi)$ is given by,

$$\tan \phi = 0.362 + 0.032 \ln(x/2) + 0.153 \ln(y) \quad [7.6.6]$$

and for insert joints it is given by,

$$\tan \phi = 0.348 + 0.013 \ln(x) + 0.193 \ln(y) \quad [7.6.7]$$

where the following non-dimensional parameters are used,

$$x = \frac{L_c}{D_{uh,brg}} \quad [7.6.8]$$

$$y = \frac{D_{avail}}{D_{uh,brg}} \quad [7.6.9]$$

7.6.3.4 Existence of a Cone and Sleeve

The existence of the sleeve is determined as follows:

If $D_{avail} > D_{lim}$, the compression zone is fully developed into a cone (or pair of cones for nut-tightened joints)

If $D_{uh,brg} > D_{avail}$, no compression cone develops and only a sleeve has to be used for calculation purposes

If $D_{uh,brg} < D_{avail} < D_{lim}$, that compression zone is formed by a partial compression sleeve and compression cone/s

The above cases, 1 to 3, correspond to the left, middle and right configurations of Figure 7-10.

7.6.4 The Compression Zone Compliance

The compliance of the clamped parts, δ_c , for the case of fully developed compression cone/s (i.e. with $D_{avail} > D_{lim}$) is given by,

$$\delta_c = \frac{2 \ln \left[\frac{(D_{uh,brg} + D_h)(D_{lim} - D_h)}{(D_{uh,brg} - D_h)(D_{lim} + D_h)} \right]}{w E_c \pi D_h \tan(\phi)} \quad [7.6.10]$$

where E_c is the modulus of elasticity of the clamped parts.

For partially developed compression cone/s (i.e. $D_{uh,brg} < D_{avail} < D_{lim}$), the clamped parts compliance is given by,

$$\delta_c = \frac{2}{w D_h \tan(\phi)} \ln \left[\frac{(D_{uh,brg} + D_h)(D_{avail} - D_h)}{(D_{uh,brg} - D_h)(D_{avail} + D_h)} \right] + \frac{4}{D_{avail}^2 - D_h^2} \left[L_c - \frac{D_{avail} - D_{uh,brg}}{w \tan(\phi)} \right] \quad [7.6.11]$$

$$E_c \pi$$

Equation [7.6.11] includes the effect of both the compression cone/s and sleeves, and is appropriate when the clamped parts have the same modulus of elasticity.

If the compliances of the cone and sleeve are calculated separately (for example when multiple materials are present in the clamped parts), it is important to calculate the clamped parts compliance by,

$$\delta_c = \frac{2}{w} \delta_{cone} + \delta_{sleeve} \quad [7.6.12]$$

where the cone's compliance is,

$$\delta_{cone} = \frac{\ln \left[\frac{(D_{uh,brg} + D_h)(D_{uh,brg} + 2 L_{cone} \tan(\phi) - D_h)}{(D_{uh,brg} - D_h)(D_{uh,brg} + 2 L_{cone} \tan(\phi) + D_h)} \right]}{E_c D_h \pi \tan(\phi)} \quad [7.6.13]$$

and the sleeve's compliance is,

$$\delta_{sleeve} = \frac{4L_{sleeve}}{E_c \pi (D_{avail}^2 - D_h^2)} \quad [7.6.14]$$

and the lengths of the cone and sleeve are given by,

$$L_{cone} = \frac{D_{avail} - d_{uh,brg}}{2 \tan(\phi)} \quad [7.6.15]$$

and,

$$L_{sleeve} = L_c - \frac{2L_{cone}}{w}. \quad [7.6.16]$$

For the case where only a compression sleeve exists ($D_{uh,brg} < D_{avail}$), Equation [7.6.16] is used for the sleeve compliance and L_{sleeve} is equal to the combined length of the clamped parts, L_c , and $w=1$ for a nut-tightened joint or $w=2$ for a threaded hole joint.

7.6.5 Gasket Compliance

If the clamped parts include a gasket, it is possible to estimate the total compliance of all clamped parts using,

$$\delta_c = \delta_e + \delta_g \quad [7.6.17]$$

where δ_e is the compliance of the elastic clamped parts (flanges, washers, etc) and δ_g is the compliance of the gasket.

However, in general, the load-displacement characteristics of gaskets are non-linear (as shown in Figure 7-14) and the compliance of the gasket is much greater than that of the other clamped parts. Therefore, deformation of the gasket often dominates the elastic behaviour of the joint. Not only does δ_g vary with the applied load, but in addition the gasket behaviour is often partially plastic (see Figure 7-15), leading to a hysteresis effect. If the load is dynamic, the hysteresis can disappear over a period of time, and therefore [it is important to analyse](#) gasket joints differently depending on whether they are intended for static or dynamic service.

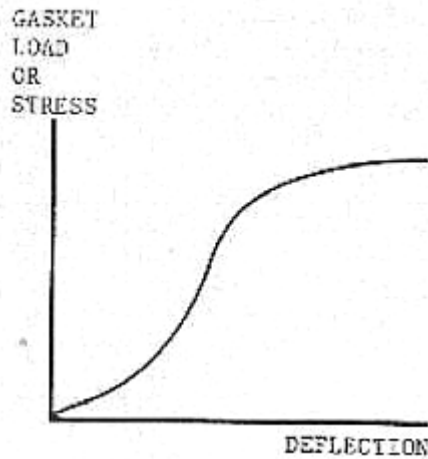


Figure 7-14 - Typical Gasket Deflection

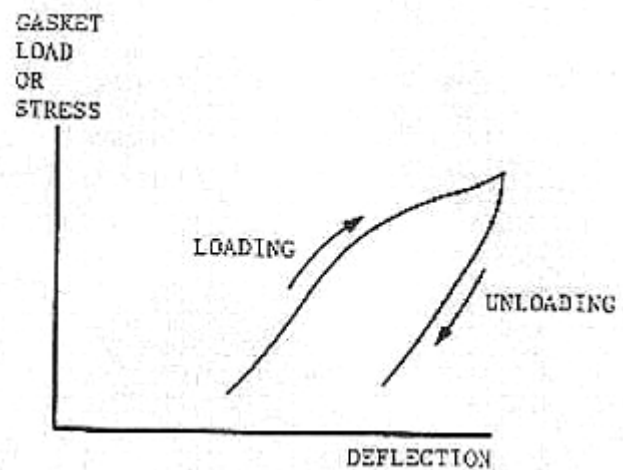


Figure 7-15 – Gasket Showing Hysteresis

The coefficient of thermal expansion of a gasket can be different from that of the other clamped parts or the fastener hence temperature changes can affect joint performance.

Including an elastic-plastic nonlinear spring applied in the joint diagram results in a joint non-linear joint diagram such as shown in Figure 7-16. In this figure the amount of creep is indicated by the difference between the dotted and full lines.

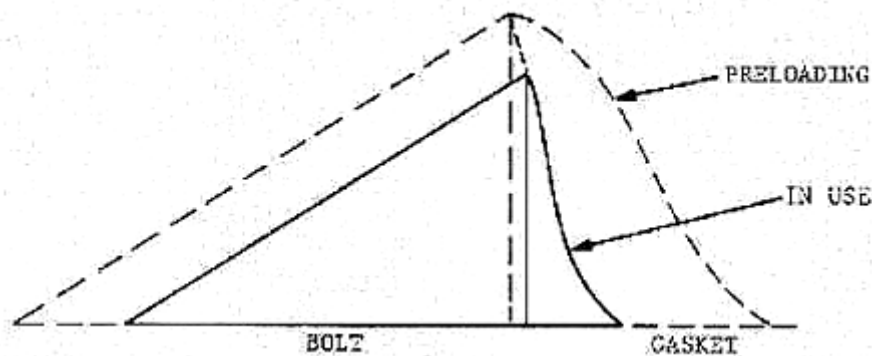


Figure 7-16- Joint Diagram for a Gasket Joint Showing Gasket Creep

The difficulties in predicting gasket creep and spring rates has led to an empirical approach, which uses experimentally derived gasket factors, y and m for each type of gasket material:

- The y factor gives the initial gasket stress which can be converted to a minimum interface clamping load, $F_{k,req}$, assuming uniform gasket loading. A typical value for a soft aluminium gasket is 60 N/mm^2 and silicon rubber 3 N/mm^2 .
- The m factor is a shape factor experimentally derived for each gasket type. It is the ratio of gasket pressure to contained pressure for an effective seal. Typical values for soft aluminium and silicon rubber are 3,25 and 1,..25 respectively.

Section 6.4.5 contains some recommendations for designing joints in order to minimise unwanted compliance effects due to gaskets.

7.7 Calculation of the Loading Plane Factor

7.7.1 Introduction

7.7.1.1 Overview

These equations in the section are only applicable for concentric axially loaded joints. Section 8.2.4 provides an extension of this method for the case of eccentric axially loaded joints.

For most joints, the effective loading planes are considered to be within the joint and separated by a distance of nL_j , as shown in Figure 7-17.

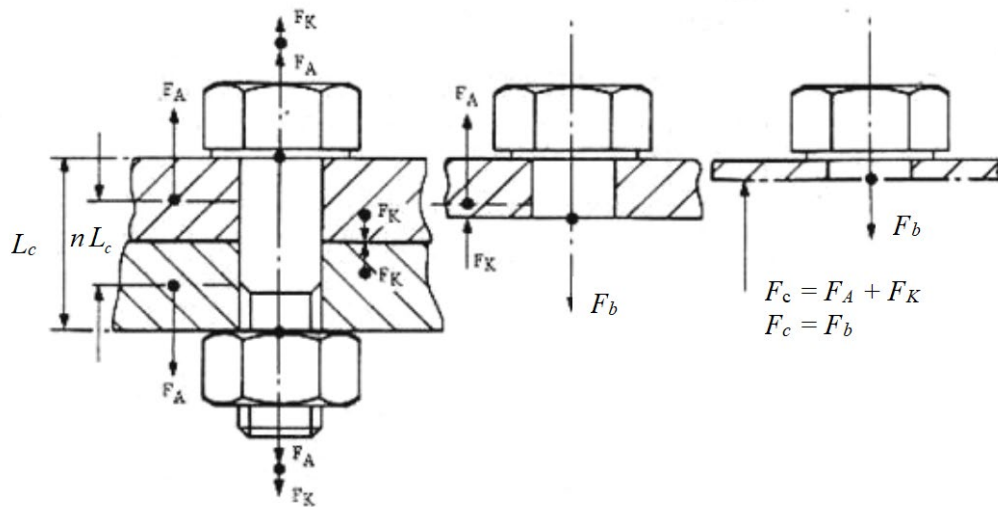


Figure 7-17 - Tension Joint Loading Planes and the Forces Acting within the Joint

Between the loading planes the joint's internal compressive stresses are relieved by the effect of the external load, F_A . Outside the loading planes the clamped material is subjected to extra compression effect of F_A in addition to the clamping load, F_K .

The effect of the loading plane factor on the joint diagram is shown in Figure 7-18. As n reduces, the effective fastener stiffness reduces and the effective joint stiffness increases (see Reference 7.4). Hence, the closer the loading planes, the smaller the fastener load increment and the larger the preload relief in the clamped parts.

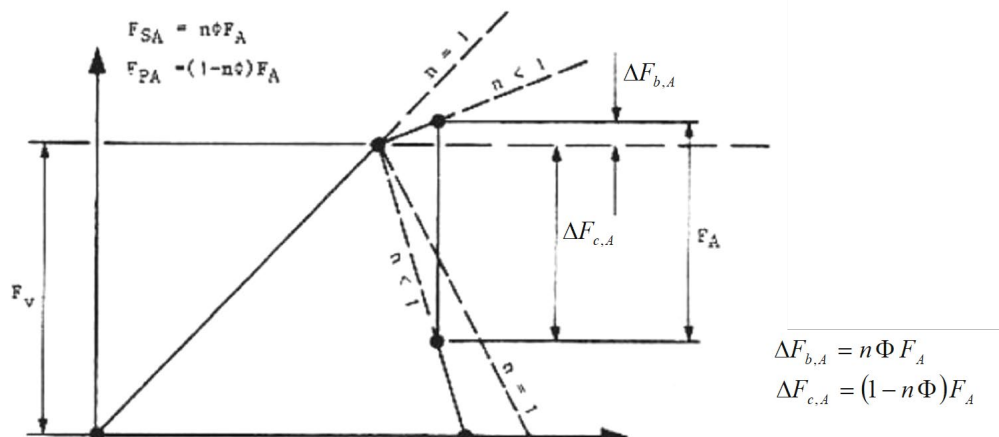


Figure 7-18 - Joint Diagram for Loading Planes within the Joint ($n < 1$)

7.7.1.2 Approximate Method

The loading plane factor depends on the deformation of the joint caused by the preload. For uncritical verification purposes with simple joint geometries the loading plane factor can be set to 0,5, which assumes that the loading planes are at the centre of each flange.

7.7.1.3 Experimental Method

A more precise value for the loading plane factor can be determined from testing by use of the relation,

$$n = \frac{\delta_j}{\delta_c} = \frac{f_{l,1} + f_{l,2}}{f_{uh,1} + f_{uh,2}} \quad [7.7.1]$$

where; δ_j is the effective compliance of the joint (equal to the relative deflection of the loading planes for 1N of externally applied axial load), $f_{l,1}$ and $f_{l,2}$ are the deflections of the points of action of the external load, and $f_{uh,1}$ and $f_{uh,2}$ are the deflections of the under-head and under-nut bearing surfaces under the same external load.

Equation [7.7.1] cannot be applied without knowing of the axial deflections of the under-head and under-nut bearing surfaces and the loading planes due to the externally applied axial load. These deflections can be determined by test or FEM modelling.

7.7.1.4 Geometric Analysis Method

The deformation of the joint is depends strongly on its geometry. For a concentric axially loaded joint, the determination of the loading plane factor is relatively simple provided there is continuous and uniform contact pressure between the flanges. In such cases, the loading plane factor depends only on the following parameters:

- $D_{uh,brg}$ The under-head bearing diameter (or diameter of the washer if it is assumed to be stiff)
- D_h The hole diameter
- a_k The distance between the edge of the bearing surface under the fastener head and the point load introduction of the external force
- a_r The shortest distance between the edge of the bearing surface and the edge of the clamped parts
- h_k The distance between the point of load introduction and the interstice

These geometric parameters are defined in Figure 7-19.

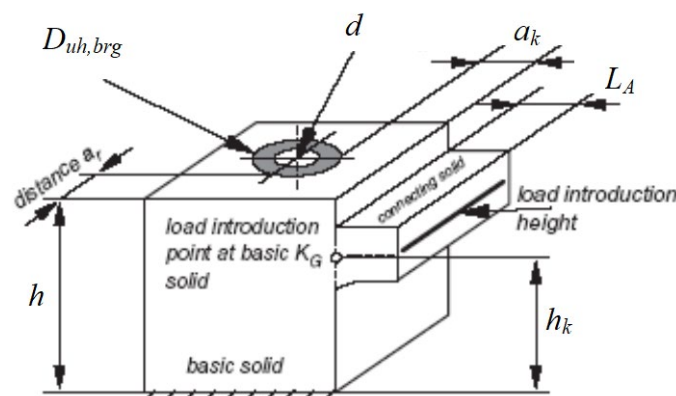


Figure 7-19 - Geometry for Determination of Loading Plane Factor

Using the geometric analysis method, the joint is first extracted from its environment by making a cut at a position where the inner moment is zero (see Figure 7-20). In joints with multiple fasteners there are interference effects between neighbouring fasteners, causing the clamped parts to be stiffer than in case of a single fastener joint. This effect is due to the mutual obstruction of lateral deformations by the neighbouring fasteners. This problem can be solved by using the distance between the hole edges of two neighbouring holes as the region of the deformation cone for the calculation of the clamped parts compliance, δ_c .

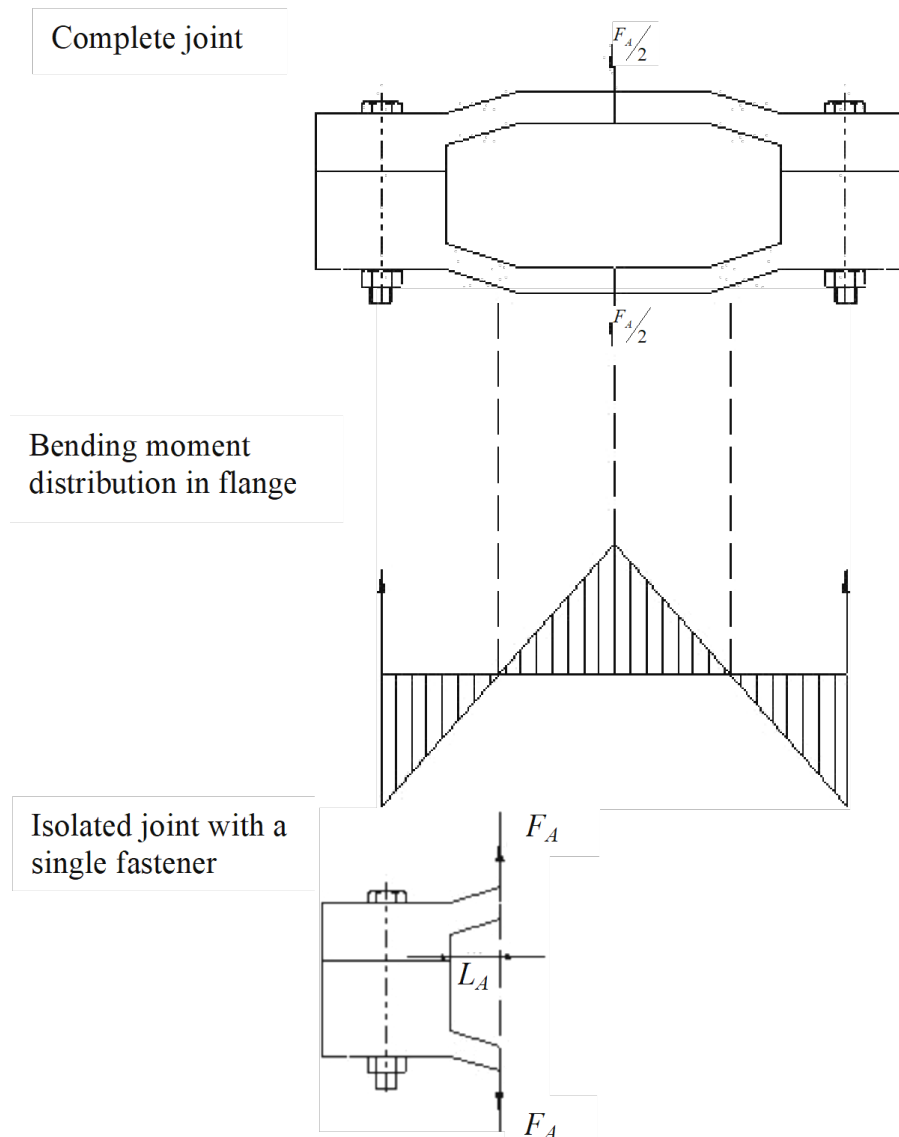


Figure 7-20 – Extraction of the Joint from its Environment

After extracting the joint from its environment, it be split into a 'basic body' and a 'connector body'. The basic body determines the elastic properties of the joint, including the deformation cone. The connector body is the part of the joint where the external forces are applied. The point of external force introduction into the basic body K_G is assumed to be at the horizontal mid-plane of the connector body.

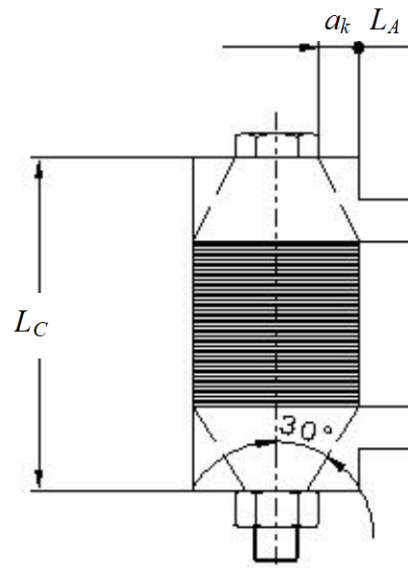


Figure 7-21 - The Basic and Connector Bodies

7.7.2 Simple Calculation of the Loading Plane Factor

7.7.2.1 Overview

This Section presents a simple method for determining the loading plane factor. The method is based on a 2-dimensional representation of the joint and it makes the following assumptions:

- No external moments act on the fastener (but the moment acting on the fastener due to the external force is considered)
- The joint's flanges have no gapping
- All clamped parts in the joint have the same modulus of elasticity
- The joint body is of prismatic shape.
- The product of the parameters concerning the 3-dimensional nature of the joint can be conservatively estimated by $k_{as} * k_{dh} * k_{dw} = 0,8$ (see Section 7.7.3.3 for the analytical definition of these parameters).

7.7.2.2 Joint Types for the Simple Method

Most commonly used joints can be approximated by a class of simplified joints shown in Figure 7-22 according to the point of force introduction into the joint. **It is important that the interstice lies inside the shaded zone of the corresponding diagram.** This zone defines the region where evenly distributed compression is assumed, and is assumed to have a cone half angle of 30°.

Figure 7-22 shows only nut-tightened joints, however the joint types 1, 2 and 4 are also applicable to threaded hole joints. In these cases the lower flange acts as the insert and the dimension L_c is only the thickness of the upper flange.

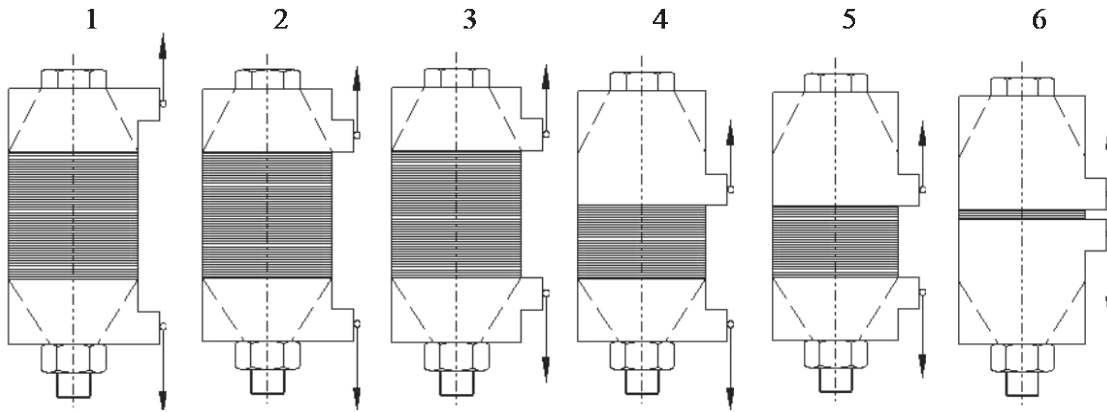


Figure 7-22 – Joint Types According to the Points of Force Introduction

7.7.2.3 Interpolation Table for the Simple Method

The loading plane factor is read from Table 7-2. For intermediate parameter values linear interpolation is applicable.

Table 7-2 - Loading Plane Factors for Simplified Method

L _A / L _C	a _k / L _C	JOINT TYPE (FROM FIGURE 7-22)					
		1	2	3	4	5	6
0,0	0,0	0,70	0,57	0,44	0,42	0,3	0,15
	0,1	0,55	0,46	0,37	0,34	0,25	0,14
	0,3	0,30	0,30	0,26	0,25	0,22	0,14
	≥0,5	0,13	0,13	0,12	0,12	0,10	0,07
0,1	0,0	0,52	0,44	0,35	0,33	0,24	0,13
	0,1	0,41	0,36	0,30	0,27	0,21	0,12
	0,3	0,22	0,21	0,20	0,16	0,15	0,10
	≥0,5	0,10	0,10	0,09	0,08	0,07	0,06
0,2	0,0	0,34	0,30	0,26	0,23	0,19	0,11
	0,1	0,28	0,25	0,23	0,19	0,17	0,11
	0,3	0,16	0,16	0,15	0,12	0,12	0,09
	≥0,5	0,07	0,07	0,07	0,06	0,06	0,06
≥0,3	0,0	0,16	0,16	0,16	0,14	0,14	0,10
	0,1	0,14	0,14	0,14	0,13	0,13	0,10
	0,3	0,12	0,12	0,12	0,10	0,10	0,08
	≥0,5	0,04	0,04	0,04	0,03	0,03	0,03

7.7.3 Analytical Calculation of the Loading Plane Factor

7.7.3.1 Overview

The loading plane factor can be determined analytically by the method presented in this section, although it is normally considered too complex for hand calculations. Thus, it is expected that the method presented here is mainly used in computer programs (or spreadsheets, etc.) for fastener analysis.

It is assumed that height of the connector body is relatively small compared to the thickness of the flanges and thus, the load introduction can be represented by a point force. Also, it is assumed that the joint consists of two flanges (such as shown in Figure 7-23), each of which can be treated separately.

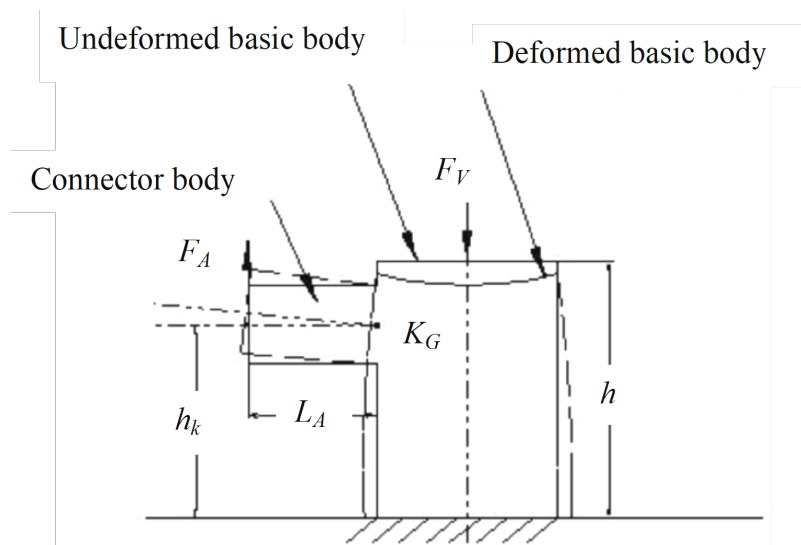


Figure 7-23 – Basic and Connector Bodies of a Flange

The (overall) loading plane factor of the joint is based on loading plane factors for the two flanges according to,

$$n = n_{upper} \left(\frac{\delta_{upper}}{\delta_j} \right) + n_{lower} \left(\frac{\delta_{lower}}{\delta_j} \right) \quad [7.7.2]$$

where; n_{upper} and n_{lower} are the loading plane factors for the upper and lower flanges respectively, and δ_{upper} and δ_{lower} are the compliances of the upper and lower flanges respectively.

7.7.3.2 Loading Plane Factor for a Single Flange

The loading plane factor for a single flange n_{flange} is given by,

$$n_{flange} = n_G - n_M \left(\frac{L_A}{h} \right) \quad (\text{only valid for } L_A/h \leq 1/3) \quad [7.7.3]$$

where n_G and n_M are the general loading plane and moment conduction factors respectively, which are given in the following Sections.

7.7.3.3 The Moment Conduction Factor

The moment conduction factor, n_M , accounts for the influence of the position of the connector body relative to the compression cone and the parameter L_A , and is calculated by,

$$n_M \approx \frac{n_G - n_G^* \left[\frac{n_{2D}}{n_{2D}^*} \right]^*}{0.1} \quad [7.7.4]$$

where;

n_G is the loading plane factor of the basic body (see 7.7.3.4),

n_G^* is the loading plane factor of the basic body whose parameter a_k/h is reduced by 0,1, and;

$\left[\frac{n_{2D}}{n_{2D}^*} \right]^*$ is the ratio of the 2D loading plane factors, where n_{2D}^* is calculated with a ratio a_k/h that is reduced by 0,1, and h_k/h is moved into the region of evenly distributed compression (for the calculation of both factors)

Figure 7-24 shows the principal trends of n_M over the height of a flange.

Equations [7.7.3] and [7.7.4] show that the loading plane factor is reduced if the connector body lies in the spreading zone of the compression cone. In some cases this leads to negative values for n , which can be interpreted as a one-sided gapping of the joint due to the bending effect of the applied load.

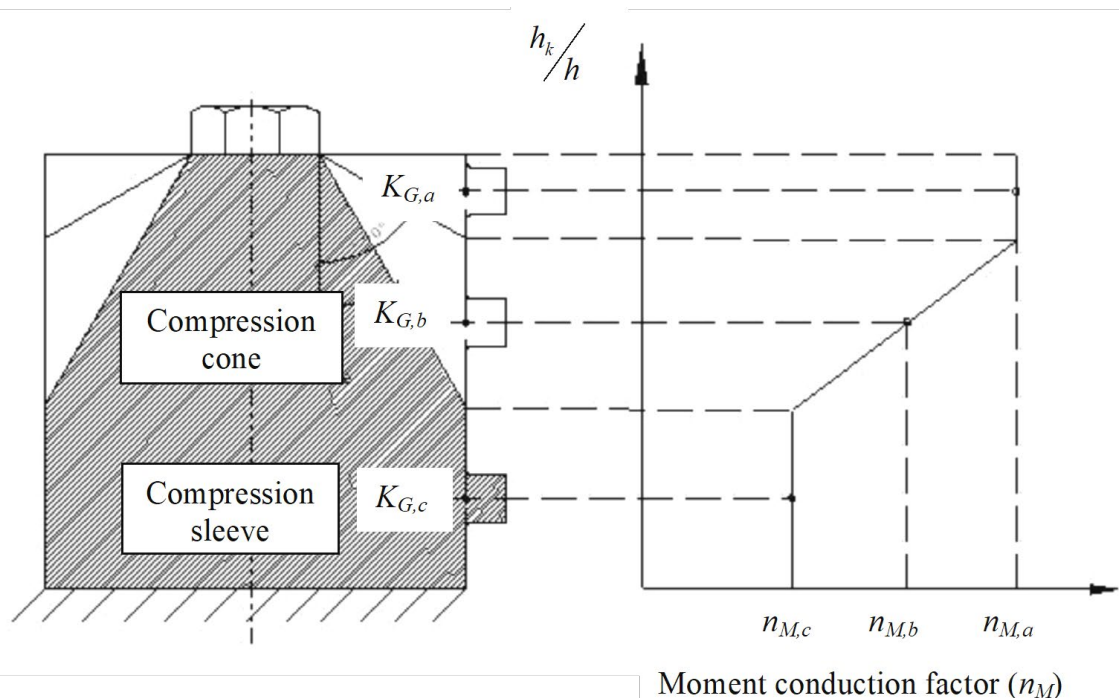


Figure 7-24- Moment Conduction Factor Variation with the Connector Body Position

7.7.3.4 The General Loading Plane Factor

The general loading plane factor of the joint is calculated by,

$$n_G = n_{2D} k_{ar} k_{dh} k_{dw} \quad [7.7.5]$$

where and n_{2D} is the loading plane factor of an equivalent two-dimensional joint calculated by,

$$\begin{aligned} n_{2D} = & \left[0.71 + 0.29 \left(\frac{a_k}{h} \right) - 1.41 \left(\frac{a_k}{h} \right)^2 \right] \left(\frac{h_k}{h} \right) \quad [7.7.6] \\ & + \left[1.31 - 5.89 \left(\frac{a_k}{h} \right) + 4.96 \left(\frac{a_k}{h} \right)^2 \right] \left(\frac{h_k}{h} \right)^2 \\ & + \left[-1.04 + 3.06 \left(\frac{a_k}{h} \right) - 1.88 \left(\frac{a_k}{h} \right)^2 \right] \left(\frac{h_k}{h} \right)^3 \end{aligned}$$

where the geometric variables a_k , h , and h_k are defined in Figure 7-19, and the factors k_{ar} , k_{dh} & k_{dw} account for the influence of the 3D spatial extension of the joint and are given by,

$$k_{ar} \approx 1 - 1.74 \left(\frac{a_r}{h} \right) + 1.24 \left(\frac{a_r}{h} \right)^2 \quad [7.7.7]$$

$$k_{dh} \approx 1 - 0.25 \left(\frac{d}{D_{uh,brg}} \right) \quad [7.7.8]$$

$$k_{dw} \approx 1 \quad [7.7.9]$$

Equations [7.7.5] to [7.7.8] are valid in the ranges,

$$0 \leq \left(\frac{h_k}{h} \right) \leq 1 \quad [7.7.10] \qquad 0 \leq \sqrt{\left(\frac{a_r}{h} \right)^2 + \left(\frac{a_k}{h} \right)^2} \leq 0.7 \quad [7.7.11]$$

$$0.2 \leq \left(\frac{d_{uh,brg}}{h} \right) \leq 0.6 \quad [7.7.12] \qquad 0.6 \leq \left(\frac{d}{D_{uh,brg}} \right) \leq 0.8 \quad [7.7.13]$$

7.8 Joint Separation

7.8.1 Introduction

Under an externally applied tensile load it is generally required that no gapping occurs at any interstice between clamped parts in a joint (i.e. the clamping force does not reach zero). Many joints have additional requirements for a positive clamping force for sealing and other operational functions. Thus, the failure mode of joint separation is defined to occur when the clamping force is reduced to its critical level, $F_{K,req}$ (which is greater than or equal to zero).

The joint diagram at the critical condition for separation failure is depicted in Figure 7-25. It can be seen that, under the action of F_A , the compression in the clamped parts is reduced from the initial preload of $F_{V,min}$ to the minimum specified level of $F_{K,req}$. Any increase in F_A results in insufficient compression in the clamped parts, thereby constituting failure by separation.

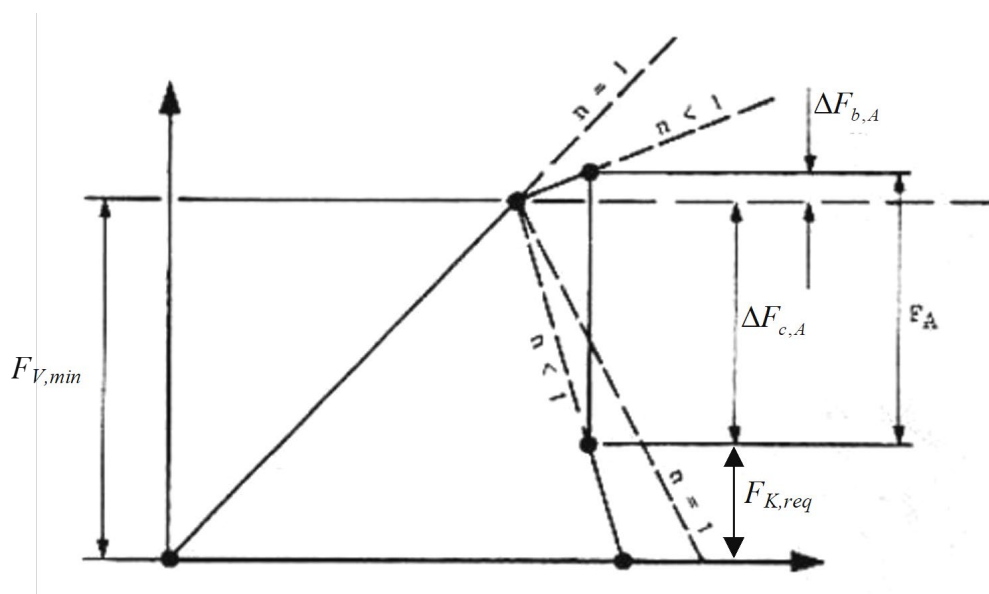


Figure 7-25 - Joint Diagram at Onset of Separation Failure

7.8.2 The Margin of Safety for Joint Separation

The MoS for joint separation is not intended to cover the case of slipping of a friction grip joint. The appropriate MoS for slipping is defined in Section 9.2.1.

The Margin of Safety for joint separation is given by,

$$MoS_{sep} = \frac{F_{V,min} - F_{K,req}}{(1 - \Phi_n) F_A sf_{sep}} - 1 \quad [7.8.1]$$

where sf_{sep} is the safety factor defined for separation as defined in Table 5-4,

and Φ_n is the force ratio defined in equation [7.4.6].

7.9 Fastener Tensile Failure

7.9.1 External Vs Overall Load

The calculations of the MoS for axial loads depend on how the joint transmits externally applied shear loads. Two modes of shear load transfer are included in these guidelines, 'Friction Grip' and 'Bearing' (see Section 9).

It is important to check the failure criterion for 'overall load' in the fastener for both types of joint. The overall load, F_{tot} , is the sum of the maximum preload, $F_{V,max}$, and the part of the externally applied axial load that is seen by the fastener, i.e.,

$$F_{tot} = F_{V,max} + \Delta F_{b,A} \quad [7.9.1]$$

Failure criteria for 'external load' are only relevant when there is gapping (i.e. zero clamping force between the flanges), which leads to the fastener transmitting the full external axial load (i.e. $F_b = F_A$).

Friction grip joints generally do not normally need assessment of this criterion since they are intended to transmit shear forces in case of minimum compression forces and therefore they are more critical in the slipping failure mode.

Table 7-3 shows which axial strength criteria be checked for each type of joint.

Table 7-3 - Criteria for Axial Load Analysis

Fastener Loading	Case	Joint Type	Check to be performed
Overall load (F_{tot})	No Gapping	Friction Grip	Yes
		Bearing	Yes
External load (F_A)	Gapping	Friction Grip	No
		Bearing	Yes

The following Section presents the equations for the relevant MoS.

7.9.2 Margin of Safety on Fastener Failure

The margins of safety for external load criteria are all based on the fastener material's yield strength, σ_y , and ultimate strength, σ_{ult} .

The margins of safety for the overall load, F_{tot} , are,

$$MoS_{tot,y} = \frac{A_s \sigma_y}{F_{V,max} + \Phi_n F_A sf_y} - 1 \quad (\text{for yield failure}) \quad [7.9.2]$$

$$MoS_{tot,ult} = \frac{A_s \sigma_{ult}}{F_{V,max} + \Phi_n F_A sf_{ult}} - 1 \quad (\text{for ultimate failure}) \quad [7.9.3]$$

If gapping is tolerable, the margins of safety on fastener failure, under the external load, F_A , become:

$$MoS_{A,y} = \frac{A_S \sigma_y}{F_A sf_y} - 1 \quad (\text{for yield failure}) \quad [7.9.4]$$

$$MoS_{A,ult} = \frac{A_S \sigma_{ult}}{F_A sf_{ult}} - 1 \quad (\text{for ultimate failure}) \quad [7.9.5]$$

Equations [7.9.2] and [7.9.3] express the force increment seen by the fastener in terms of the external axial load, and include the appropriate loading plane factor and safety factors. The safety factors are only applied to the external axial load, F_A , since the uncertainty in preload is already factored into $F_{V,max}$.

7.10 Thread Failure by Shear Pull-Out

7.10.1 Introduction

To guarantee the pull-out (striping) strength capacity of the thread a certain length of the engaged thread, L_{eng} , is necessary. In nut-tightened joints the full length of the female thread is normally engaged, i.e. $L_{eng} = L_n$. For manufacturing reasons, threaded hole joints often only have engaged thread for only a portion of the hole's length.

Fastener systems with 'normed' nuts are completely bearing capable when the strength class of the nut is at least as high the strength class of the fastener.

It is recommended to use nuts with lower stiffness than the fastener in order to give more uniform load transfer through the threaded interface. If calculations indicate that the female thread is too weak, **it is important to consider** the use of a thread insert of higher strength (e.g. a helicoil). The calculation methods presented in this section are applicable to any thread system, including helicoils.

7.10.2 Failure of the Female Thread

The critical fastener load for failure of the female thread is given by,

$$F_{ult,th,n} = \tau_{ult,n} * A_{th,n} * c_1 * c_3 \quad [7.10.1]$$

where; $\tau_{ult,n}$ is the ultimate tensile shear strength of the material forming the female thread, $A_{th,n}$ is the surface area around the female thread that is assumed to fail during thread pull-out, and c_1 & c_3 are empirical coefficients (**derived for ISO metric threads**) accounting for the depth of supporting material behind the female thread and the strength ratio of the two threads (see **equations [7.10.4], [7.10.5] and [7.10.6]** below).

The female thread's failure surface area is calculated by (**see Reference 7.2**),

$$A_{th,n} = \pi d \left(\frac{L_{eng,eff}}{p} \right) \left[\frac{p}{2} + (d - D_2) \tan(\theta) \right] \quad [7.10.2]$$

where p is the thread pitch, and D_2 is the pitch diameter of the female thread, θ is the half angle of the thread groove, and $L_{eng,eff}$ is the effective length of engaged thread given by,

$$L_{eng,eff} = L_{eng} - 2 * p \quad [7.10.3]$$

which accounts for the beginning portion of the engaged thread, which does not transmit any significant load (**1,0p on the upper part and 1,0p on the lower part of the engaged length, for a total of 2p**).

The coefficient c_1 is either 1,0 for a threaded hole, or calculated by the following equation for a threaded nut:

$$c_1 = 3.8 \left(\frac{s_w}{d} \right) - \left(\frac{s_w}{d} \right)^2 - 2.61 \quad [7.10.4]$$

where s_w is the wrench size as indicated in Figure 5-5.

Equation [7.10.4] is only valid for metric threads with $1.4 \leq \left(\frac{s_w}{d} \right) \leq 1.9$.

The coefficient c_3 is given by,

$$c_3 = 0,897 \quad \text{for } R_s \geq 1,0, \text{ or} \quad [7.10.5]$$

$$c_3 = 0,728 + 1,769R_s - 2,896R_s^2 + 1,296R_s^3 \quad \text{for } 0,4 < R_s < 1 \quad [7.10.6]$$

where for $R_s \leq 0,4$: $R_s=0,4$

where; R_s is the shear strength ratio of the female and male threads according to;

$$R_s = \frac{\tau_{ult,n} A_{th,n}}{\tau_{ult,b} A_{th,b}} \quad [7.10.7]$$

where; $\tau_{ult,b}$ is the ultimate tensile shear strength of the material forming the male thread and $A_{th,b}$ is the failure surface area of the male thread calculated by (see Reference 7.2),

$$A_{th,b} = \pi D_1 \left(\frac{L_{eng,eff}}{p} \right) \left[\frac{p}{2} + (d_2 - D_1) \tan(\theta) \right] \quad [7.10.8]$$

where D_1 is the minor diameter of the female thread and d_2 is the pitch diameter of the male thread (see Section 5.4).

If the both threads are steel, Equation [7.10.7] can be replaced with;

$$R_s = \frac{\sigma_{ult,n} A_{th,n}}{\sigma_{ult,b} A_{th,b}} \quad [7.10.9]$$

where; $\sigma_{ult,n}$ and $\sigma_{ult,b}$ are the ultimate tensile strengths of the female and male thread materials respectively.

Table 7-4 - <<deleted>>

Using equations [7.10.2] and [7.10.3] the necessary length of engaged thread can be expressed as,

$$l_{eng,req} = \frac{F_{th} p}{c_1 c_3 \tau_{ult,n} \pi d \left[\frac{p}{2} + (d - D_2) \tan(\theta) \right]} + 2 p \quad [7.10.10]$$

where F_{th} is the axial load transmitted by the thread, from both maximum preload and the applicable proportion of the axial applied force, as defined by the joint stiffness ratio.

The most unfavourable case for the load-bearing capacity of the threaded joint is when the external diameter d of the bolt thread is at the lower tolerance limit and the pitch flank diameter D_2 of the nut thread is at the upper tolerance limit. Equation [7.10.10] for finding the necessary length of thread engagement is for this reason modified as follows for the case when the effective thread dimensions are not known:

$$l_{eng,req,min} = \frac{F_{th} p}{c_1 c_3 \tau_{ult,n,min} \pi d_{min} \left[\frac{p}{2} + (d_{min} - D_{2,max}) \tan(\theta) \right]} + 2 p \quad [7.10.11]$$

7.10.3 Failure of the Male Thread

Normally the fastener's material strength is higher or equal to that of the nut, so when 'normed' nuts with equal or lower material strength to the fastener are used, there is no need to calculate failure of the male thread.

If the fastener's material is weaker than the nut or insert, $R_s > 1$ from Equation [7.10.7], the analysis is the same except for Equation [7.10.1] in which the variables, $\tau_{ult,n}$ and $A_{th,n}$, are replaced by $\tau_{ult,b}$ and $A_{th,b}$ respectively and it is important to use the correction factor c_2 (derived for ISO metric threads) instead of c_3 .

Thus, the strength of the male thread is calculated by,

$$F_{ult,th,b} = \tau_{ult,b} A_{th,b} c_1 c_2 \quad [7.10.12]$$

where $\tau_{ult,b}$ is the ultimate shear strength of the fastener material, $A_{th,b}$ is the failure area of the male thread as calculated by Equation [7.10.8], and the coefficient c_1 is calculated as for the female thread.

The coefficient c_2 is given by,

$$c_2 = 1,187 \quad \text{for } R_s \geq 2,2, \text{ or} \quad [7.10.13]$$

$$c_2 = 5,594 - 13,682R_s + 14,107R_s^2 - 6,057R_s^3 + 0,9353R_s^4 \quad \text{for } 1,0 < R_s < 2,2 \quad [7.10.14]$$

The minimum required engagement length is calculated as follows:

$$l_{eng,req,min} = \frac{F_{th} p}{c_1 c_2 \tau_{ult,n,min} \pi d_{min} \left[\frac{p}{2} + (d_{2min} - D_{1max}) \tan(\theta) \right]} + 2 p \quad [7.10.15]$$

7.10.4 Margin of Safety on Thread Pull-Out

The margin of safety on shear pull-out of the thread under the external load is calculated by,

$$MoS_{th,A} = \frac{F_{th,crit}}{F_A s f_{ult}} - 1 \quad [7.10.16]$$

and for the overall load,

$$MoS_{th,tot} = \frac{F_{th,crit}}{F_{V,max} + \Phi_n F_A s f_{ult}} - 1 \quad [7.10.17]$$

where $F_{th,crit}$ is the critical thread failure load (lower of the male and female thread strengths).

No MoS calculations are necessary for yield failure of the thread.

7.11 Crushing of Flanges

The margins of safety on flange crushing are calculated with the following equations,

$$MoS_{crush,y} = \frac{A_{uh,min} \sigma_{br,y}}{F_{V,max} + \Phi_n F_A s f_y} - 1 \quad \text{(for yield)} \quad [7.11.1]$$

$$MoS_{crush,ult} = \frac{A_{uh,min} \sigma_{br,ult}}{F_{V,max} + \Phi_n F_A s f_{ult}} - 1 \quad \text{(for ultimate)} \quad [7.11.2]$$

where σ_{br} is the maximum compressive stress that occurs under the head or nut for either the F_{tot} or F_A (refer to Table 7-3 for applicable fastener load criteria). Note that considering bearing stresses allowables is rather conservative. (It is known that for some ductile metallic materials a bearing stress up to twice the yield limit of the flange material does not result in flange indentation).

However, in case the margins of safety are low and a simple approximation cannot be accepted, such as for honeycomb crushing, it is advised to determine the crushing allowable by test (see, for example, the ECSS-E-HB-32-22).

7.12 Repeated Loading to a Point above Yield

Point E of Figure 7-26 represents a joint tightened to a preload F_{V1} , which induces stresses in the fastener that are below its yield stress. At the first application of the external load, F_A , the fastener feels an extra load $\Delta F_{b,A,1}$, which takes its highest stressed region beyond its yield strength (along the path EFG.). This causes permanent deformation of the fastener ΔL_b and local work hardening of the deformed material. If the applied external load is then removed, the fastener's preload can reduce from point E to a lower value, point H. If F_A is reapplied, the fastener load needs to exceed point G before that work hardened part of the fastener can yield again. However, there can be an adjacent part of the fastener that yields at a lower load (as it has not workhardened) allowing further permanent deformation to take place.

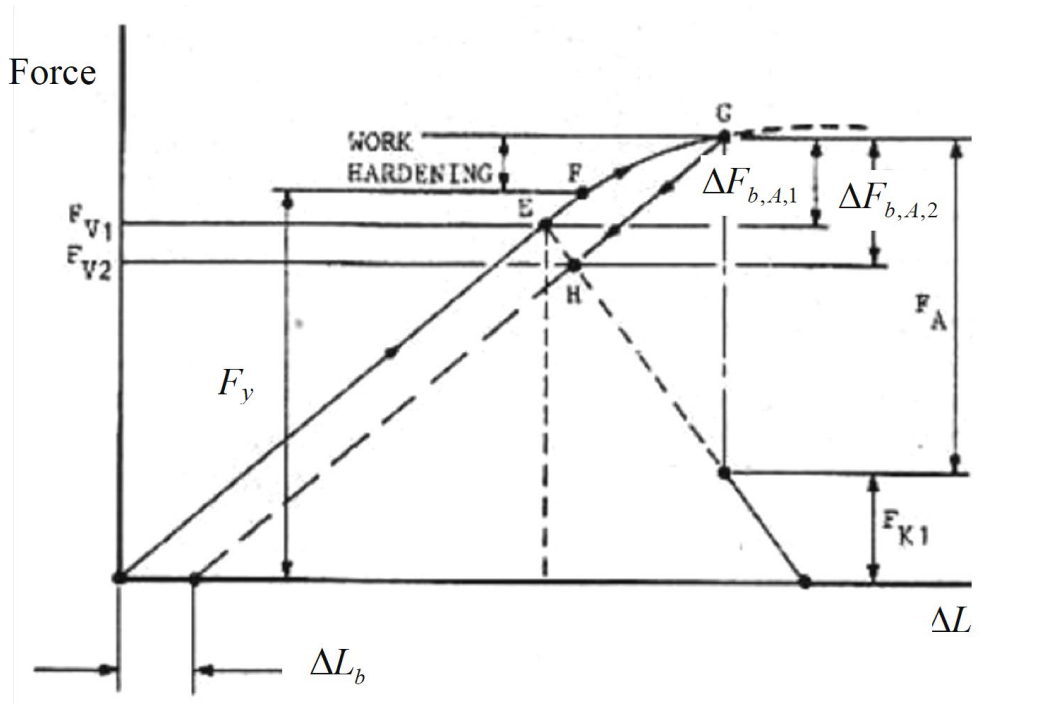


Figure 7-26 – Joint Diagram Showing Repeated Loading into the Plastic Region

The result of continued loading as shown in Figure 7-26 is a non-linear preload reduction with each subsequent load application as shown in Figure 7-27 (see Reference 7.3). This is not a desirable situation, and therefore, in normal circumstances it is important to avoid a loading above the fastener yield.

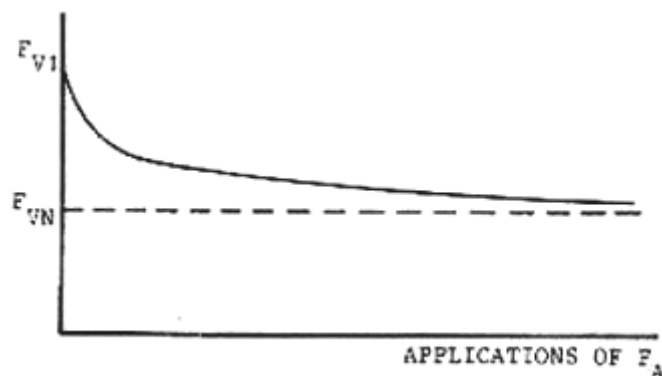


Figure 7-27 – Preload Loss with Repeated Loading into Yield

7.13 Dynamic Loading

A simple example showing the effects of dynamic loading is given in Figure 7-28. Here, an alternating external axial load varying from zero to F_A is applied to a joint. The fastener experiences a dynamic load with amplitude of $\Delta F_{b,A}/2$.

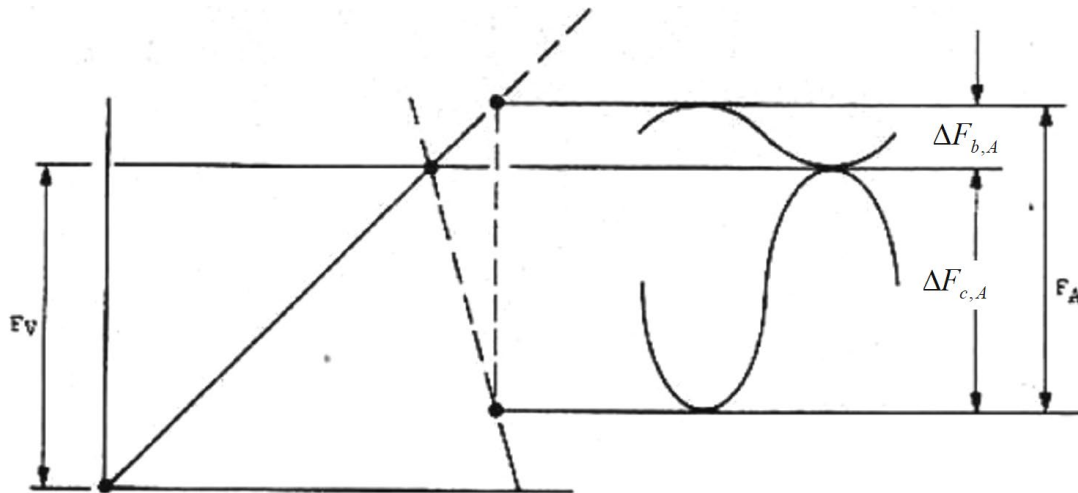


Figure 7-28 – Joint Diagram Showing a Dynamic External Load

The dynamic stress amplitude in the fastener due to the external load $\Delta\sigma_{b,A}$ is given by,

$$\Delta\sigma_{b,A} = \frac{\Delta F_{b,A}}{2 A_S} \quad [7.13.1]$$

where A_S is the fastener stress area (see Section 5.4).

Figure 7-29 is a typical S-N curve that relates the applied stress in a component to its number of cycles to failure. As $\Delta\sigma_{b,A}$ reduces, the number of cycles to failure increases, until the stress is below a certain threshold $\Delta\sigma_{b,\infty}$, after which the fastener is termed fatigue resistant.

In Section 7.4 it was shown that $\Delta F_{b,A}$ is reduced by decreasing the fastener's stiffness relative to that of the clamped parts. Hence, to improve fatigue resistance, it is recommended to use reduced shank fasteners.

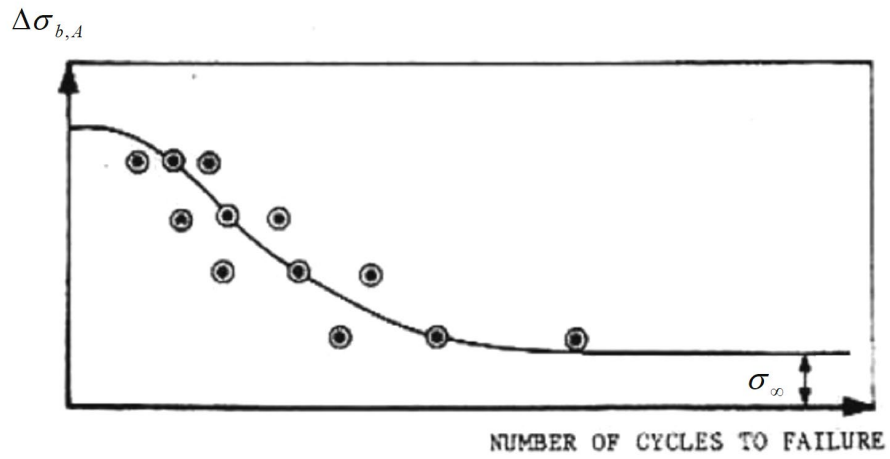


Figure 7-29 – Typical S-N Curve (For a Given Mean Stress)

7.14 Worked Examples

7.14.1 Preload in a Concentric Axially Loaded Joint

7.14.1.1 Overview

The geometry of this example problem is shown in Figure 7-30.

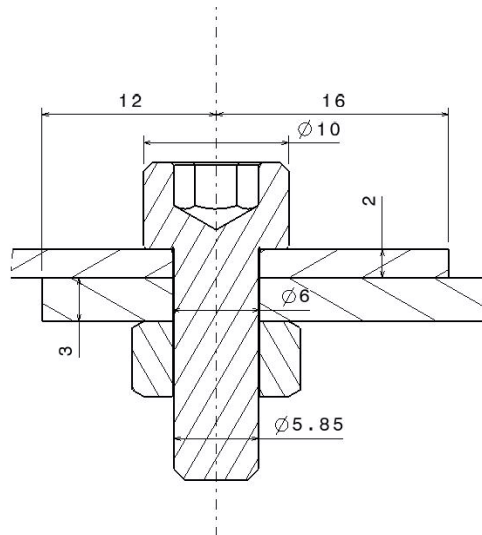


Figure 7-30 - Example problem of concentric axially loaded joint

7.14.1.2 Initial Data

The fastener to be used for this joint is a LN 29949 M6 x 14 with an anchor nut LN 29693. This fastener has the following material properties:

Table 7-5: Preload in a Concentric Axially Loaded Joint, fastener material properties

Material	A-286 steel
Yield allowable	950 MPa
Ultimate allowable	1100 MPa
Shear yield allowable	548 MPa
Shear ultimate allowable	655 MPa
Young's modulus (E_b)	201 GPa
Thermal expansion coefficient (α_b)	1,68e-5 K-1

The following thread parameters can be calculated using the standard relations for metric threads:

Table 7-6: Preload in a Concentric Axially Loaded Joint, Thread parameters

Thread pitch (p)	1 mm (standard)
Fastener nominal diameter (d)	6 mm (M6 fastener)
Pitch diameter (d_2)	5,35048 mm
Minor diameter (d_3)	4,77313 mm
Stress diameter (d_s)	5,062 mm
Cross-section area at minor diameter (A_3)	17,894 mm ²
Stress area (A_s)	20,123 mm ²

The upper flange is 2 mm thick with an edge distance of 16mm. The lower flange is 3 mm thick with an edge distance of 12 mm. The diameter of the holes through the flanges is 6,5 mm.

The flanges have the following material properties:

Table 7-7: Preload in a Concentric Axially Loaded Joint, flange material properties

Material	Al 7075 T 7351
Young's modulus (E_c)	71 GPa
Thermal expansion coefficient (α_c)	2,2e-5 K-1
Shear ultimate allowable	262 MPa
$\sigma_{br,y,2.0}$	613 MPa
$\sigma_{br,ult,2.0}$	882 MPa
$\sigma_{br,y,1.5}$	524 MPa
$\sigma_{br,ult,1.5}$	689 MPa

The joint is assembled at a reference temperature of 21°C. The maximum operating temperature is 50°C and the minimum operating temperature is 4°C.

The joint is subjected to an external axial load of 1000N.

The strength of this structure is **only** verified by analysis. Thus, **it is important that** the safety factors for yield and ultimate loads **are taken** from Table 5-4. These values are then multiplied by the joint fitting factor of 1,15. Thus, the safety factors to be applied to the design justification are:

$$sf_y = 1,25 \times 1,15 = 1,4375$$

$$sf_{ult} = 2 \times 1,15 = 2,3$$

7.14.1.3 Calculation of the Nominal Preload

For the preload ratio, the default value of 0,8 is chosen. With this starting point the preload stress is calculated,

$$\sigma_V = 0,8 * \sigma_y = 760MPa$$

With this, the nominal preload can be calculated,

$$F_V = \sigma_V \cdot A_s = 15,294 kN$$

7.14.1.4 Calculation of the Force Ratio

First the compliance of the fastener has to be determined (see Section 7.5). The joint is nut-tightened and has a cylindrical fastener head. Therefore the appropriate substitution lengths from Table 7-1 are as follows:

$$L_{h,sub} = 0,4 d$$

$$L_{eng,sub} = 0,5 d$$

$$L_{n,sub} = 0,4 d$$

Using these substitution lengths the fastener's compliance can be calculated using equation [7.5.5],

$$\delta_b = \frac{1}{E_b} \left[\frac{L_{h,sub}}{A_{nom}} + \frac{L_{eng,sub}}{A_3} + \frac{L_{n,sub}}{A_{nom}} + \sum \frac{L_i}{A_i} \right]$$

where the modulus of elasticity of the nut is equal to that of the fastener.

It is assumed that the entire shank length is threaded, which leads to,

$$\sum \frac{L_i}{A_i} = \frac{5}{17.89} \text{ [mm}^{-1}\text{]}$$

Therefore, the fastener compliance is evaluated as,

$$\delta_b = \frac{1}{201000} \left[\frac{0.4 \times 6}{28.27} + \frac{0.5 \times 6}{17.89} + \frac{0.4 \times 6}{28.27} + \frac{5}{17.89} \right] = 3,0689e^{-6} \text{ mm/N}$$

Now, the compliance of the clamped parts is calculated. The available diameter for compression cone is determined from the minimum edge distance,

$$D_{avail} = 24 \text{ mm (minimal edge distance of 12mm occurs in upper flange)}$$

The length of the compression zone is the full length through the clamped parts,

$$L_c = 5 \text{ mm}$$

The underhead bearing diameter is equal the diameter of the fastener head

$$D_{uh,brg} = 10\text{mm}$$

The non-dimensional compression cone parameters x and y are evaluated as,

$$x = \frac{L_c}{D_{uh,brg}} = \frac{5}{10} = 0.5$$

$$y = \frac{D_{avail}}{D_{uh,brg}} = \frac{24}{10} = 2.4$$

Thus, tan of the compression cone half angle is calculated from Equation [7.6.6],

$$\begin{aligned}
 \tan(\phi) &= 0.362 + 0.032 \ln(x/2) + 0.153 \ln(y) \\
 &= 0.362 + 0.032 \ln(0.5/2) + 0.153 \ln(2.4) \\
 &= 0.4516
 \end{aligned}$$

The limit diameter of the compression cone is calculated with Equation [7.6.5], with $w=1$ for a nut-tightened joint:

$$D_{lim} = D_{uh,brg} + w \cdot L_c \cdot \tan(\phi) = 10mm + 1 \cdot 5mm \cdot 0,4516 = 12,2579mm$$

The criteria in Section 7.6.3.4 are used to determine that the compression cone is fully developed since $D_{avail} > D_{lim}$. Therefore, Equation [7.6.10] is used to calculate the compliance of the clamped parts,

$$\begin{aligned}
 \delta_c &= \frac{2 \ln \left[\frac{(D_{uh,brg} + D_h) \cdot (D_{lim} - D_h)}{(D_{uh,brg} - D_h) \cdot (D_{lim} + D_h)} \right]}{w \cdot E_c \cdot \pi \cdot D_h \cdot \tan(\phi)} = \frac{2 \ln \left[\frac{(10mm + 6,5mm) \cdot (12,258mm - 6,5mm)}{(10mm - 6,5mm) \cdot (12,258mm + 6,5mm)} \right]}{1 \cdot 71GPa \cdot \pi \cdot 6,5mm \cdot 0,4516} \\
 &= 1,1289e^{-6} \frac{mm}{N}
 \end{aligned}$$

The (basic) force ratio is now calculated using Equation [7.4.2],

$$\Phi = \frac{\delta_c}{\delta_c + \delta_p} = \frac{1,1289e^{-6}}{1,1289e^{-6} + 3,0689e^{-6}} = 0,2689$$

The geometry of the joint is simple, so the loading plane factor, n , can be assumed 0.5 with adequate accuracy. Thus, the force ratio of the joint with loading plane adjustment is given by,

$$\Phi_n = n \cdot \Phi = 0,5 \cdot 0,2689 = 0,1345$$

7.14.1.5 Calculation of the preload loss due to embedding

The preload loss due to embedding is assumed to be 5% of the nominal preload. Therefore,

$$F_z = 0,05 \cdot 15294N = 764,7N$$

7.14.1.6 Calculation of the thermal induced loads

This calculation is performed with Equations [6.3.23] and [6.3.24],

$$\begin{aligned}
 F_{\Delta T^+,b} &= \frac{L_j (\alpha_c - \alpha_b) \Delta T_{max}}{\delta_b + \delta_c} = \frac{5 \cdot (2,20e^{-5} - 1,68e^{-5}) \cdot (50 - 21)}{3,0689e^{-6} + 1,1289e^{-6}} N = 179,6N \\
 F_{\Delta T^-,b} &= \frac{L_j (\alpha_c - \alpha_b) \Delta T_{min}}{\delta_b + \delta_c} = \frac{5 \cdot (2,20e^{-5} - 1,68e^{-5}) \cdot (4 - 21)}{3,0689e^{-6} + 1,1289e^{-6}} N = -105,3N
 \end{aligned}$$

7.14.1.7 Calculation of the maximum and minimum preload

The following values of the underhead and thread friction coefficients are read from Annex B for the specific fastener and nut combination:

$$\mu_{uh,max} = 0,296 \qquad \mu_{uh,min} = 0,179$$

$$\mu_{th,max} = 0,176 \qquad \mu_{th,min} = 0,086$$

The following maximum and minimum prevailing torques are read from Table 6-2:

$$M_{p,max} = 2,0 \text{ Nm} \qquad M_{p,min} = 0,4 \text{ Nm}$$

The effective diameter of the application of the underhead torque is determined using Equation [5.4.6],

$$d_{uh} = 0.5(D_{uh,brg} + D_h) = 0.5(10 + 6.5) = 8,25\text{mm}$$

The tan of the thread helix angle is determined using the relation in Equation [6.3.9],

$$\tan \varphi = \frac{p}{\pi d_2} = \frac{1}{\pi \times 5.35048} = 0.0595$$

The thread tooth angle is 60° therefore,

$$\cos \theta = \cos \frac{60^\circ}{2} = 0,866$$

Now a trial value of the maximum applied torque is set to 13,65Nm. Assuming a torque wrench scatter of 5%, this leads to a maximum applied torque of 14,3Nm and a minimum applied torque of 13,0Nm. The applied torque is specified as part of the manufacturing process so it is important that it is rounded to an accuracy of 0,1 Nm. The bolt utilization, torque and preload are directly linked with each other. Any of these parameters can be chosen as baseline for the bolt evaluation process and the other than calculated out of the selected one.

Now the maximum and minimum in-service preloads are calculated using Equations [6.3.14] and [6.3.15],

$$\begin{aligned} F_{V,max} &= \frac{M_{app,max} - M_{p,min}}{\frac{1}{2} \cdot d_2 \cdot \left(\tan \varphi + \frac{\mu_{th,min}}{\cos \theta} \right) + \frac{1}{2} \cdot d_{uh} \cdot \mu_{uh,min}} + F_{\Delta T^+} \\ &= \frac{14,3 - 0,4}{\frac{1}{2} \cdot 5,3505 \cdot \left(0,0595 + \frac{0,086}{0,866} \right) + \frac{1}{2} \cdot 8,25 \cdot 0,179} + 179,6 = 12129\text{N} \end{aligned}$$

$$\begin{aligned} F_{V,min} &= \frac{M_{app,min} - M_{p,max}}{\frac{1}{2} \cdot d_2 \cdot \left(\tan \varphi + \frac{\mu_{th,max}}{\cos \theta} \right) + \frac{1}{2} \cdot d_{uh} \cdot \mu_{uh,max}} + F_{\Delta T^-} - F_Z \\ &= \frac{13,0 - 2,0}{\frac{1}{2} \cdot 5,3505 \cdot \left(0,0595 + \frac{0,176}{0,866} \right) + \frac{1}{2} \cdot 8,25 \cdot 0,296} - 105,3 - 764,7 = 4848\text{N} \end{aligned}$$

Finally, it is important to determine the margin of safety on the tightening process. The load in the fastener is composed of a tensile stress due to the preload and a torsional stress due to the applied torque. First the torsional stress is calculated.

The polar section modulus is calculated with equation [6.5.5], which considers the case of total plastic deformation (ultimate),

$$W_p = \frac{\pi d_0^3}{12} = \frac{\pi \times 5.062^3}{12} = 33,95 \text{ mm}^3$$

The minimum moment absorbed by friction under the fastener head is determined with Equation [6.5.3], with $\lambda=180$ degrees for a flat screw head

$$M_{uh,min} = \frac{d_{uh}}{2} \cdot (F_{V,max} - F_{\Delta T+}) \cdot \mu_{uh,min} \cdot \frac{1}{\sin(\lambda/2)} = \frac{8,25}{2 \cdot 1000} \cdot (12129 - 179,6) \cdot 0,179 \cdot 1 = 8,82 \text{ Nm}$$

The maximum shear stress due to torsion is then calculated with Equation [6.5.2],

$$\tau_{max} = \frac{M_{app,max} - M_{uh,min}}{W_p} = \frac{14,3 - 8,82}{33,95e^{-9}} = 161,3 \text{ MPa}$$

The maximum tensile stress is calculated with Equation [6.5.6],

$$\sigma_{v,max} = \frac{F_{V,max} - F_{\Delta T+}}{A_0} = \frac{12129 - 179,6}{20,12e^{-6}} = 593,8 \text{ MPa}$$

Now the von Mises equivalent stress can be calculated using Equation [6.5.1],

$$\sigma_{v.m.} = \sqrt{\sigma_{v,max}^2 + 3 \cdot \tau_{max}^2} = \sqrt{593,8^2 + 3 \cdot 161,3^2} = 656,3 \text{ MPa}$$

The ultimate margin of safety on tightening is then calculated with Equation [6.5.8],

$$MoS_{ti,ult} = \frac{\sigma_{ult}}{\sigma_{v.m.}} - 1 = \frac{1100}{656,3} - 1 = 0,676$$

The next step in the analysis process is to check the shear pull-out of thread. Because the nut is made of the same material than the fastener (the nut is like the fastener made of A-286 steel.), the shear pull out of thread is not critical. Nevertheless, the following example shows a calculation of the nut's pull-out strength.

7.14.2 Thread Shear Pull-Out Example

The thread of joints that use normed nuts of the same material grade as the fastener (or higher) can always be at least as strong as the fastener itself. However, an example of thread pull-out for such a joint is documented here to show the analysis process.

First, the effective length of the engaged thread is calculated with Equation [7.10.3]. The effective engaged thread length l_{eff} of the LN 29693 anchor nut is 5 mm (although the fastener protrudes beyond the length of the nut).

$$L_{eng,eff} = L_{eng} - 2 \cdot p = 5 - 2 \cdot 1 = 3 \text{ mm}$$

Now, the failure surface areas of the threads are calculated with Equations [7.10.2] and [7.10.8]. The pitch diameter of the female thread, D_2 , is equal to that of the fastener, d_2 .

$$A_{th,n} = \pi \cdot d \cdot \left(\frac{L_{eng,eff}}{p} \right) \left[\frac{p}{2} + (d - D_2) \tan(\theta) \right] = \pi \cdot 6 \cdot \left(\frac{3}{2} \right) \left[\frac{1}{2} + (6 - 5,35) \tan(30) \right] = 49,48 \text{ mm}^2$$

$$A_{th,b} = \pi \cdot D_1 \cdot \left(\frac{L_{eng,eff}}{p} \right) \left[\frac{p}{2} + (d_2 - D_1) \tan(\theta) \right] = \pi \cdot 4,92 \cdot \left(\frac{3}{2} \right) \left[\frac{1}{2} + (5,35 - 4,92) \tan(30) \right] = 34,77 \text{ mm}^2$$

The female-to-male thread strength ratio is calculated with Equation [7.10.7],

$$R_S = \frac{\sigma_{ult,n} \cdot A_{th,n}}{\sigma_{ult,b} \cdot A_{th,b}} = 1 \cdot \frac{49,48}{34,77} = 1,423$$

Now, the empirical coefficients c_1 and c_3 are calculated using Equations [7.10.4] to [7.10.6]. The joint uses an anchor nut, and therefore the wrench size, s_w , is not defined. Therefore, in order to evaluate the constant c_1 , it is important to use the outer diameter of the anchor nut, which is 7,5 mm.

$$c_1 = 3,8 \left(\frac{s_w}{d} \right) - \left(\frac{s_w}{d} \right)^2 - 2,61 = 3,8 \times \left(\frac{7,5}{6} \right) - \left(\frac{7,5}{6} \right)^2 - 2,61 = 0,578$$

$$R_S \geq 1: c_3 = 0,897$$

Now the critical axial forces for shear pull-out of the female (nut) thread is determined with Equation [7.10.1],

$$F_{ult,th,n} = \tau_{ult,n} \cdot A_{th,n} \cdot c_1 \cdot c_3 = 655 \cdot 49,48 \cdot 0,578 \cdot 0,897 = 16,8 \text{ kN}$$

The empirical coefficient c_2 is calculated using Equation [7.10.14],

$$\begin{aligned} c_2 &= 5,594 - 13,682 \cdot R_S + 14,107 \cdot R_S^2 - 6,057 \cdot R_S^3 + 0,9353 \cdot R_S^4 \\ &= 5,594 - 13,682 \cdot 1,423 + 14,107 \cdot 1,423^2 - 6,057 \cdot 1,423^3 + 0,9353 \cdot 1,423^4 \\ &= 1,072 \end{aligned}$$

Now the critical axial forces for shear pull-out of the male (bolt) thread is determined with Equation [7.10.12],

$$F_{ult,th,b} = \tau_{ult,b} \cdot A_{th,b} \cdot c_1 \cdot c_2 = 655 \cdot 34,77 \cdot 0,578 \cdot 1,072 = 14,1 \text{ kN}$$

That gives all necessary input for the calculation of the margins of safety for thread failure under external and overall axial loads with Equations [7.10.16] and [7.10.17], with

$$F_{th,crit} = \min(F_{ult,th,n}, F_{ult,th,b})$$

$$MoS_{th,A} = \frac{F_{th,crit}}{F_A \cdot sf_{ult}} - 1 = \frac{14100}{1000 \cdot 2,3} - 1 = 5,131$$

$$MoS_{th,tot} = \frac{F_{th,crit}}{F_{V,max} + \Phi_n \cdot F_A \cdot sf_{ult}} - 1 = \frac{14100}{12129 + 0,1345 \cdot 1000 \cdot 2,3} - 1 = 0,134$$

With equivalent material class, the nut thread pull-out is not verified because covered by the screw strength.

7.15 References

7.1	G. Meyer & D. Strelow	Simple Diagrams Aid in Analysing Forces in Bolted Joints, Assembly Engineering, Jan. 1972, pp. 28-33
7.2	VDI - RICHTLINIEN	VDI 2230, Nov. 2015, Systematic Calculations of High Duty Bolted Joints
7.3	S.D. Rossides	Behaviour of a Simple Tension Joint with Fasteners Tightened into Yield, British Aerospace Report BT.12065 July 1981
7.4	J. Olmstead	Space Station SPDM Body Joint Load Factor Summary, MDA internal document

Eccentric Axially Loaded Joints

8.1 Effects of Eccentricity

8.1.1 Overview

In the case of an eccentrically fastened joint, such as shown in Figure 8-1, there are three important axes:

- the joint axis (O-O)
- the fastener axis (S-S)
- the axis of the external axial load (A-A)

The relative positions of these axes are defined two variables; the clamping eccentricity, s , and the loading eccentricity, a (see Figure 8-1).

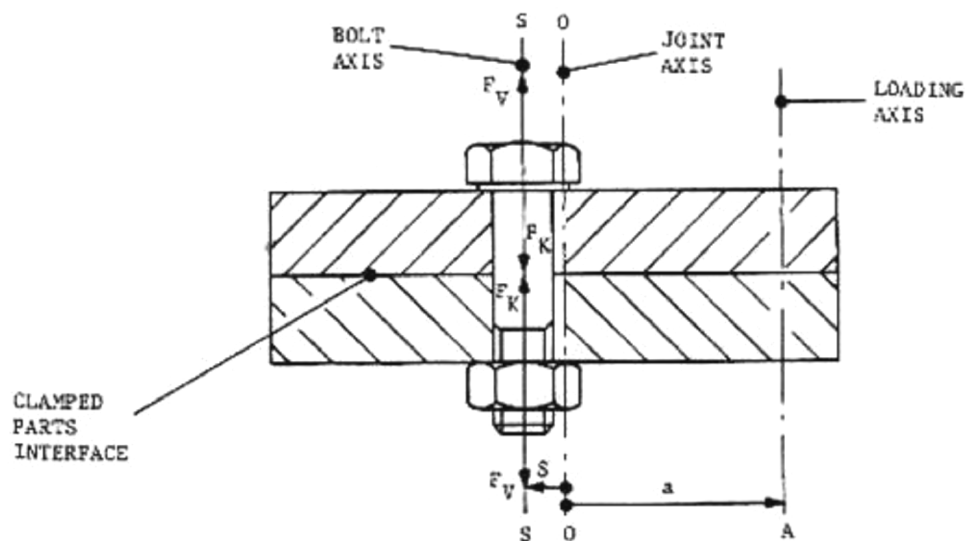


Figure 8-1 - A Typical Eccentric Joint

During assembly the fastener can be pretensioned causing an interface clamping pressure with a peak at (or near) the fastener axis (S-S) as shown in Figure 8-2. The joint axis (O-O) is defined to lie at the centroid of the interface pressure distribution. For eccentrically clamped joints the joint axis does not necessarily coincide with the fastener axis.

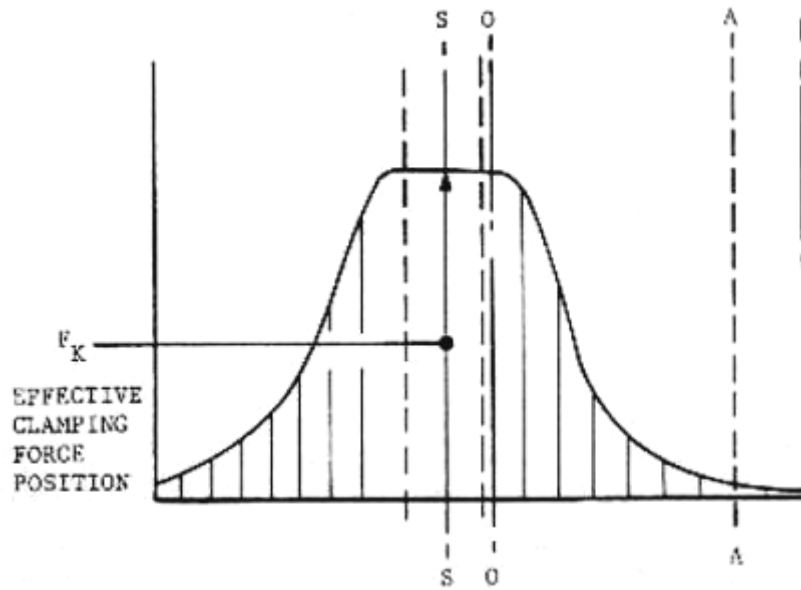


Figure 8-2 - Interface Pressure Distribution after Preloading

As the external eccentric tensile load $F_{A,1}$ is applied the reaction under the fastener head the centroid of interface pressure (joint axis) F_K moves away as indicated in Figure 8-3 and Figure 8-4. At the same time the centroid of the under-head reaction, $\Delta F_{b,A,1} + F_V$, moves towards the external load.

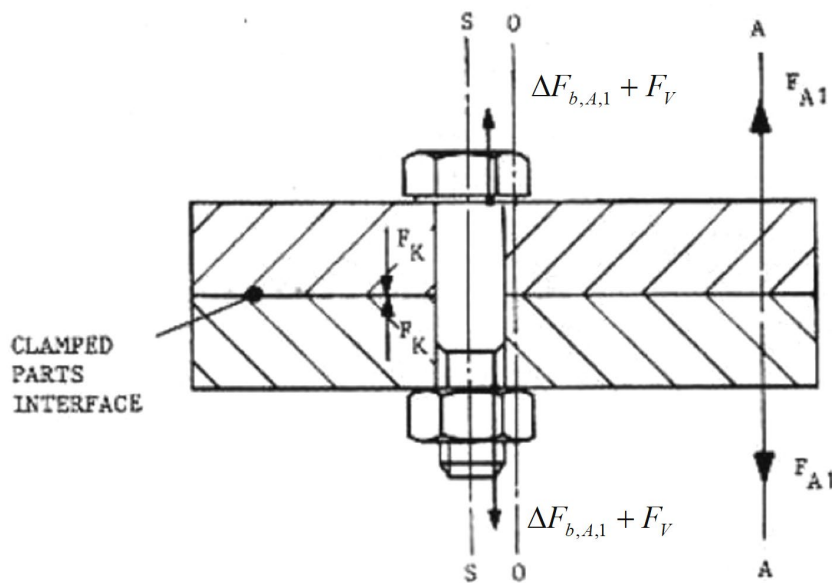


Figure 8-3 - Typical Joint Eccentrically Loaded

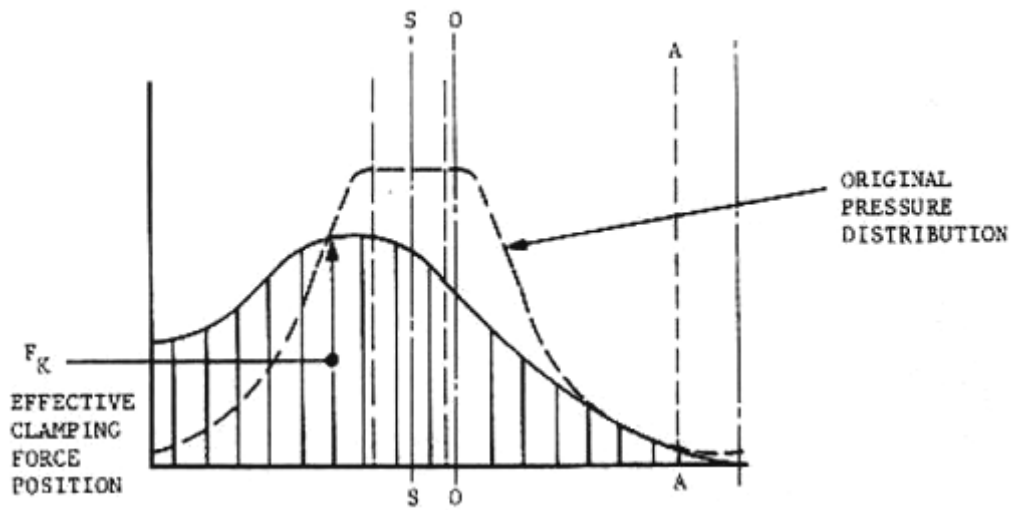


Figure 8-4 - Redistribution of interface pressure (with force F_{A1} not sufficient to cause gapping)

Figure 8-5 and Figure 8-6 show a typical interface pressure distribution caused by an eccentric load sufficient to cause one-sided opening of the joint. Such separation occurs if the axial load F_{A2} exceeds a certain value, which is dependent on the preload and the eccentricities, s and a . One-sided opening of the joint interface causes substantial increase in the fastener stress. This is discussed in Section 8.4 (see also References 8.1 and 8.2).

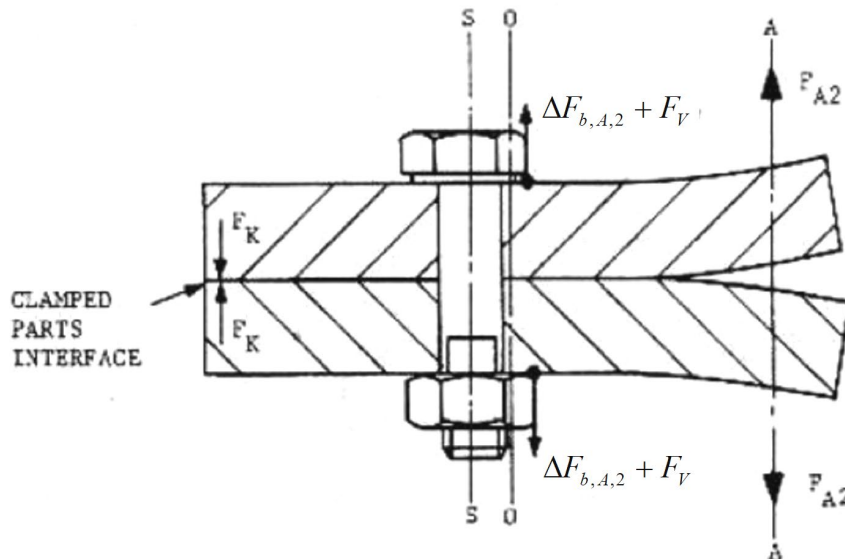


Figure 8-5 - An Eccentrically Loaded Joint with Gapping

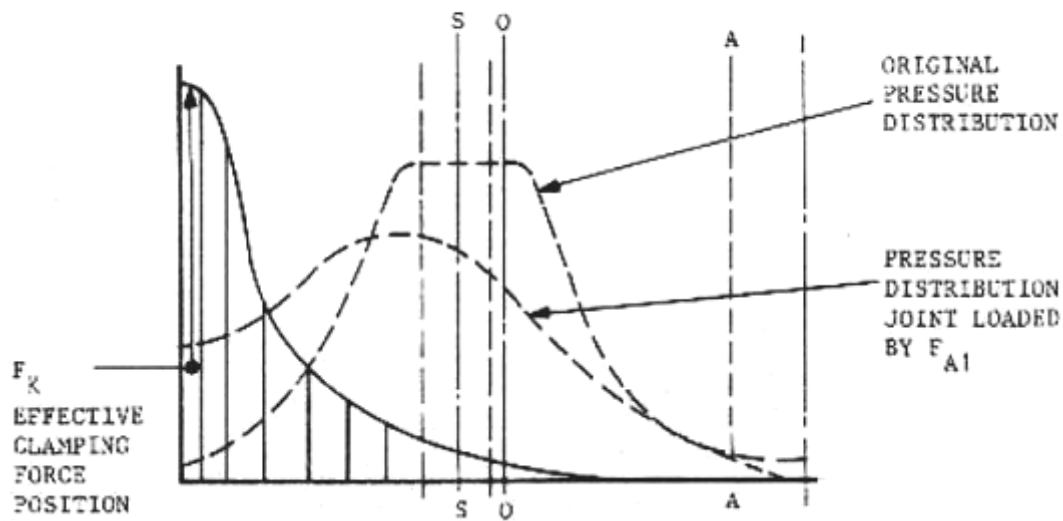


Figure 8-6 - Redistribution of Interface Pressure (Force F_{A2} Causes Gapping)

The joint indicated in Figure 8-1, Figure 8-3 and Figure 8-5 has flange contact surfaces that are relatively wide compared to the fastener diameter. Such joints are referred to as 'Joints With Large Areas of Contact', and the compliance equations are provided in Section 8.2.1.

Joints that employ a gasket, seal or sealing ring which is narrow with respect to the flange width, and with a flange that is stiff enough to prevent contact elsewhere on the interface surface, are referred to as 'Cantilevered Flange Joints' (see Figure 8-17). For such joints the interface pressure distribution does not significantly change with F_A and the compliance equations are given in Section 8.3.

8.1.2 Prying

In joints with eccentric loads, the fastener load increment due to the action of the external load is greater than that of the equivalent concentric joint. This effect is often called prying or prising. Reference 8.3 provides some analytical methods and examples of this effect.

8.2 Joints with Large Areas of Contact

8.2.1 Compliance of the Clamped Parts

8.2.1.1 Overview

The equations for calculating the compliance of the clamped parts in the concentric loading case were given in Section 7.6. The eccentric case is more complicated since, in addition to longitudinal deformation, the eccentricity of the external load produces bending deformations in the flanges leading to additional extension of the joint. Hence, the longitudinal compliance of the flanges in an eccentric joint is greater than that of a concentrically loaded joint. Also, for joints with large areas of contact, the distribution of the clamping pressure depends on the magnitude of the external load (as discussed in Section 8.1), producing further changes in compliance.

A relatively simple analysis (modified from Reference 8.4) of eccentric joint deformation is possible if the following assumptions are made:

- The clamped parts form a prismatic bending solid
- There is no one-sided gapping (i.e. the interface pressure is always positive)
- All the cross-sections of this prismatic solid remain flat under loading
- A linear stress distribution is established in these cross-sections
- The bending resistance of the fastener is much lower than that of the bending solid and **can** be neglected

These simplifying assumptions limit the joints that can be considered to those in which the interface area loaded by one fastener, A_j , is not much greater (3 to 5 times) the underhead area. Serious errors can occur if larger areas are assumed (see Reference 8.2). Additionally, **it is important that** the joint's transverse width, C , and clamping eccentricity, s , satisfy the following relations:

$$C \leq (D_{uh,brg} + h_{min}) \quad [8.2.1]$$

$$s \leq \frac{(D_{uh,brg} + h_{min})}{2} \quad [8.2.2]$$

where C is the distance from the fastener joints axis to the flange edge as indicated in Figure 8-7. **It is important that** joints that do not satisfy these criteria **are** analysed using FEM or testing.

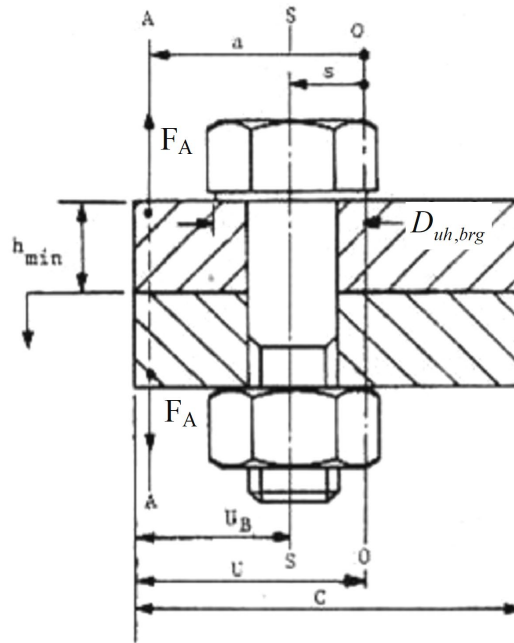


Figure 8-7 - Limitations of the Eccentric Joint Analysis Method

In a multi-fastener joint such as Figure 8-8 the spacing between fasteners (fastener pitch) is defined as t , and the flange length assumed to be loaded by each fastener is defined as b , which is assumed to be given by,

$$b = \begin{cases} D_{uh,brg} + h_{min} & \text{if } t > (D_{uh,brg} + h_{min}) \\ t & \text{if } t \leq (D_{uh,brg} + h_{min}) \end{cases} \quad [8.2.3]$$

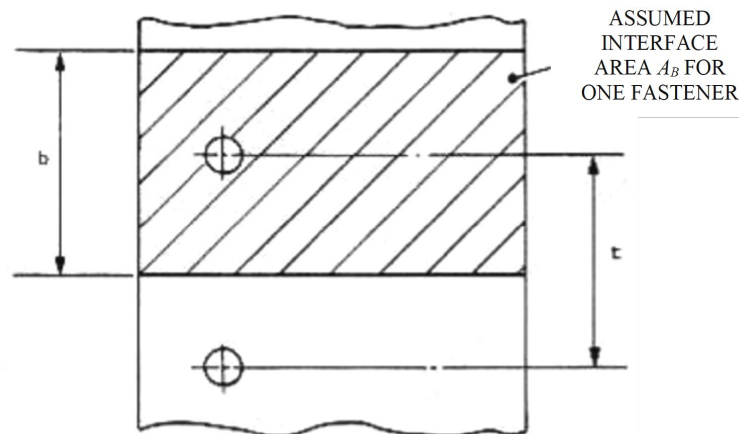


Figure 8-8 - The Interface Area for Multiple Fastener Joints

The clamped interface area shown in Figure 8-8 has an area, $A_c = b.C$, and a radius of gyration,

$$G_c = \left[\frac{I_c}{A_c} \right]^{\frac{1}{2}} \quad [8.2.4]$$

where I_c is the second moment of area of the clamped interface (about its neutral axis), which is given by $bt^3/12$ for the interface shown in Figure 8-8.

Subject to the above assumptions, clamped parts compliance values can be calculated for the two classes of eccentric joints shown in the following [sections](#).

8.2.1.2 Eccentric Joints Loaded at the Fastener Axis

This class of joints has the external load is introduced at the fastener axis (i.e. $s = a$), as shown in Figure 8-9.

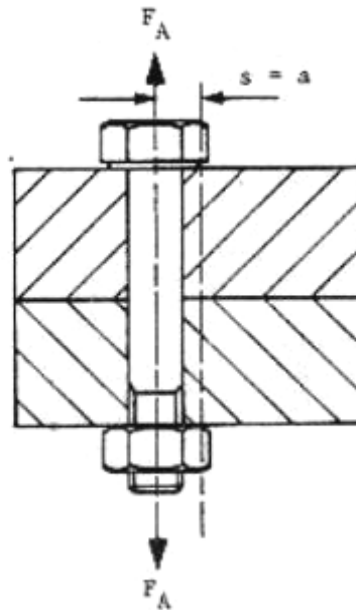


Figure 8-9 - An Eccentrically Loaded Joint where $s = a$

The compliance of the clamped parts, δ_c^* , is higher than δ_c and is calculated by multiplying the compliance of an equivalent concentric joint by an eccentricity factor, according to,

$$\delta_c^* = \delta_c \left[1 + \frac{s^2}{\frac{G_c^2 A_c}{A_{sub}}} \right] \quad [8.2.5]$$

which can be written in a more simple form as,

$$\delta_c^* = \delta_c (1 + \lambda^2) \quad [8.2.6]$$

where λ is the length ratio given by,

$$\lambda = \frac{s / G_c}{\sqrt{A_c / A_{sub}}} \quad [8.2.7]$$

where A_{sub} , is the effective clamping area defined below in [Section 8.2.1.4](#).

8.2.1.3 General Case of an Eccentric Joint

This (more general) class of joints is shown in [Figure 7.2.4](#), and has clamped parts compliance given by,

$$\delta_c^{**} = \delta_c \left(1 + \frac{a}{s} \lambda^2 \right) \quad [8.2.8]$$

where; λ is defined by equation [8.2.7].

The value of a in equation [8.2.8] is always taken as positive. The value of s is positive if S-S and A-A are on the same side of O-O or negative if they are on opposite sides. Thus, δ_c^{**} can be either greater than or less than δ_c .

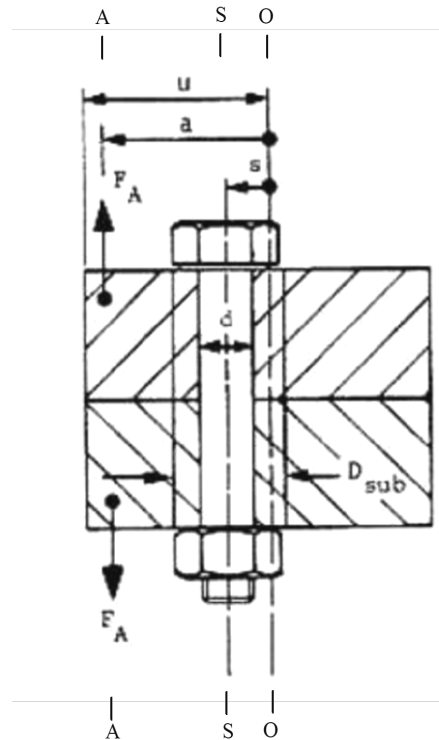


Figure 8-10 - The General Eccentrically Loaded Joint

8.2.1.4 The Effective Clamping Area

The effective clamping area, A_{sub} , used in equation [8.2.7] is the cross-sectional area of the assumed compression zone (see Section 7.6.2) at its greatest extent, and is calculated as follows,

- a. For a clamped sleeve with narrow flanges with $D_{avail} \leq D_{lim}$,

$$A_{sub} = \frac{\pi}{4} (D_{lim}^2 - d^2) \quad [8.2.9]$$

- b. For wide flanges with $D_{avail} > 3D_{lim}$;

$$A_{sub} = \frac{\pi}{4} \left[\left[D_{uh,brg} + \frac{L_c}{10} \right]^2 - d^2 \right] \quad [8.2.10]$$

- c. For the intermediate case with $D_{lim} < D_{avail} \leq 3D_{lim}$

$$A_{sub} = \frac{\pi}{4} (D_{uh,brg}^2 - d^2) + \frac{\pi}{8} \left[\frac{D_{lim}}{D_{uh,brg}} - 1 \right] \left[\frac{D_{uh,brg} L_c}{5} + \frac{L_c^2}{100} \right] \quad [8.2.11]$$

8.2.2 The Joint Diagram

The joint diagram developed for concentric joints in Section 7 can also be used to describe the characteristics of eccentric axially loaded joints.

Triangle S_1, V_1, P_1 of Figure 8-11 represents the preloaded condition where the fastener tension F_b is equal and opposite to the compressive load on the clamped parts F_K . As the external eccentric load F_A increases from zero the fastener extends under the partial load $\Delta F_{b,A,1}$. This causes the clamped parts to lose compression linearly until the point when the joint begins to separate at the side nearest the load F_A . During this phase the straight line V_1 to H_1 represents the behaviour of the clamped parts. If F_A is further increased, the joint characteristics change to that of a hinge and lever producing a nonlinear load-deflection response of the clamped parts. The fastener therefore feels a high proportion of the external load $\Delta F_{b,A,1}$ than predicted by extrapolation of the line V_1H_1 .

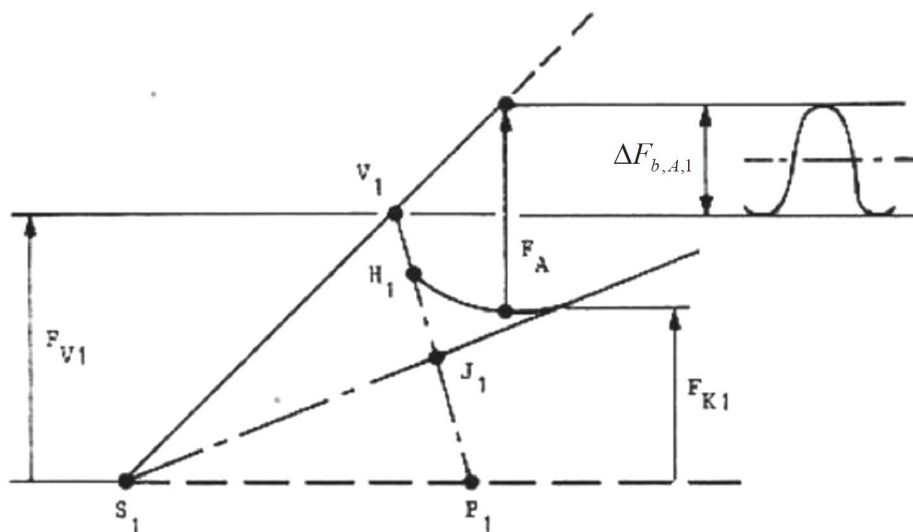


Figure 8-11 - The Joint Diagram for Eccentrically Loaded Joints showing the Non-Linearity of the Clamped Parts

Figure 8-12 shows the load increment in the fastener due to the same dynamic external load F_A , and illustrates the fact that higher preload (indicated by F_{V2}) delay the onset of separation and thus $(V_1 - H_1) < (V_2 - H_2)$. The figure also indicates that, after one-sided opening commences, the higher the preload reduces the load increment in the fastener, i.e. $\Delta F_{b,A,2} < \Delta F_{b,A,1}$.

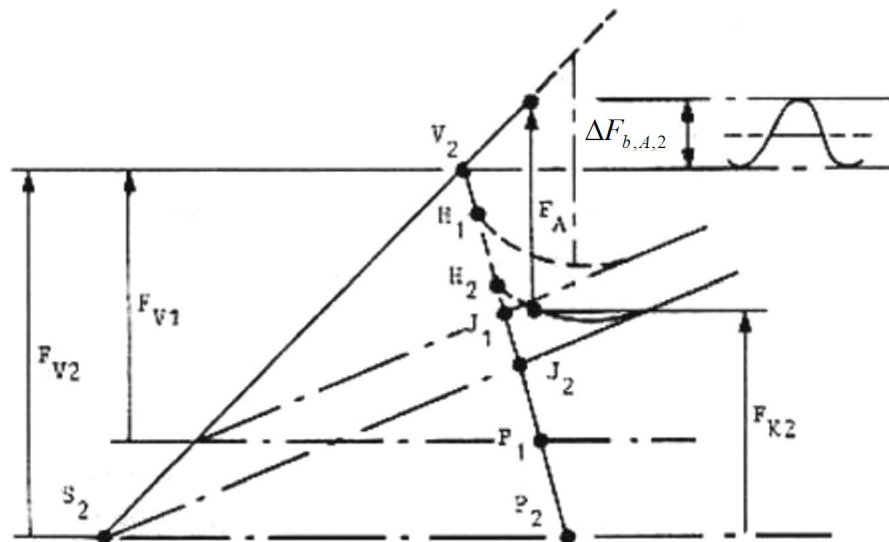


Figure 8-12 - Joint Diagram with a Higher Preload

8.2.3 The Force Ratio

For an eccentric axially loaded joint with a large contact area, assuming the clamped parts behave linearly, it can be shown that the force ratio, $\Phi_{e,n}$, prior to one-sided opening is given by,

$$\Phi_{e,n} = n_{ecc} \left[\frac{\delta_c^{**}}{\delta_b + \delta_c^*} \right] \quad [8.2.12]$$

where δ_c^* and δ_c^{**} are defined in Section 8.2.1, and n_{ecc} is defined below in Section 8.2.4.

As was the case for concentric joints, the force ratio is used to determine the incremental loads experienced by the fastener and clamped parts due to the externally applied force according to the relations; $\Delta F_{b,A} = \Phi_{e,n} F_A$ and $\Delta F_{c,A} = (1 - \Phi_{e,n}) F_A$.

The difference in the force ratio compared with that of the equivalent concentric joint is the quantitative consequence of the “prying” effect (see Section 8.1.2).

8.2.4 Loading Plane Factor

For eccentric axially loaded joints, the loading factor derived in Section 7.7 need to be corrected. The assumption is made that all cross-sections stay planar during deformations of the joint. First the loading plane factor has to be determined for a theoretical joint, where the fastener’s longitudinal axis is moved to a point that leads to a concentric axially loaded joint. Then the eccentric loading plane factor is calculated with,

$$n_{ecc} = \frac{n_{con} + a s \frac{L_c}{E_c I_c}}{1 + s^2 \frac{L_c}{E_c I_c}} \quad [8.2.13]$$

where; n_{con} is the concentric loading plane factor from Section 7.7.

8.2.5 The Interface Opening Limit

Figure 8-13 shows the limiting value of the external load, $F_{A,sep}$, at which the interface begins to open. This is calculated by,

$$F_{A,sep} = \frac{F_V}{\left[1 + \frac{au}{G_c^2}\right] \left[1 + \frac{su}{G_c^2}\right] - \Phi_{e,n}} \quad [8.2.14]$$

where u is the eccentricity of the point of first gapping (relative to the joint axis O-O).

Conversely for a given external load, F_A , there can be a value of preload, $F_{V,sep}$, at which one-sided opening can just occur,

$$F_{V,sep} = F_{K,sep} + (1 - \Phi_{e,n})F_A \quad [8.2.15]$$

where $F_{K,sep}$ is the clamping force at the onset of interface gapping as given by,

$$F_{K,sep} = \frac{(a-s)u}{G_c^2 + su} F_A \quad [8.2.16]$$

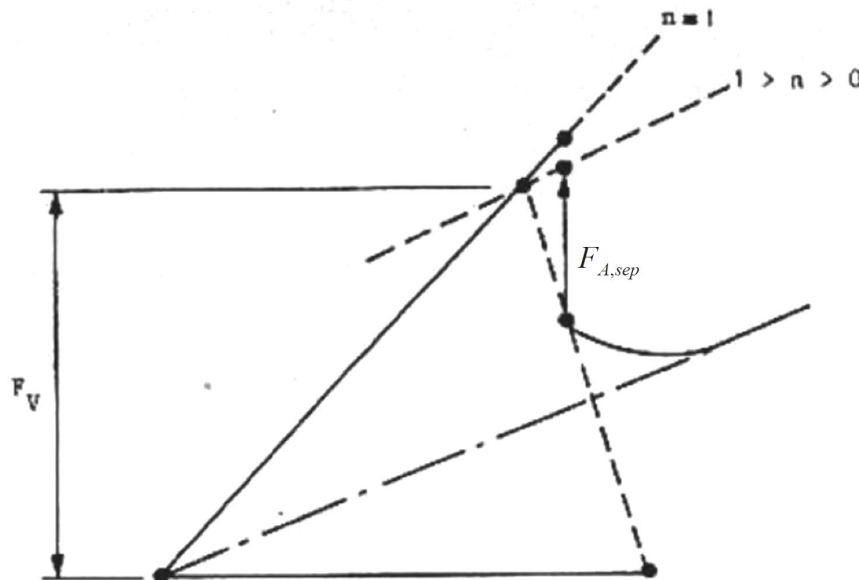


Figure 8-13 - An Eccentrically Joint Loaded to the Interface Opening Limit with the Loading Plane Inside the Joint

See Reference 8.4 for the derivation of the equations [8.2.14] and [8.2.15].

8.2.6 Preload Considerations

8.2.6.1 Preload Scatter

The effects of preload scatter due to friction variables during assembly are the same for eccentric joints as for concentric joints, and are described in Section 6.

8.2.6.2 Preload Loss

Embedding, as described in Section 6.4.2, mainly occurs after preloading but before external loading is applied. The amount of embedding preload loss for an eccentric joint can be calculated as for a concentric joint from,

$$F_z = \frac{f_z(1 - \Phi_{e,n})}{\delta_c} \quad [8.2.17]$$

where f_z is the plastic deformation caused by embedding as given by Table 6-3, and $\Phi_{e,n}$ is the force ratio.

8.3 Cantilevered Flange Joints

8.3.1 Overview

These joints have small contact areas at the interstice, leading to bending moments being transmitted through the flange. This results in the axis of the clamped parts being fixed rather than moving with change in external load F_A (the case for joints with large areas of contact).

For this class of joints, the procedure for determining the flange compliance can be complex and time consuming. The theory presented in the following Sections applies to the special case of circular joints with cantilevered flanges. For more general cases with non-circular flanges it is recommended to use testing or FEM.

8.3.2 Compliance of Circular Flanges

8.3.2.1 Overview

References 8.3 and 8.5 give empirical relationships for joints with cantilevered circular flanges. This category of joints often occurs when gaskets or sealing rings are used.

8.3.2.2 Linear Superposition of Deformations

For cantilevered flange joints, three compliances are used in combination to describe the flanges' bending displacements. Figure 8-14 indicates three modes of deformation that determine the deflections of the flange between the axis of the fastener and the axis of the clamped parts. These compliances are calculated as follows:

$$\delta_1 = \frac{\Delta L_1}{F_V} \quad \text{This is the compliance of the flanges under the preload taking into account the bending effects due to the eccentric clamping load.} \quad [8.3.1]$$

$$\delta_2 = \frac{\Delta L_2}{\Delta F_{b,A}} \quad \text{This is the bending compliance of the flanges due to the corresponding portion of the applied load seen by the fastener. In other words it is the flange bending due to the couple } \Delta F_{b,A} \text{ with forces acting at the axes of the fastener axis and externally applied load.} \quad [8.3.2]$$

$$\delta_3 = \frac{\Delta L_3}{\Delta F_{c,A}} \quad \text{This is the bending compliance of the flanges due to the load seen by the clamped parts and the corresponding portion of the applied load. In particular, it is the flange bending due to the couple } \Delta F_{c,A} \text{ with forces acting at the axes of the clamped parts and the externally applied load.} \quad [8.3.3]$$

Assuming no gapping occurs, the elongation of the flange due to the external load is the linear sum of the three extension modes of Figure 8-14, i.e.,

$$\Delta L_{c,A} = \Delta L_3 + \Delta L_2 + \Delta L_{b,A} \quad [8.3.4]$$

Thus the compliance of the flange is,

$$\delta_c = \frac{\Delta L_3 + \Delta L_2 + \Delta L_{b,A}}{\Delta F_{c,A}} \quad [8.3.5]$$

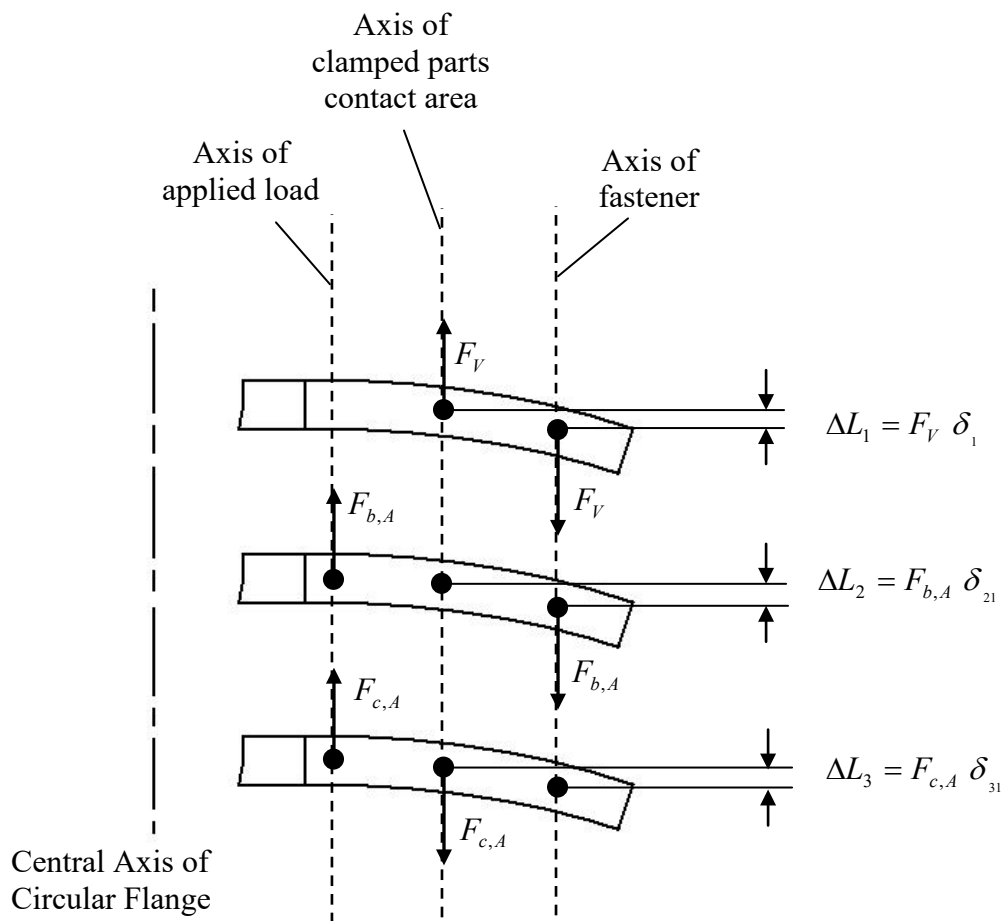


Figure 8-14 - Definition of Flange Compliance due to Bending Loads at Different Points

Two types of flanges are frequently employed for circular joints, fixed flanges and loose flanges. Fixed flanges are rigidly connected to the remaining structures. Loose flanges are separate annular rings that compress the mating parts together. The following two Sections provide analytical equations for the compliance of both types of flanges.

8.3.2.3 Compliance of Fixed Circular Flanges

Figure 8-15 shows a typical fixed flange with a small contact area such as a sealing ring. For this type of flange the three compliances of Figure 8-14 are given by the following equations (see Reference 8.5):

$$\delta_1 = \psi a_D^2 \quad [8.3.6]$$

$$\delta_2 = \psi a_D a_R \quad [8.3.7]$$

$$\delta_3 = \psi a_D (a_R - a_D) \quad [8.3.8]$$

where ψ is the inversion compliance (defined in Section 8.3.2.5 below).

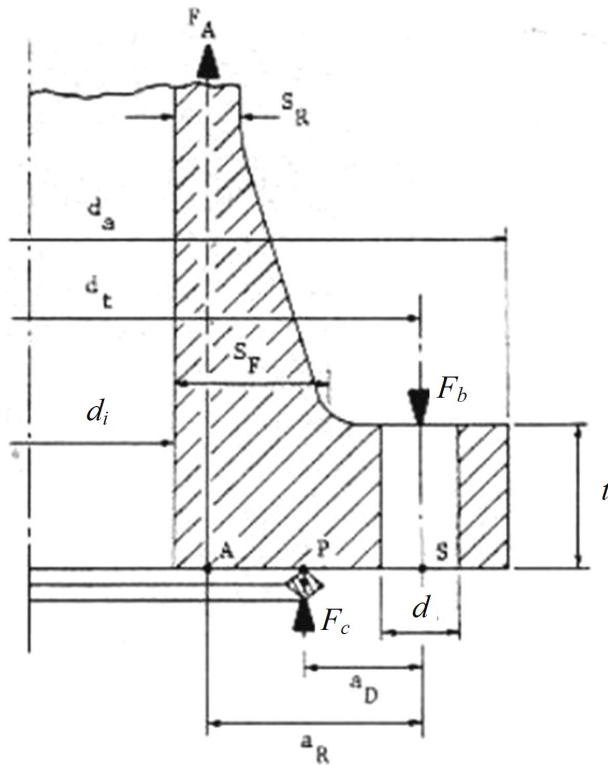


Figure 8-15 - Dimensions of a Fixed Circular Flange (with a Weldneck)

In general, the contacting interstice between the fixed flanges can be either a large area or a small area. Only the case of the small contact area is considered in this theory.

8.3.2.4 Compliance of Loose Circular Flanges

Figure 8-16 shows the bending dimensions and bending deformations of a loose circular flange. For this flange the joint axis (O-O) and the external load axis (A-A) are generally coincident and as a result δ_3 is zero. Thus, the bending deformation due to an external load F_A is only due to the increase in fastener load $\Delta F_{b,a}$ and is given by,

$$\Delta L = \Delta F_{b,a} \psi a_F^2 \quad [8.3.9]$$

This is rearranged to give the flange compliance,

$$\delta_c = \frac{\Delta L}{F} = \psi a_F^2 \quad [8.3.10]$$

where ψ is the inversion compliance (defined in Section 8.3.2.5 below).

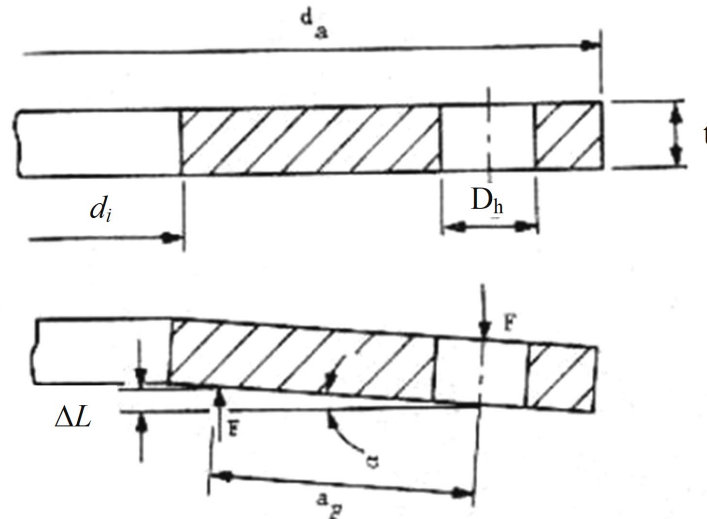


Figure 8-16 - Bending Deformation of Circular Loose Flange

8.3.2.5 Inversion Compliance

The inversion compliance, ψ , is given by,

$$\psi = \frac{d_a + d_i}{4\pi E h W} \quad [8.3.11]$$

where W is a factor accounting for the presence of the holes in the flange given by,

$$W = \frac{1}{12}(d_a - d_i - d^*)h^2 \quad (\text{for loose flanges}) \quad [8.3.12]$$

$$\text{or} \quad \frac{1}{12}(d_i + S_F)S_F^2 + \frac{1}{12}(d_a - d_i - d^*)h^2 \quad (\text{for fixed flanges}) \quad [8.3.13]$$

where d_a and d_i are flange annulus' outer and inner diameters (see Figure 8-15 and Figure 8-16), S_F is the radial thickness of the weldneck (see Figure 8-15), h is the thickness of the flange, and d^* is defined by,

$$d^* = \begin{cases} \frac{d}{2} & \text{for } W_{nom} \geq 500 \\ \left(1 - \frac{W_{nom}}{1000}\right)d & \text{for } W_{nom} < 500 \end{cases} \quad [8.3.14]$$

where d is the diameter of the fastener holes, and W_{nom} is the flange nominal width specified in mm.

8.3.3 Force Ratio for Circular Cantilever Flanges

8.3.3.1 Single Flange

Consider a weld neck flange such as the one illustrated in Figure 8-15, fastened to an infinitely stiff surface such that only the flange undergoes bending deflections. During preloading the fastener extends by ΔL_b and the flange deflects by,

$$\Delta L_1 = \delta_1 F_V \quad [8.3.15]$$

When the external load F_A is added the fastener is stretched by,

$$\Delta L_{b,A} = \delta_b \Delta F_{b,A} \quad [8.3.16]$$

The force ratio for the cantilevered flange joint, Φ_C , can be defined as follows,

$$\Phi_C = \frac{\Delta F_{b,A}}{\Delta F_{b,A} + \Delta F_{c,A}} = \frac{1}{\left(1 + \frac{\Delta F_{c,A}}{\Delta F_{b,A}}\right)} \quad [8.3.17]$$

Using Equations [8.3.1], [8.3.2], [8.3.3] and [8.3.5],

$$\Delta F_{b,A} (\delta_b + \delta_2) = \Delta F_{c,A} (\delta_c - \delta_3) \quad [8.3.18]$$

Therefore, combining Equations [8.3.17] and [8.3.18] the force ratio expressed as a function of the compliances is,

$$\Phi_C = \left[1 + \frac{\delta_b + \delta_2}{\delta_c - \delta_3}\right]^{-1} \quad [8.3.19]$$

For loose flanges where the clamping load and applied load are coincident $\delta_3 = 0$ and Equation [8.3.19] is simplified to,

$$\Phi_C = \left[1 + \frac{\delta_b + \delta_2}{\delta_c}\right]^{-1} \quad [8.3.20]$$

8.3.3.2 Twin Flanges

The compliances derived in sections 8.3.2.2, 8.3.2.3, 8.3.2.4 and 8.3.2.5 are for individual cantilevered flanges. In many cases, the joint has two symmetric cantilevered flanges. For such a joint, with fixed flanges and m bolts the force ratio is given by,

$$\Phi_C = \left[1 + \frac{\delta_b/m + 2\delta_2}{\delta_c - 2\delta_3}\right]^{-1} \quad [8.3.21]$$

where δ_b and δ_c include the effects of both flanges and the increased L_c (unlike those values used in the above sections 8.3.2.2 to 8.3.2.5).

For loose flanges, $\delta_3 = 0$, and Equation [8.3.21] becomes simplified to,

$$\Phi_C = \left[1 + \frac{\delta_b/m + 2\delta_2}{\delta_c}\right]^{-1} \quad [8.3.22]$$

where δ_b and δ_c are redefined to account for both flanges, as in equation [8.3.21].

8.3.4 Simplified Joint Diagram for Eccentric Joints

8.3.4.1 Overview

Consider a weld neck type flange, as shown in Figure 8-15 with m bolts. If the fasteners are equally preloaded by F_v/m and consequently stretched by $(\delta_b F_v)/m$, the two flanges can bend by $2\delta_1 F_v$ while also being compressed by $(\delta_c F_v)/m$. This preloading is represented in the joint diagram of Figure 8-17 by the triangle SPV .

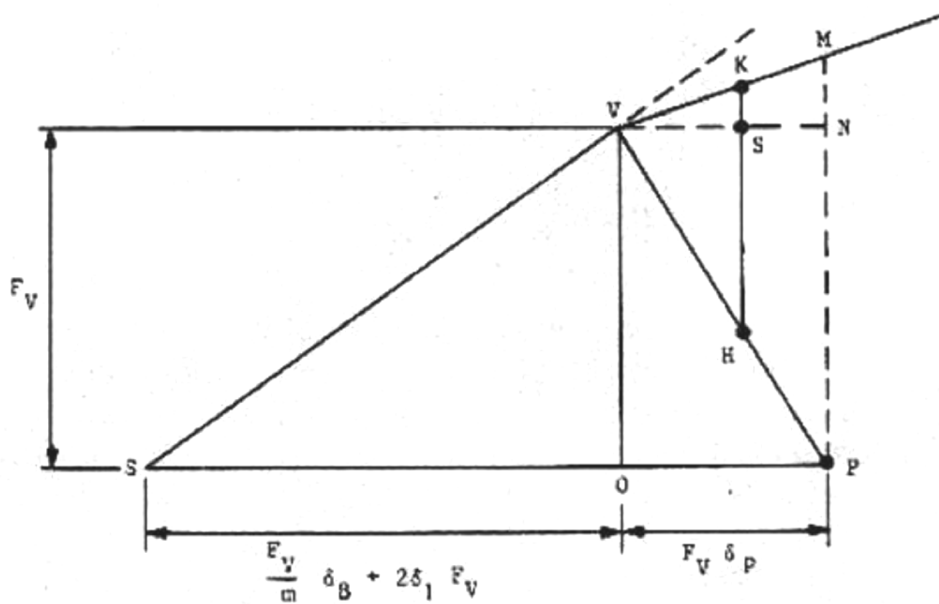


Figure 8-17 - Simplified Joint Diagram for Cantilevered Flanged Joints

8.3.4.2 Onset of Separation

Separation occurs when the preload reduces to zero, which is represented by the line PM in Figure 8-17.

At the onset of separation $F_A = |PM|$ (where $|MN|$ is equal to $\Delta F_{b,A}$ and $|NP|$ is equal to $\Delta F_{c,A}$).

Thus,

$$\Delta F_{c,A} = F_v \quad [8.3.23]$$

8.3.5 Joint Diagram for Eccentric Nonlinear Joints

In the case of symmetrically flanged joint with a gasket or seal which has non-linear deformation characteristics, the clamped parts compliance δ_c is dependent upon the load.

Assuming m fasteners, Equation [8.3.23] can be rearranged to give;

$$\Delta F_{b,A} = \left(\frac{\delta_c - \delta_3}{\delta_b/m + \delta_2} \right) \Delta F_{c,A} = \frac{\Delta L_{c,A} - \Delta F_{c,A} \delta_3}{\delta_b/m + \delta_2} \quad [8.3.24]$$

Since $\Delta L_{c,A}$ and $\Delta F_{c,A}$ are nonlinear, the joint diagram is also linear. To construct the joint diagram, a range of values of $\Delta L_{c,A}$ are assumed and using the gasket characteristics, the corresponding values of $\Delta F_{c,A}$ can be determined. Hence, the values of $\Delta F_{b,A}$ can be calculated and used to construct the joint diagram.

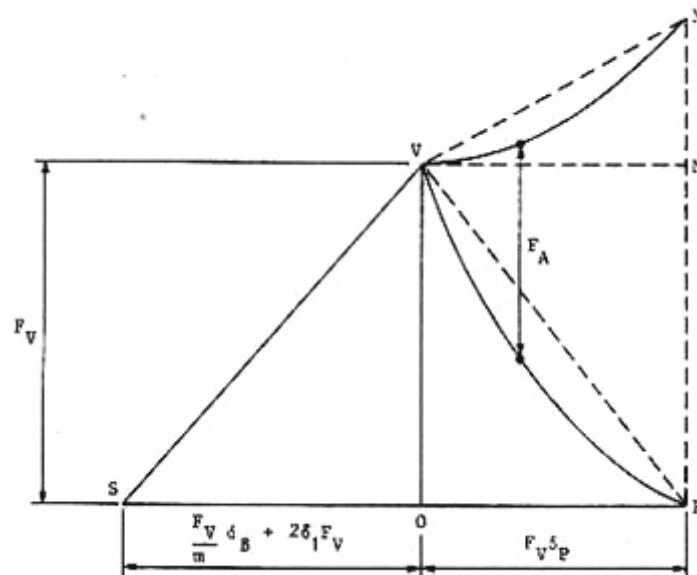


Figure 8-18 - The Joint Diagram for Non-Linear Gasket Joints

8.4 Fastener Loads in Eccentric Joints

8.4.1 Bending Moments

8.4.1.1 Overview

The bending moment in an eccentric joint causes bending stress in the fastener. This stress needs to be considered in addition to the direct stresses caused by F_A and $\Delta F_{b,A}$ and be taken into account, particularly when determining the fatigue endurance limit.

Considering the loads acting on the upper clamped part of Figure 8-19, the sum of moments about the joint axis O-O is,

$$M = F_A a - \Delta F_{b,A} s - F_V s \quad [8.4.1]$$

The change in M due to the externally applied load F_A is given by the first two terms in the right hand side of Equation [8.2.17]. Thus, the increment to the moment can be written as,

$$\Delta M_A = F_A a - \Delta F_{b,A} s = \left(1 - \frac{s}{a} \Phi_{e,n}\right) a F_A \quad [8.4.2]$$

According to Reference 8.3 this moment increment is partly absorbed by the clamped parts, as $\Delta M_{c,A}$, and partly by the fastener as $\Delta M_{b,A}$ (as is the case for axial loads), according to the ratio of the bending compliances. This leads to the relation,

$$\Delta M_{b,A} = \Delta M_A \left[\frac{1}{1 + \beta_b / \beta_c} \right] \quad [8.4.3]$$

which can be simplified for $\beta_b \gg \beta_c$ to give,

$$\Delta M_{b,A} \approx \frac{\beta_c}{\beta_b} \Delta M_A \approx \frac{\beta_c}{\beta_b} \left(1 - \frac{s}{a} \Phi_{e,n}\right) a F_A \quad [8.4.4]$$

where β_c is the bending compliance of the clamped parts given by,

$$\beta_c = \frac{L_c}{G_c^2 A_c E_c} \quad [8.4.5]$$

and β_b is the bending compliance of the fastener given by,

$$\beta_b = \frac{1}{E_b} \sum_i \frac{L_i}{I_i} \quad [8.4.6]$$

where L_i is the length of the i 'th segment of the fastener, and I_i is the second moment of area of the i 'th segment of the fastener, and E_b is the young's modulus of the fastener.

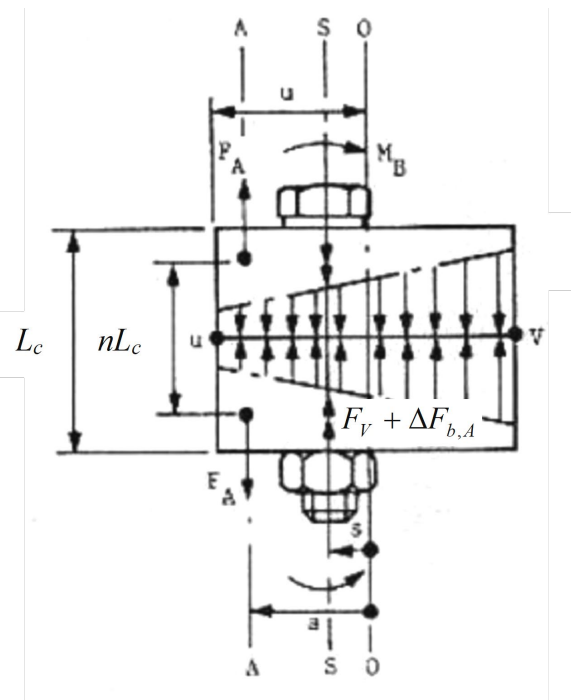


Figure 8-19 - Idealised Linear Pressure Distribution across an Eccentrically Loaded Joint's Interface

8.4.1.2 Fastener Stress under Combined Axial and Bending Loads

The determining factor for the endurance limit of the fastener in an eccentrically loaded joint is generally the nominal stress σ_{nom} . This arises from the longitudinal force $\Delta F_{b,A}$ and the moment $\Delta M_{b,A}$ for the tension fibre subject to the greatest stress in the minor cross-section at the first load-bearing thread turn. This is calculated from,

$$\sigma_{nom} = \sigma_{axial} + \sigma_{bending} \quad [8.4.7]$$

$$\begin{aligned} &= \frac{\Delta F_{b,A}}{A_3} + \frac{\Delta M_{b,A}}{I_3} \frac{d_3}{2} \\ &= \Phi_{e,n} \frac{F_A}{A_3} + \frac{\beta_c}{\beta_b} \left(1 - \frac{s}{a} \Phi_{e,n} \right) a \frac{F_A}{I_3} \frac{d_3}{2} \end{aligned}$$

Substituting for β_c , β_b and A_3 , [8.4.7] can be rewritten as,

$$\sigma_{nom} = \left[1 + \left(\frac{1}{\Phi_{e,n}} - \frac{s}{a} \right) \frac{L_c}{L_{sub}} \frac{E_b}{E_c} \frac{a \pi d_3^3}{8 A_c G_c^2} \right] \frac{\Phi_{e,n} F_A}{A_3} \quad [8.4.8]$$

where; the expression to the right of the brackets is the stress arising only from the force $\Delta F_{b,A}$, and the expression in brackets is its relative increase as a result of the additional bending stress.

8.5 References

8.1	G.H. Junker & P.W. Wallace	The Bolted Joint: Economy of Design Through Improved Analysis and Assembly Methods, Proc. Instn. Mech. Engrs. Vol. 198B No. 14., 1984
8.2	AGATONOVIC P	Beitrag zur Berechnung von Schrauben-Verbindungen, Drahtwelt S8, Part 2 P. 130-137, 1972
8.3	Wheeler A.T., Clarke M. J., Hancock G. J., Murray T. M.	Design Model for Bolted Moment End Plate Connections using Rectangular Hollow Sections, University of Sydney, Centre for Advanced Structural Engineering, June 1997.
8.4	VDI 2230, Nov. 2014 , VDI - RICHTLINIEN	Systematic Calculations of High Duty Bolted Joints
8.5	VDI 2505	Calculation of Flanged Joints

Shear Loaded Joints

9.1 Introduction

9.1.1 Overview

Shear loaded joints are often used to connect sheet or plate material and usually have multiple fasteners. These types of joints transmit loads transverse to the longitudinal of the fastener. A typical shear joint is illustrated in Figure 9-1.

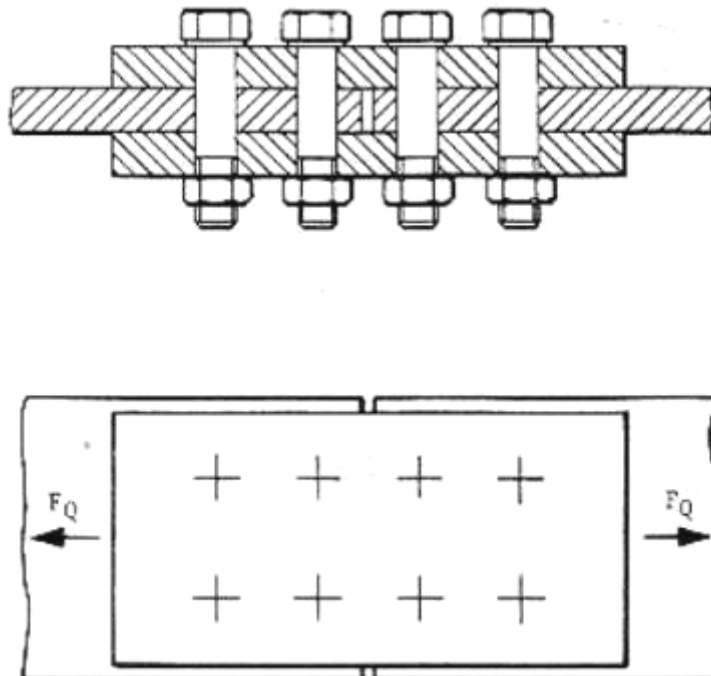


Figure 9-1 - Typical Double Lap Shear Joint

Shear loaded joints can be designed according to two fundamentally different philosophies.

- a. Friction grip (or slip resistant) design
- b. Bearing type (or slipped joint) design

As the name suggests, friction grip joints rely on friction between the flanges to transmit the shear loads. Bearing joints rely on the fasteners to transmit the shear loads, which are generated at the interface between the fastener shank and the flange hole.

In practice joints can generally behave as friction grip joints until the load is sufficiently high to slip the flanges. Figure 9-2 shows a typical force vs. extension curve for a shear joint showing how a friction grip joint can “slip” into a bearing joint configuration as the transverse force F_Q increases. The extent of the deformation occurring during the slip depends on the fastener pattern, the hole clearance and the alignment of the holes.

For the reasons explained below in Section 9.2.1, when feasible, friction grip design is the preferred option for joints in spacecraft structures.

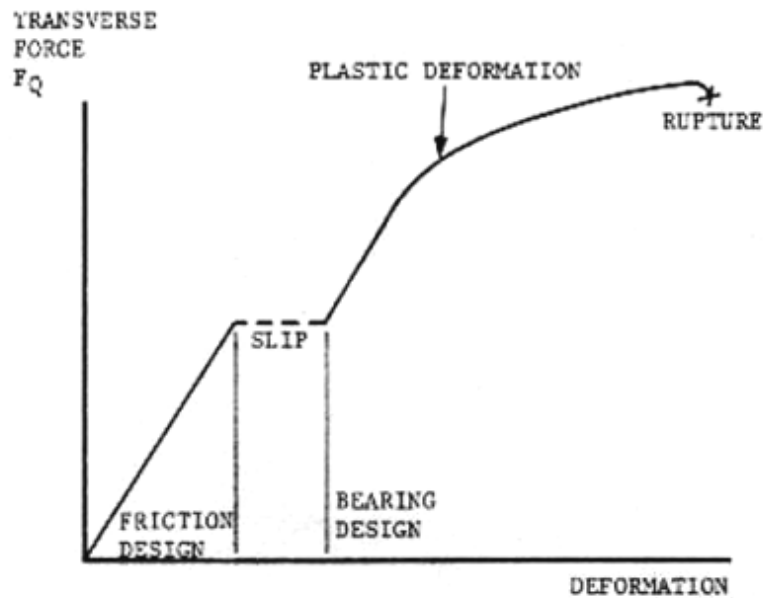


Figure 9-2 - Load Deformation Curve for a Fastener in Direct Shear

9.1.2 Analysis Approach

Friction grip joints and bearing joints need analysis of different failure cases. The margins of safety related for shear loads that need to be calculated for each type of joint are summarised in Table 9-1.

Table 9-1 - Failure Modes of Shear Joint Types

Margin of safety	Friction grip joint	Bearing joint	Refer to section
Slipping	Yes	No	9.2.2
Fastener shear	No	Yes	9.3.2
Hole bearing	No	Yes	9.3.4
Flange net tension section	Yes	Yes	9.3.3
Flange crushing	Yes	No	7.11
Fastener combined bending and shear	No	Yes	[1]
[1] This failure mode is not covered in this version of the handbook.			

9.2 Friction Grip Joints

9.2.1 Design Principles

Friction grip design relies on a sufficiently high clamping force maintained by the fasteners to prevent transverse slippage of the clamped plates due to transverse load. It has the principal advantage that, providing slip does not occur, the fastener feels only the tensile preload in the case of symmetric joints (double shear and two faying surfaces) shown in Figure 9-3. In the unsymmetrical case of a single faying surface (single shear) shown in Figure 9-5 and Figure 9-6 the joint's deformation creates relatively small tension load in the fasteners, which is usually insignificant. This handbook addresses the load transfer by the friction between the clamped parts as a basic design principle. Note that this approach is not followed by other standards like, e.g., NASA-STD-5020 that, for human spaceflight missions, does not allow to use friction to react applied shear forces between the clamped parts for ultimate loads assessment.

There are also some other additional advantages provided by the friction grip design approach:

- Large clearance holes can be used, which facilitates manufacture, assembly and interchangeability.
- For stiffness and load transfer considerations the mating flanges in a friction grip joint can be treated as a single elastic body.
- In the absence of slip, vibration loosening does not occur.
- Friction grip design is simple to implement since the fastener preload, provided it is above the slip threshold, is not critical. Therefore, friction grip fasteners can be sized on tensile clamping strength alone.
- Since there is generally additional strength in the bearing load (at least before its ultimate failure), friction grip design can be considered "fail-safe".

It is important that for friction grip joints the clamped parts strength are calculated by the "net section tension" method (see Section 9.3.3).

If desired, a friction grip joint can also be analysed for slippage into bearing using the methods in Section 9.3.

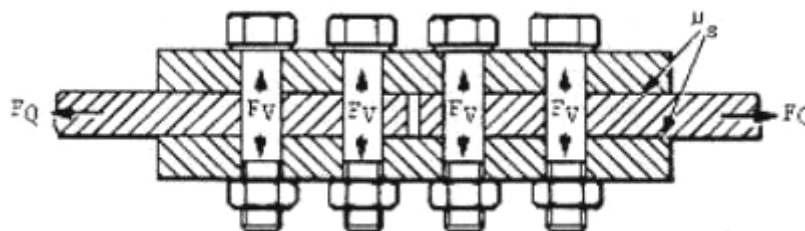


Figure 9-3 - A Symmetrical Shear Joint

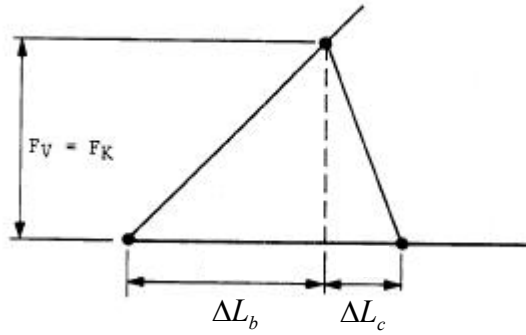


Figure 9-4 - The Joint Diagram for Each Fastener in Figure 9-3

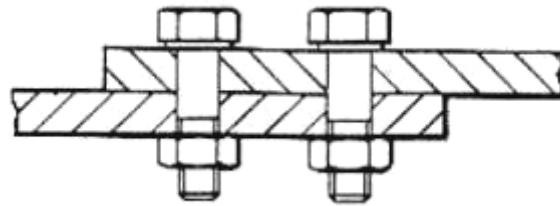


Figure 9-5 - Typical Unsymmetrical Friction Grip Shear Joint

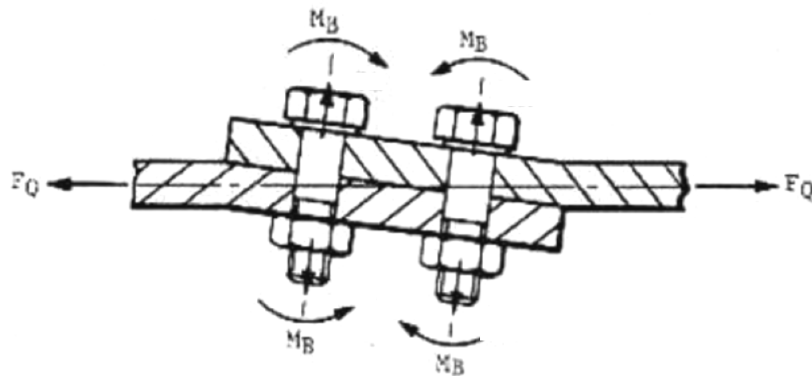


Figure 9-6 - Fastener Bending and Tension in an Unsymmetrical Shear Joint

9.2.2 Slip Resistance

9.2.2.1 Overview

Slip resistance depends on the friction force at the interface's faying surfaces. This force is in turn dependent on the fastener clamping load and the friction coefficient at those faying surfaces.

9.2.2.2 Pure Shear Loading

When no external axial load is applied to the joint, the clamping load is equal to the sum of the preloads and the slip resistance is given conservatively by,

$$S_r = x \mu_s \sum_{i=1}^m F_{V,\min,i} \quad [9.2.1]$$

where; μ_s is the **minimum** slip coefficient of the flange interface, x is the number of faying surfaces, and $F_{V,\min,i}$ is the minimum preload in the i^{th} fastener taking into account variations in preload and thermal effects (see [Section 6.3.5](#) and [6.4](#)).

If all of the fasteners in the joint have the same minimum preload, $F_{V,\min}$, Equation [9.2.1] is simplified to,

$$S_r = x \mu_s m F_{V,\min} \quad [9.2.2]$$

where m is the number of fasteners in the joint.

In multi-fastener joints Equation [9.2.2] can be overly conservative since it assumes that all fasteners are tightened to the lower bound of their preload range. Therefore, if the joint has enough fasteners (typically 5 or more), the slip resistance of the joint can be calculated with,

$$S_r = x \mu_s m F_{V,nom} \quad [9.2.3]$$

where $F_{V,nom}$ is the nominal preload

In case of local bending moment, the impact can be a variation of the spread of the local pressures, without influence on the sum of the compression pressures (due to fasteners preload), and with an increase of the maximum local pressure, which can only have a positive impact on the friction coefficient. So the local bending moment can be neglected.

9.2.2.3 Slip Resistance For Axial Loaded Joints

Provided the joint does not slip, the fastener **can** experience only tensile load. For the simple joints shown in Figure 9-7 the external axial load F_A is partly absorbed in stretching the bolt but is mainly absorbed in releasing the clamped parts. The axial load reduces the interface clamping, F_k , and thereby reduces the shear load capacity of the joint.

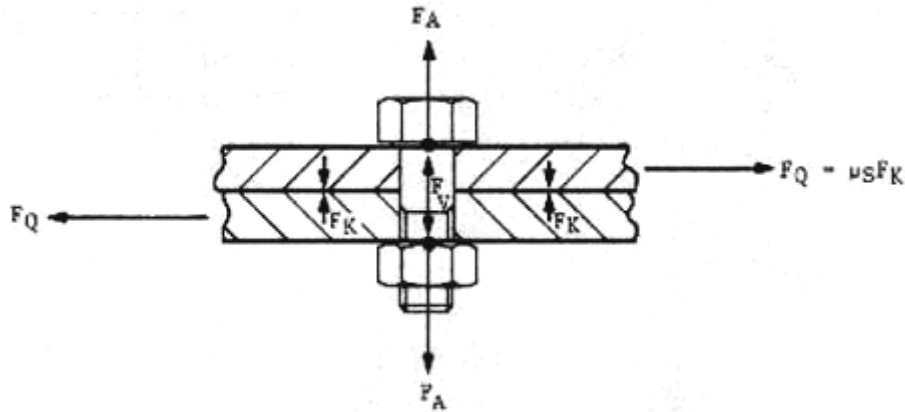


Figure 9-7 - Simple Friction Grip Joint with Added Tension Loading

A friction grip joint is considered to have failed when the joint has slipped. It is therefore necessary to ensure that,

$$S_r = x \mu_s m F_c > F_Q \quad [9.2.4]$$

where F_c is the flange compression force.

The flange compression is relieved according to,

$$F_c = (F_V - (1 - \Phi_{e,n}) F_A) \quad [9.2.5]$$

where the force ratio term $\Phi_{e,n}$ takes into account any adjustments for the loading plane factor (see Section 7.5) or eccentricity (see Section 8.2.3).

The relationship between the axial load and slip resistance is linear (see Figure 9-8).

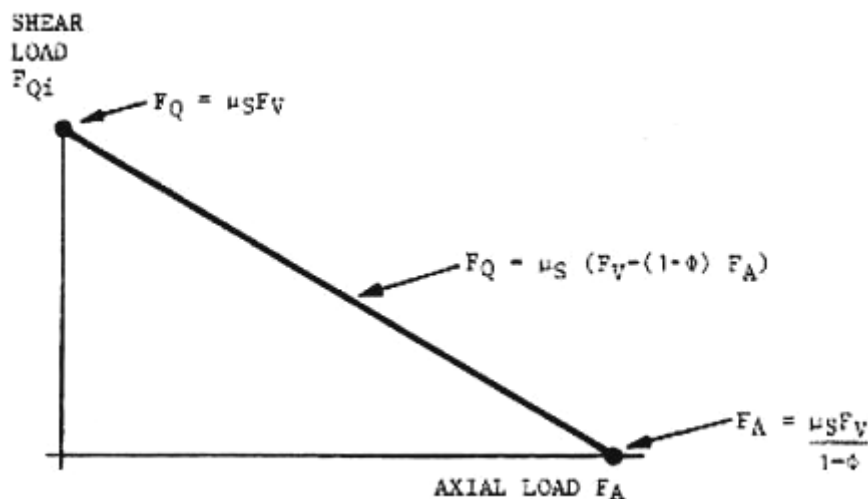


Figure 9-8 - Reduction of Shear Capacity with Increasing External Axial Load

9.2.2.4 Friction Coefficients at the Interface

Friction is subject to high variability. Therefore, to ensure safety in the design calculations, it is assumed that μ_s is at the minimum of its range, and it is important that the surface roughness of interfaces is taken into account. It is important to remember that although an increase in surface roughness increases the slip coefficient, it also increases the preload loss due to embedding which can be the more important effect (see Section 6.4.2).

Annex C lists typical friction coefficients for commonly used joint materials.

9.2.2.5 Design Features that Increase Slip Resistance

The joint can be designed with specific features that increase its slip resistance such as those shown in Figure 9-9. However, the calculation of the shear capacity of such joints is beyond the scope of this document.

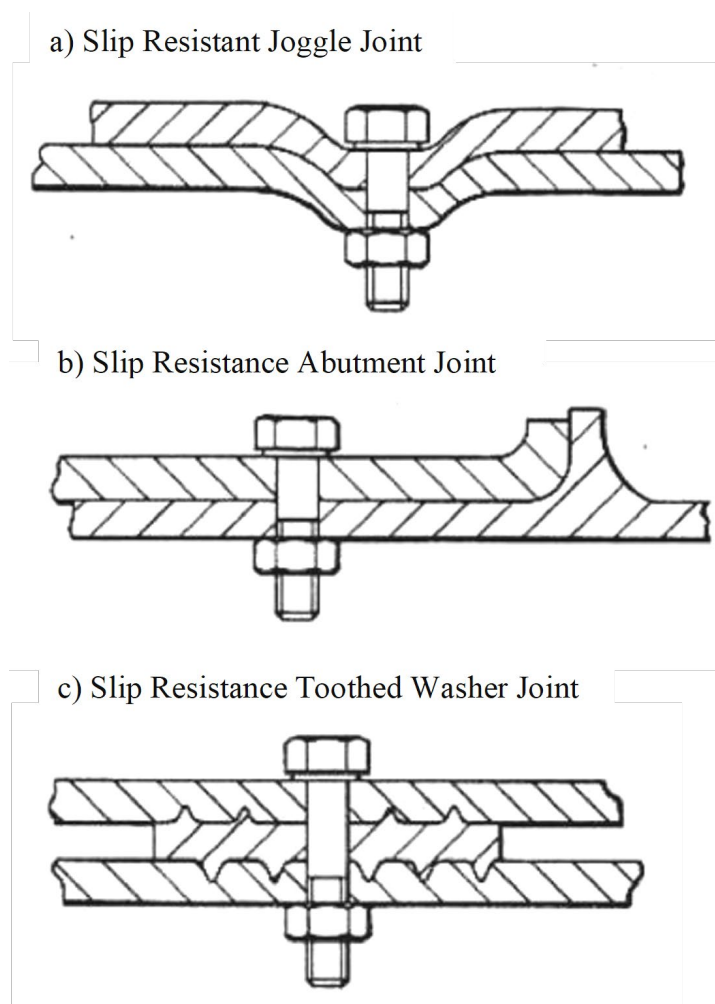


Figure 9-9 - Joint Design Features that Increase Slip Resistance

9.2.3 Friction Grip Strength Analysis

It is important that the strength analysis documentation for such a joint clearly identify it as a “friction grip joint” and the margin of safety for slipping is stated.

The margin of safety for slipping is calculated taking into account the lowest possible preload, $F_{V,min}$, and the safety factor for ultimate loads (see Table 5-4). It is defined as;

$$MoS_{slip} = \frac{(F_{V,min} - (1 - \Phi_{e,n})F_A) \mu_s x}{F_Q sf_{slip}} - 1 \quad [9.2.6]$$

If the MoS for slipping is positive, the margin of safety on separation defined in Section 7.8 is also positive. If used, it is important to clearly state this fact in the strength analysis documentation.

It is important that the net tension section of each flange also have sufficient strength to carry the shear load. See Section 9.3.3 for the net section evaluation method.

It can also exist a design requirement that, if the friction grip joint slip into bearing, the joint does not fail in any of the other modes described in the next section for bearing joints.

9.3 Bearing Joints

9.3.1 Design Principles

9.3.1.1 Overview

A “bearing” joint is one which has slipped until the fasteners “bear” on the holes as illustrated by Figure 9-10. A joint is also considered to be a bearing joint when a tight tolerance shaft (or plug gauge) is used.

Bearing type joints are mostly used where the necessary clamping force to prevent slip exceeds the clamped material’s under-head crushing strength (see Section 7.11). Such joints are therefore preloaded to a level below the flange’s crushing strength, but sufficiently high to lock the fastener under transverse vibration. The joint is then allowed to slip into bearing, where the shear load is transmitted via the fasteners into the flanges via bearing stress within holes.

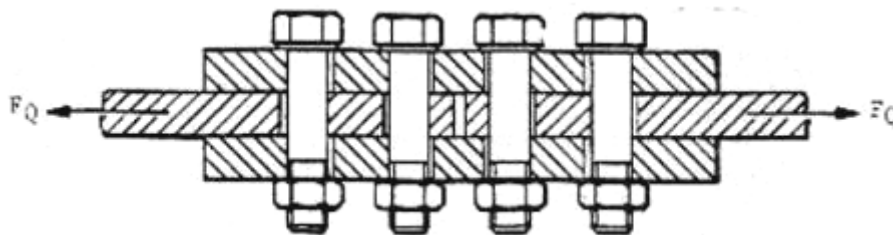


Figure 9-10 - Shear Joint in Bearing

Figure 9-11 shows a lap joint with a large number of fasteners. In such joints some of the fasteners, due to their position at the end of the fastener row, take a higher load than others. When the external shear load is applied, some load redistribution invariably takes place due to local line contact yielding. However, after this redistribution the outer fasteners can still experience shear loads some 15 % above average.

Note that this type of joints are not recommended. A preferred design is to have the joint transferring the shear loads by friction.

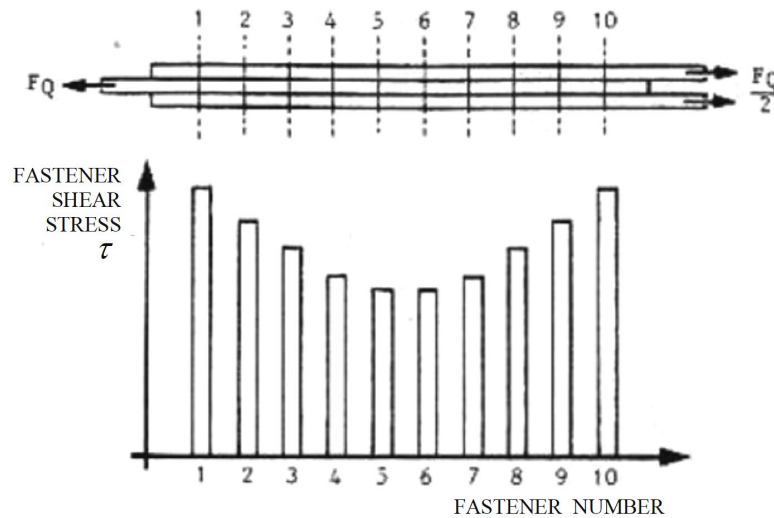


Figure 9-11 - Long Bearing Shear Stress Distribution

9.3.1.2 Thread Within the Hole

An important design feature of any bearing joint is the number of disengaged threads in the load path within the joint. This is illustrated by Figure 9-10, in which the threaded regions of the fasteners extend partially into the hole, proportionately increasing the hole bearing stress. In the extreme case where the interface plane passes through a threaded part of the fastener, its shear area is reduced from the shank cross-sectional area, A_{sh} , to the thread's stress area, A_s . For these reasons, it is recommended that the thread be carefully dimensioned to minimise the length of disengaged thread in the joint, while also ensuring that there is sufficient thread to account for manufacturing tolerances.

9.3.1.3 Pivoting Bearing Joint

Another type of bearing joint that is commonly found in mechanisms where relative rotation of the flanges about a single fastener pivot (scissors action) is a design requirement. In this case the nut needs a locking mechanism and the fastener preload is negligibly low. The fastener is therefore predominantly subject to transverse shear and bearing loads between fastener and hole. Also, depending on the degree of eccentricity of the applied load, the bending stresses within the fastener can be significant.

9.3.1.4 Strength Analysis of Bearing Joints

The strength of a bearing designed shear joint depends on its resistance in three failure modes; fastener shear, hole bearing and flange shear-out failure. The strength calculation methods for each of these failure modes are given in the following Sections.

9.3.2 Fastener Shear Failure

9.3.2.1 Overview

For the calculation of the shear resistance of the fastener's cross-section at the joint's shearing plane has to be used. If the thread is lying in the shear plane, the fastener's stress cross-sectional area to be used is A_s . Otherwise, the fastener's shank is in the shear plane and **it is important to use** its cross-sectional area A_{sha} .

9.3.2.2 Pure Shear

The MoS for shear failure of the fastener are as follows:

$$MoS_{Q,y} = \frac{\tau_y A_s}{F_Q s f_y} - 1 \quad (\text{for yield}) \quad [9.3.1]$$

$$MoS_{Q,ult} = \frac{\tau_{ult} A_s}{F_Q s f_{ult}} - 1 \quad (\text{for ultimate}) \quad [9.3.2]$$

where τ_y and τ_{ult} are the yield and ultimate shear stresses for the fastener, and A_s is the cross-sectional area at the shear plane (either A_{sha} or A_s).

9.3.2.3 Combined Shear and Axial Loads

In a bearing design the preload is chosen to ensure that the assembled joint **can** slip into bearing at the first external shear load application. It is therefore necessary to calculate the slip load and preload the fasteners to a level below that the one to prevent slip.

The joint's strength depends not only on the shear and tension interaction in the fastener but also on the dimensions and material properties of the clamped parts. The relative magnitude of the axial and shear components of the combined loading **can** make it necessary to reduce the axial preload in order to allow more of the fastener's strength to be used in shear. It is therefore necessary, when designing a bearing joint experiencing both tension and shear loads, to work backwards to a remaining clamping force rather than size the fastener by the preload requirements.

The fastener's shear capacity depends not only on the bolt size and its material shear strength, but also on the levels of axial and torsional stress in the triaxial stress system in its shearing planes.

The equations [9.3.3], [9.3.4], [9.3.5] and [9.3.6] assume that all torsional stresses (due to torque tightening) are removed by embedding, and bending stresses are small. Under these assumptions only the interaction between axial and shear stress are considered within the fastener.

In cases where it cannot be assumed that bearing joints have negligible fastener bending, **it is important to apply** more comprehensive fastener failure theories.

Thus, the verification of the combined loaded bearing joint uses stress interaction relations. If the thread is in the shear plane (not a recommended design practice), **it is important to satisfy** the following combined stress interaction relations:

$$R_{comb,y} = \sqrt{R_{A,y}^2 + R_{S,y}^2} \leq 1 \quad (\text{for yield}) \quad [9.3.3]$$

$$R_{comb,ult} = \sqrt{R_{A,ult}^2 + R_{S,ult}^2} \leq 1 \quad (\text{for ultimate}) \quad [9.3.4]$$

If the shank is in the shear plane, the following stress interaction relations can be used:

$$R_{comb,y} = \sqrt{R_{A,y}^2 + R_{S,y}^3} \leq 1 \text{ (for yield)} \quad [9.3.5]$$

$$R_{comb,ult} = \sqrt{R_{A,ult}^2 + R_{S,ult}^3} \leq 1 \text{ (for ultimate)} \quad [9.3.6]$$

The above equations [9.3.3] to [9.3.6] use the following ratios for the fastener's strength utilisation ratios:

$$R_{A,y} = \frac{(F_{V,max} + \Phi_{e,n} F_A sf_y)}{\sigma_y A_S} \quad [9.3.7]$$

$$R_{A,ult} = \frac{(F_{V,max} + \Phi_{e,n} F_A sf_{ult})}{\sigma_u A_S} \quad [9.3.8]$$

$$R_{S,y} = \frac{F_Q sf_y}{\tau_y A_S} \quad [9.3.9]$$

$$R_{S,ult} = \frac{F_Q sf_{ult}}{\tau_{ult} A_S} \quad [9.3.10]$$

If gapping is tolerable, the stress interaction relations is also to be checked with Equations [9.3.7] and [9.3.8] replaced by the following (overall axial load) equations respectively:

$$R_{A,y} = \frac{F_A sf_y}{\sigma_y A_S} \quad [9.3.11]$$

$$R_{A,ult} = \frac{F_A sf_{ult}}{\sigma_u A_S} \quad [9.3.12]$$

The margins of safety for combined axial and shear forces acting on the fastener are,

$$MoS_{comb,y} = \frac{1}{R_{comb,y}} - 1 \quad [9.3.13]$$

$$MoS_{comb,ult} = \frac{1}{R_{comb,ult}} - 1 \quad [9.3.14]$$

The calculation of the margin of safety on combined loads for equation [9.3.3&4] is graphically depicted in Figure 9-12. Point A represents a loading case that results in a combined margin of safety below the critical level. Point B represents the margin of safety for a higher loading case at the critical level but with the same ratio between the combined loads. This graphical interpretation cannot be used for the cubic terms in equations [9.3.5&6].

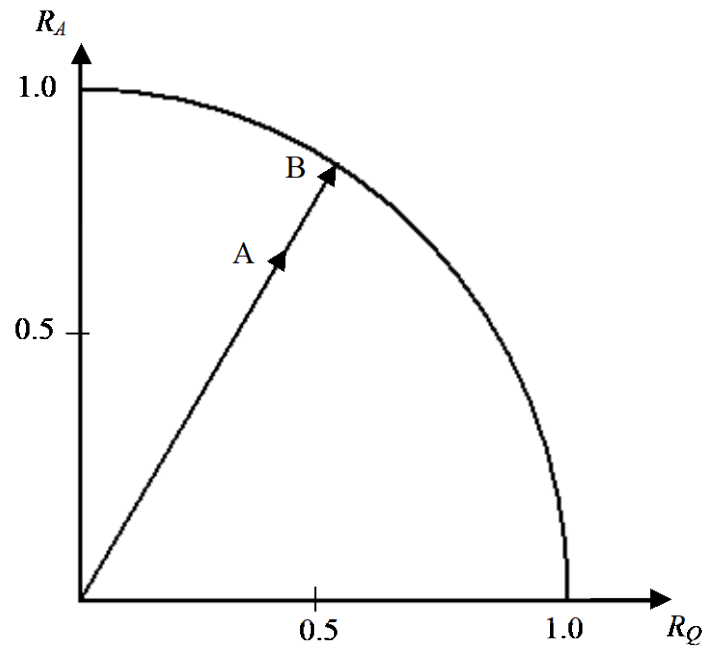


Figure 9-12 - Graphical Determination of the Margin of Safety on Combined Loads

9.3.2.4 Shear Strength of Fastener Group with Hole Tolerance

When a joint has more than one fastener, hole tolerances cannot be perfect and thus a clearance between hole and fastener. This clearance requires extra deformations to bring the full set of fasteners into bearing, and creates a reduction in the strength of the joint.

The theory in Reference 9.1 can be used to calculate the total bearing strength of a fastener group with hole clearances at their maximum tolerance bounds. The theory makes the following limiting assumptions:

Steel fasteners in aluminium flanges

Fastener shanks are in bearing (i.e. no thread in holes)

The theory use a conservative approach whereby the first fastener to fail is in the hole at the maximum tolerance bound, whereas as all other holes are at the centre of their tolerance bounds. This situation is shown in Figure 9-13.

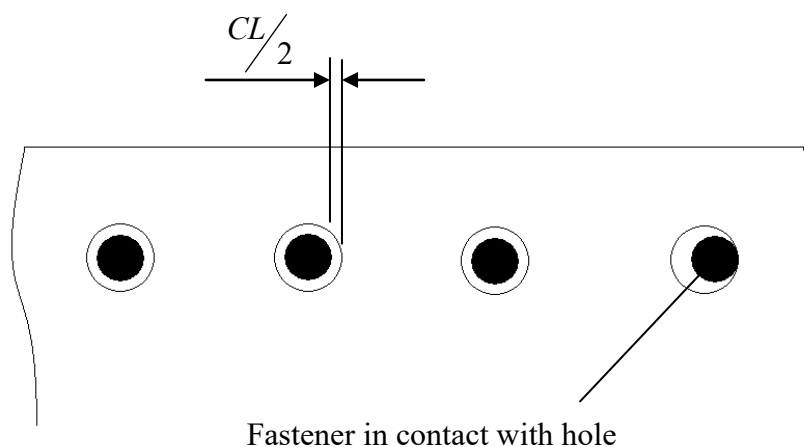


Figure 9-13 - Fastener Group with hole clearance

The combined strength of the fastener group is the ideal strength assuming perfect tolerances (i.e. the total shear strength of all fastener shanks), minus the force capable to bring all fastener shanks into bearing, i.e.

$$\text{Fastener Group Bearing Strength} = n \left(\frac{A_S \tau_{ult}}{s f_{ult}} \right) - (n - 1) F_{CL} \quad [9.3.15]$$

where n is the number of fasteners in the bearing joint and F_{CL} is the shear force capable to move the fastener shank by a distance equal to the hole clearance.

$$F_{CL} = \frac{t_1 t_2 F_{CL}^*}{t_1 + t_2} \quad [9.3.16]$$

Where F_{CL}^* is a parameter given by the empirical relation,

$$F_{CL}^* = -3.2245e^{10} (CL)^3 + 2.4222e^9 (CL)^2 + 1.2697e^7 (CL) - 3.7262e^3 \quad [9.3.17]$$

The variable, CL , is the hole clearance, which is defined as $D_h - d$.

Equation [9.3.17] is graphically presented in Figure 9-14.

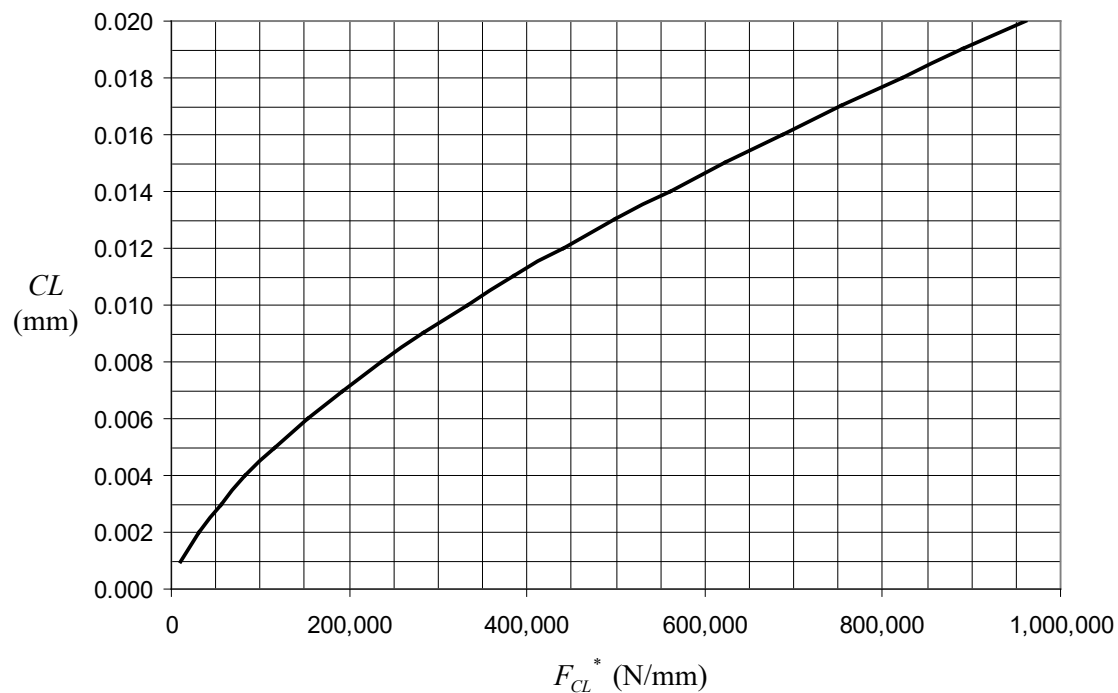


Figure 9-14 - Shear load parameter versus hole clearance

9.3.3 Net Tension Section Failure of Flanges

9.3.3.1 Overview

The method for evaluating net tension section failure is taken from Reference 9.2. By this theory, the net tension section is defined as the smallest area that is obtained by deducting the summed area of all holes lying in any potential failure path (straight or zig-zag) across a flange from the gross cross-sectional sectional area. **It is important to consider t** his failure mode considered for both friction grip joints and bearing joints.

In order to obtain a sufficiently large net tension section area to transmit the tension load through the flange, it is necessary to meet the following condition:

$$A_{net,min} > \frac{F_Q}{K_R \sigma_{ult}} \quad [9.3.18]$$

where σ_{ult} is the yield strength of the respective flange, and K_R is a reduction factor for the flange material's ultimate strength (see Section 9.3.3.2 below), and $A_{net,min}$ is the smallest net tension section area calculated by,

$$A_{net,min} = A_{gross} - \max(A_{holes,i}) \quad [9.3.19]$$

where A_{gross} is the flange area ignoring the presence of the holes, and $A_{holes,i}$ is the summation of the hole areas along the i 'th potential path across the flange.

The summation of the holes' areas, A_{holes} , considers the full area of the first hole but then only fractional parts of each succeeding hole, and is calculated by,

$$A_{holes} = t d \left(1 + \sum_{i=2}^m \left\langle 1 - \frac{p_i^2}{4 s_i d} \right\rangle \right) \quad [9.3.20]$$

where p_i and s_i are the lateral and longitudinal distances between the centres of the i 'th and $(i-1)$ 'th holes (see Figure 9-15), and t is the thickness of the flange, and **it is important that** the expression inside the angled brackets **is** replaced with zero if it evaluates to a negative value.

Figure 9-15 shows the nomenclature used to define the net tension section.

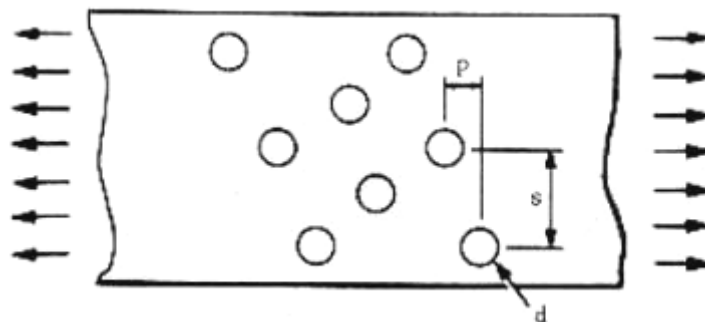


Figure 9-15 - Nomenclature for Net Tension Section Calculation

The margin of safety on net tension section failure is therefore given by,

$$MoS_{Q,net} = \frac{K_R \sigma_{ult} A_{net,min}}{F_Q s f_{ult}} - 1 \quad [9.3.21]$$

9.3.3.2 Net Section Data for Some Aluminium Alloys

Aluminium alloys develop a net ultimate stress that varies according to the proportion of area lost through holes. The curves in Figure 9-16 give reduction factors to be applied in Equation [9.3.20]. The curves correspond to the following general groups of alloys:

- Al-Cu solution treated and naturally aged sheet and plate (e.g. L163 2014 A CLAD 1050A-T3)
- Al-CuAl-Zn solution treated and artificially aged sheet or plate (e.g. L165 2014 A CLAD 1050A-T6, L88 7075 CLAD 7072-T6)
- Al-Cu solution treated and naturally aged extruded bar (e.g. L102 2014 A T4),
- Al-Cu solution treated and artificially aged extruded bar (e.g. L168 2014 A - T6510, DTD 5124 Al-Zn, 7075-T6)

With the exception of curve 3, the data in Figure 9-16 is applicable to loadings that are either longitudinal or transverse to the grain (or final direction of rolling). There is also some limited evidence that curve 1 can be applicable to naturally aged extruded bar loaded in the transverse direction.

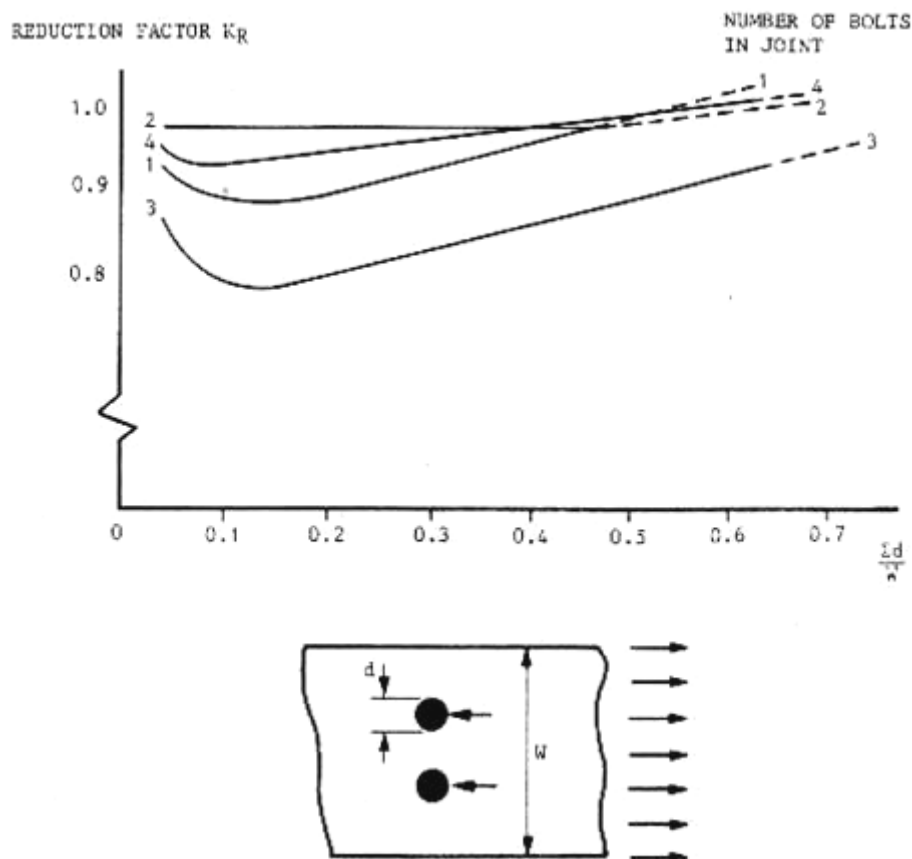


Figure 9-16 - Ultimate Strength Reduction Factors for Net Tension Section Failure

The curves in Figure 9-16 are based on data from tests on specimens with unfilled holes, however spot checks have shown that they can be applied to loaded holes. The data was derived from specimens where the edge distance of the holes was $4d$. From the general shape of the curves it can be assumed that they are applicable at lower edge distances, say to $2d$.

9.3.4 Hole Bearing Failure

After slipping one or more fasteners bear against the side of their holes. Initially, an elastic bearing stress is developed in the plate material adjacent to the hole, as indicated in Figure 9-17, peaking at the line contact. An increase in the shear force F_Q causes further plastic elongation of the hole, as shown in Figure 9-18. In most cases a linear stress F_Q distribution, shown in Figure 9-19, can give an adequate approximation, whereby the bearing stress is,

$$\sigma_{br} = \frac{F_Q}{dt} \quad [9.3.22]$$

where t is the thickness of the flange, and d is the diameter of the fastener.

If the fastener's thread extends within the hole, it is important to assume that the threaded region of the fastener is not capable of transmitting any bearing stress. In such cases, it is important to decrease the value of t in Equation [9.3.22] accordingly.

In most cases, the value of d in Equation [9.3.22] is equal to the nominal hole diameter, D_h . However, if the fastener's diameter is significantly smaller than that of the hole, it is important to use the smaller (fastener) diameter. This situation typically occurs in multi-fastener joints where deliberately loose tolerances are needed to ensure assembly of pre-drilled parts.

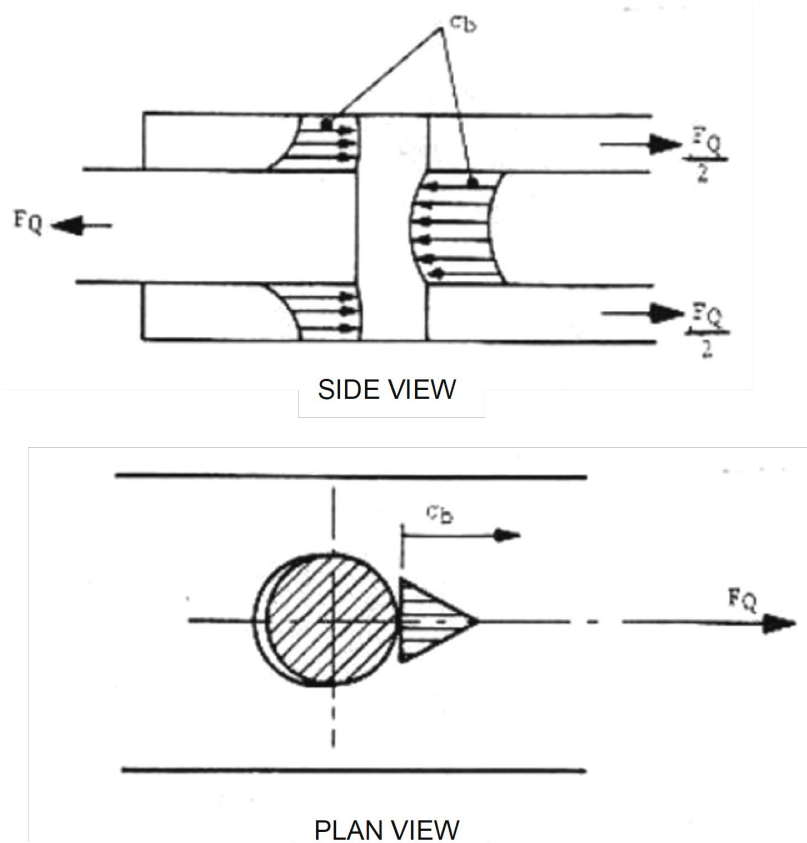


Figure 9-17 - Initial Bearing Contact Elastic Stresses and Deformations

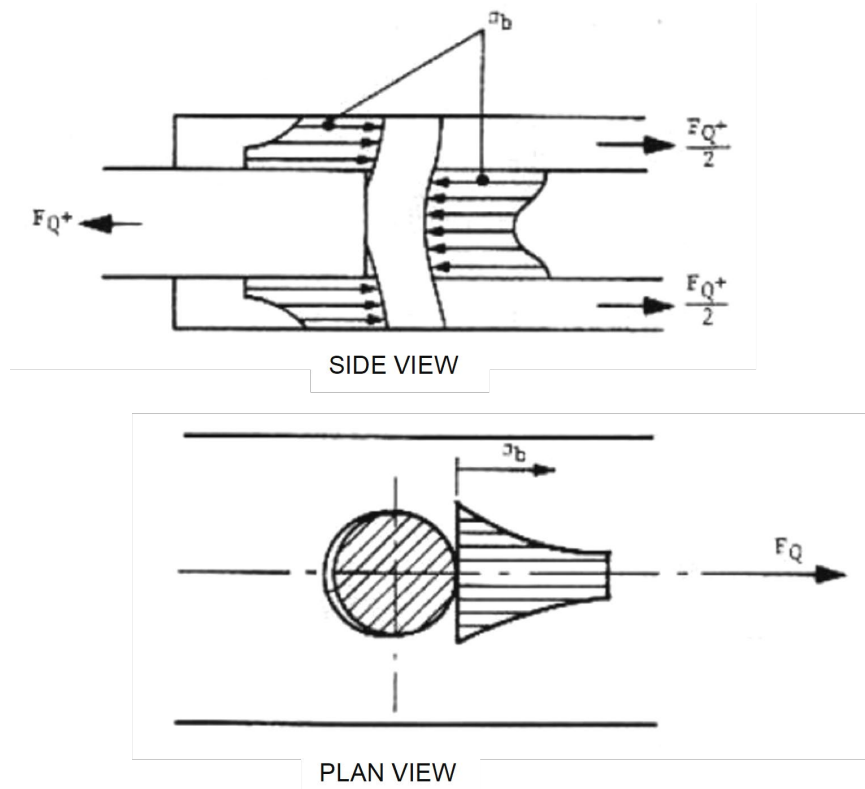


Figure 9-18 - Elastic / Plastic Stresses and Deformations After Increased Loading

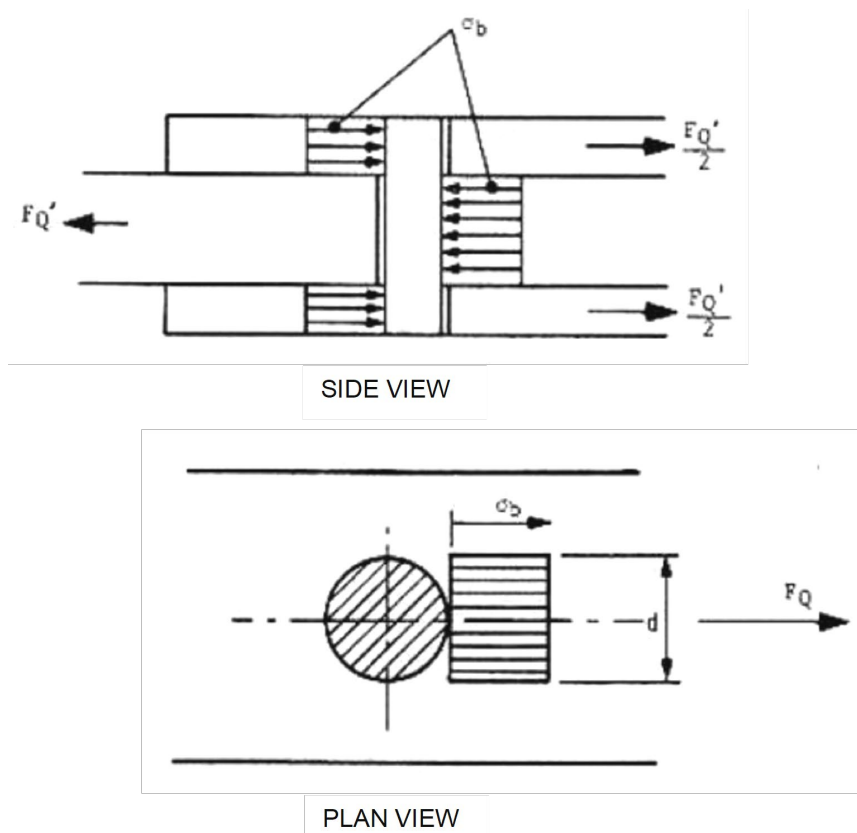


Figure 9-19 - Idealised Bearing Stresses

It is important to compare the bearing stress calculated with equation [9.3.22] to the allowable values for yield, $\sigma_{br,y}$, and ultimate, $\sigma_{br,ult}$, bearing strength of the flange material. These allowable values are listed in Reference 9.3 for spaceflight-proved materials for edge distance ratios a/D_h of 1,5 and 2,0, and for flange thickness ratios t/D_h in the range 0,25 to 0,5.

For a/D_h less than 1,5 it can be assumed that the shear-out failure mode can be more critical (see Section 9.3.5 below). Above an edge distance ratio of 2,0 the bearing strength is constant. If the edge distance is in the intermediate range (i.e. $1,5 < a/D_h < 2,0$), it is important to interpolate the bearing strength linearly from the values at 1,5 and 2,0.

The margins of safety on hole bearing strength are calculated as follows:

$$MoS_{br,y} = \frac{\sigma_{br,y} D_h t}{F_Q s f_y} - 1 \quad (\text{for yield}) \quad [9.3.23]$$

$$MoS_{br,ult} = \frac{\sigma_{br,ult} D_h t}{F_Q s f_{ult}} - 1 \quad (\text{for ultimate}) \quad [9.3.24]$$

Note that the variable, d , in the above equations is the diameter of the fastener and not the diameter of the hole. This distinction is important for joints with oversized holes, in which case the bearing area is determined by the fastener diameter.

9.3.5 Shear-Out or Tear-Out Failure

Shear-out or tear-out failure, as illustrated in Figure 9-20 and Figure 9-21 respectively, can occur when the fasteners are located close to the edge of the plate. These modes of failure do not need to be considered for fasteners that are more than $2d$ from a flange edge.

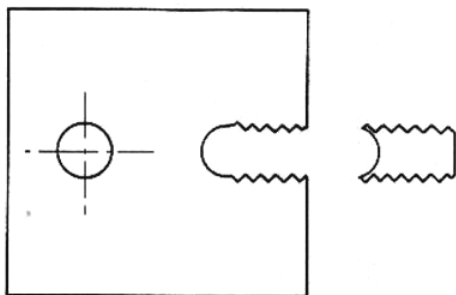


Figure 9-20 - Shear-Out Failure

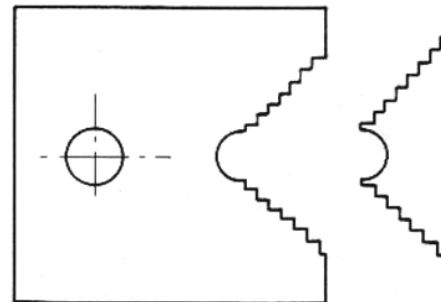


Figure 9-21 - Tear-Out Failure

To calculate the shear stress in the flange, τ , the minimum shear-out length is used. Referring to the notation of Figure 9-22, this length is given by,

$$2a_1 = |ef| + |gh| \quad [9.3.25]$$

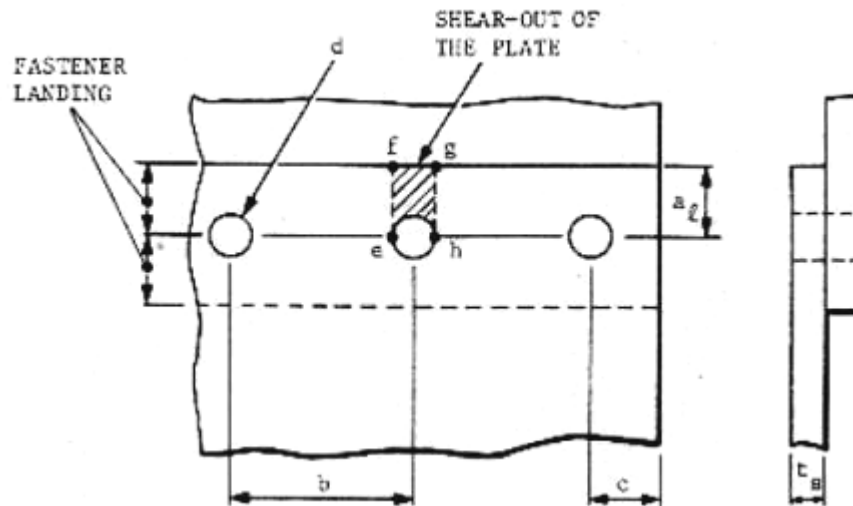


Figure 9-22 - Nomenclature for Plate Shear Out Calculation

The following condition is the relation to be satisfied by the design, for each fastener near (within $2d$) an edge:

$$\tau = \frac{F_Q}{2a_1 t} < \tau_{ult} \quad [9.3.26]$$

where t is the thickness of the flange, and F_Q is the component of the fastener's load acting towards the nearest edge of the flange.

This leads to the following margin of safety on shear-out,

$$MoS_{so} = \frac{2\tau_{ult} a_1 t}{F_Q s f_{ult}} - 1 \quad [9.3.27]$$

9.4 Eccentrically Loaded Shear Joints

9.4.1 Overview

When the line of action of the applied shear load F_Q does not pass through the centroid of a fastener group the joint is said to be eccentrically loaded. A typical eccentrically loaded shear joint is shown in Figure 9-23.

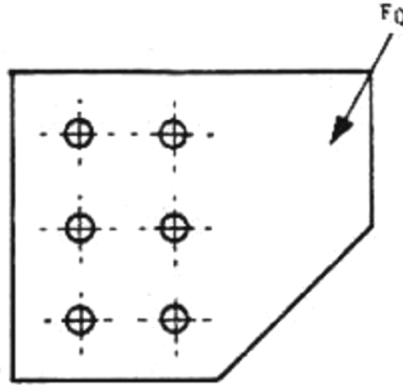


Figure 9-23 - A Typical Eccentric Loaded Shear Joint

The type of load felt by individual fasteners depends whether the joint is operating as a friction grip or as a bearing type joint. The load-rotation curve for a typical joint loaded through friction grip and into bearing is shown in Figure 9-24.

Before the joint slips, the flanges are assumed deform together as a single elastic body. After the onset of slippage it is important to assume that all loads are transmitted via the bearing load paths.

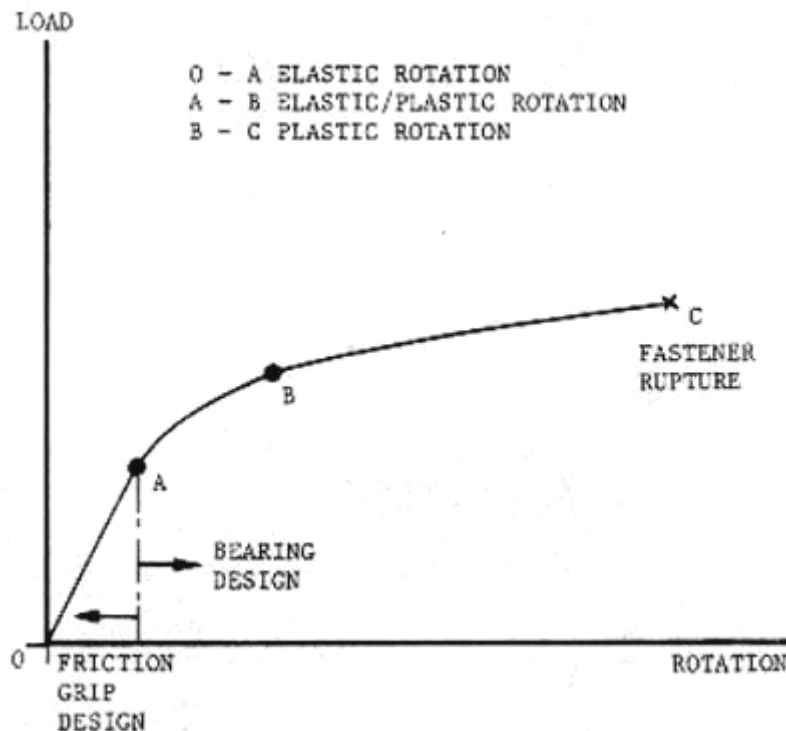


Figure 9-24 - Load v Rotation Curve for a Typical Eccentric Loaded Shear Joint

9.4.2 Fastener Group Centroid

The centroid of the fastener group can be determined by assuming any two axes X and Y and applying the equations,

$$\bar{y} = \frac{A_{sha,1} y_1 + A_{sha,2} y_2 + \dots + A_{sha,n} y_n}{\sum_{i=1}^m A_{sha,i}} \quad [9.4.1]$$

$$\bar{x} = \frac{A_{sha,1} x_1 + A_{sha,2} x_2 + \dots + A_{sha,n} x_n}{\sum_{i=1}^m A_{sha,i}} \quad [9.4.2]$$

where x_i and y_i are the coordinates of the i 'th fastener, and $A_{sha,i}$ is its shank area.

In some cases symmetry can also be used to determine the fastener group centroid.

9.4.3 Bearing Design of Eccentric Shear Joints

In Figure 9-23 the eccentric load F , can be resolved to the centroid of the fastener group as a force F_Q and a moment $M_Q = F_Q e$ (where e is the eccentricity of loading). Each fastener experiences a load due to F (in a direction parallel to it) and a load due to M acting in a direction perpendicular to a line passing through that fastener's centre and the centroid of the fastener group.

The externally applied shear force F_Q can then be distributed amongst the fasteners proportionally to their shear areas according to,

$$F_{Q,i} = \frac{A_{sha,i} F_Q}{\sum_{j=1}^m A_{sha,j}} \quad [9.4.3]$$

where $A_{sha,i}$ is the shank area of the i 'th fastener, and m is the total number of fasteners.

Similarly, the applied moment M_Q can be distributed amongst the fasteners proportionally to their bearing and shear areas and to their distance from the centroid according to,

$$F_{M,i} = \left[\frac{A_{sha,i} r_{c,i}}{\sum_{j=1}^m A_{sha,j} r_{c,j}^2} M_Q \right] \quad [9.4.4]$$

$r_{c,i}$ is the distance of the i 'th fastener from the centroid.

The force vectors resulting from Equation [9.4.3] act parallel to the externally applied shear load. The force vectors resulting from Equation [9.4.4] act perpendicularly to the moment arm from the fastener group centroid to the relevant fastener. The shear load acting on each fastener is determined by the vectorial addition of these two forces.

Equation [9.4.4] uses the fastener shank areas ($A_{sha,i}$) as the weighting factor for the load division. However, in some cases the bearing area and fastener stiffness can also be significant (e.g. for groups of dissimilar fasteners or when the flange thickness is not constant). In such cases it is recommended to replace the area, $A_{sha,i}$, with the strength of the fastener-hole pair, which is given by,

$$F_{Q,ult,i} = \min \left[F_{Q,br,i}, F_{Q,sha,i} \right] \quad [9.4.5]$$

where $F_{br,i}$ is the ultimate bearing strength of the i 'th hole (calculated using Section 9.3.4) and $F_{b,i}$ is the ultimate shear strength of the i 'th fastener (calculated using Section 9.3.2).

Using the shear force resulting from equation [9.4.3], **it is important to calculate** the relevant margins of safety for each fastener according to the complete set of bearing joint analysis methods in Section 9.3.

A worked example of eccentric bearing joints is given in Section 9.5.3.

9.4.4 Friction Grip Design of Eccentric Shear Joints

9.4.4.1 Overview

In a friction grip joint the load is transmitted between the flanges via frictional forces at the clamped interstice. Hence, the rotational slip resistance is needed to estimate the loading capacity of the joint. This is calculated in Reference 9.2 by assuming that the slipping movement is about an instantaneous centre of rotation. The location of the centre of rotation depends on the fastener pattern and the line of action of the applied load, as illustrated in Figure 9-25.

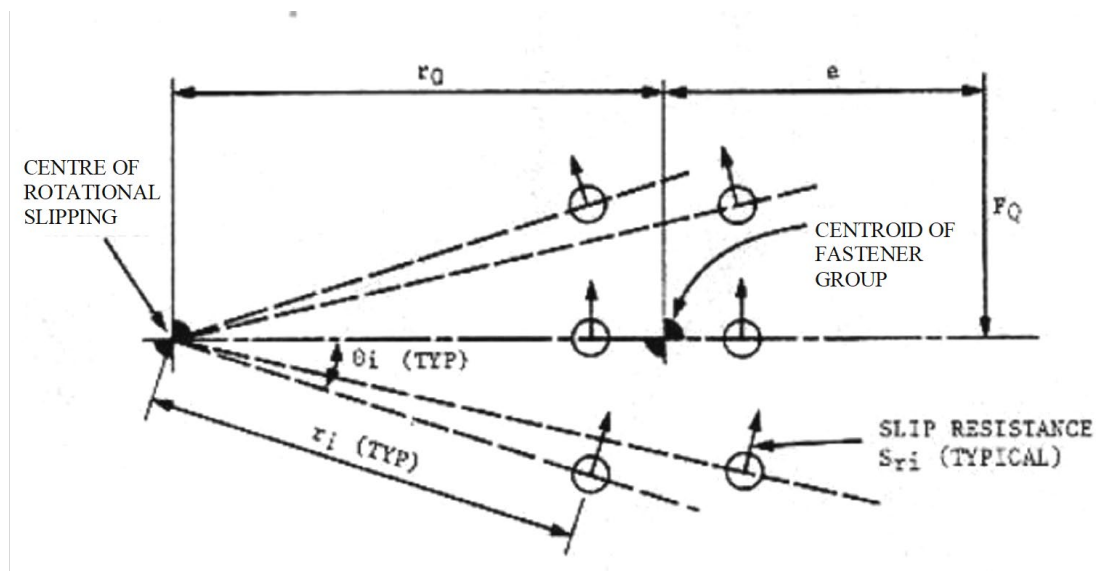


Figure 9-25 - Shear Resistance Relative to the Centre of Rotation

It is assumed that, at the onset of slipping, the magnitudes all fastener shear loads are equal. Thus, the slip resisting force transmitted by fastener i is given by;

$$S_{r,i} = S_r / m \quad [9.4.6]$$

where S_r is the overall slip resistance of the joint as calculated from Equations [9.2.1], [9.2.2] or [9.2.3], (see Section 9.2.).

It is also assumed that, at the onset of slipping, each fastener carries a reaction force in a direction perpendicular to the radial line emanating from the centre of rotation (see Figure 9-25). The angle of the radial line is given by;

$$\theta_i = \tan^{-1} \left(\frac{y_i - y_0}{x_i - x_0} \right) \quad [9.4.7]$$

where x_i and y_i are the coordinates of fastener i and x_0 and y_0 are the coordinates of the centre of rotation, which can be found by the iterative process described below in Section 9.4.4.2.

9.4.4.2 Determination of the Centre of Rotation

A trial centre of rotation is chosen and used as the origin for X and Y axes. Then the following three equilibrium equations are checked;

$$\frac{S_r}{m} \sum_{i=1}^m \sin(\theta_i) = 0 \quad (\text{force equilibrium in } X \text{ direction}) \quad [9.4.8]$$

$$\frac{S_r}{m} \sum_{i=1}^m \cos(\theta_i) - F_Q = 0 \quad (\text{force equilibrium in } Y \text{ direction}) \quad [9.4.9]$$

$$F_Q(e + r_0) - \frac{S_r}{m} \sum_{i=1}^m \sin(\theta_i) = 0 \quad (\text{moment equilibrium about } r_0) \quad [9.4.10]$$

where θ_i is a function of the assumed centre of rotation.

It is important to use then a suitable iterative algorithm to find a centre point that satisfies all three equations.

Due to symmetry, the centre of rotation for the fastener group shown in Figure 9-25 lies on a line, which is perpendicular to the externally applied load and passing through the centroid of the fastener group. Therefore, in that case, the search for the centre of rotation only needs variation of one parameter. If the fastener pattern is non-symmetric (with respect to the applied load), the location of the centre of rotation is unknown in both the X and Y directions.

9.5 Worked Examples

9.5.1 Shear Loaded Joint Example

This example calculation uses the joint defined in Figure 9-26.

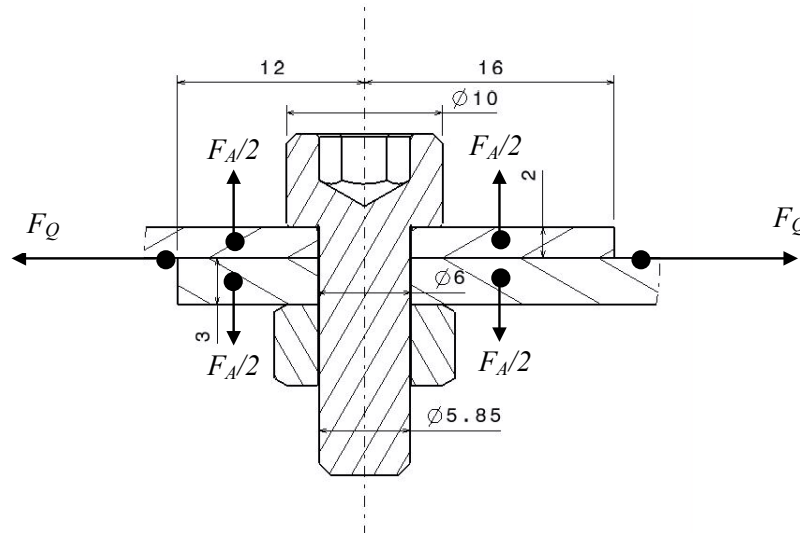


Figure 9-26 - Shear loaded joint example

The friction coefficient at the interface between the flanges,

$$\mu_s = 0,3$$

The strength of this structure is verified only by analysis. The safety factor for yield sf_y , ultimate loads sf_{ult} and slipping sf_{slip} is read from Table 5-4. The value of sf_y and sf_{ult} is multiplied with the joint fitting factor 1,15.

$$sf_y = 1,25 \times 1,15 = 1,4375$$

$$sf_{ult} = 2 \times 1,15 = 2,3$$

$$sf_{slip} = 1,25 \text{ (non safety critical)}$$

In addition to the axial load of Section 7.14, the joint is also subject to a shear load. Thus, the loads to which this joint is subjected are as follows:

$$F_A = 1000 \text{ N}$$

$$F_Q = 1000 \text{ N}$$

The joint is first checked for its friction grip capacity. This is done by calculating the margin of safety on slipping using Equation [9.2.6]. There is only one interstice in this joint so $x = 1$.

$$MoS_{slip} = \frac{(F_{V,min} - (1 - \phi_{e,n}) F_A) \mu_s \chi}{F_Q sf_{slip}} - 1 = \frac{(4848 \text{ N} - (1 - 0,1345) * 1000 \text{ N}) * 0,3 * 1}{1000 \text{ N} * 1,25} - 1 = -0,04$$

The MoS for slipping is below zero, therefore it is important to re-analyse the joint as a bearing joint. Alternatively, if the joint has multiple fasteners, MoS_{slip} can be recalculated with the average preload $F_{V,av}$.

Therefore, the margins of safety on fastener shear loads are determined for yield and ultimate using the theory of Section 9.3.2. First, the fastener's strength utilisation ratios are determined using equations [9.3.7] to [9.3.10],

$$R_{A,y} = \frac{F_{V,max} + \phi_{e,n} F_A s f_y}{\sigma_y A_s} = \frac{12129N + 0,1345 * 1000N * 1,4375}{950MPa * 20,12 mm^2} = 0,6446$$

$$R_{A,u} = \frac{F_{V,max} + \phi_{e,n} F_A s f_u}{\sigma_u A_s} = \frac{12129N + 0,1345 * 1000N * 2,3}{1100MPa * 20,12 mm^2} = 0,5619$$

$$R_{S,y} = \frac{F_Q s f_y}{\tau_y A_s} = \frac{1000 \times 1,4375}{548 \times 20,12} = 0,130$$

$$R_{S,u} = \frac{F_Q s f_{ult}}{\tau_{ult} A_s} = \frac{1000 \times 2,3}{655 \times 20,12} = 0,175$$

Since the thread is in the shear plane of the joint, it is important to use equations [9.3.3] & [9.3.4] to calculate the combined stress utilisation ratios,

$$R_{comb,y} = \sqrt{R_{A,y}^2 + R_{S,y}^2} = \sqrt{0,6446^2 + 0,130^2} = 0,658$$

$$R_{comb,u} = \sqrt{R_{A,u}^2 + R_{S,u}^2} = \sqrt{0,5619^2 + 0,175^2} = 0,588$$

Thus, the MoS on fastener failure can be calculated using equations [9.3.13] and [9.3.14],

$$MoS_{comb,y} = \frac{1}{R_{comb,y}} - 1 = \frac{1}{0,658} - 1 = 0,521$$

$$MoS_{comb,u} = \frac{1}{R_{comb,u}} - 1 = \frac{1}{0,588} - 1 = 0,700$$

Next, it is important to check the strength of both flanges for hole bearing and shear-out. Both flanges consist of AA 7075 T7351.

For flange 1;

Thickness $t_1 = 2$ mm

Hole diameter $D_h = 6,5$ mm

Edge distance ratio $a_1/D_h = 16/6,5 = 2,46$

That is above 2,0, so the bearing strength of the material is the value for the edge distance ratio of 2,0. The margins of safety on hole bearing is analysed for flange 1 are calculated using equations [9.3.23] and [9.3.24],

$$MoS_{brg,y} = \frac{\sigma_{brg,y,2.0} D_h t_1}{F_Q s f_y} - 1 = \frac{613 \times 6.5 \times 2}{1000 \times 1.4375} - 1 = 4.54$$

$$MoS_{brg,ult} = \frac{\sigma_{brg,ult,2.0} D_h t_1}{F_Q s f_{ult}} - 1 = \frac{882 \times 6.5 \times 2}{1000 \times 2.3} - 1 = 3.99$$

For flange 2;

Thickness $t_2 = 3$ mm

Hole diameter $D_h = 6,5$ mm

Edge distance ratio $a_l/D_h = 12/6,5 = 1,85$

The edge distance ratio is less than 2,0 so the bearing allowables can be found by linear interpolation between the value for $a_l/D_h = 1,5$ and $a_l/D_h = 2,0$,

$$\begin{aligned} \sigma_{brg,y,1.85} &= \sigma_{brg,y,1.5} + \frac{(a_l/D_h - 1.5)}{0.5} \times (\sigma_{brg,y,2.0} - \sigma_{brg,y,1.5}) \\ &= 524 + \frac{(1.85 - 1.5)}{0.5} \times (613 - 524) \\ &= 585.6 \text{ MPa} \end{aligned}$$

$$\begin{aligned} \sigma_{brg,ult,1.85} &= \sigma_{brg,ult,1.5} + \frac{(a_l/D_h - 1.5)}{0.5} \times (\sigma_{brg,ult,2.0} - \sigma_{brg,ult,1.5}) \\ &= 689 + \frac{(1.85 - 1.5)}{0.5} \times (882 - 689) \\ &= 822.6 \text{ MPa} \end{aligned}$$

Now, the margins of safety on hole bearing for flange 2 are,

$$MoS_{brg,y} = \frac{\sigma_{brg,y,1.85} D_h t_1}{F_Q s f_y} - 1 = \frac{585.6 \times 6.5 \times 3}{1000 \times 1.4375} - 1 = 6.94$$

$$MoS_{brg,ult} = \frac{\sigma_{brg,ult,1.85} D_h t_2}{F_Q s f_{ult}} - 1 = \frac{822.6 \times 6.5 \times 3}{1000 \times 2.3} - 1 = 5.97$$

Finally, the MoS for flange shear-out is calculated using equation [9.3.27],

For flange 1;

$$MoS_{SO} = \frac{2 \tau_{ult} a_l t_1}{F_Q s f_{ult}} = \frac{2 \times 262 \times 16 \times 2}{1000 \times 2.3} - 1 = 6.29$$

For flange 2;

$$MoS_{SO} = \frac{2 \tau_{ult} a_l t_2}{F_Q s f_{ult}} = \frac{2 \times 262 \times 12 \times 3}{1000 \times 2.3} - 1 = 7.20$$

9.5.2 Net Tension Section Failure Example

This example is based on the shear joint in Figure 9-27. The shear load is 50kN and the material ultimate stress is 427MPa.

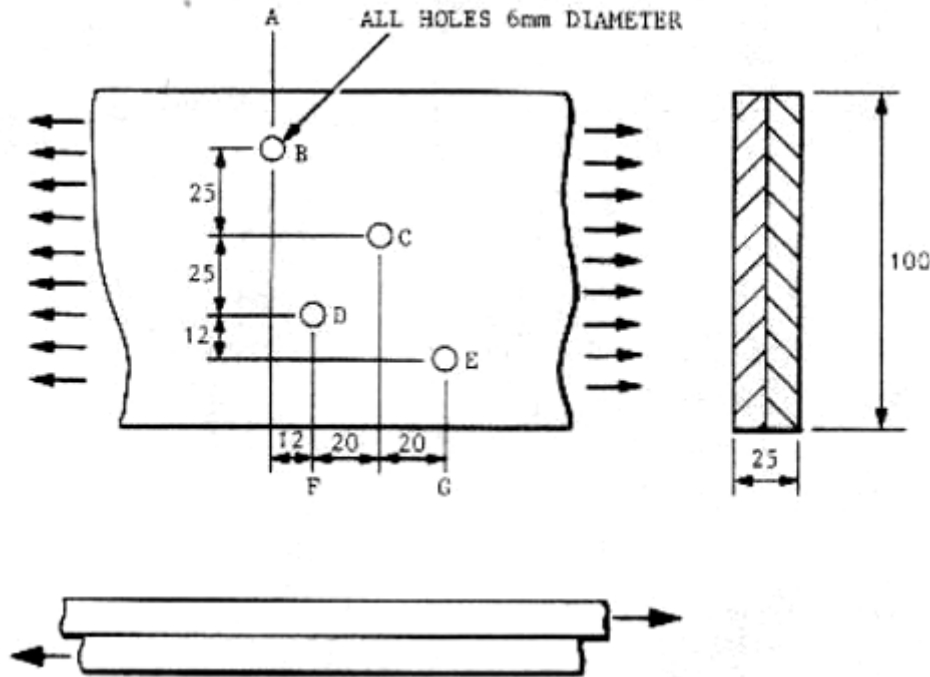


Figure 9-27 - Shear Joint Example to Show the Method of Net Tension Section Calculation

Inspection of the joint shows three potential fracture paths across the joint; *ABDF*, *ABCDF* and *ABCEG*.

The summed hole areas for each potential failure path across a flange are calculated using equation [9.3.20],

ABDF:

$$A_{holes} = t \times d \left(1 + \sum_{i=2}^2 \left[1 - \frac{p_i^2}{4 \times s_i \times d} \right] \right) = 12.5 \times 6 \times \left(1 + \left[1 - \frac{12^2}{4 \times 50 \times 6} \right] \right) = 141 \text{ mm}^2$$

ABCDF:

$$A_{holes} = t \times d \left(1 + \sum_{i=2}^3 \left[1 - \frac{p_i^2}{4 \times s_i \times d} \right] \right) = 12.5 \times 6 \left(1 + \left[1 - \frac{32^2}{4 \times 25 \times 6} \right] + \left[1 - \frac{20^2}{4 \times 25 \times 6} \right] \right) = 100 \text{ mm}^2$$

ABCEG:

$$A_{holes} = t \times d \left(1 + \sum_{i=2}^3 \left[1 - \frac{p_i^2}{4 \times s_i \times d} \right] \right) = 12.5 \times 6 \left(1 + \left[1 - \frac{32^2}{4 \times 25 \times 6} \right] + \left[1 - \frac{20^2}{4 \times (25 + 12) \times 6} \right] \right) = 116.2 \text{ mm}^2$$

The largest value of A_{holes} is 141mm^2 , which occurs for failure path $ABDF$.

The smallest net tension section is now calculated with equation [9.3.19],

$$A_{net,min} = A_{gross} - \max(A_{holes}) = 100 \times 12,5 - 141 = 1109 \text{ mm}^2$$

The proportion of net section lost by holes is calculated with

$$\frac{\sum_{i=1}^m d_i}{W} = \frac{2 \times 6}{100} = 0.12$$

The reduction factor for ultimate strength in the net tension section is now found using the graph in Figure 9-14. For the material type 1. Section 9.3.3.2 shows that the reduction factor K_R is found to be approximately 0.9.

The margin of safety on net tension section failure can now be calculated using equation [9.3.21],

$$MoS_{Q,net} = \frac{K_R \sigma_{ult} A_{net,min}}{F_Q s f_{ult}} - 1 = \frac{0.9 \times 427 e^6 \times 1109 e^{-6}}{50000 \times 1.4} - 1 = 5.07$$

9.5.3 Eccentric Shear Bearing Joint Example

This example is taken from Reference 9.1. This example considers an eccentric shear load acting on the group of six symmetric fasteners shown in Figure 9-28.

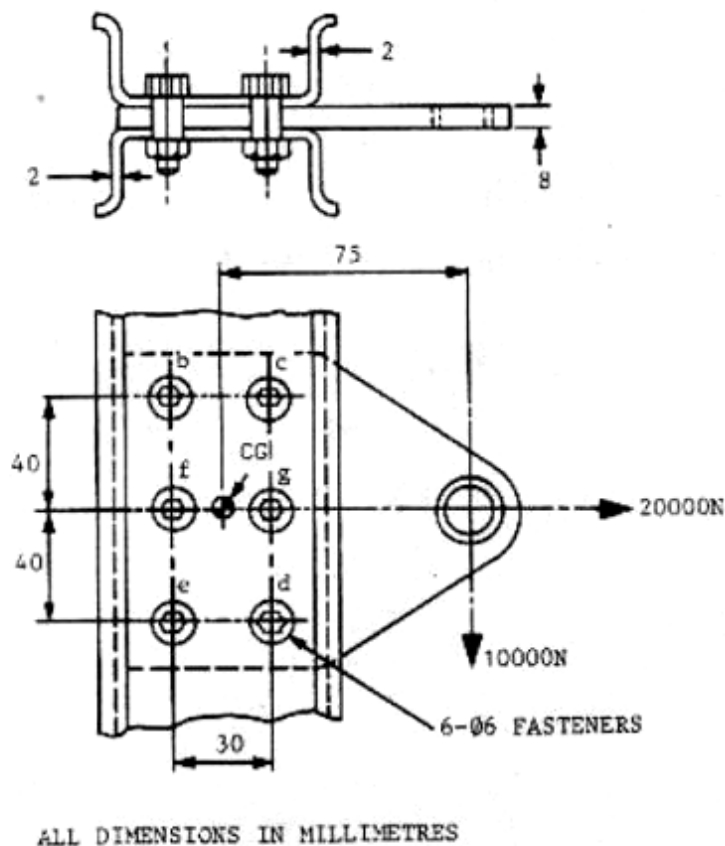


Figure 9-28 - Offset Loads on Fastener Groups

The centroid of the group (marked 'CG' in Figure 9-28) is determined by symmetry. The fasteners all have the same bearing and shear areas, therefore, relatively simple calculations can be made to determine the shear loads on the fasteners,

$$\text{Horizontal load on each fastener: } \frac{20000}{6} \text{ N}$$

$$\text{Vertical load on each fastener: } \frac{10000}{6} \text{ N}$$

$$\text{Moment at CG: } M_Q = 10000 \times 0,075 = 750 \text{ Nm}$$

Load due to moment on fasteners *b, c, e* and *d* with equation [9.4.4]:

$$F_{M,bced} = \left[\frac{A_{sha,bced} r_{c,bced}}{\sum_{j=1}^6 A_{sha,j} r_{c,j}^2} M_Q \right] = \frac{28.27e^{-6} \times 0.04272}{(4 \times 28.27e^{-6} \times 0.04272^2) + (2 \times 28.27e^{-6} \times 0.015^2)} \times 750 = 4134 \text{ N}$$

Load due to moment on *f* and *g* with equation [9.4.4]:

$$F_{M,fg} = \left[\frac{A_{sha,fg} r_{c,fg}}{\sum_{j=1}^6 A_{sha,j} r_{c,j}^2} M_Q \right] = \frac{28.27e^{-6} \times 0.015}{(4 \times 28.27e^{-6} \times 0.04272^2) + (2 \times 28.27e^{-6} \times 0.015^2)} \times 750 = 1452 \text{ N}$$

The force components for each fastener are shown in Figure 9-29. For more complex fastener group geometry equation [9.4.3] is needed.

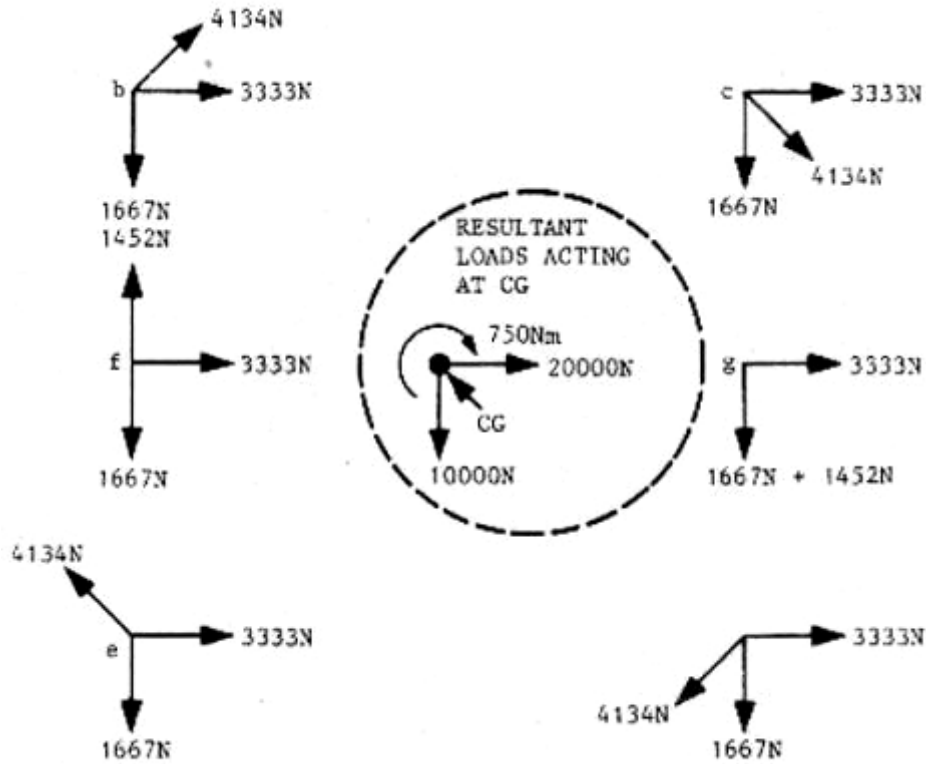


Figure 9-29 - Vector addition of the fastener loads

It can be seen by inspection that fastener *c* is the critical fastener, since all components of force act in the same quadrant (downwards to the right). Now that the most highly loaded fastener has been determined, it is important to determine the margins of safety for bearing joints according to Section 8.3.

9.6 References

9.1	LEE H.M.	Shear Joint Capability Versus Bolt Clearance, NASA TM-108378
9.2	BAe	Structural Design Data Handbook, British Aerospace Dynamics Group, Filton, 1985
9.3	DOT/FAA/AR-MMPDS-01	Metallic Materials Properties, Development and Standardization, Office of Aviation Research, Washington, D.C. 20591 (supersedes MIL-HDBK-5)

10

Low Duty Joints

10.1 Introduction

Previous sections have dealt with joints that designed primarily for strength criteria. There are however cases where the joint has to be modified to meet other criteria. These cases usually results in low duty (low stressed) joints. These joints can be assumed to be strong enough provided the external load on the joint does not exceed a threshold value. Low duty joints do not normally need detailed strength checks as were shown in previous sections. Section 10.4 describes the threshold loading that determines whether or not a joint is low duty.

10.2 Low Duty Joint Design Guidelines

10.2.1 Overview

Low duty joints can result from consideration of the following design requirements:

- Insert pull out strength (sandwich panel constructions)
- Joint thermal conductivity
- Joint electrical conductivity
- Handling size
- Stiffness
- Tolerancing
- Redundancy (fail safe)

Each of these is expanded in the following Sections 10.2.2 to 10.2.8.

10.2.2 Insert Pull out Strength

Threaded inserts (Reference 10.1) in sandwich panels are normally potted into the panel (see Figure 10-1). Generally the shear strength of the insert is high but its pull out strength is low. For an M4 insert, typical shear and pull-out strengths are 2kN and 0.4kN respectively. This limits the loads transmitted by the joint to be substantially less than the tensile strength of a steel M4 fastener, which is approximately 11kN. Therefore, it can be assumed that the critical failure mode of the joint is insert pull-out.

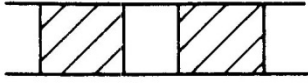
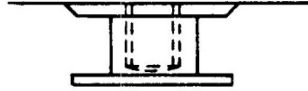

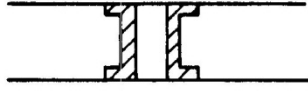
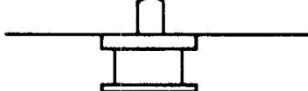
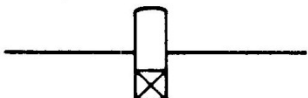
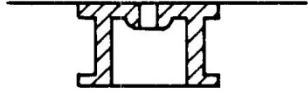
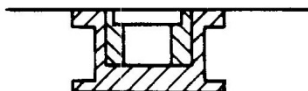


	TYPE	FASTENING PRINCIPLE	SHAPE	DIA (mm)	MATERIAL
(A)	1	BONDING DURING SANDWICH PRODUCTION		17-30	Al
(B)	2	POTTING		11-22	Al St Ti
	3			11-12	Al St Ti
	4			11-14	Al
	5			6-14	St Ti
	6			3-6	St Ti
	7			19-70	Al
	8			19-25	Al INSERT Ti NUT
	(C)		9	MECHANICALLY CLAMPED OR SCREWED	
10			14-22		Al St Ti

Figure 10-1 - Types of Inserts Used in Honeycomb Panels

10.2.3 Joint Thermal Conductance

Joint thermal **conductance** is a design requirement for certain space applications. A common example is electronics **units** for which it is necessary to conduct most of the heat generated internally away into the mounting structure. This needs a good thermal **conductance through this interface**. The topic of thermal conductance through interfaces is a complex one, and is treated in detail in ECSS-E-HB-31-01 Part 4A, Section 5 (Reference 10.2).

10.2.4 Joint Electrical Conductivity

The requirements for good electrical conductivity are similar to those for thermal conductivity. The necessary interface area is normally small. Thus, a single small fastener, properly preloaded, and standard washer generally provide adequate clamping force and sufficiently low electrical contact resistance. Typical examples of this type of joint are given in Figure 10-2.

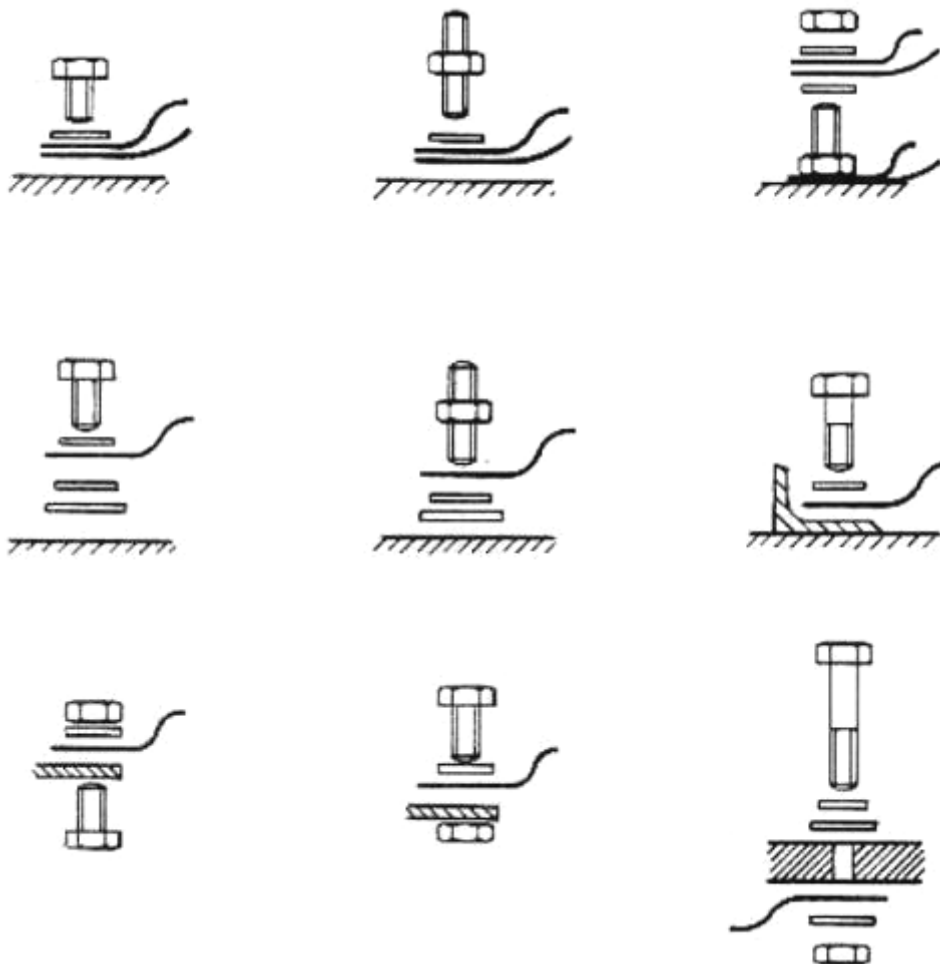


Figure 10-2 - Typical Earthing Arrangements

10.2.5 Handling Size

There are clear advantages in handling fasteners that have reasonable size. Very small fasteners are more easily dropped or damaged and assembly tends to be more time consuming when they are used. Additionally, very small fasteners cannot be reliably torque tightened. M4 is commonly held to be the smallest useful fastener size for general use, although other constraints [can](#) dictate the use of smaller fasteners. Thus, low duty joint often occur for ease of handling reasons, typical examples being are cable and pipe clamps, see Figure 10-3.

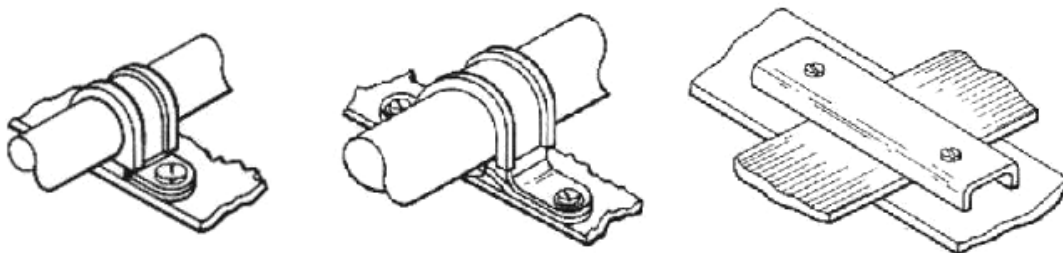


Figure 10-3 - Typical Low Duty Clamp Connections

10.2.6 Stiffness

The fastener size or number of fasteners used has a significant effect on the joint stiffness, it can also affect the stiffness of the mounted assembly. For example, by increasing the number of mounting points for an equipment box, its stiffness when mounted [can](#) increase, eliminating the need for complex stiffening structure within the box (thus saving weight and reducing cost).

10.2.7 Tolerances

In order to [reduce costs it is important to](#) minimise the tolerances. The larger the fastener, the larger the acceptable hole clearance whilst maintaining sufficient under-head bearing area, and hence the greater the misalignment that can be accommodated. This is particularly important for large lightweight assemblies where the distance between the mounting hole centres [can](#) be large, hence requiring relatively large positional tolerance to avoid the need for excessive manufacturing precision.

10.2.8 Redundancy

For some structures it [can](#) be deemed prudent to add additional fasteners to maintain the structural integrity should a fastener fail. This is more important in joints with few fasteners and hence can lead to a substantial reduction in duty.

10.3 Non-Metallic Joints

Low duty connections [can](#) also be found in wire wrap mounts and thermal blanket anchorages. These connections can be done without high clamping loads and, in the case of thermal blankets, metals are undesirable due to their high conductivity. As a result, plastic joint members and fasteners in conjunction with adhesives are often used. These types of connections are considered to be beyond the scope of this guidelines document.

10.4 Low Duty Threshold

In the absence of other information it can be assumed that a joint is of the low duty type if the applied joint load, either shear or axial, is less than 20% of the 0,2% proof load of the fastener, in the corresponding loading direction.

This assumes that the fastener can be preloaded to 75% of yield stress although in some circumstances the preload can differ, in which case the external load limit can be changed.

10.5 Example: Low Duty Thermal Joint

10.5.1 Overview

This example considers the equipment box shown in Figure 10-4.

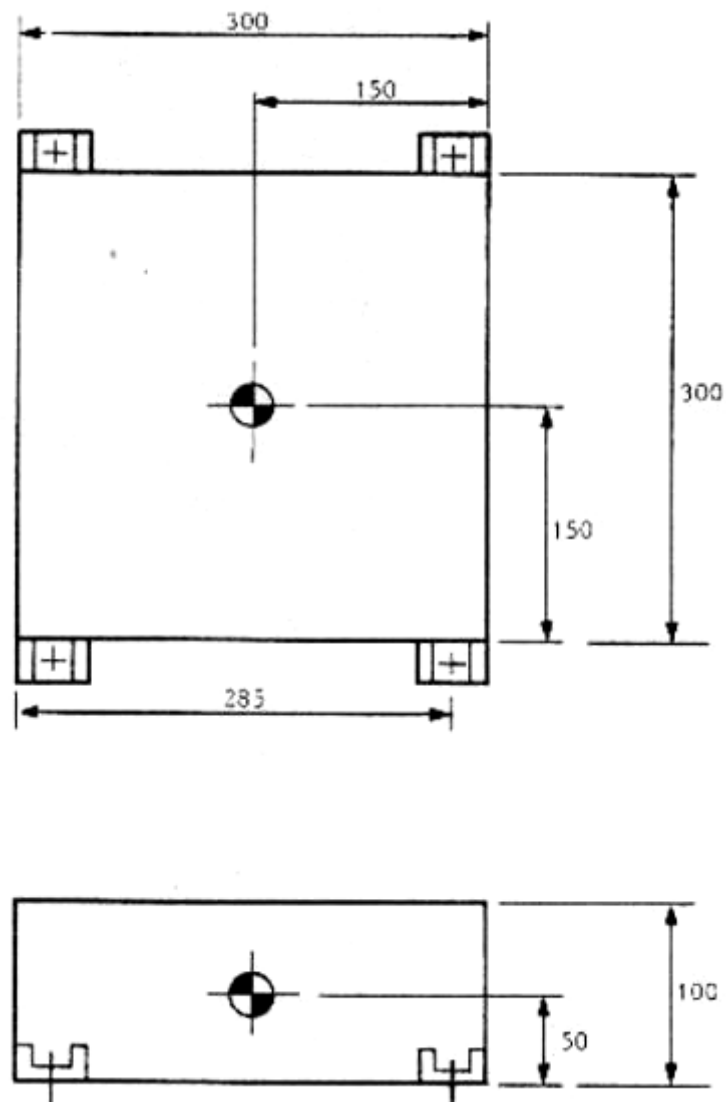


Figure 10-4 - Equipment Mounting Box Geometry

The box is to operate in a space environment as follows:

- Mass including contents: 5kg
- Fastener size to be used: M4
- Maximum acceleration: 20g into the base of the box.
- Heat to be dissipated: 5W
- Maximum allowable equipment temp: 70°C
- Maximum ambient temp: 45°C
- Pull out strength of insert joints: 400 N
- Shear out strength of insert joints: 2 kN
- Box and panel material: Aluminium 2024-T4
- Feet dimensions: 30 mm x 20 mm x 3mm thick

10.5.2 Initial Assumptions

The feet of the box each have a single fastener loaded to 65% of yield. The four fasteners experience the following tensile forces due to the box's inertia under acceleration:

Inertia force = mass x acceleration = 5 x 20 x 9,81 = 981N

Therefore, the load per fastener is 981/4 = 245N

An M4 x 0.7 fastener with 8,8 grade steel has the following properties:

Nominal diameter (d)	4 mm
Pitch (p)	0,7 mm
Yield strength (σ_y)	640 MPa
d_2 (Equation [5.4.1])	3,545 mm
d_3 (Equation [5.4.2])	3,141 mm
d_s (Equation [5.4.3])	3,343 mm
A_s (Equation [5.4.7])	8,779 mm ²

The yield load of the fastener is calculated with the stress area,

$$F_y = \sigma_y A_s = 640 \times 8.779 = 5619 \text{ N,}$$

The applied load to the fastener is only 4.3% of this yield strength. Therefore, low duty criteria apply (see Section 10.4) so no further strength checks need to be performed for the fastener.

The load acting on the inserts is below their pull out strength.

10.5.3 <<deleted>

10.6 References

10.1	ECSS-E-HB-32-22	Insert Design Handbook
10.2	ECSS-E-HB-31-01 Part 4A	Thermal design handbook – Part 4: Conductive Heat Transfer

Fatigue and Fracture Control of Fasteners

11.1 Introduction

This Section is intended to give the designer a broad understanding of Fatigue and Fracture Control analysis of fasteners, presenting **in addition some** hand calculation methods suitable for preliminary design purposes only.

The areas of fatigue and fracture mechanics are very much inter-related, in many cases, the relevant analysis tasks are complementary but usually a **potential** fracture critical item (PFCI) is designed to only one of these methods.

The differences between fatigue and fracture mechanics analyses are in their basic philosophies; fatigue estimates the life to failure of an **initially** uncracked item while fracture mechanics calculates whether or not an **initial** crack of a given size **can** propagate in a catastrophic manner under service loading.

In general, **it is important to verify** threaded fastener joints for adequate fatigue. Fasteners that are of aerospace quality and design that are used on a single mission (i.e. non-reusable items) **and verified to remain elastic and without gapping during their life** are generally not fatigue (**initiation**) critical since they are not subject to significant cyclic loading other than launch and acceptance testing, **unless there are significant other cyclic loads e.g. on orbit**.

It is important that potentially fracture critical (PFCI) joints **are** designed in accordance with ECSS-E-ST-32-01 "Fracture Control" (Reference 11.1).

Where possible, it is recommended that the latest version of the approved ESA/NASA computer program be used. The current version is ESACRACK, which incorporates ESALOAD, NASGRO¹ and ESAFATIG (see References 11.2 and 11.9).

11.2 Fastener Fatigue

11.2.1 Fundamentals

Fatigue failure occurs in a material under the cumulative effect of a number of cycles of alternating, repeated or varying stresses (usually tensile) of a level lower than the maximum static failure (or yield) stress. Such failures occur due to progressive extension of a micro crack initiating at the point of highest stress in a local stress field.

The initial speed of extension of the crack, **after its initiation**, is dependent on the crack propagation properties of the material and the applied loading cycle. Eventually a point of rapid and unstable crack growth occurs resulting in ultimate failure of the fastener.

The number of cycles to failure decreases as the range of alternating stress increases. For some materials an indefinitely long crack free life **can** be expected provided that the range of alternating stress is sufficiently low. However, some materials (such as Aluminium alloy) have no fatigue limit, although

¹ Fatigue Crack Growth Computer Program, originally developed at NASA Johnson Space Center, now further developed by Southwest Research Institute and the NASGRO Consortium.

the slope at high values of N becomes very low. A typical alternating stress versus number of cycles to failure ($S-N$) curve is shown in Figure 11-1. The $S-N$ curve approach generally assumes that the crack initiation time is much longer than the time to propagate the crack to failure.

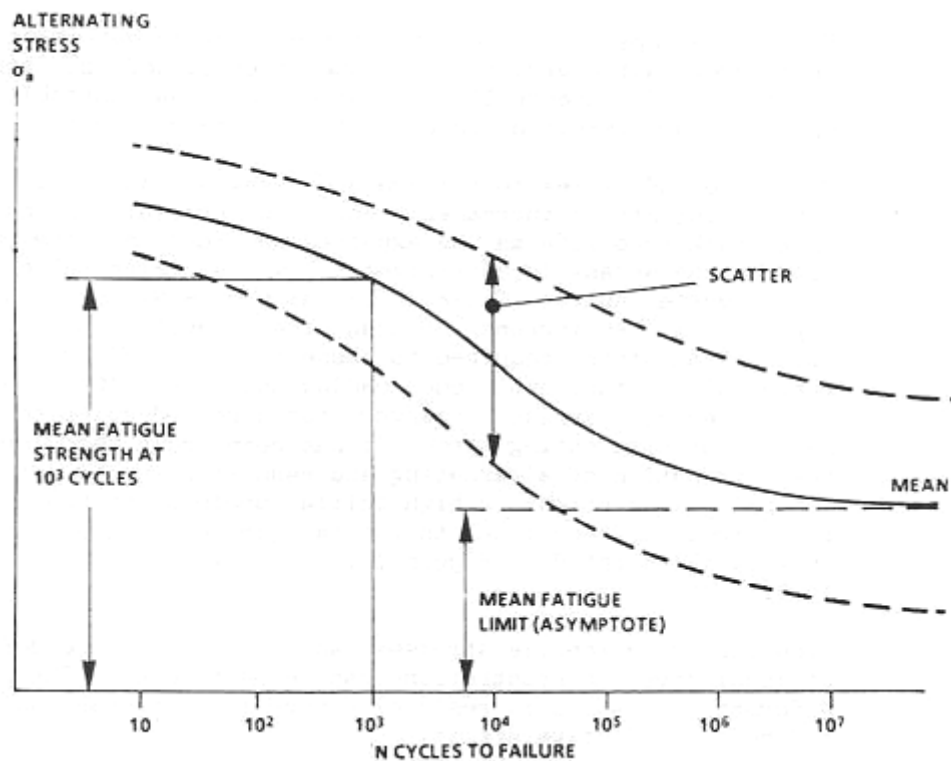


Figure 11-1 - Typical Fatigue Curve at Constant Mean Stress

An increase of the mean stress level reduces the alternating stress that causes failure. Figure 11-2 shows a typical constant amplitude loading and Figure 11-3 shows the effect of changed mean stress.

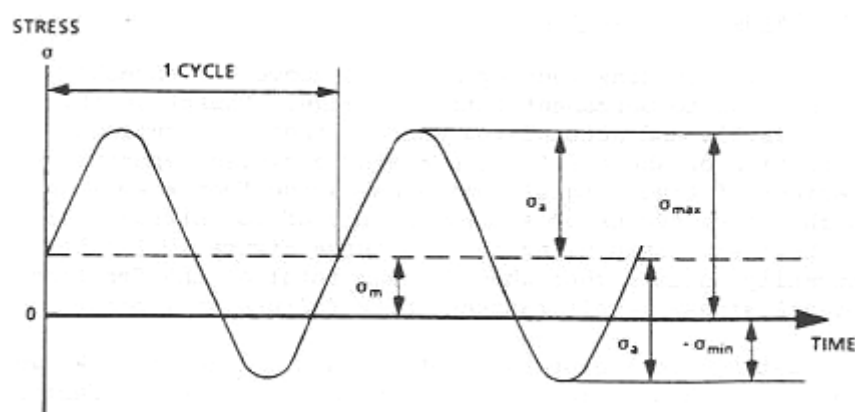


Figure 11-2 - Typical Constant Amplitude Loading

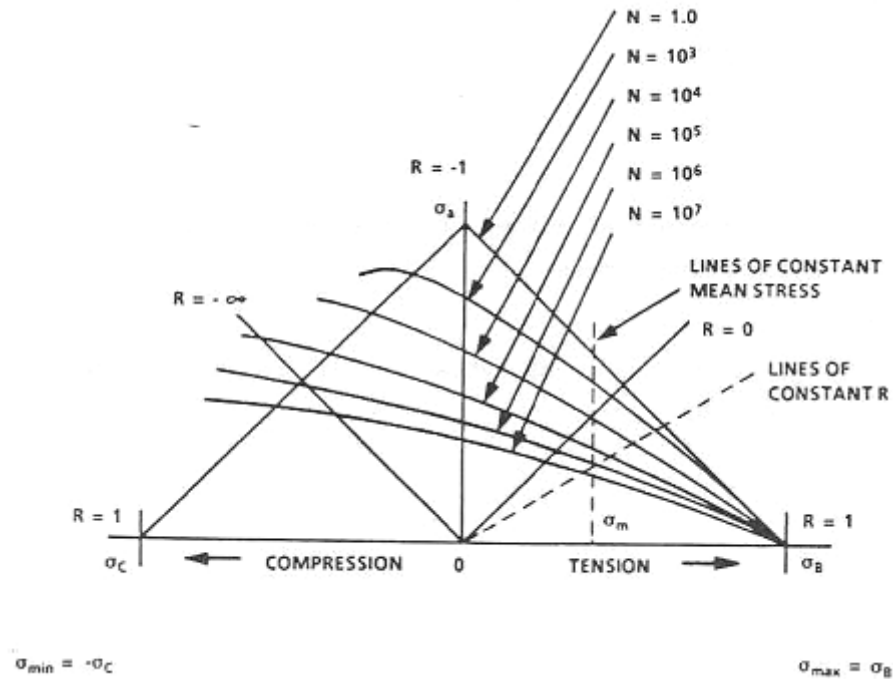


Figure 11-3 - Typical Stress Ratio – Mean Stress Diagram

Provided the combination of alternating and mean stresses does not exceed the fastener yield stress, a high initial preload is beneficial to the fatigue crack initiation resistance of the fastener. This is illustrated in Figure 11-4. Even very high tensile stresses, which cause plastic deformation at local stress concentrations, can be beneficial. Plastic deformation results in residual compressive stresses, which reduce the effective stress.

The ESAFATIG software (reference 11.2) contains specific fastener data. The available fastener data is illustrated below in Figure 11-5 to Figure 11-8.

Where:

$$\log N_f = A - B \log(S_{eq} - C), \text{ and } S_{eq} = S_{\max} (1 - R)^P$$

See reference 11.2 for more details.

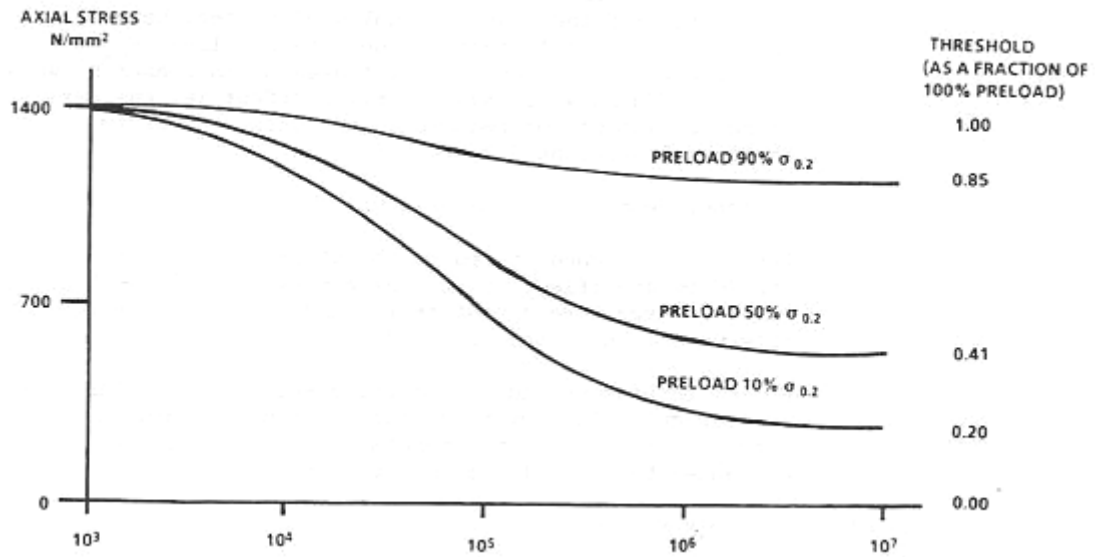
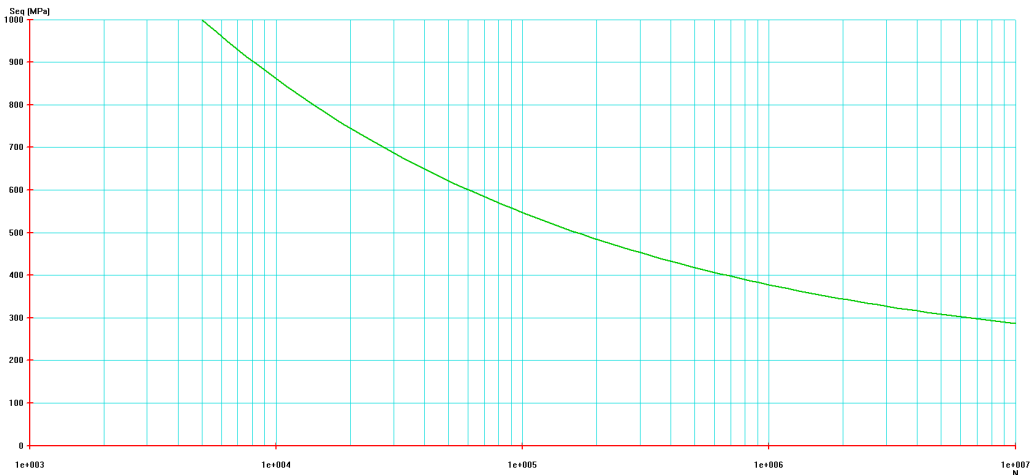


Figure 11-4 - Typical Preload Effects on Fatigue Life of Fasteners
 (taken from reference 11.6)

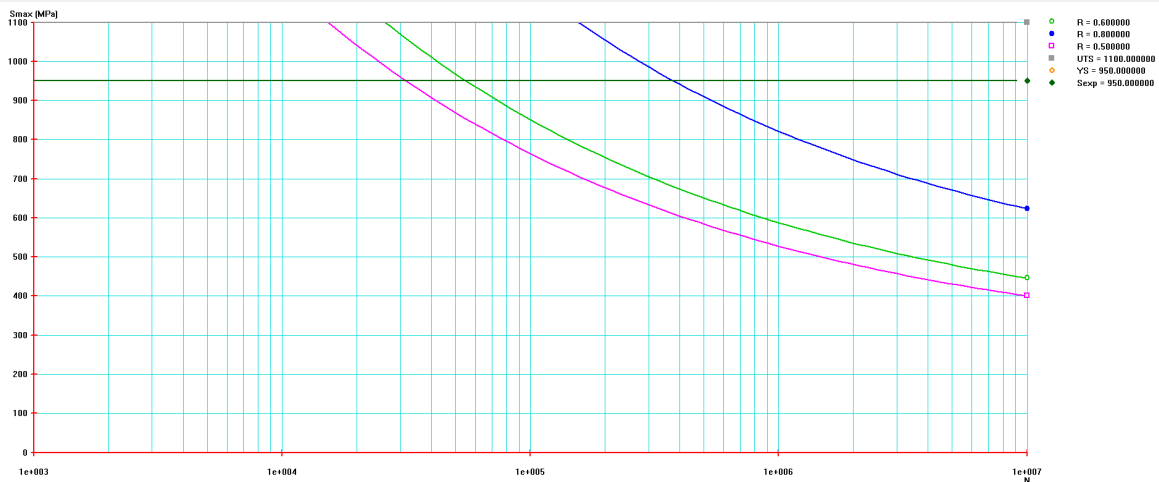
Material Group :	Material Alloy :	Material Description :					
stainless steel [d] ->	A286 ---[1] ->	[d1] A-286, STA d=3/16" p:32/inch NAS-6703-12M screw R=[0. ->					
Material Data - Fatigue Curvefit Constants :							
P: 0.483	A: 14.545	B: 3.722	C: 180.000	L: 180.000	UTS: 1100	YS: 950	Sexp: 950

(a)



(b)

Material Group :	Material Alloy :	Material Description :					
stainless steel [d] ->	A286 ---[1] ->	[d1] A-286, STA d=3/16" p:32/inch NAS-6703-12M screw R=[0. ->					
Material Data - Fatigue Curvefit Constants :							
P: 0.483	A: 14.545	B: 3.722	C: 180.000	L: 180.000	UTS: 1100	YS: 950	Sexp: 950



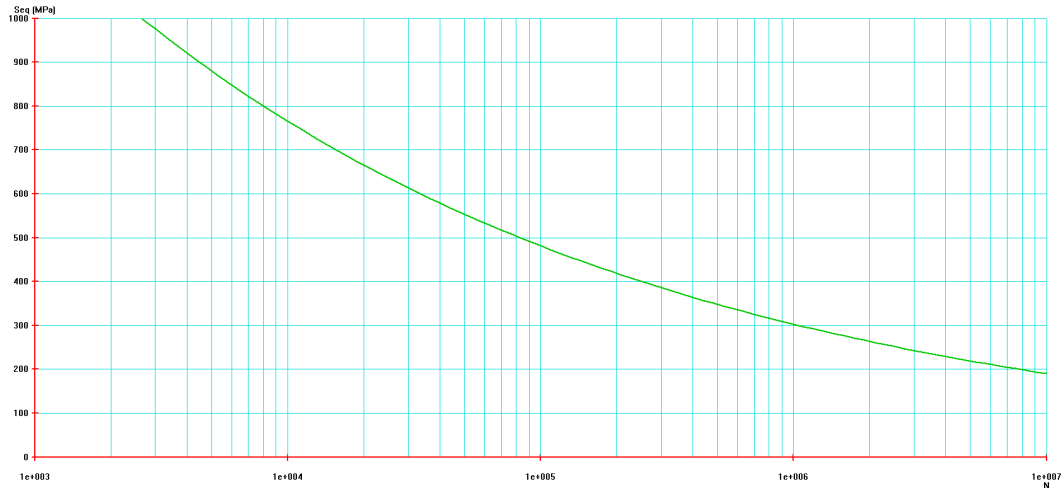
(c)

(a) Model parameters; (b) Seq-N; (c) Smax-N (for R=0.5, 0.6, 0.8)

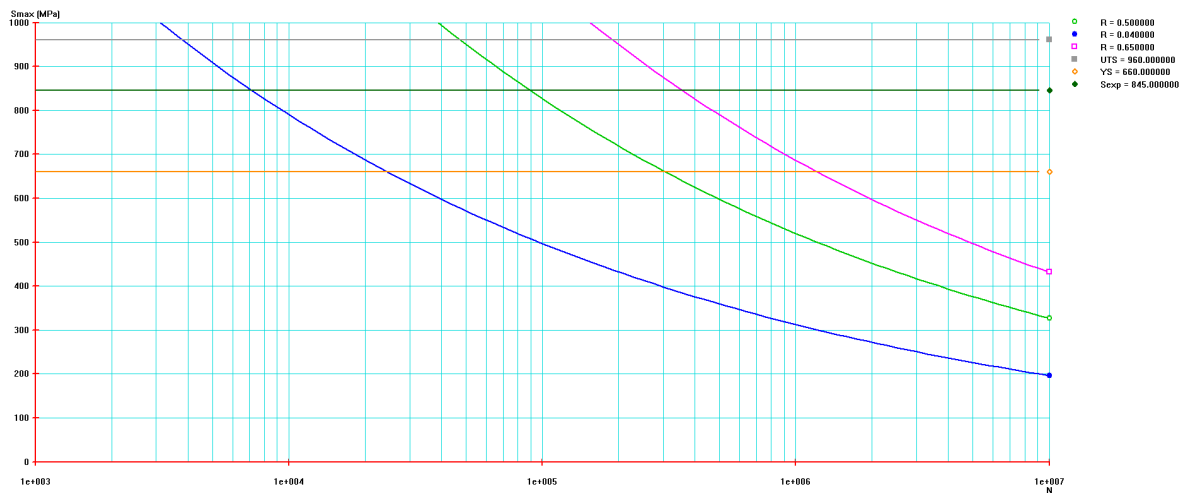
Figure 11-5 – ESALOAD S-N curves for A286 steel bolts (UTS=1100MPa)

Material Group :	Material Alloy :	Material Description :
stainless steel [d] ->	A286 --[1] ->	[d2] A-286 M5, W. No. 1.4944.4 screw R=(0.04;0.65) ->
Material Data - Fatigue Curvefit Constants :		
P: 0.780	A: 18.316	B: 4.964
C: 0.000	L: 119.719	UTS: 960
YS: 660	Sexp: 845	

(a)



(b)



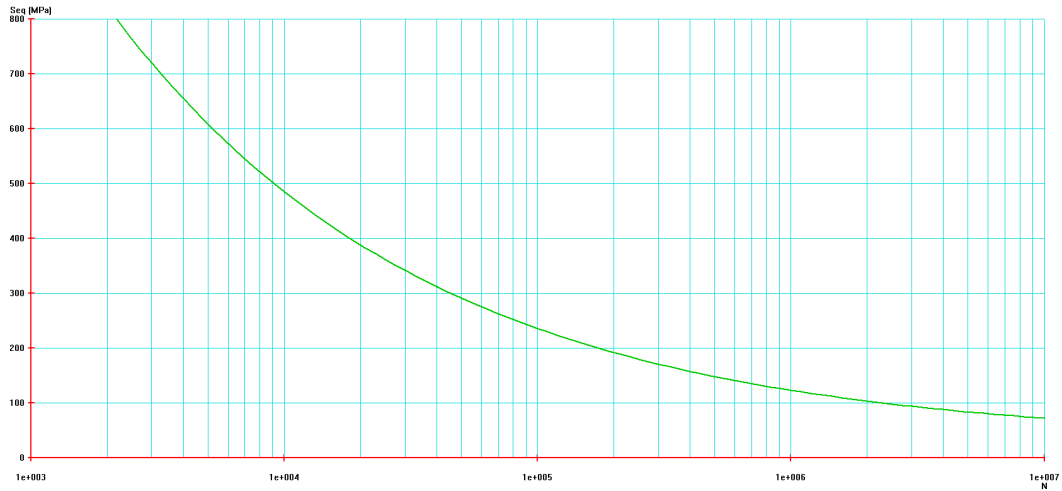
(c)

(a) Model parameters; (b) Seq-N; (c) Smax-N (for R=0.04, 0.5, 0.65)

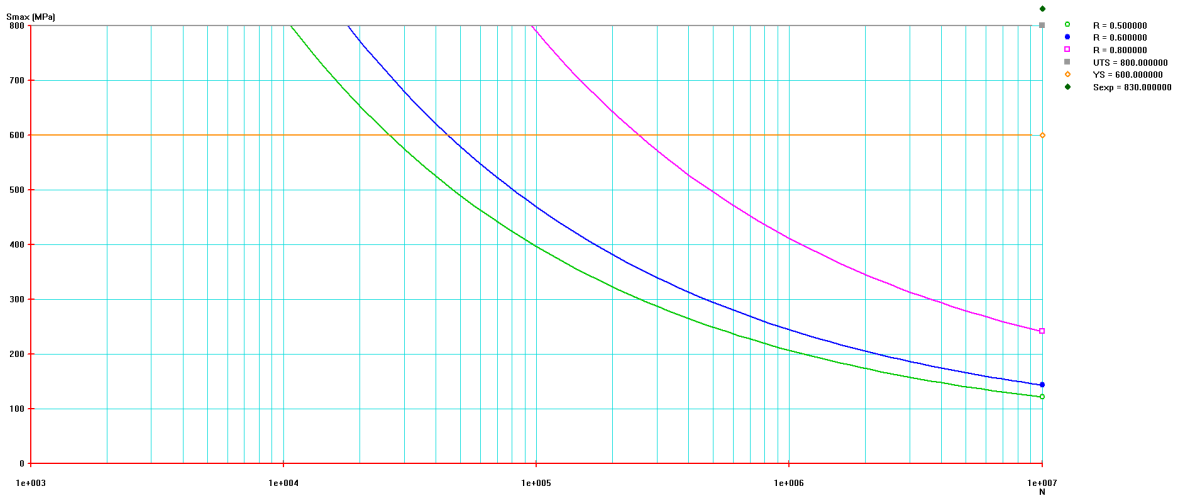
Figure 11-6 – ESALOAD S-N curves for A286 steel bolts (UTS=960MPa)

Material Group :	Material Alloy :	Material Description :
stainless steel [d] ->	A2-80 SCREW --[2] ->	[a1] A2-80, M5, ISO 3506-1979 austenitic screw R=(0.6;0.8) ->
Material Data - Fatigue Curvefit Constants :		
P: 0.752	A: 11.689	B: 2.893
C: 30.000	L: 30.000	UTS: 800
YS: 600	Sexp: 830	

(a)



(b)



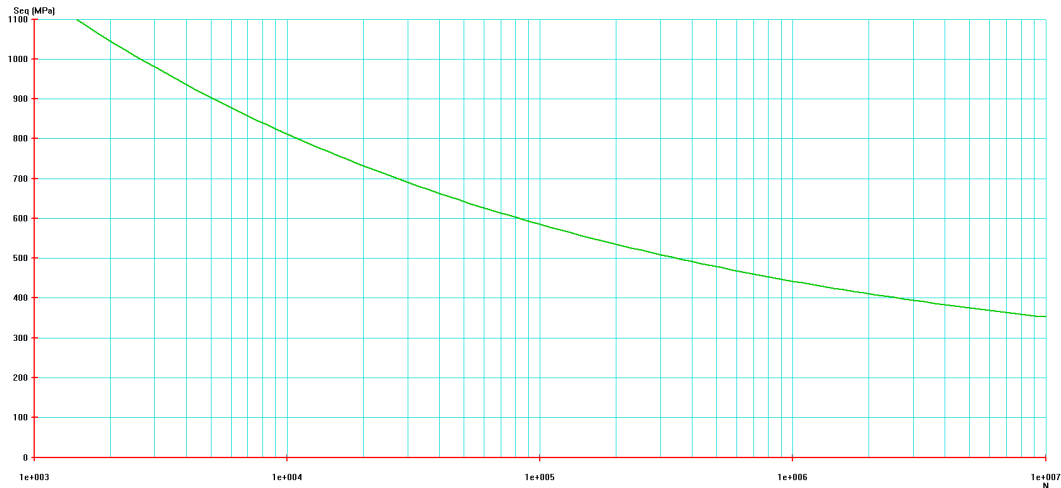
(c)

(a) Model parameters; (b) Seq-N; (c) Smax-N (for R=0.5, 0.6, 0.8)

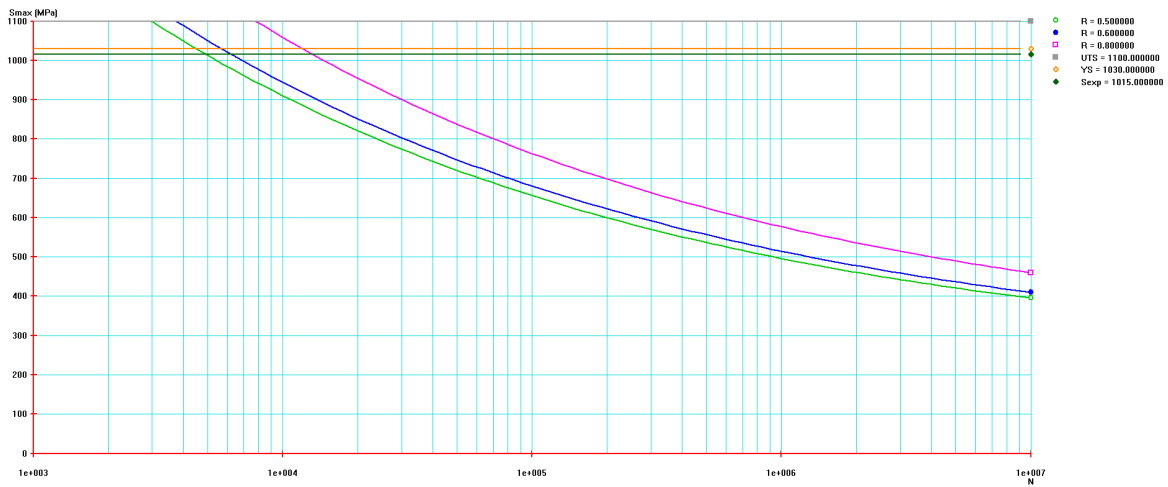
Figure 11-7 – ESALOAD S-N curves for A2-80 stainless steel bolts (UTS=800MPa)

Material Group :	Material Alloy :	Material Description :					
titanium alloys [p] ->	6Al-4V --[1] ->	[d1] Ti-6Al-4V , d=3/16" p:32/inch ABS 0114-12-P screw R=[0.6] ->					
Material Data - Fatigue Curvefit Constants :							
P :	A :	B :	C :	L :	UTS :	YS :	Sexp :
0.165	17.861	4.974	200.000	200.000	1100	1030	1015

(a)



(b)

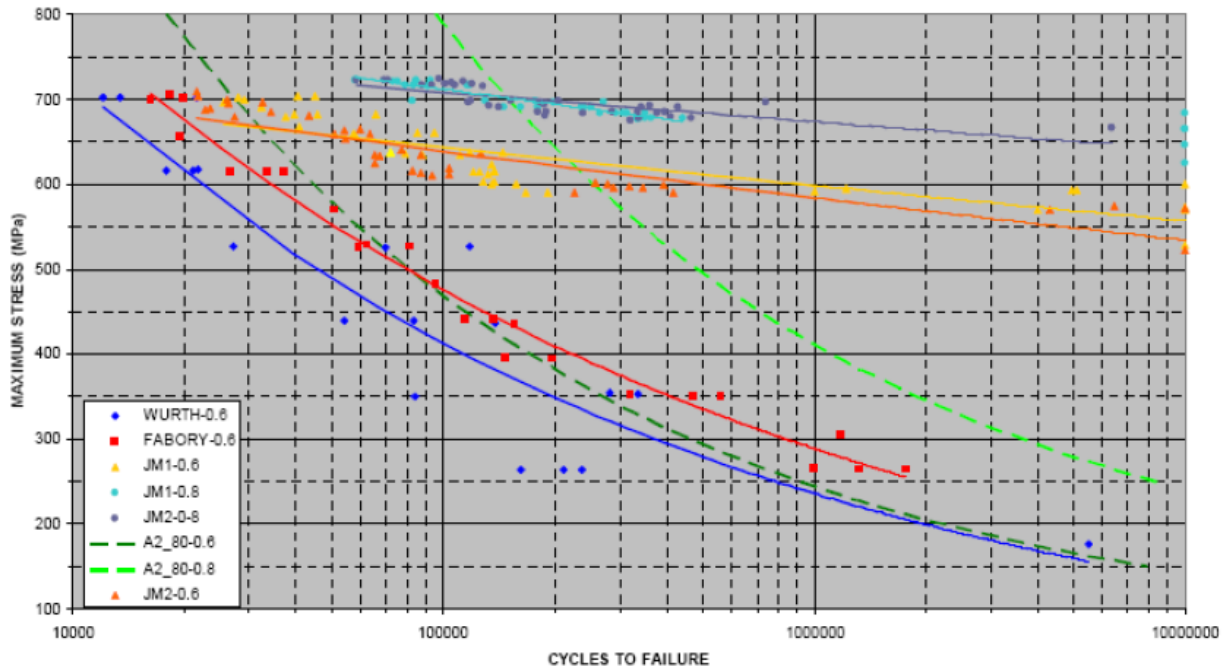


(c)

(a) Model parameters; (b) Seq-N; (c) Smax-N (for R=0.5, 0.6, 0.8)

Figure 11-8 – ESALOAD S-N curves for Ti6Al4V bolts (UTS=1100MPa)

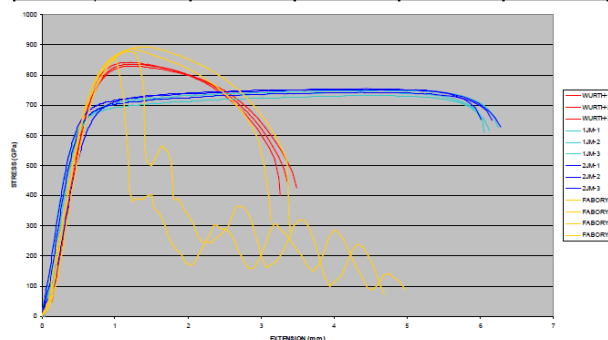
Note that the data provided in ESAFATIG is determined for aerospace grade fasteners. A small study has shown that industrial grade fasteners can perform significantly worse (reference 11.7). The figure below, from reference 11.7, compares the same type of stainless steel screws (DIN 912) procured to aerospace (DIN65058. 'JM') and industrial standard (Würth and Fabry).



Industrial grade (Wurth & Fabory) tested at R=0.6, aerospace grade (JM, 2 batches) tested at R=0.6 and 0.8. ESAFATIG data for A2-80 screws is provided for reference

Figure 11-9 – Fatigue test results for M5 DIN 912 stainless steel screws, A2-70

BATCH	SPECIMEN	STRESS (MPa)		AVERAGE STRESS (MPa)	
		YIELD	RUPTURE	YIELD	RUPTURE
JM1	1	579	747	584	746
	2	594	754		
	3	580	736		
JM2	1	612	759	612	754
	2	618	757		
	3	606	747		
WURTH	1	723	843	720	842
	2	720	835		
	3	716	847		
FABORY	1	748	891	731	884
	2	715	885		
	3	714	861		
	4	748	900		



Industrial grade (Wurth (red) & Fabory (yellow)) screws show higher strength and lower ductility than aerospace grade (JM, 2 batches (blue)) screws

Figure 11-10 – Tensile test results for M5 DIN 912 stainless steel screws, A2-70

Some observations (reference 11.7):

- Fatigue properties for ‘aerospace grade’ fasteners tested were very good. Very little dispersion within and between the 2 batches tested was observed.
- Fatigue properties of ‘industrial grade’ fasteners were significantly below those of aerospace grade. Possible causes:
 - Fastener quality was in fact closer to class A2-80 (more cold worked);
 - Potentially lower quality of commercial fasteners, e.g. lower surface hardness and lower surface quality.
- Based on these test results it can be prudent to use fatigue properties of the stronger A2-80 material to verify fatigue life of A2-70 fasteners, or alternatively to make sure that properties are really below those of A2-80 when using the properties of this study. Fastener strength classes are defined by minimum strength properties. There upon, no separate A2-70 material properties were included in ESAFATIG at the time.

It is important that truly fatigue critical fasteners are procured to a standard that ‘fatigue rates’ the fasteners by a batch fatigue test. Be aware that some of the smaller or shorter sizes are not be actually batch tested per such standards and will need to be fatigue tested in custom set-ups. Example: NASA-STD-5019A requires ‘low risk’ (i.e. ‘high quality’) fasteners, which operate at stress levels $>0,3 \times UTS$ (incl. preload), to be batch fatigue tested. This is a category not included in the current ECSS-E-ST-32-01.

11.2.2 Palmgren – Miner rule

All cyclic stresses above the fatigue threshold level give rise to permanent fatigue damage. Damage accumulates whether there is continuous load variation or whether there are single cycles separated by long periods of time. Equal damage can arise from a small number of high stress cycles or a large number of low stress cycles. This is best envisaged using the S-N curve Figure 11-1.

It is normally assumed that when the sum total of the fractional damage at all stress levels reaches unity, failure can occur.

The mathematical expression of the above concept is known as the Palmgren - Miner Linear cumulative damage rule. A scatter factor of 4 is typically applied to fatigue damage to allow for uncertainty in the fatigue analysis (see Reference 12.4). Thus, for fatigue resistant design, it is necessary to satisfy the following inequality,

$$f = 4\Omega \leq 1 \quad [11.2.1]$$

where f is the total fatigue damage and Ω is the fatigue damage.

The fatigue damage Ω is given by,

$$\Omega = \sum_{i=1}^m \frac{n_i}{N_{f,i}} \quad [11.2.2]$$

where n_i is the number of cycles that have occurred at a particular mean and alternating stress, $N_{f,i}$ is the number of cycles to failure at the same stress condition, and m is the number of stress conditions that the joint is subjected to.

11.2.3 Fatigue Design Principles

11.2.3.1 Overview

Any factors that affect stress can affect fatigue life. Such factors give rise to the basic design principles as listed in the following sections.

11.2.3.2 Static and Dynamic Loading

Appropriate joint design can greatly reduce the external loads felt by the fasteners and increase the life of the joint. Any features of the design that increase the fastener compliance or decrease clamped part's compliance can have a similar effect, e.g. smaller diameter, longer, or reduced shank bolts. For more information on fastener compliance, refer to Section 7.5. The choice of fastener material can also have a significant impact. The joint diagram in Figure 11-11 illustrates that a titanium fastener with half the elastic modulus of a steel fastener feels only half of the external load ($\Delta F_{b,A}/2$). Figure 11-12 compares the fatigue performance of M8 fasteners made from the two materials operating at a mean stress of $0,75 \sigma_y$.

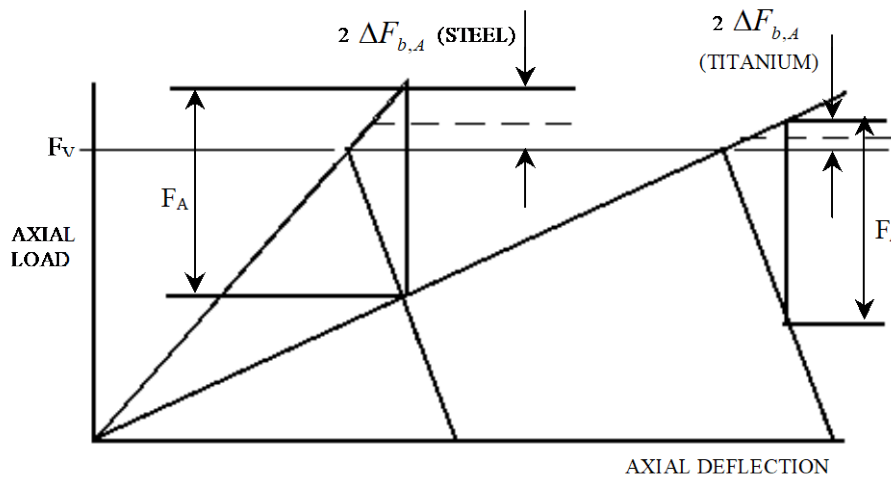


Figure 11-11 - Joint Diagram Comparing Steel and Titanium Fasteners

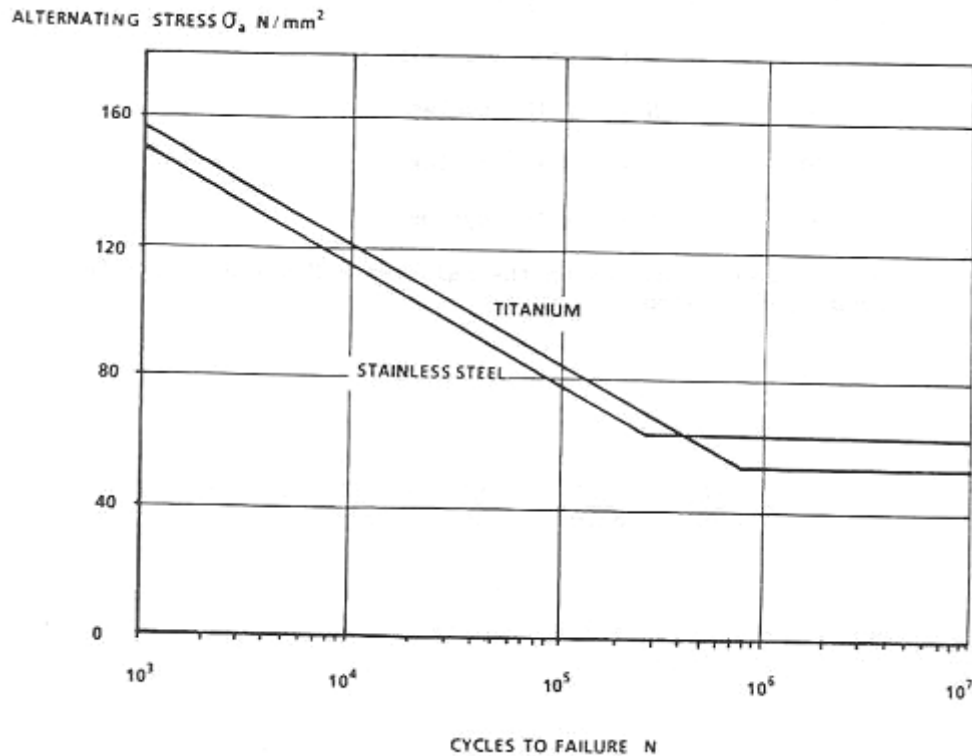


Figure 11-12 - Typical Fatigue Comparison, Ref. 11.8

11.2.3.3 Fastener Geometry and Manufacturing

It is important to specify fasteners that are designed to reduce the stress concentrations, and to incorporate all features such as large under head radius, large thread root radius and close tolerance threads.

It is also important to specify rolled threads, and in particular, thread rolling and cold working of the under head radius is carried out as the final manufacturing operation to guarantee beneficial compressive stresses.

11.2.3.4 Assembly Methods

Preload is the most important joint parameter in resisting external loads (see Section 6). It is important to use the most accurate preloading method (appropriate to the assembly) together with a dry lubrication system that gives the most consistent (rather than the lowest) friction conditions.

It is important to measure prevailing torque during each assembly operation and that torque is added to the torque specified for preloading.

11.2.3.5 Surface Finish Defects and Other Damage

It is important to pay special attention to surface finish and Non Destructive Inspection (NDI) procedures for safe life PFCI fasteners. Fatigue life can be greatly reduced by flaws, scratches or abrasions arising either during manufacturing or while in service.

Other effects that are important to be considered are differential thermal stresses, stress corrosion and fretting under load.

11.3 Fundamentals of Fracture Control and Fracture Mechanics

11.3.1 Fracture Control

Fracture control is multi-disciplinary and includes the engineering disciplines of fracture mechanics for the assessment of damage tolerance (safe operating life), non-destructive inspection to screen for damage, quality and process controls, material lot traceability and proof testing to assure the highest quality part. The combination of these disciplines into a viable fracture control plan ensures that parts whose failure can lead to loss of life or vehicle provide adequate safety [ref 11.10].

The basic assumptions that underlie implementation of fracture control include:

- All structural elements can contain crack-like defects located in the most critical area of the component in the most unfavourable orientation.
- The fact that the applied non-destructive inspection (NDI) do not detect (significant) defects does not negate this assumption, but merely establishes a lower bound on the initial size of the cracks to be used for verification.
- All critical spaceflight hardware is of a good design, certified for the application, adequately acceptance tested, and manufactured and assembled using high quality aerospace processes. It is important that it contains no detected defects, unless specifically justified and approved.

The implementation of fracture control utilizes part classifications to identify their criticality (Ref. 11.1) potential fracture critical (PFCI) and fracture critical (FCI).

Non-fracture critical PFCI include safe life parts (with standard initial crack size), low released or contained masses, redundant (fail safe) structure, non-hazardous leak-before-burst (LBB) pressurized components, low speed and low momentum rotating machinery, and high quality (low risk) parts with high margins on cycle life and strength (i.e. with low risk of failure caused by a crack-like defect).

Note that historically the term 'safe life' is used for spaceflight hardware where a safe crack growth life is demonstrated. This is still the case in ECSS standards. This differs from usage of this term in e.g. aeronautics. In more recent standards (e.g. NASA-STD-5019) NASA has changed towards the term 'damage tolerant'.

Sometimes fracture control and fracture mechanics verification are understood to be the same thing. However, by applying non-fracture critical categories like fail-safe, low risk and containment, it can be possible to implement fracture control without fracture mechanics analyses or tests.

Sometimes fracture mechanics assessments are used outside the formal framework of the fracture control standards, e.g. to conservatively assess fatigue life (durability). The initial crack size can then be based on other experiences and information than the applied crack detection methods, for example $a = c = 0,125$ mm (corner or surface crack) per ECSS-E-ST-32-01.

Normally, safety critical fasteners are procured in accordance with aerospace practices, following standards like references 11.12, 11.13 or equivalent. In addition, a method for assurance of fastener integrity is required.

According to ECSS-E-ST-32-01 all PFCI fasteners are procured and tested in conformance with aerospace standards for structural fasteners or equivalent specifications agreed with the customer. For example, LN, AIR and NAS standards, or ISO, EN and national standards which are explicitly intended for aerospace applications. '*Fasteners procured and tested in conformance with aerospace standards for non-structural fasteners shall not be used*' (example Ref. 11.21). However, for secondary connections where

significant redundancy exists and fatigue is not a major concern, sometimes such non-structural fasteners are applied.

Preferably, fasteners be designed and verified to be fail safe.

According to ECSS-E-ST-32-01 threaded fasteners can only be considered 'low risk' when the stress (incl. preload) does not exceed $0,3 \times UTS$ during the life, which limits this category generally to threaded fasteners used as shear pins with low preload.

Safe life fasteners have to be sufficiently large in diameter (minimum 5mm but preferably larger) and of the highest aerospace quality manufactured from A286 steel, Inconel 718, MP35 N alloy or similarly tough and environmentally compatible alloys.

It is important that fracture critical (or low risk) bolts in tension applications are not been fabricated from low fracture toughness alloys or specifically titanium (unless agreed otherwise, see below).

The eddy current method is the preferred method for inspection of fracture critical threaded fasteners. General guidance can be found in the ECSS-Q-ST-70-15C (Ref. 11.14) on NDT, more specific information can be found in e.g. NASA-JSC PRC 6509 (Ref. 11.15). The associated standard surface crack size for eddy current is: depth $a=1,27\text{mm}$, length $2c=2,54\text{mm}$. Dye penetrant inspection is generally considered insufficient, because rolled threads, and other rolled radii cannot be etched as normally required before penetrant inspection for fracture control, in order to avoid degradation of the fastener quality. Penetrant inspection is sometimes performed without etching, but more as a general quality check instead of basis for safe life analysis.

In case preloaded fasteners without threads rolled after all thermal treatment of the material be used, in agreement with the customer, in addition to the crack size associated with the NDI, also a so-called 'maximum machining defect' (of depth $0,127\text{mm}$ all along the thread) that is generally smaller than the reliably detectable crack size, if often considered as additional risk mitigation (Ref. 11.9).

Performing a proof test for crack screening of fasteners is generally not easy. See also ECSS-E-ST-32-01. Sometimes this is agreed between customer and supplier, but most of the time it is some sort of compromise for risk mitigation as part of implementation of the 'reduced fracture control programme' for non-human spaceflight, and often supported by NDI after proof testing (some sort of 'proof test enhanced NDI'). This works best if only small crack growth is predicted, and no significant SCC, EAC or SLC (as can be the case for titanium fasteners) has to be accounted for.

Titanium fasteners

Over the years, a lot of debate has occurred about the risks associated with the application of titanium preloaded fasteners. The latest NASA fracture control standard [ref 11.16] prohibits titanium for low risk fasteners, while for fracture critical and safe life fasteners titanium is discouraged (esp. for fracture critical ones) and subject to approval of the responsible fracture control authority. The ECSS standard [Ref 11.1] prohibits titanium safe life fasteners generally, but defines no specific limitation for fail-safe titanium fasteners.

The concerns highlighted in NASA-STD-5019A are: generic environmentally assisted or sustained load cracking failure modes, as well as low fracture toughness. For safe life (damage tolerant) titanium fasteners: Titanium alloys, such as Ti-6Al-4V (including annealed and STA conditions), cp-Ti, and other titanium alloys, have potential generic EAC or SLC failure modes that are to be addressed in the assessment with test data from flawed fasteners in the applicable service life environments (incl. air).

Additional background information on sustained load cracking of titanium can be found in Ref. [11.17].

In addition, NASA-STD-5019A explains: Growth of a pre-existing crack in susceptible metallic alloys under sustained stress without assistance from an external environment. SLC, because of the presence

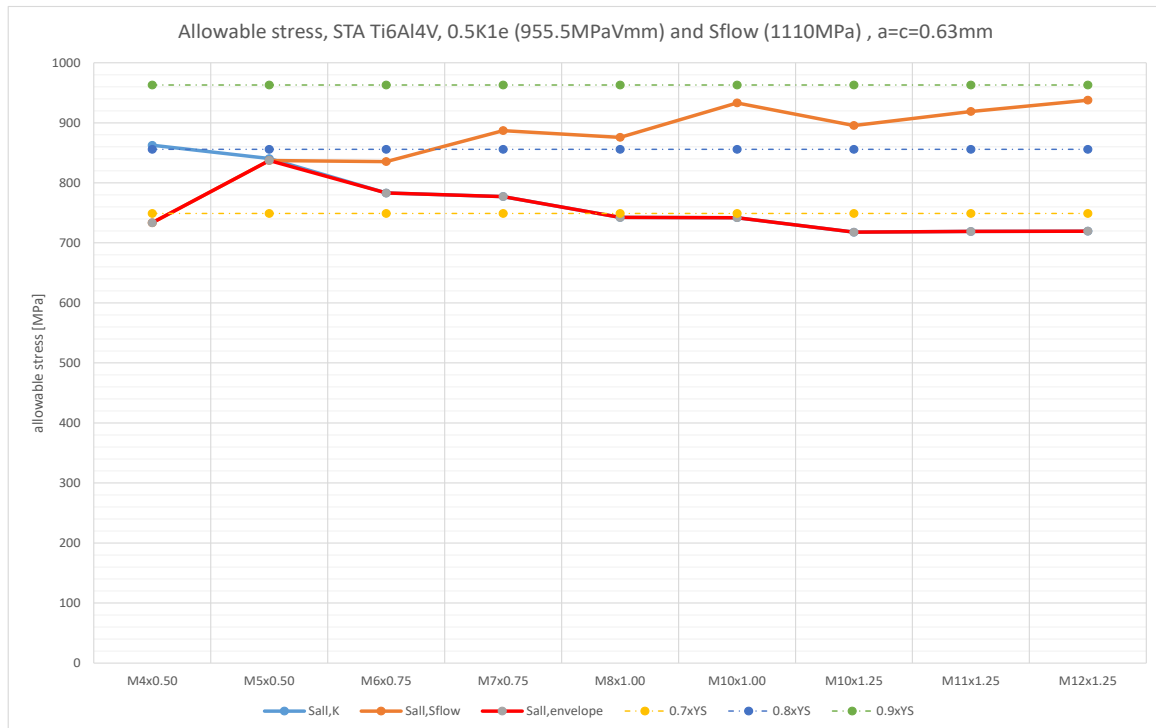
of interstitial hydrogen, occurs in titanium alloys, including commercially pure titanium (cp-Ti) and Ti-6Al-4V (Ti64), in both annealed and solution treated and aged (STA) conditions. Testing is necessary to determine the threshold stress intensity for the titanium alloy metallurgical condition and interstitial hydrogen content. Other materials with different crystalline structures such as steel and aluminum alloys that do not allow interstitial hydrogen can still exhibit SLC behaviours. A threshold stress intensity factor can be obtained by procedures such as those in ASTM E1681 for the case of an inert or vacuum environment. One publication determines the effects of hydrogen content and temperature on SLC in Ti-6Al-4V (Boyer and Spurr, 1978, Ref. [11.18]).

An update of the ECSS fracture control standard was released in 2021 (Rev. 2 of Ref. [11.1]). For uncrewed application titanium safe life fasteners are now permitted, based on a sustained load cracking threshold of 50% of the fracture toughness. This 50% value is considered a reasonable lower bound of the values observed in literature (Ref. [11.17] and specifically [11.19] and [11.20]).

For more critical applications (esp. human spaceflight), additional test data can be required for verification.

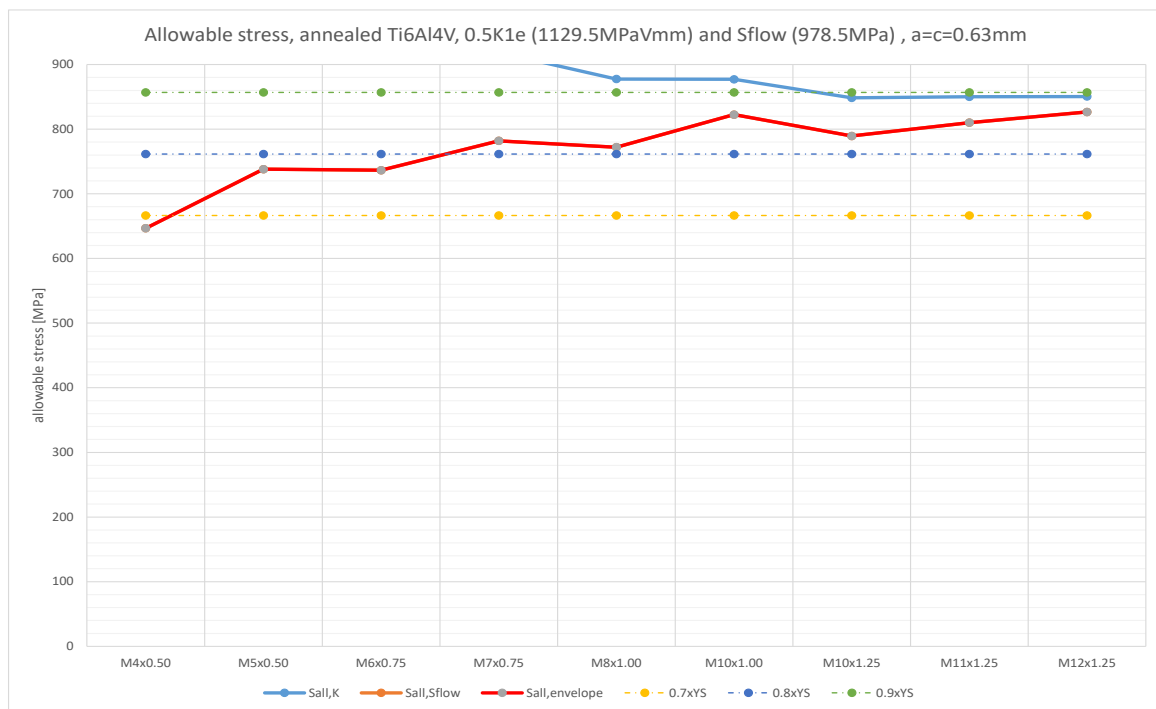
As part of the so-called 'reduced fracture control programme' (applicable to non-human spaceflight) a new risk-based approach for safe life fasteners is included, based on the fact that a crack of the order of 0,63mm (a value of 0,025" used also in some NASA standards) can be considered as unlikely to exist in a high-quality part, independent of the applied NDI. Note that for critical applications a larger initial crack size can apply. In Figure 11-13 to Figure 11-18 some residual bolt strength curves are presented for some commonly applied fastener materials, which provide rough indications of the maximum sustained stress level allowed in the fasteners in the limiting case that no significant fatigue crack growth occurs. The curves are defined using the NASGRO (v.9) model SC08 (see also Figure 11-20) with crack size $a=c=0,63\text{mm}$. The red lower bound curves is defined by the minimum strength defined by toughness (K_{Ic} or 50% of K_{Ic} for titanium; blue curves) and flow stress (average of yield and ultimate strength; orange curves). In most cases, the flow stress criterion is driving, except for Ti6Al4V STA (Figure 11-13). The toughness curve tends to be slightly decreasing for increasing bolt size, because the larger root radius causes an increased depth affected by high stresses (size effect of stress concentration). The curve based on the flow stress criterion tends to be slightly increasing, due to the relative decrease of the crack size w.r.t. the cross-sectional area. For reference, lines at applied sustained stress levels 70% (yellow), 80% (blue) and 90% (green) of the yield strength (for uncracked geometry) are also provided.

Internal thread in safe life items can be of particular concern, because it will be difficult to inspect and cracks could emanate from sharp notches, and only few suitable standard cracked geometries exist in crack-growth software like NASGRO. It is recommendable to avoid this wherever possible. Such threads will not only be directly loaded by the bolt, but can also be loaded by other loads applied to the item, and the resulting stress distribution can be complex. This can be the most critical location of the part, even if the corresponding bolt pattern is verified as fail safe. The acceptance rationale can also benefit from the risk-based approach, using 0.63mm initial crack size, mentioned above (see ref. 11.1, rev.2, clause 11.2.2.6), at least for non-human spaceflight. In some cases also the a so-called 'maximum machining defect' (of depth 0,127mm all along the thread), mentioned above for external thread, can be considered as additional risk assessment.



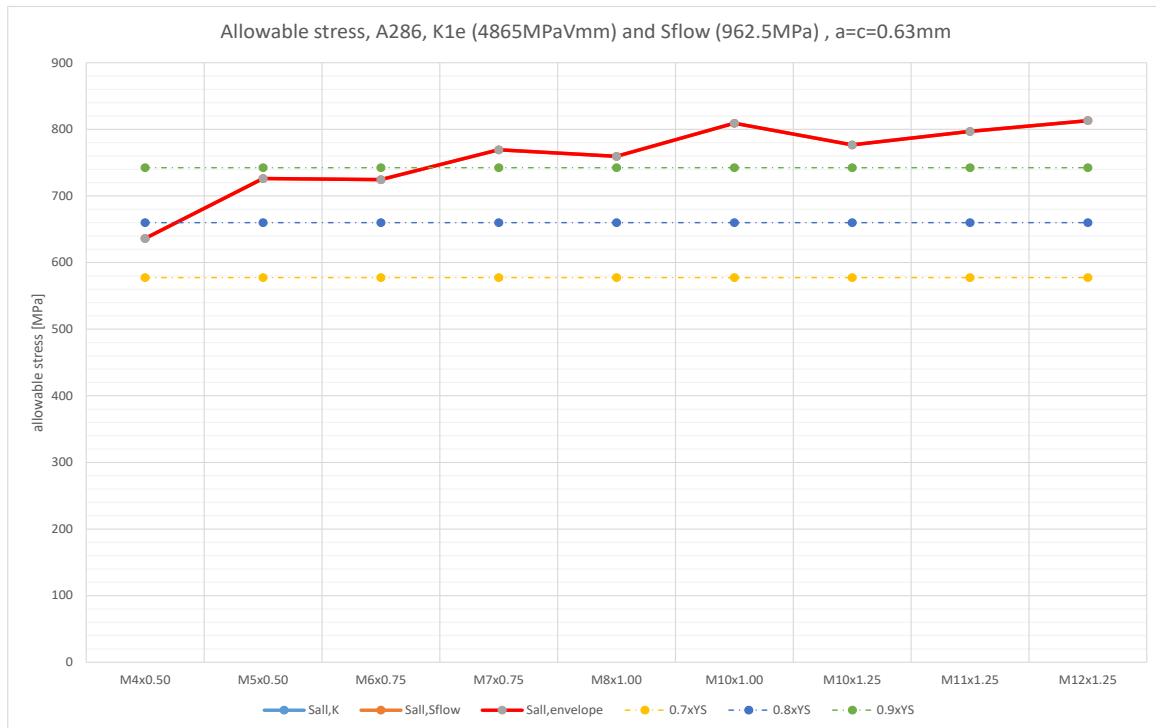
YS=1070MPa; $K_{1e}=1910\text{MPa}\sqrt{\text{mm}}$; sustained stress limited by $0.5x K_{1e}$

Figure 11-13 – Residual bolt strength under sustained loads, Ti6Al4V STA



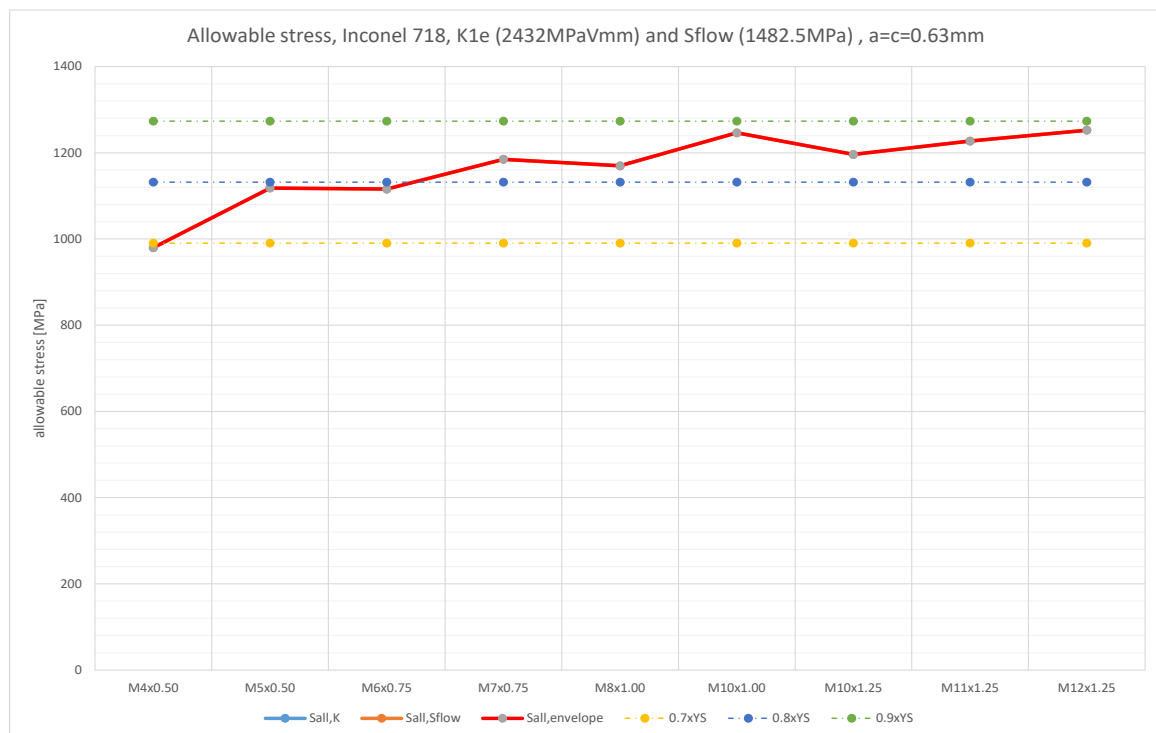
YS=950MPa; $K_{1e}=2260\text{MPa}\sqrt{\text{mm}}$; sustained stress limited by $0.5x K_{1e}$

Figure 11-14 – Residual bolt strength under sustained loads, Ti6Al4V annealed



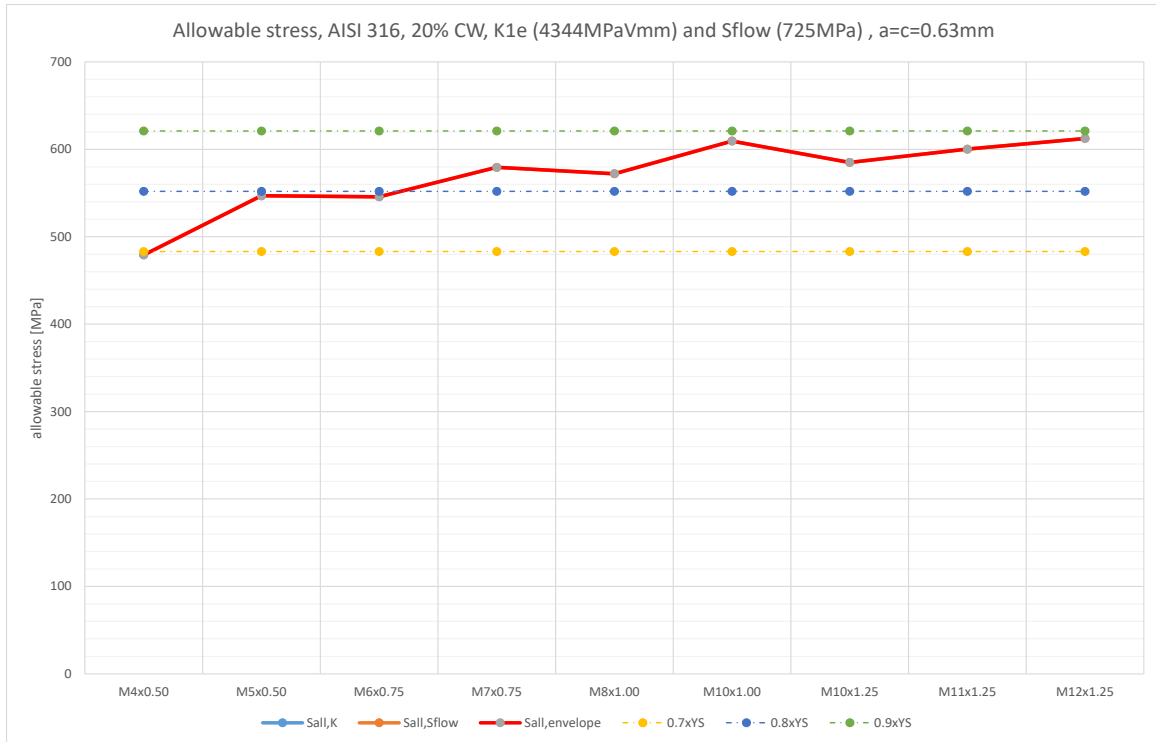
YS=825MPa; K_{1e}=4865MPa√mm

Figure 11-15 – Residual bolt strength under sustained loads, A286 steel



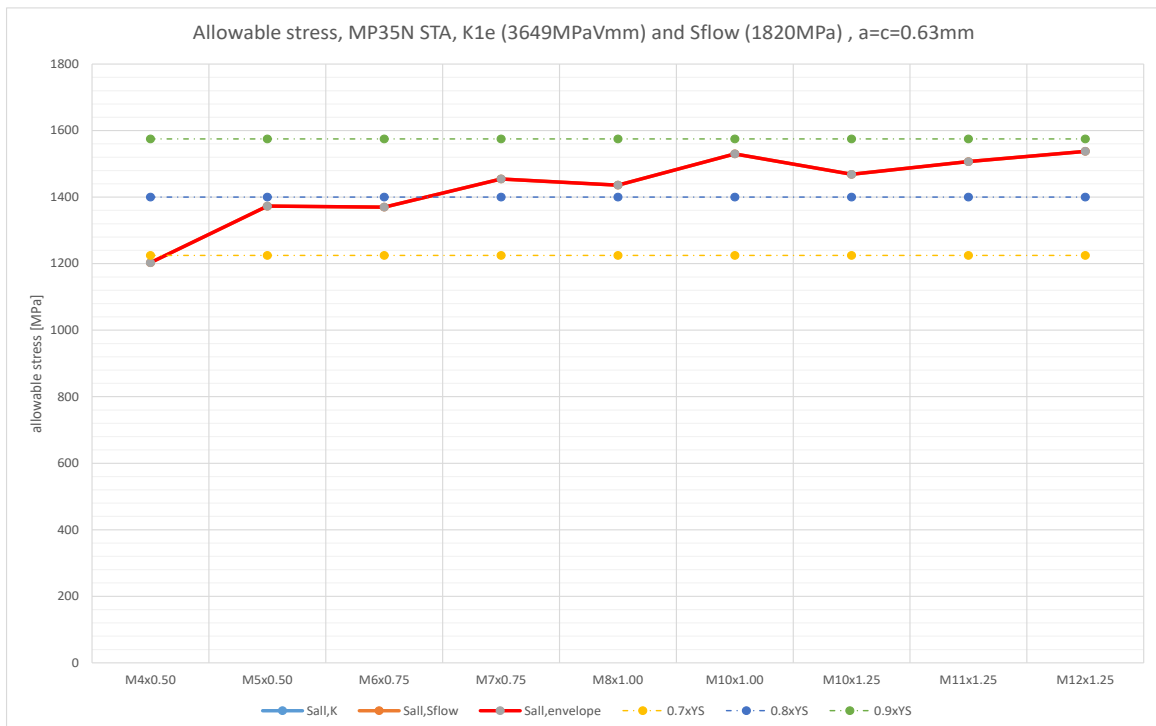
YS=1415MPa; K_{1e}=2430MPa√mm

Figure 11-16 – Residual bolt strength under sustained loads, Inconel 718



$YS=690MPa; K_{1e}=4345MPa\sqrt{mm}$

Figure 11-17 – Residual bolt strength under sustained loads, AISI 316 stainless steel



$YS=1750MPa; K_{1e}=3650MPa\sqrt{mm}$

Figure 11-18 – Residual bolt strength under sustained loads, MP35N STA

11.3.2 The Stress Intensity Factor

Fracture Mechanics theory is still under development and a number of different approaches can be found in the literature. The most well-established and useful concept is the stress intensity factor, a parameter used to characterise the stress distribution around a crack tip.

The stress intensity is the basis of Linear Elastic Fracture Mechanics (LEFM) theory, which applies in cases of plane strain such as a radial crack propagating from a fastener thread root.

From Reference 11.5, the stress intensity factor is given by,

$$K_I = \sigma \sqrt{\pi a} F \quad [11.3.1]$$

where K_I is the stress intensity factor for the tensile opening mode (as opposed to K_{II} and K_{III} for the shear and torsion crack opening modes), σ is the gross axial fastener stress (calculated using the fastener's nominal cross-sectional area, A), a is the crack length measured radially into the bolt, and F is the stress intensity correction factor (accounts for the geometry and location of the crack).

To develop an LEFM analysis using Equation [11.3.1] it is assumed an initial crack length, a_0 , either from knowledge of the initial crack size or from an estimation of the largest crack that can escape detection with the relevant NDI techniques. The equation can be used to calculate the stress intensity factor for a cracked component, and allows estimation of either the critical static stress corresponding to the crack length, or the instantaneous stress intensity for dynamic loading crack growth analysis.

11.3.3 The Stress Intensity Correction Factor

11.3.3.1 Overview

This section is based on an older version of the NASGRO software (Ref. [11.3] or [11.4]) as well as other literature and will not be fully up to date with the latest NASGRO version (Ref. [11.9]). Cracked fastener models are still being further developed.

In a fastener subjected to both tensile and bending loads the correction factor for stress intensity factor is calculated by,

$$K_I = \sqrt{\pi a} (\sigma_0 F_0 + \sigma_1 F_1) \quad [11.3.2]$$

where σ_0 and σ_1 are the tensile and bending components of the normal stress at the crack location (see Section 11.3.3.2 below), and, F_0 and F_1 are that amplification factors specific to the tensile and bending stress fields respectively.

The following three types of cracks are most likely to occur in fasteners:

circumferential crack at the thread (most likely in fasteners with cut threads),

thumbnail crack at the thread (most likely in fasteners with rolled threads loaded in bending), and thumbnail cracks at the fillet under the fastener head

The ESACRACK/NASGRO software calculates stress intensity factors for these and other crack types, including those mentioned in this section. The following sections briefly describe the theory adopted by ESACRACK/NASGRO.

11.3.3.2 Components of Local Stress

In Equation [11.3.2] the tensile and bending components of the local bending stress at the crack are given by,

$$\sigma_0 = \frac{4F_b}{\pi d_{local}^2} \quad [11.3.3]$$

and,

$$\sigma_1 = \frac{32M_b}{\pi d_{local}^3} \quad [11.3.4]$$

where F_b is the tensile force in the fastener, M_b is the bending moment in the fastener, and d_{local} is the assumed local diameter of the fastener at the crack location, which is either:

- d for circumferential cracks, or
- d_3 for thumbnail cracks

11.3.3.3 Circumferential Cracks around the Thread

Figure 11-19 shows the assumed stress distributions (left) and geometry (right) of the ESACRACK/NASGRO model for circumferential fastener cracks.

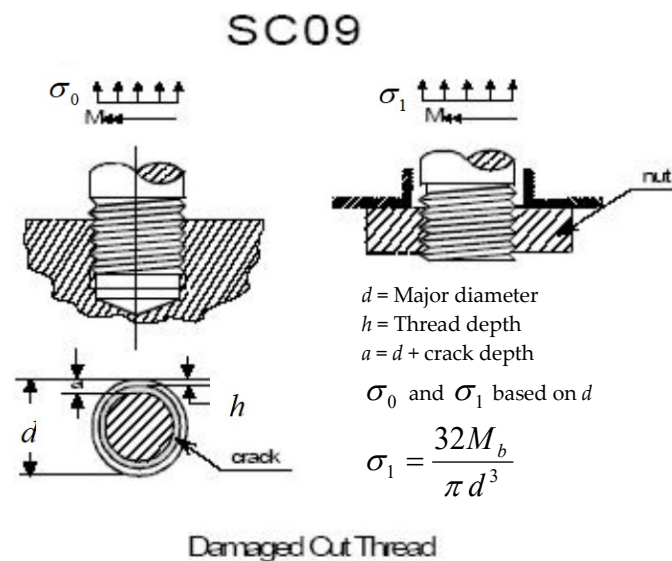


Figure 11-19 - ESACRACK Model of a Circumferential Crack

The following equations are used by ESACRACK/NASGRO to determine the stress intensity correction factors for circumferential cracks in the fastener thread:

$$F_0 = \frac{G_0}{k^{3/2}} \quad [11.3.5]$$

where;

$$G_0 = 0,5 + 0,25 k + 0,1875 k^2 - 0,1815 k^3 + 0,3655 k^4,$$

$$k = 1 - 2 a/d,$$

And,

$$F_1 = G_1 \frac{\sqrt{r}}{r^3} \quad [11.3.6]$$

where;

$$G_1 = 0,375 (1 + 0,5r + 0,375r^2 + 0,3125r^3 + 0,2734r^4 + 0,531r^5)$$

$$r = (d - 2a) / d$$

11.3.3.4 Thumbnail Cracks at the Thread Root

Figure 11-20 shows the assumed stress distributions (left) and geometry (right) of the ESACRACK/NASGRO model for thumbnail fastener cracks.

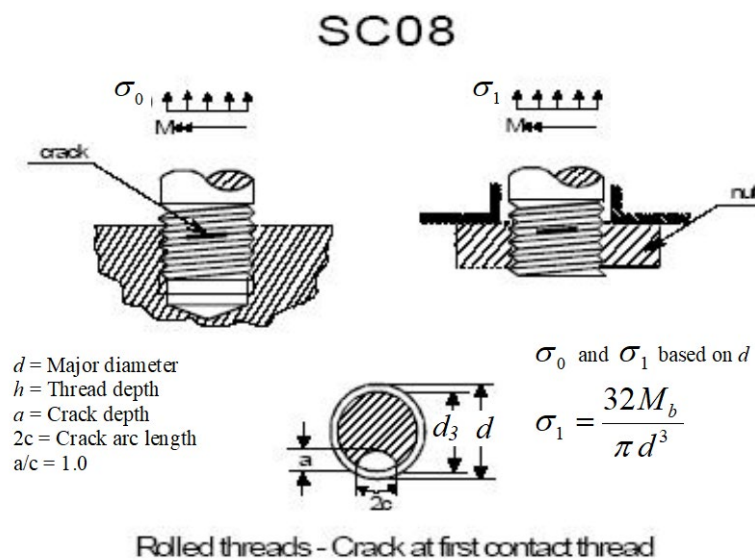


Figure 11-20 - ESACRACK Model of a Thumbnail Crack

For this type of crack, the stress intensity correction factors for tension (F_0) and bending (F_1) are shown in Table 11-1 (from Reference 11.3).

Table 11-1 - Stress Intensity Factors for Thumbnail Crack in a Fastener Thread

a/d	Tension Correction Factor (F_0)		Bending Correction Factor (F_1)	
	a/c = 0,645	a/c = 1,0	a/c = 0,645	a/c = 1,0
0,0	$K_t f_x$	1,00	$K_t f_x$	0,60
0,05	-	0,84	-	0,54
0,1	0,95	0,76	0,61	0,48
0,2	0,90	0,65	0,54	0,37
0,3	0,98	0,59	0,55	0,31
0,4	1,29	0,62	0,64	0,30
0,5	2,05	1,0	0,84	0,50

For $a/d = 0,05$ it is important to use interpolation.

For the case of no crack (i.e. $a/d = 0$) the stress intensity correction factor is determined by the stress concentration factor K_t , which can be interpolated from Table 11-2, and an extra factor, f_x , which is given by,

$$f_x = \begin{cases} \left[1 + 1.464 \left(\frac{a}{c} \right)^{1.65} \right]^{-1/2} & \text{for } \frac{a}{c} \leq 1 \\ \left[1 + 1.464 \left(\frac{a}{c} \right)^{-1.65} \right]^{-1/2} & \text{for } \frac{a}{c} > 1 \end{cases} \quad [11.3.7]$$

Table 11-2 - Stress Concentration Factors at a Fastener Minor Diameter

r/d	0,005	0,01	0,015	0,02	0,025	0,03	0,035	0,04	0,045	0,05
K_t	10,8	7,89	6,55	5,73	5,17	4,77	4,48	4,19	3,97	3,79
r/d	0,055	0,06	0,065	0,07	0,075	0,08	0,085	0,09	0,095	0,10
K_t	3,63	3,49	3,37	3,26	3,16	3,07	2,97	2,91	2,84	2,78

11.3.3.5 Thumbnail Crack at Fillet Under Fastener Head

Figure 11-21 shows this type of crack.

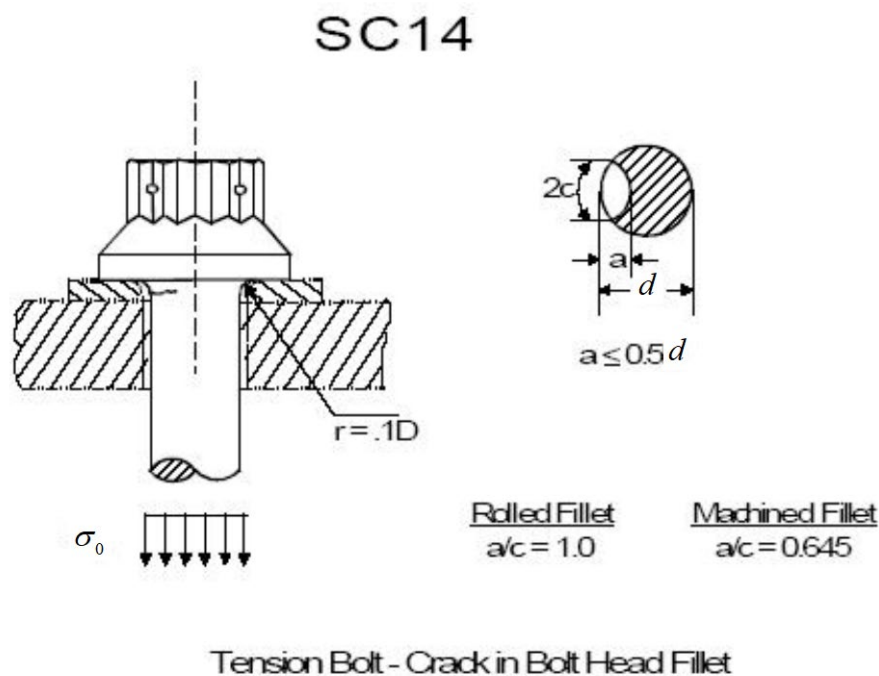


Figure 11-21 - ESACRACK Model of a Fillet Crack under a Fastener Head

The stress intensity factors for this type of crack are calculated as for a thumbnail crack at the thread root in Section 11.3.3.4 above except the following additional assumptions are made:

- For a machined fillet $a/c = 0,645$
- For a rolled fillet $a/c = 1,0$
- $r/d = 0,1$
- For $a/d = 0$ the stress concentration factor of 2,78 is used
- For $a/d = 0,05$ smooth interpolation is used

11.3.4 Crack Growth Calculations

To predict safe life for a particular potential fracture critical (PFCI) fastener it is necessary to assume an initial crack size, calculate the stress intensity at the first load cycle, calculate the change in crack length due to that cycle and then calculate a new stress intensity. Comparison of this with the critical value for the material, K_{Ic} or K_{ISCC} , can determine if failure can occur. If not, the next cycle can be calculated and the process repeated until the critical crack length is reached.

As this process can extend over thousands of cycles it is generally beyond the scope of hand calculations and the use of computer-based methods such as ESACRACK/NASGRO are advised.

NAGRO provides added ability to include effects of preload on bolted joint analysis for crack case SC08 (crack at first contact thread) and SC14 (semi-elliptical surface crack in bolt head fillet).

As an example of the procedure, the SC08 crack solution needs the following inputs:

- Tensile stress, S_0
- Bolt preload value, P (in kip or Newton)
- Length of the grip (combined member thicknesses), L
- Threaded part of grip length, L_t
- Elastic Modulus of bolt, E_b
- Elastic Modulus of members, E_m

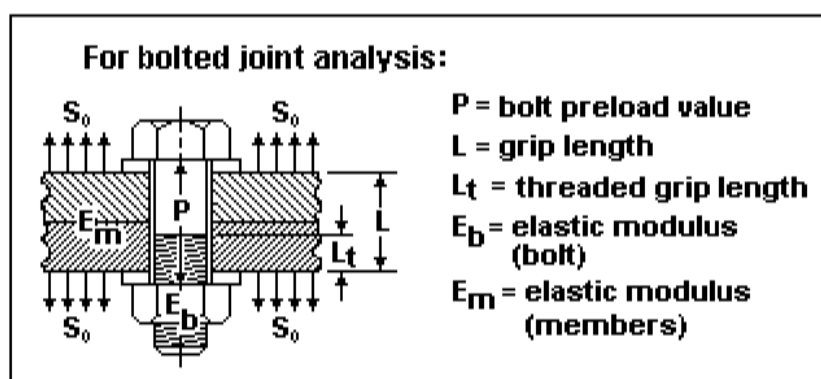


Figure 11-10 – NASGRO inputs for the bolt analysis, SC08 case

The code computes stiffnesses and net axial stress of bolt and members, and the stress intensity factor with corresponding crack growth.

The approach is explained in Annex N of the NASGRO manual and based on Shigley, J.E. and Mischke, C. R., "Mechanical Engineering Design (in SI Units)," Sixth Edition, Tata McGraw-Hill Book Company, 2003.

It is up to the user to ensure that the stress cycles generated by NASGRO are consistent with those calculated in the stress analysis, using the guidelines of this handbook. Alternatively, a spectrum can be derived using the ESALOAD software (Ref. [11.2]).

11.3.5 Corrosion Considerations

The principal means by which corrosion affects the fatigue life is the formation of pits, which create geometric stress concentrations in the same areas as a chemically degraded metallic surface. Many of the same features that affect basic fatigue life are also corrosive. Therefore, good design against fatigue also eliminates many possible corrosion hazards.

Good fatigue performances need avoidance of stress corrosion cracking (SCC, or more generally environmentally assisted cracking, EAC) at locations in the joint where corrosion is likely. The elimination of residual tensile stress, as well as adequate corrosion protection and the correct choice of material is essential.

Reference 11.9 provides some information about susceptibility to stress corrosion cracking of some materials in the presence of cracks. These are generally considered as indicative, but need to be confirmed by test for critical applications, see also e.g. Reference 11.17. It has been shown that with some materials there is a threshold value, below which stress corrosion cracking **cannot** occur. This threshold is denoted K_{ISCC} (or, more generally, K_{EAC}) and is a material property, which can be measured. However, the threshold can depend on many factors, and only a limited number of threshold values can be found in literature.

It is important to note that K_{EAC} is dependent upon the environment. Therefore, comparison between different materials and/or different environments can be **incorrect**.

The combined effect of corrosion and fatigue is a more rapid failure than either acting alone. This is called corrosion fatigue. The calculation of the effect of corrosion on fatigue life is not possible in the original design calculations. To make the design calculations realistic it is essential to ensure that the possibility of corrosion is minimised and later to assess the effect of salvage schemes if they become necessary.

More information on corrosion can be found in Section 13.

11.4 Worked Examples

11.4.1 Fatigue of a Threaded Fastener Example

11.4.1.1 Overview

A critical threaded fastener joint design uses an M8 diameter Titanium fastener to the following loading spectrum during each mission:

- 50 cycles at a stress amplitude of 160 MPa
- 4000 cycles at a stress amplitude of 50 MPa
- 880 cycles at a stress amplitude of 60 MPa
- 300 cycles at a stress amplitude of 130 MPa

- 100 cycles at a stress amplitude of 90 MPa

What is the life of the fastener in numbers of missions?

11.4.1.2 Analysis

From the S-N curve in Figure 11-12 the cycles to failure for each spectrum block are as follows:

Table 11-3 - Analysis of cycles to failure

Alternating Stress, σ_a (MPa)	Cycles per Mission, n	Cycles to Failure, N
160	50	10^3
50	4000	below endurance limit
60	880	5×10^5
130	300	7×10^3
90	100	8×10^4

From Section 11.2.2, using the Palmgren - Miner Rule, the fatigue damage per mission is given by,

$$\begin{aligned}
 f &= 4\Omega \\
 &= 4 \sum_{i=1}^m \frac{n_i}{N_{f,i}} \\
 &= 4 \times \left[\frac{50}{1e^3} + \frac{880}{5e^5} + \frac{300}{7e^3} + \frac{100}{8e^4} \right] \\
 &= 0.37
 \end{aligned}$$

The fatigue life of the fastener is therefore $1 / 0,37 = 2,7$ missions.

11.4.2 Threaded Fastener Fracture Mechanics Example

This example is based on an older version of the NASGRO software (Ref. [11.3] or [11.4]) as well as other literature and will not be fully up to date with the latest NASGRO version (Ref. [11.9]). Cracked fastener models are still being further developed.

11.4.2.1 Problem Description

A M8 Titanium fastener (TA28 (Ti6Al4V)) is used to clamp together two 10mm thick flanges made from Aluminium. The external axial load applied to the joint is 18 kN and the fastener has a 0,5mm deep thumbnail crack at the first thread into the nut.

Determine the static strength of the fastener.

The following assumptions and properties apply:

- The yield stress for a TA 28 fastener is 1100 N/mm²
- The stress area of an M8 fastener = 32,8 mm²
- The fastener is preloaded to between 60 and 65% of yield

- The fastener sees no bending loads
- The flanges are sufficiently wide to allow fully developed compression cones
- No thermal effects apply.

11.4.2.2 Solution

The yield load of the fastener is,

$$F_{b,y} = A_S \times \sigma_y = 1100 \times 32.8 = 36.1 \text{ kN}$$

Thus, the maximum fastener preload is

$$F_{V,\max} = 0.65 \times 36.1 = 23.5 \text{ kN}$$

Now the force ratio is calculated. Since $L_j > 2d$,

$$D_{\text{lim}} \approx 3d_{uh,brg}$$

It is assumed for the sake of this example that the force ratio is,

$$\Phi \approx 0.47$$

The loading plane is assumed to be at the mid-point of the joint members, i.e. $n = 0,5$.

Thus,

$$\Phi_n = n \cdot \Phi = 0.235 = \frac{F_{b,A}}{F_A}$$

Therefore, since $F_A = 18\text{kN}$, the load increment in the fastener due to the external load is given by,

$$F_{b,A} = 18 \text{ kN} \times 0,235 = 4,2 \text{ kN}$$

The maximum fastener tensile load is,

$$F_{b,\max} = F_V + F_{b,A} = 23,5 \text{ kN} + 4,2 \text{ kN} = 27,7 \text{ kN}$$

The gross axial stress is,

$$\sigma_0 = \frac{F_{b,\max}}{A_S} = \frac{27.7}{32.8} \times 1000 = 844 \text{ MPa}$$

For the thumbnail crack with an initial assumed length $a = 0,5\text{mm}$ and $c = 0,5\text{mm}$ the stress intensity correction factor for tensile stress, F_0 , can be read from Table 11-1 to be 0,84.

Thus, the stress intensity factor can be calculated with Equation,

$$K_1 = \sqrt{\pi a} \sigma_0 F_0 = \sqrt{\pi \times 0.5} \times 844 \times 0.84 = 889 \text{ MPa}\sqrt{\text{mm}}$$

$$K_1 = \sqrt{\pi a} \sigma_0 F_0 = \sqrt{\pi \times 0,5} \times 844 \times 0,84 = 889 \text{ MPa}\sqrt{\text{mm}}$$

Note that assuming such small crack size (0,5 mm) would require special NDT procedure, acc. Reference [11.14].

For TA28 fasteners a typical value for the critical stress intensity factor, K_{Ic} , is 2780 MPa√mm (see Reference 11.3), therefore the Margin of Safety on fastener fracture is,

$$MoS = \frac{K_{Ic}}{K_1} - 1 = \frac{2780}{889} - 1 = 2,13$$

Note: Using K_{Ic} (instead of K_{Ic}) will generally be conservative. The value of 2780 MPa√mm is one of the highest in the NASGRO database for Ti6Al4V, so it needs to be confirmed for the actual fastener material grade used. Depending on the nature of the loading (sustained or varying) it can be appropriate to use a reduced toughness value to cover sustained load cracking phenomena (see section 11.3.1).

Hence, given the assumptions in this calculation, it can be concluded that a thumbnail crack of 0,5 mm length (or depth) does not represent a critical defect and can be tolerated.

To find the critical defect size for this joint it is necessary to repeat this calculation for a number of crack lengths until K_{Ic} is exceeded and interpolate for the critical length.

NASGRO can be used more conveniently. In version 9.2 the result for a 0,5 mm crack in an M5 bolt at 844 MPa is: 785 MPa√mm.

11.5 References

11.1	ECSS-E-ST-32-01C Rev. 2	Space engineering - Fracture control
11.2	ESA	ESACRACK User's Manual - Version 4.4.0.a, TEC-MCS/2006/1448/In/GS, Issue 5.1.a, March 2018
11.3	NASA	Fatigue Crack Growth Computer Program "NASGRO" 2000. JSC 22267B (included in ESACRACK manual)
11.4	NASA	Fatigue Crack Growth Computer Program, "NASA/FLAGRO", August 1986. JSC 22267
11.5	BROEK D.	Elementary Engineering Fracture Mechanics, Noordhof (Netherlands) 1974.
11.6	RAYMOND L	'Infinite Life High Strength Bolts', Assembly Engineering, April 1975
11.7	ISQ	Fatigue Test On Threaded A2-70 Size M5 Fasteners - Final Report, ISQ, 2008
11.8	KELLERMAN R., TURLACH G.	'Bolts for light weight construction made of ultra high strength steels and titanium alloys.'
11.9	NASGRO	Fracture Mechanics and Fatigue Crack Growth Analysis Software - Reference Manual, Version 9.2, July 2020
11.10	S.C. Forth	'Fracture control', in: G.E. Musgrave, et al. (Ed.), Safety Design for Space Systems, Butterworth-Heinemann, 2009, pp. 567-568
11.11	G. Sinnema	'8th Paolo Santini memorial lecture on safety of spaceflight structures -The application of fracture and damage control', Acta Astronautica 162 (2019) 469-480
11.12	ECSS-Q-ST-70-46C	Space product assurance - requirements for manufacturing and procurement of threaded fasteners, ECSS, Rev. 1 (2009).
11.13	NASA-STD-8739.14	NASA Fastener Procurement, Receiving Inspection, And Storage Practices For NASA Mission Hardware, NASA, 2020 (Superseding NASA-STD-6008)

11.14	ECSS-Q-ST-70-15C	Space product assurance - Non-destructive testing, March 2021
11.15	PRC-6509 Rev. E	Process Specification for Eddy Current Inspection, December 2019, NASA Johnson Space Center
11.16	NASA-STD-5019A	Fracture Control Requirements for Spaceflight Hardware, NASA, 2016 (Change 3, Aug 2020).
11.17	G. Sinnema	SCC - A Historical Perspective, at: ESA TIM on Fracture Control of Spacecraft, Launchers and Their Payloads and Experiments, (November 2015) Noordwijk, The Netherlands.
11.18	Boyer, R.R.; Spurr, W.F.	(January 1978). "Characteristics of Sustained-Load Cracking and Hydrogen Effects in Ti-6Al-4V," Metallurgical Transactions A. Vol. 9A, pp. 23-29.
11.19	Kostrivas, Smith, Gittos (TWI)	'Sustained load cracking of titanium alloy weldments', Proceedings of OMAE 2005, June 12-16, 2005, Halkidiki, Greece
11.20	Kostrivas, Smith, Gittos (TWI)	'Sustained load cracking in titanium alloys', 10th World Conference on Titanium, 13-18 July 2003, Hamburg, Germany
11.21	DIN 65149, Luft- und Raumfahrt	Schrauben aus Stahl für nichttragende Bauteile M 3 und M 4. Technische Lieferbedingungen (Aerospace - Steel Screws for non-structural components M 3 and M 4 Technical specifications), 1980

Preloaded Fastener Installation

12.1 Overview

This section discusses a variety of methods for controlling the preload in fasteners. For each method, descriptions are provided for the theoretical basis of each method. Also, recommendations are given regarding practical limitations and the expected levels of accuracy.

This section also presents some guidelines for the preload effects that result from reuse of a fastener by subjecting to multiple tensioning cycles.

12.2 Torque Controlled Tightening

Torque Control Tightening is the most commonly used tightening method as it is relatively simple and cost-effective to apply. The torque is usually applied with a calibrated torque wrench. Often an audible “click” signal is given when the required torque is reached.

The theoretical torque-preload relation is discussed in Section 6.3.

The main drawback of the torque-control method is that the scatter in achievable preload is rather significant as most of the applied torque is consumed by the various friction contributors and only 10% is converted into stretching the bolt (see Section 6.3.1). The pre-load for a torque controlled tightening can vary by more than 100 % between min Preload and max Preload, depending on the scatter in the friction coefficients (thread and underhead). Note that the up to 35% deviation shown in Table 6-1 (tooling uncertainty) applies to the preload between each tightening application for KNOWN friction figures.

Therefore, a good knowledge of the friction characteristics of a given joint assembly is essential to ensure that the resulting preload remains within the design range. It is important to determine these characteristics by torque-tension characterization testing as e.g. described in Ref. 12.16 or 12.17 or any equivalent method. Since friction characteristics are lot dependent a confirmation of derived characteristics by lot testing is recommended.

12.3 Yield Load Controlled Tightening

12.3.1 Introduction

Yield load or gradient controlled tightening techniques are based on the fact that when the yield load of the fastener material is reached, the tightening torque, M_{app} ceases to increase linearly with the angle of rotation. That is when,

$$\frac{dM_{app}}{d\theta} \text{ ceases to be constant,}$$

or equivalently,

$$\frac{d^2 M_{app}}{d\theta^2} \neq 0 \quad [12.3.1]$$

When this condition is detected, a control system automatically stops the tightening process. Proprietary fastener tightening systems based on this yield controlled tightening are available and they are claimed to reduce the preload scatter to less than $\pm 8\%$.

Since each fastener is treated as unique by the control system, this technique is largely independent of the factors that contribute to high values of preload scatter when using other assembly methods. However, the method is susceptible to variations in the fastener's yield stress and stress section area. Variations in the proportions of these stresses, which might arise due to effects such as variations in friction conditions, can change the value of axial tensile stress at which yield occurs and hence the observed fastener preload. This is examined theoretically in 12.3.2 and 12.3.3.

12.3.2 Method of Operation

The basis of the method is an algorithm that accurately detects the occurrence of yield in the fastener. Typical curves illustrating the system characteristics are shown in Figure 12-1 and Figure 12-2. It is seen that the gradient of the torque-rotation curve has a characteristic shape with a peak or plateau followed by a marked reduction in magnitude, to about 20 - 30% of the maximum value. This feature is observed under varying friction conditions and for different joint materials and hardness. The rapid drop in gradient corresponds to the onset of yield and provides the basis on which yield is detected.

From Figure 12-1 it is apparent that the complete torque-rotation curve includes an initial zone of low gradient corresponding to embedding. It is important to eliminate this by tightening the fastener to a predetermined torque before commencing automated measurement of the torque-rotation gradient.

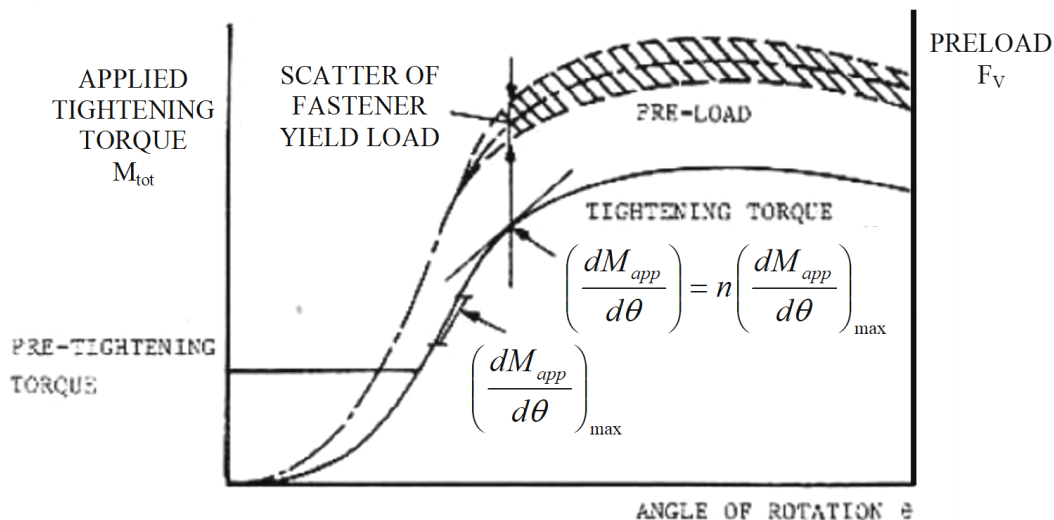


Figure 12-1 - Yield Load Controlled Tightening

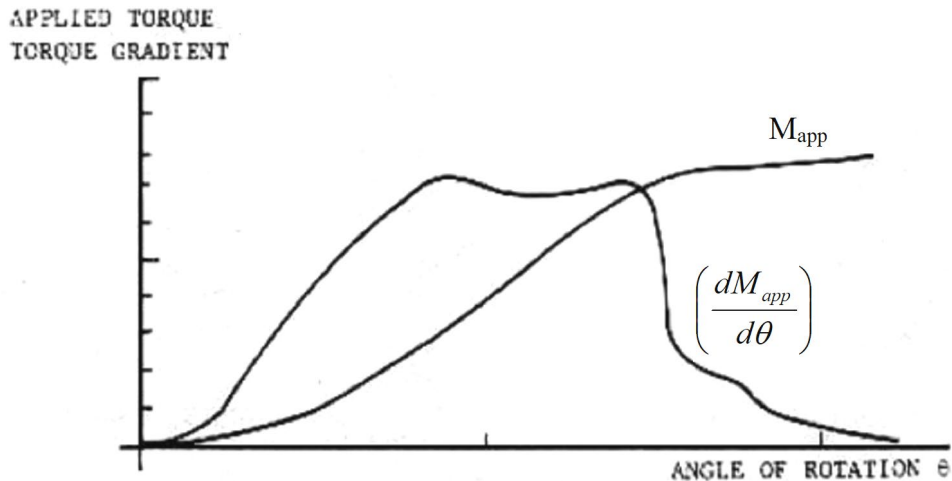


Figure 12-2 - Torque and Gradient Values as a Function of θ

From this point the control algorithm is as follows:

- a. Determine the torque-rotation gradient: $\left[\frac{dM_{app}}{d\theta} \right]$
- b. Detect and store the maximum value of : $\left[\frac{dM_{app}}{d\theta} \right]$
- c. Compare current value of $\left[\frac{dM_{app}}{d\theta} \right]$ with $\left[\frac{dM_{app}}{d\theta} \right]_{max}$
- d. Cease tightening when: $\left[\frac{dM_{app}}{d\theta} \right] \leq n \left[\frac{dM_{app}}{d\theta} \right]_{max}$

A typical range of values for n is 0,5 to 0,7.

12.3.3 Preload Developed in Fastener

For yield controlled tightening the Von Mises Yield criterion is adopted,

$$\sigma_{v.m.} = \sqrt{\sigma_V^2 + 3\tau^2} = \sigma_y \quad [12.3.2]$$

where; σ_V and τ are the axial and torsional stresses at the smallest cross-section of the fastener respectively, and σ_y is the axial yield stress of the fastener.

In Equation [12.3.2] the cross-section at which the stresses are computed usually corresponds to the thread minor diameter, d_3 , unless reduced diameter shank fasteners are used, in which case d_0 is used.

Rearranging Equation [12.3.2] yields,

$$\frac{\sigma_{0.2}}{\sigma_V} = \sqrt{1 + \frac{3\tau^2}{\sigma_V^2}} \quad [12.3.3]$$

Thus,

$$\frac{\sigma_{0,2}}{\sigma_V} = \left[1 + \frac{48 M_{th}^2}{F_V^2 d^2} \right] \quad [12.3.4]$$

where M_{th} is the thread torque (transmitted by the fastener shank), which from Section 6.4.2 is given by,

$$M_{th} = \frac{F_V}{2} \left[\frac{p}{\pi} + d_2 \frac{\mu_{typ}}{\cos \alpha} \right] \quad [12.3.5]$$

From Equation [12.3.4] it is clear that the ratio $\sigma_{0,2}/\sigma_V$ is always greater than 1, and thus the preload stress developed in a fastener tightened to yield, σ_V , is less than that corresponding to the axial yield stress, $\sigma_{0,2}$.

Since M_{th} is function of the thread friction coefficient variations in the friction conditions lead to preload scatter. However, assuming lubrication and other factors are controlled, the variation is considerably less than that observed for torque-tightened fasteners.

Significant differences in preload are expected between lubricated and unlubricated fasteners. This is illustrated in Table 12-1 where σ_y/σ_V is calculated for a range of metric fastener sizes and lubrication conditions.

Table 12-1 - σ_y/σ_V for a Range of Fastener Sizes and Typical Friction Conditions

Fastener size	p [mm]	d [mm]	d ₂ [mm]	σ_y/σ_V		
				$\mu_{typ} = 0,10$	$\mu_{typ} = 0,15$	$\mu_{typ} = 0,20$
M3	0,5	2,459	2,675	1,198	1,330	1,483
M3.5	0,6	2,850	3,110	1,203	1,337	1,490
M4	0,7	3,242	3,545	1,207	1,341	1,496
M5	0,8	4,134	4,480	1,191	1,321	1,472
M6	1,0	4,917	5,350	1,192	1,330	1,483
M8	1,25 ^[2]	6,647	7,188	1,187	1,316	1,466
M10	1,5 ^[2]	8,376	9,026	1,181	1,309	1,457
NOTE 1: Assumes $\theta = 30^\circ$;						
NOTE 2: It is important for MJ fasteners that M8 has p=1,0mm and M10 has p=1,25mm						

12.4 Angle of Rotation Controlled Tightening

12.4.1 Introduction

This method of tightening (also called 'turn or the nut controlled tightening') is based on the fact that it is possible to stretch the fastener a prescribed amount by turning the nut or fastener a certain number of degrees. Therefore, control by angle of rotation is indirectly control by measuring the elongation.

The method, although simple in concept, is dependent on a number of parameters specific to a particular joint. Therefore, it is **important to consider** an empirical method.

There are two variations on the method:

- a. Elastic range tightening, where the fastener is not plastically deformed.
- b. Plastic range tightening, where the fastener is taken beyond its yield point.

The second method (b) is usually not used in space applications, the first method is discussed in the following section 12.4.2.

12.4.2 Elastic Range Tightening

This variant is based on the measurement of **the angle of rotation during tightening** of the nut or fastener. The effect of frictional variations is eliminated except for the effect they have on the 'snug torque', which determines the starting point of angle measurement. However, this method is subject to a number of shortcomings related to variations in the effective stiffness of the fastener, and the joint clamped parts.

Since the part of the fastener's length is not under tension, an allowance needs to be made for the diffusion of stress and strain in the threads that are engaged to the nut. The region of unengaged thread region below the nut needs also to be considered since this has a lower effective cross-sectional area, and hence stiffness, than the unthreaded shank. Without close dimensional control over the shank and thread lengths it is impossible to be certain how many threads **can** be in the tensile strain region. Furthermore, some deformation of the nut takes place near the first few threads, adding to the uncertainty in the elongation.

Some of these points are illustrated in Figure 12-3, which shows a section through a typical joint with the variation of strain along the length of the fastener. The reduction in strain in the shank is apparent and indicates the importance of controlling the lengths of the shank and the thread to a reasonable degree of accuracy in order to predict the elongation of the fastener under load.

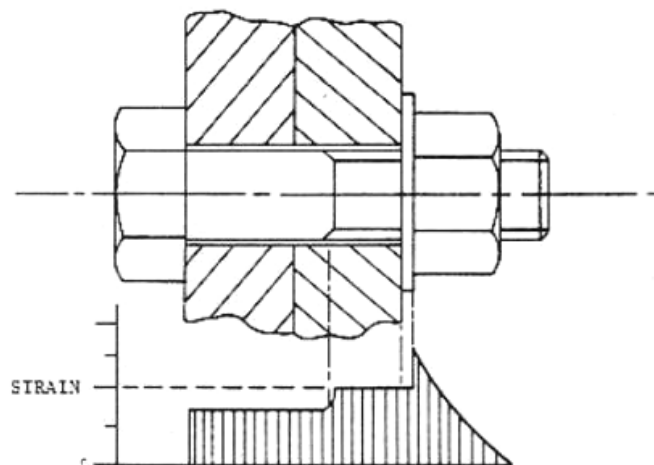


Figure 12-3 - Variation of Strain along Fastener

The second important element in this method is control of the clamped parts' stiffness. Compression of the joint members and crushing of the surfaces under the fastener head and nut have to be considered. These factors can cause significant uncertainty and can be alleviated by the use of hardened steel washers.

Associated with this aspect is non-alignment of the flanges prior to assembly. The method assumes that the flanges are perfectly parallel, and in close uniform contact and that there is no deflection of the flanges. The first assumption can be ensured by specifying a 'snug' torque to which the fastener is tightened prior to commencing measurement of the rotation angle. This ensures that the joint faces are effectively in close uniform contact before assembly. The second assumption can be ensured by careful design, and by consideration of the effects of any gasket materials that can be included in the joint.

The accuracy with which the operator can set the rotation angle depends on the accessibility of the fastener and having specifications that involve simple fractional rotations (e.g. $\frac{3}{4}$ of a revolution). It is important to note, that pumping (turning the torque wrench forth and back) can lead to significant errors, since the resolution of the optical angle measurement usually is in the range of 0,5 to 1,0 degrees, whereas the resolution of the mechanical mechanism is in the range of 3 to 5 degrees.

Most of the described shortcomings can be overcome by a proper approach for the angle driven tightening, including a dedicated calibration of the joints to be tightened.

In practice, to assess the stress state in the fastener it is feasible to start with a classic bolt analysis, where the friction variation is reduced from the unknown large scatter, to a scatter of around 20% (i.e. 0,08-0,096) and a utilization of the bolt around 0,8 to 0,9. This can provide the analyst with a preload, which the junction is capable of. It is important to take care of the selection of the lower friction bound, which is in line with the selected type of connection (lubricated, non-lubricated).

The next step is to setup up a calibration joint, which has identical compliances for the clamped parts and the fastener, including a force-measuring device. With this calibration setup, the 'snug torque' and the angle needed to derive the defined preload can be defined. The 'snug torque' is ideally at a region, where the force-torque or force-angle diagram gets into the linear relation.

The shortcomings of handling activities like pumping remain and have to be avoided by proper AIT.

The large advantage with this method is, that compared to the classical uncalibrated torque tightening approach a significant smaller variation in the preload can be achieved, which enhances the overall performance of the junction.

12.5 Ultrasonic Methods

12.5.1 Introduction

As the fastener is tightened its length increases, changing both the transit time (or 'time of flight') of an ultrasonic signal and the resonant frequency of axial vibration. The change in either of these can be used to determine fastener extension. Thus, two main ultrasonic methods exist;

- a. the "transit time system", in which the time taken for a pulse of ultrasound to travel from one end of the fastener to the other and back again is measured, and
- b. the "resonant oscillator system" in which the ultrasonic resonant frequency of the fastener is measured.

Once the length of the fastener is reliably obtained, the preload can then be calculated from its strain.

12.5.2 Ultrasonic Extensometers

12.5.2.1 Overview

Extensometers employ a technique based on the transit time of an ultrasonic pulse traveling along the fastener's axis, but with allowance for the reduction of sonic velocity with increasing stress.

The principle of operation is as follows:

- a. A pulser within the instrument shocks a transducer that then delivers a brief, highly damped pulse of ultrasound to one end of the fastener.
- b. This pulse travels down the fastener, echoes off the far end, and returns to the original transducer.
- c. The instrument measures and records the transit time of the pulse.
- d. The fastener is then tightened, increasing the length of the path to be covered by the signal and decreasing the sonic velocity.
- e. The new increased transit time is recorded.
- f. Using this data, the instrument (typically incorporating a microprocessor) computes the total change in transit time, computes and discards that portion of the change which resulted from the change in velocity, and then displays the actual change in fastener length.

A further important factor, which has to be considered, is the effect of temperature. A temperature change can affect the length of the fastener and the sonic velocity. If temperature of the fastener changes between the unstressed and stressed readings, it is good practice to factor out its influence on length and velocity by the measuring equipment.

Therefore, before commencing preload measurement, three factors can be set into the instrument. These are 'velocity' and 'stress' factors for the fastener material and a 'temperature' factor. It is important to determine these factors experimentally determined, since theoretical calculation of the relationship between preload and change in transit time is not possible. Extensometer manufacturers have determined factors for many materials and these are available to the user. In cases where the data is not available, the instrument can be user-calibrated on a sample of the fastener. Subsequent recalibration is usually done by means of a calibration block provided with the instrument.

12.5.2.2 Using an Ultrasonic Extensometer

After calibration a typical procedure (Reference 12.1) for tightening a joint is as follows:

- a. The instrument is set in the length mode.
- b. The temperature of the fastener to be tightened is measured and the appropriate temperature factor input into the instrument.
- c. An acoustic couplant such as glycerine or oil is applied to the fastener and the transducer set in place. This **can** be attached to either end of the fastener.
- d. The initial length of the fastener is ultrasonically measured and recorded for future reference.
- e. Steps 3 and 4 are repeated for other fasteners in the joint.
- f. The instrument is switched to the change of length mode and the extension necessary to give the desired preload is calculated.
- g. The joint is pulled together by tightening each fastener to approximately 30% of the required preload. Torque control is commonly used for this pass. The length of the fasteners can be monitored at the end of the pass to confirm that results are reasonable.
- h. Additional passes are made, tightening the fastener to a higher percentage of the required preload. A small sample of fasteners is measured with the extensometer at the end of each pass, but torque is still used for control.
- i. The extensometer is used to control the tightening process for values of preload above, typically, 70% of the required preload.
- j. It is recommended to remeasure every fastener in the joint after the final pass to monitor the relaxation effects such as embedding.

12.5.2.3 Practical Considerations

In laboratory conditions instruments are capable of resolving to between 2,5 mm and 0,25 mm. However, in the field the performance **can** be significantly worse, by an order of magnitude or more.

The accuracy to which preload can be controlled is a function of fastener length. **It is important to take into the account** the fastener diameter if it is less than ten times the sonic wavelength.

As for the angle controlled tightening method, variations in fastener and joint stiffness **are** reflected in preload scatter and **are to** be considered.

Transducers vary in frequency, diameter, signal strength, acoustic damping, etc, and at present, selection is still largely a matter of trial and error.

Good and consistent acoustic coupling of the transducer is necessary. However, it is not possible to couple all fastener configurations since a sufficiently large mounting area **is** available for the transducer and the opposite end provides a substantial signal reflection. Hexagon headed fasteners usually work well but socket head cap screws, **do** not permit this method unless they are large enough to allow the transducer to be mounted in the wrench socket, or beside it. If the transducer is too large, it **can** receive unwanted reflections from the underhead interstice, etc.

Fastener identification markings can prevent a satisfactory acoustic coupling and machining of the head **can** be necessary to eliminate air, which creates acoustic impedance. Even with perfectly flat surfaces, consistent coupling can be difficult to achieve, since varying the contact pressure between the transducer and the fastener can significantly alter results. In critical applications, it **can** be necessary to accurately control the pressure between the surfaces, as described in Section 12.4.2.

Different materials have different effects on the acoustic signal with regard to absorption and scattering. For example, some stainless steels are grainy and can distort the signal. The American A286 material is believed to contain Titanium platelets within it that cause false echoes and severe attenuation. Irregular hardness, e.g. case hardening, can also warp the signal.

The fact that preload is actually calculated from the strain needs that the length of the portion of the fastener under tension is accurately known. This is usually not the case and therefore, the standard method of calibration can be inadequate in cases where a high degree of accuracy is needed.

12.5.2.4 Increasing the Accuracy of Preload Measurement

Although the procedures described in [section 12.2](#) and [12.3](#) above enable fastener preload to be controlled far more accurately than is possible by torque control or angle controlled tightening methods, generally the methods lead to preload scatter of greater than 5%. Higher accuracy can be achieved by making two main modifications to the procedure.

- a. Increasing the repeatability of the coupling between the transducer and fastener head. This can be achieved by using transducers that can be screwed into a tapped recess in the head. By tightening the transducer to a predetermined torque, more consistent coupling is achieved. It is **important to note**, that the fasteners need to be specially machined and the transducers have to be specially made.
- b. Using a direct method for deriving a set of calibration data, specific to the fasteners being used. As mentioned previously, the usual method of calibration involves measuring the fastener extension to calculate preload with the inherent inaccuracies mentioned in [section 12.4.2](#). These inaccuracies can be eliminated by measuring the fastener load and extension relationship as follows:
 1. The fastener is passed through two small steel plates sandwiching a suitable load washer, the total thickness being equal to the thickness of the clamped parts of the real joint.
 2. The nut is tightened to give various increments of preload.
 3. For each increment the preload and extension readings (given by the load washer and ultrasonic extensometer) are recorded.
 4. Any desired preload can now be obtained, knowing the required extension reading.

Approximate values of the calibration factors are input into the instrument at the start. These do not need to be exact, since any error in the extension reading is unimportant, as the output has been calibrated against load required. However, it is important to use the same factors for all future measurements for the calibrated joint configuration.

An appreciable amount of data has been obtained using this method (References 12.2 and 12.3) but it tends to be very specific to a certain type and size of fastener. If only a small number of different fasteners are involved, it **can** be practicable to calibrate each type of fastener for its specific required preload. However, if the number is large this **is often** not possible. It is possible to use data obtained for a limited variety of specimens to develop empirical formulae that hold true for fasteners of different dimensions, (see Reference 12.4). It has been found that the following relationship can be applied:

$$\frac{\Delta L_b}{F_V} = a + b L_1 + c L_2 \quad [12.5.1]$$

where L_1 is the plain length of the fastener and L_2 is the threaded length of the fastener up to the face of the nut, and, a , b and c are constants, to be evaluated for the particular fastener system.

12.5.2.5 Resonant Oscillator Methods

Examples of these methods include the Reflection Oscillator Ultrasonic Spectrometer (ROUS) and improved Pseudo Continuous Wave (PCW) methods. The first step is to establish a resonant condition in the fastener. As the fastener is stressed the wave velocity through it decreases. The frequency of exciting is held constant by the transducer and thus the wavelength therefore decreases (since the velocity is the product of the wavelength and the frequency). Therefore, to re-establish a resonant condition, it is necessary to decrease the transducer frequency.

The reader is directed to References 12.5 to 12.9 for more detailed information.

12.5.2.6 Scatter

It is not possible to give an accurate "maximum error" figure covering all fastener configurations, since this depends on many factors, including fastener dimensions, fastener material and the type of nut. However, as a guide to the order of magnitude of errors, Table 12-2 shows values of 'B' value scatter, for extensometer readings for fasteners of six different diameters that were tested as described in Section 12.4.2 (see also Reference 12.4). It is important to note that, for each diameter, different lengths of fastener were tested. Since the largest errors are likely to be incurred with the shortest fastener, the minimum length used is quoted.

It can be seen that the worst cases in this set of tests produced scatter values in the region of 6%, while it is possible in some cases to obtain results within 1%.

Table 12-2 - Typical Scatter of Ultrasonic Extensometer Preload Readings Using a Direct Load Method of Calibration

Fastener Diameter (mm)	Fastener Length (mm)	Fastener Material	'B' Value Scatter
8	51,2	Inconel	5,5 %
10	40,7	Inconel	6,4 %
12	52,6	Inconel	4,9 %
14	61,7	Inconel	2,8 %
18	70,0	Titanium	6,2 %

12.6 Direct Measurement

12.6.1 Overview

This method of preload control is long established and is included here for completeness. It has a number of disadvantages that are outlined below.

12.6.2 Method of Application and Practical Considerations

A micrometer is used to measure the fastener extension by taking readings before and after tightening. To make accurate measurements, it is necessary to provide gauging surfaces at each end of the fastener. This is usually done by grinding the end faces square or by providing a conical recess into which a steel ball can be located.

The method needs access to both ends of the fastener and sufficient clearance to accommodate a caliper type micrometer.

The method also needs the application of both analytical and practical judgment, and most of the disadvantages cited for the angle controlled tightening method apply. Tension cannot be rechecked without slackening the nut and retightening it unless a log is kept of all fastener dimensions.

The level of accuracy to which the preload can be controlled, assuming a uniform precision in measurement, is primarily a function of the fastener length.

12.7 Reuse of Fasteners

12.7.1 Overview

In many situations a threaded fastener has to be loosened and retightened again, e.g. Mechanical Ground Support Equipment (MGSE) hardware during service on the ground or parts of a test model that are later reused as flight hardware. Reuse of fasteners is desirable since new fasteners are often expensive, however additional analysis [and/or testing](#) is recommended. Two major parameters are affected by reuse; the friction coefficients, and the prevailing torques of the locking device.

12.7.2 Effects on Friction Coefficients

During the tightening procedure the surfaces of the threads are at first planated by the force acting perpendicular to the surface. Under the effect of an increased preload during the tightening, the grinding of the two moving surfaces creates scratches and grooves on both surfaces, thus resulting in higher friction coefficients. The friction coefficients of unlubricated fasteners [can](#) increase by up to 100%, and further increases can occur with a higher coefficient of utilisation. This effect depends mainly on the hardness of the engaged materials and their surface treatments. Therefore, the use of experimental data is recommended when determining the effects of reuse on the friction coefficient.

The results of a series of reuse tests are summarised in Table 12-3, which [are important to](#) be used in place of Table B-1 if fastener reuse is expected. The values in Table 12-3 are the maximum and minimum values for the 2nd to 5th applications of tightening torque. As friction coefficients [can](#) increase with further retightening, [it is important to use](#) this data with care and [to avoid](#) extensive reuse. Nonetheless, the first retightening results in the highest increase of friction coefficients. Depending on the fastener size and nut type, the friction coefficients after the first retightening are 50% to 75% of the value after the 5th

retightening. The data in Table 11.51 is not applicable for MJ type threads; in that case see ISO 5858 and DIN 65349.

Using a separate lubricant added on the fastener prior to each installation significantly reduces the effects of retightening on the friction coefficients. Here also, an increase of the friction coefficients occurs, but it is around 10% - 15% of the value measured at the first use. For fasteners with a coated lubricant (i.e. dicronite) it is important to consider, that the coated lubricant is wearing off each time the fastener is installed. Not only this generates some debris, but also the friction is increasing. This applies to the friction in the thread and underhead of the fastener. Therefore it is strongly recommended to verify the impact for connections, where a precise control of preload is needed.

Table 12-3 - Friction Coefficients of Unlubricated Reused Fasteners

Fastener	Type of Nut or Insert	$\mu_{th,max}$	$\mu_{th,min}$	Flange material AA 7075 T7351	
				$\mu_{h,max}$	$\mu_{h,min}$
LN 29949 M4 (A-286)	Anchor nut (floating) LN 29693	-	-	-	-
	Helicoil LN 9499 made of bronze CuSn6	-	-	-	-
	Nut LN 9161 (self-locking, hexagon flanked)	-	-	-	-
LN 29949 M5 (A-286)	Anchor nut (floating) LN 29693	0,226	0,129	0,316	0,229
	Helicoil LN 9499 made of bronze CuSn6	0,190	0,154	0,330	0,217
	Nut LN 9161 (self-locking, hexagon flanked)	0,196	0,100	0,171	0,098
LN 29949 M6 (A-286)	Anchor nut (floating) LN 29693	0,306	0,144	0,346	0,259
	Helicoil LN 9499 made of bronze CuSn6	0,184	0,152	0,333	0,278
	Nut LN 9161 (self-locking, hexagon flanked)	0,140	0,094	0,257	0,087
LN 29949 M8 (A-286)	Anchor nut (floating) LN 29693	-	-	-	-
	Helicoil LN 9499 made of bronze CuSn6	0,399	0,236	0,352	0,294
	Nut LN 9161 (self-locking, hexagon flanked)	-	-	-	-

12.7.3 Effects on Prevailing Torques

Some self-locking devices use a thread cross-section that is deformed after manufacturing in order to form a slightly elliptical shape. When used for the first time, the elliptical shape is deformed to a circle. This deformation is partially plastic, leaving a permanent deformation for the next use. Thus, the prevailing torque reduces after the first use. Subsequent usage involves mainly elastic deformation, and thus the prevailing torque reductions are small. The increase of the prevailing torque due to increased friction coefficients (as discussed in Section 12.7.2) is negligible compared to the decrease due to plastic deformation. Therefore, the choice of lubricant has only a minor effect on the prevailing torque after multiple reuses.

Some experimental data for prevailing torque loss is shown in Figure 12-4. The data indicates that, by the 5th retightening, no further plastic deformation occurs in the locking device (i.e. the prevailing torque is generated purely by elastic deformations). Therefore, when analysing fasteners with locking devices that can be reused, it is important to use the elastic range prevailing torques of Table 12-4, in place of Table 6-2.

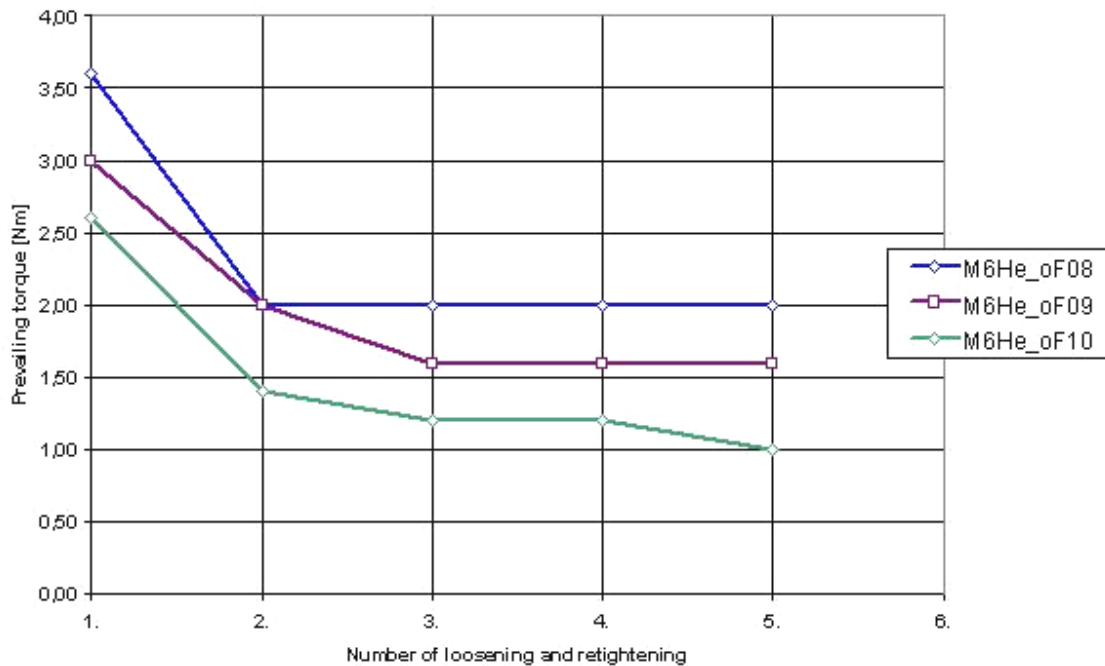


Figure 12-4 - Prevailing torques during a series of loosening and retightening cycles of a LN 29949 M6 fastener and with Helicoil LN9499 made of CuSn6

Table 12-4 - Prevailing Torques of Locking Devices after Several Loosening and Retightening Cycles for Unlubricated Fasteners

Fastener Type	Locking Device Type	Size	M_P (Nm)		
			Min.	Max.	Mean
LN 29949	Helicoil (screwlock) LN 9499 bronze (not cadmium plated)	M4	-	-	-
		M5	0,20	0,90	0,69
		M6	1,20	2,00	1,63
		M8	1,60	3,60	2,28
	Anchornut LN 29693	M4	-	-	-
		M5	-	-	-
		M6	0,40	1,60	0,87
		M8	-	-	-
	Nut LN 9161-M	M4	-	-	-
		M5	0,90	1,60	1,15
		M6	0,20	0,70	0,33
		M8	-	-	-

12.7.4 Recommended Practice for Fastener Reuse

Two approaches to determining the number of times that a fastener can be reused are recommended. The first approach is to rely on experimental data in order to determine limits. The second approach, much more accurate, is to measure the prevailing (also known as running or self-locking) torque during the installation of every fastener and add it to the specified seating torque to calculate the installation torque that is finally applied. In this approach, the fastener is considered unusable if the prevailing torque is outside the range specified by the insert manufacturer. However, this second approach is only covering the friction change within the thread. It is neglecting the under head friction change which is having an impact on the final preload. Therefore it is recommended to perform a characterization / validation test for the critical junctions.

12.8 References

12.1	BICKFORD J.H.	Ultrasonic Control of Bolt Preload, Hydrocarbon Processing., Jan 1982.
12.2	BENNET J.K. and D. de VILLIERS	Procedure for Deriving and Verifying Calibration Data for bolt preload extensions using Raymond Bolt Gauge PDX 934 (BAe. Doc. No. PR-BAe-0072)
12.3	HUTCHINS A. R.	Test Report - Deriving and Verifying Calibration Data for bolt preload extensions using Raymond Bolt Gauge PDX 934 (BAe. Doc No. RP-BAe-0120)
12.4	MORGAN E.	Assessment of Calibration Tests of Rayhmond Extensometer PDX 934 (BAe. Doc. No. TN-BAe-50-oo8-82)
12.5	YAMAMOTO E.	Direct Stress Measurement by Ultrasound Proc. Ninth World Conf. on Hon-Dest - nuctine Testing 1979.

12.6	DEPUTAT J.	Ultrasonic Technique for Measuring Stress in Screws. Proc. Ninth World Conf. on Non Destructual Testing, 1979.
12.7	BOBRENKO V. M.	Ultrasonic Method of Measuring et a1 Stresses in Parts of Threaded Joints: Soviet Journal of Non-Destructual Testing 1974.
12.8	HEYMAN J.S. and CHERN E.J.	Ultrasonic Measurement of Axial Stress: Journal for Testing and Evaluation, September 1982.
12.9	SMITH J.F., GREINER J.D.	Stress Measurement and Bolt Tensioning by Ultrasonic Methods: Journal of Metals, July 1980
12.10	BAe report GHFM/TST/S Dec 85	Examination of Factors Affecting Torque Tightening and the Production of Design Recommendations.
12.11	FISHER J.W., STRUIK J.H.A.	"Guide to Design Criteria for Bolted and Riveted Joints", John Wiley and Sons 1974
12.12	BICKFORD J.H.	"That Initial Preload - What Happens to it?", Mechanical Engineering 1983
12.13	VDI RICHTLINIEN	VDI 2230, Nov. 2015, Systematic Calculations of High Duty Bolted Joints
12.14	BICKFORD J.H.	An introduction to the Design and Behaviour of Bolted Joints, Marcel Dekker, 1981
12.15	Pfaff, H.	Calculation of the preload at the yielding point of hyperelastic tightened screws, Konstruktion 47 (1995 Nr.7/8 S.237/240)
12.16	ISO-16047	Fasteners – Torque/clamp force testing
12.17	NASM 1312-15	Fastener Test Methods, Method 15, Torque-Tension

13

Corrosion

13.1 Overview

Corrosion can be defined as the chemical reaction of a metallic material with its environment. The products of this reaction can be solid, liquid or gaseous and the physical and chemical natures of the products are important as they often influence the subsequent rate of reaction.

Handbooks and reference charts are available, providing information on the behaviour of metals and other materials in certain well-defined environments. Unfortunately the precise operational environment is, in practice, difficult to predict and can vary considerably, e.g. for reusable space components.

Additionally, the method of fabrication and fastening can affect the susceptibility to, and rate of, corrosion.

Thus to avoid corrosion problems, the factors to be considered by a designer are:

- The working environment and exposure to it
- The probable reactivity of the materials involved in fabrication
- The features of the design that can modify that reactivity

Figure 13-1 shows the types of corrosion that have been identified as most relevant to space applications. The following sections briefly describe the various types of corrosion and some recommendations are given for overcoming corrosion problems.

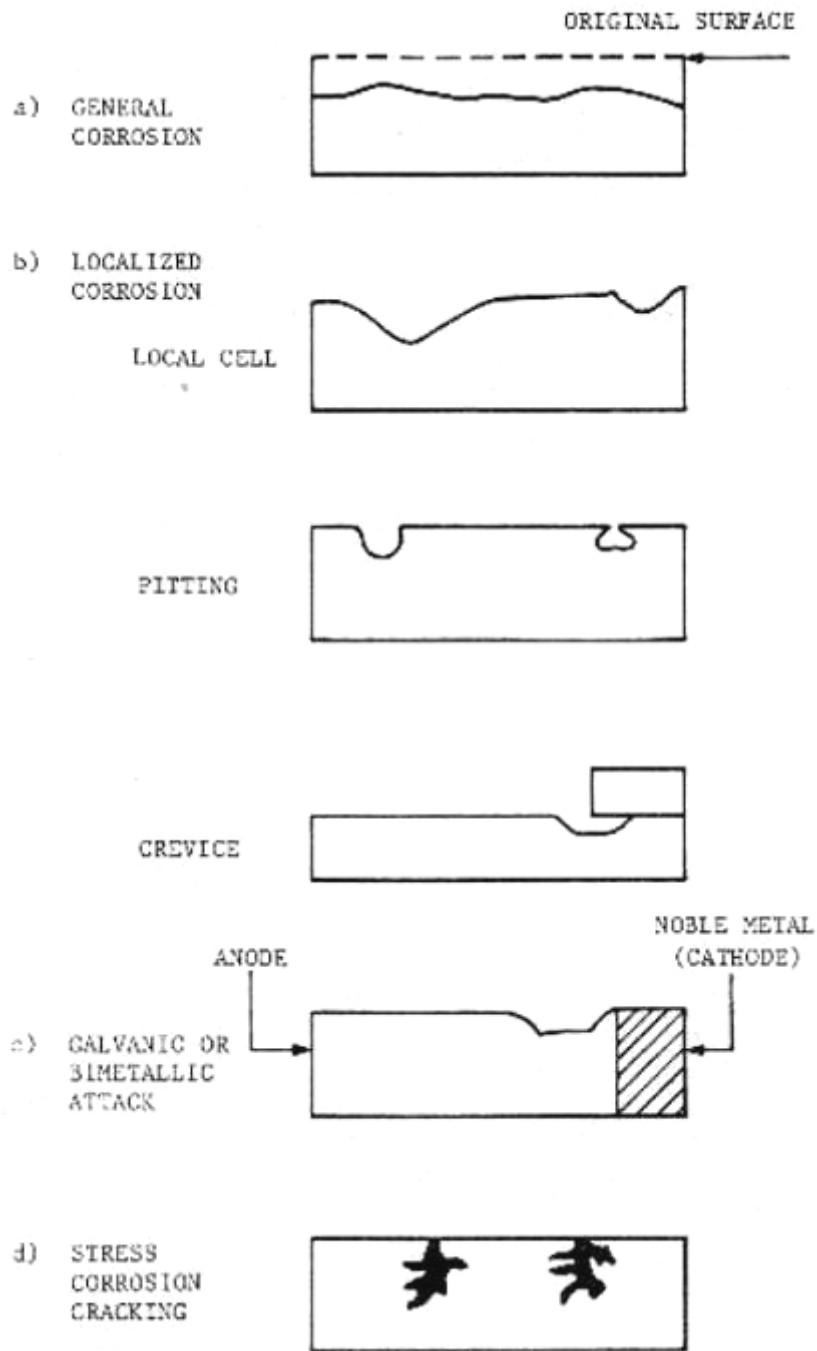


Figure 13-1 - Forms of Corrosion

13.2 Galvanic Corrosion

13.2.1 Introduction

Aqueous corrosion processes generally need oxygen and water in intimate contact to achieve measurable corrosion rates. In space environments, both these substances are virtually non-existent and hence aqueous corrosion processes **can** be essentially ignored.

However during manufacture, test and storage the structure experiences Earth environments with high levels of oxygen and water, therefore the corrosion process cannot be ignored.

When dissimilar metals are joined, accelerated corrosion can occur at the interface due to galvanic corrosion. This corrosion occurs on a metal (the anode) as a result of current flow from the anode to a less reactive (more noble) metal (the cathode), when they are in electrical contact and in the presence of an electrolyte. The anode corrodes due to dissolution of the metal and the process is balanced (in most practical applications) by the reduction of dissolved oxygen in the electrolyte.

13.2.2 Factors Which Affect the Rate of Corrosion

13.2.2.1 Electrolyte

Electrolyte factors that have major implications for galvanic corrosion are as follows:

- a. Electrolyte composition
- b. Degree of acidity or alkalinity
- c. Electrical conductivity

In general the severity of corrosion often increases with increasing electrical conductivity since in practical situations high conductivity is often caused by the presence of aggressive ions such as chloride or by acid or alkali.

13.2.2.2 Area Ratio

For many situations the rate of corrosion is dependent upon the rate of diffusion of dissolved oxygen to the cathode and is thus proportional to the area of the cathode metal surface. Thus, for a constant area of cathode material, the amount of corrosion of the anode area is constant but the intensity of corrosion increases as the area of the anodic metal is decreased. Since adverse area ratios **can** occur in threaded fastener joints, **it is important that** the fastener metal **is** of the same polarity as the clamped parts, or be relatively cathodic to them.

13.2.2.3 Metallurgical Condition and Composition

Differences in corrosion potential can exist between coupled metals or alloys of nominally the same composition. The cold working of an alloy/metal tends to make it more anodic. Bimetallic corrosion can also occur between generic alloys with slightly differing compositions.

13.2.3 Prevention of Bimetallic Corrosion

The prevention or minimisation of galvanic corrosion is best addressed during the design stage (see Reference 13.1). When dissimilar metals are joined, it is important to take care to protect the anodic member by proper electrical insulation of the joint or by excluding the electrolyte if this is feasible.

Table 13-1 lists metals in the order of their relative activity in an aqueous environment. The list begins with the more active (anodic) metal and proceeds down to the least active (cathodic) metal of the galvanic series. A galvanic series pertains to a particular electrolyte solution and hence for each specific solution encountered, a different series can apply. Usually a seawater environment is chosen as the basis for comparison since it is one of the most corrosive environments and is readily encountered. Galvanic series relationships are useful as a guide for selecting the metals used for a joint. Generally the closer one metal is to another in the series, the more compatible they can be. In a galvanic couple the metal higher in the series represents the anode and can corrode preferentially in the environment. It is therefore necessary to protect metals widely separated in the galvanic series, if they are intended to be joined.

Methods of preventing or minimising galvanic attack are based upon breaking the electrical path in the metallic or electrolytic parts of the system, by excluding oxygen from the electrolyte, or by sacrificial corrosion. This strategy cannot be used if the galvanic couple needs to act as an electrical connection. Electrical insulation can be achieved by interposing a gasket or washer between the dissimilar metals prior to connecting them. If the couple has to act as an electrical connection, a compatible metallic gasket or washer can be placed between the two metals prior to fastening, or the cathodic member can be plated with a metal compatible with the anode. Jointing compounds applied to the contacting surfaces of fasteners and lap joints do not normally provide electrical insulation, they are however very useful in preventing water penetrating the joint and hence preventing galvanic and crevice corrosion.

Table 13-1 - Galvanic Series of Metals in an Aqueous Environment

Material Category	Variant
Mg alloy	AZ - 31B
Beryllium (hot pressed)	-
Al alloy	2014 - T3
Al alloy	1160 - H14
Al alloy	7079 - T6
Al alloy	5052-0
Al alloy	5052-H12
Al alloy	5456-0, H353
Al alloy	5052 - H32
Al alloy	1100 - 0
Al alloy	6061 - T6
Al alloy	7075 - T6
Al alloy	1160 - H14
Al alloy	6061 - 0
Al alloy	2014 - 0
Al alloy	2024 - T4
Al alloy	5052 - H16
Stainless steel	430 (active)
Stainless steel	410 (active)
Copper (plated, cast or wrought)	-
Nickel (plated)	-
Tantalum	-
Stainless Steel	AM350 (active)
Stainless Steel	301 (active)
Stainless Steel	304 (active)
Stainless Steel	17-7 PH (active)
Tungsten	-
Copper 110	-
Stainless Steel	Carpenter 20 (active)
Stainless Steel	321 (active)
Stainless Steel	316 (active)
Stainless Steel	309 (passive)
Stainless Steel	17-7 PH (passive)
Stainless Steel	304 (passive)
Stainless Steel	301 (passive)



Material Category	Variant
Stainless Steel	321 (passive)
Stainless Steel	201 (passive)
Stainless Steel	AM 355 (active)
Stainless Steel	Carpenter 20 (passive)
Stainless Steel	AM 355 (passive)
Stainless Steel	A286 (passive)
Titanium (annealed)	13V, 11Cr, 3Al
Titanium (solution treated and aged)	6 Al, 4v
Titanium (annealed)	6 Al, 4V
Titanium (solution treated and aged)	13V, 11Cr, 3Al
Stainless Steel	Am 350 (passive)
Silver	-
Gold	-
Graphite	-

Surface coatings are very effective in protecting metals. **It is important that** both members of the couple **are** coated, but where this is not possible then the cathodic metal be coated as this increases the effective anode area ratio and reduces the corrosion intensity.

It is important that the non-metallic materials that are joined to metals **are** treated with caution. For example, composite materials **can** contain carbon or graphite, which being very noble, **can** result in corrosion of the metal. Graphite pencil markings on aluminium aircraft structures have given rise to galvanic corrosion problems in the past. It is important to ensure that the non-metallic material does not contain any other corrosive agents. **It is important that** in particular they **are** free of the following:

- a. Ionic salts
- b. Acid or alkaline materials
- c. Carbon or metallic particles
- d. An ability to wick or absorb water.

It is important that gaskets used in RF shielding (typically a metallic loaded or metallic mesh supported in an elastomeric medium) **are** carefully screened to achieve compatibility with the mating surfaces, otherwise the mating surfaces and fasteners can need to be treated in some way.

13.3 Stress Corrosion Cracking

13.3.1 Introduction

Stress Corrosion Cracking (SCC) occurs where certain alloys are subjected to a continuous tensile stress in the presence of a specific corrosive environment. The failures appear to be of a brittle type even where the material is recognised to be ductile. Surfaces in the region of the crack do probably not appear

affected by general corrosion that often makes SCC more difficult to diagnose. Time to failure is a matter of minutes under severe conditions, or years when conditions are less severe.

SCC is often associated with aerospace structures constructed from high strength materials and operating at high stresses. The Apollo Program suffered many SCC failures and much was learned about the design of space structures as a result (see Reference 13.2). Subsequently NASA issued design criteria for controlling SCC (Reference 13.3), to be met by all contractors for NASA flight hardware. It contains a list of materials that are resistant to SCC and also those which are most susceptible. A similar document called ECSS-Q-ST-70-36 "Material Selector for Controlling Stress Corrosion Cracking" exists within ECSS. (Reference 13.4).

The following Sections aim to highlight the aspects of SCC relevant to threaded fastener joints and to make designers aware of the methods available to avoid or reduce the occurrence of SCC.

13.3.2 Factors Affecting Stress Corrosion Cracking

13.3.2.1 Overview

The prerequisites for SCC are as follows:

- a. a susceptible material
- b. a specific corrosive environment
- c. a tensile stress

Each of these is discussed in Sections 13.3.2.2 to 13.3.2.4 below.

13.3.2.2 The Susceptibility of Materials to SCC

It is worth mentioning that SCC is sometimes more generally named environmentally assisted cracking (EAC). The effect of alloy composition and metallurgical condition (grain size and orientation, distribution of precipitates, etc.) on SCC is sufficiently understood to specify certain preferred alloys and treatments to minimise the effect of SCC (see Reference 13.3).

In high strength aluminium alloys the effects of heat treatment and cold work are significant in determining resistance to SCC. For example when wrought aluminium products are manufactured by rolling, extrusion or drawing the alloy microstructure becomes distorted into elongated grains in the direction of working. This is designated the longitudinal direction, the width of the sheet is the transverse direction, and the thickness is designated the short transverse direction (as shown in Figure 13-2 for a number of section shapes).

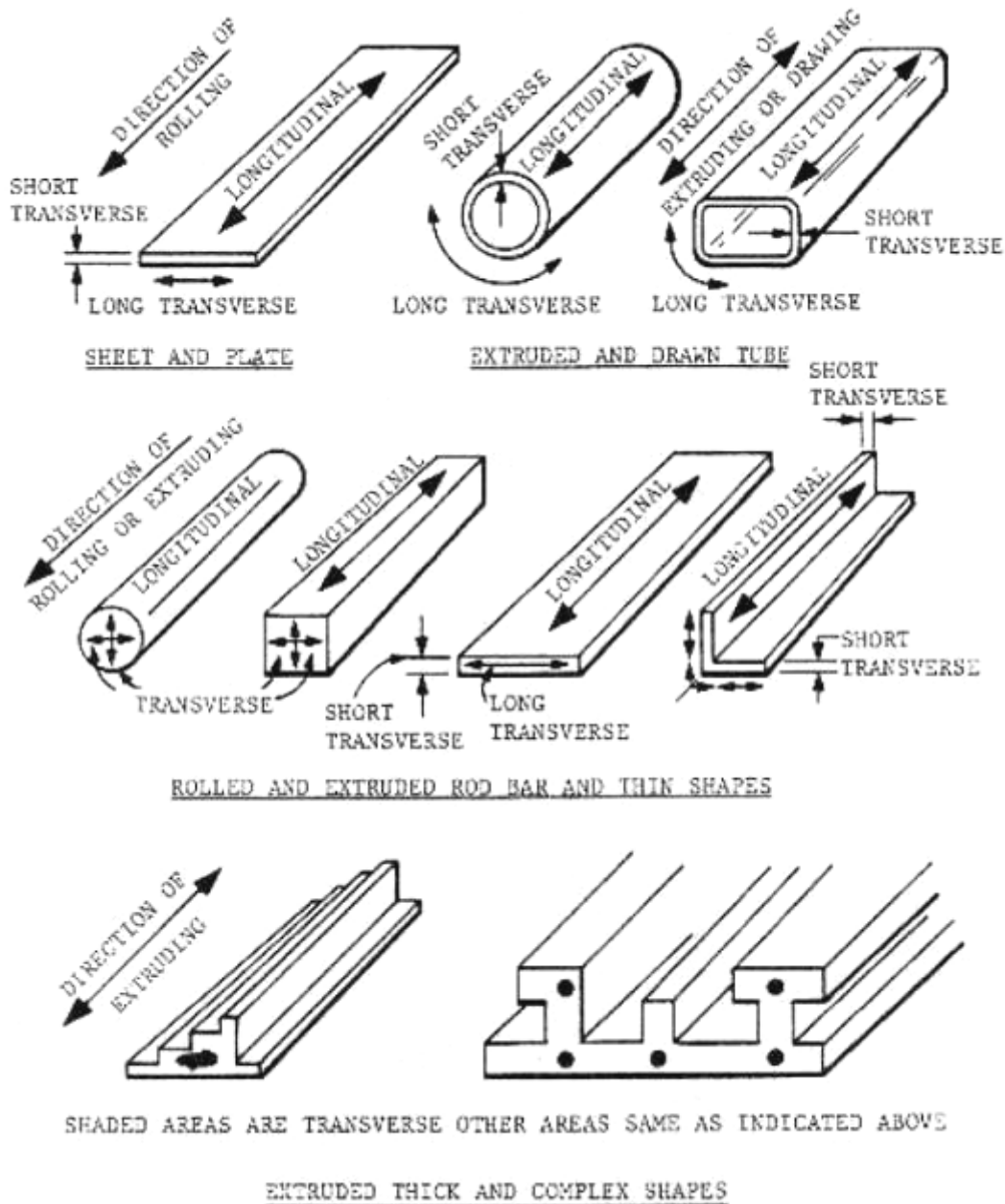
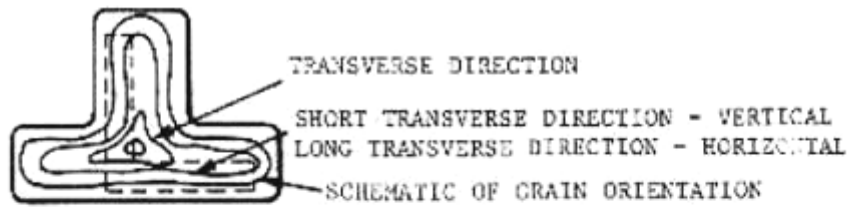


Figure 13-2 - Grain Orientations in Standard Wrought Forms

Material properties vary depending on the direction of testing with the longitudinal direction being strongest. The short transverse direction is usually the weakest and as a result is most prone to the effects of SCC. It is therefore desirable to design components that are not heavily stressed in the short transverse direction. Figure 13-3 and Figure 13-4 illustrate examples of poor joint design that can lead to high stresses in the short transverse direction.



LOCATION OF MACHINED ANGLE WITH RESPECT TO TRANSVERSE GRAIN FLOW IN THICK TEE

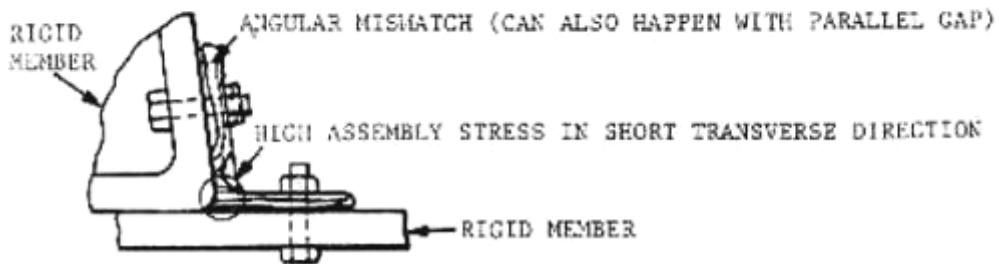
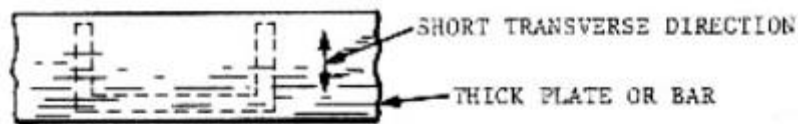


Figure 13-3 - Assembly Stress Resulting from Mismatch



LOCATION OF MACHINED CHANNEL IN PLATE OR BAR

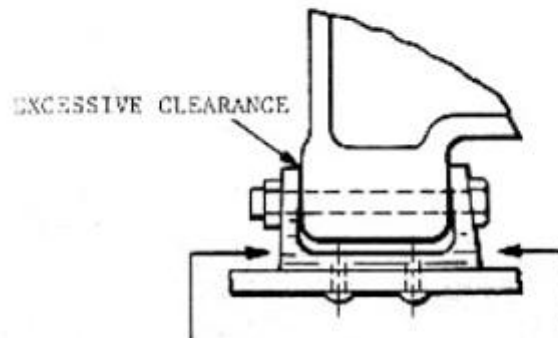


Figure 13-4 - High Assembly Stresses in Short Transverse Direction

The short transverse direction of a forged component is perpendicular to its parting plane as shown in Figure 13-5. In this case any bush or fastener with an interference fit in the bore indicated is likely to accelerate failure by SCC.

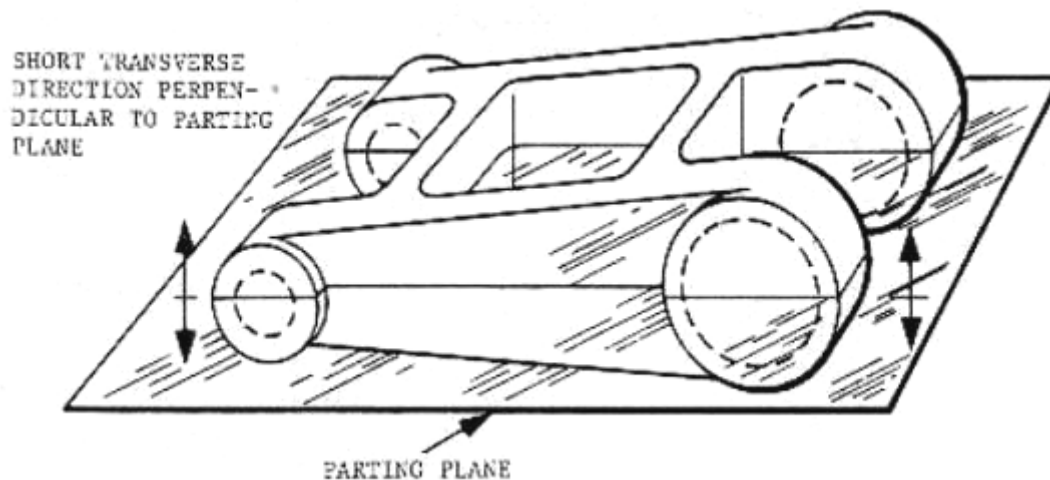


Figure 13-5 - Examples of Tensile Stresses in Short Transverse Direction Resulting from Assembly

Heat treatments have been developed to reduce the susceptibility of high strength aluminium alloys to SCC and [it is important to specify](#) these where possible.

When specifying alloys for use on space systems ECSS-Q-ST-70-36 on prevention of SCC is applicable (Reference 13.4). This document collects in a table the alloys with high resistance to SCC that can be used, and prescribes their conditions of use. Where an alloy is not listed and SCC data is not available, it is necessary to conduct suitable tests for SCC resistance, such as those given by ECSS-Q-ST-70-37 (see Reference 13.6). The results [are](#) submitted for approval on a Stress Corrosion Evaluation Form. A similar situation exists for material approval to NASA standards.

13.3.2.3 The Role of the Environment in Stress Corrosion Cracking

Environments that give rise to SCC are often specific to particular alloys, thus making SCC very difficult to predict unless tests have been conducted simulating the operating conditions or failures have been noted previously under similar conditions.

As the corrosive environment is essential for SCC to occur, [it is important that](#) the designer ensures that approved protective anti-corrosion coatings are specified.

13.3.2.4 The Influence of Stress on Stress Corrosion Cracking

The effect of applied tensile stress on SCC varies with materials. In some cases a threshold stress concentration factor K_{iscc} can be specified, below which failure by SCC cannot occur (see Section 11.3.5). In other cases, SCC occurs at all values of applied tensile stress, the time to failure being dependent on the stress level.

Tensile stresses in joint assemblies that can give rise to SCC [can](#) be imposed by several sources, in addition to the normal working stresses in the system. Misalignment or gaps between joint faces can cause high surface tensile stresses which when combined with an unfavourable grain orientation can result in rapid SCC failures. Such failures can be avoided by ensuring that gaps are properly shimmed, and the alignment of assemblies is checked.

Fasteners with substantial interference fits can impose high tensile stresses in the flange's transverse grain direction, leading to longitudinal cracks. **It is important to take care** to specify alloys that are highly resistant to SCC in these regions.

In some cases, manufacturing processes **can** leave components with residual surface tensile stresses. Examples of such processes are bending, tube drawing, stretch forming, electro discharge machining (EDM) and some cutting operations. An indication of what level of residual stresses can be imparted by these operations is given in Reference 13.5. Heat treatment processes **can** also leave residual stresses, especially for components with complex shapes. **It is important that all** residual tensile stresses **are** reduced or eliminated by thermal treatments or by mechanical means.

Compressive surface stresses can be introduced in many components by shot peening. This process is very useful for controlling SCC in critical parts.

13.4 Crevice Corrosion

13.4.1 Introduction

Accelerated corrosive attack is often observed in crevices that are exposed to wet conditions. Assemblies joined together by fasteners are particularly prone to this type of corrosion due to the difficulty in avoiding crevices between the joint elements. However, it is possible to minimise the problem by preventing moisture from penetrating the crevice.

13.4.2 Methods of Avoiding Crevice Corrosion

It is recommended to avoid, where possible, crevices in design. If they cannot be avoided, **it is important that they are** covered with a continuous paint film. Thread sealants are very useful in combating crevice corrosion and in most cases a good paint film prevents the ingress of water.

It is important that joints are carefully cleaned and dried before assembly since even small amounts of debris can prevent mating faces from contacting, resulting in crevice conditions. Similarly any moisture trapped between joint faces is likely to initiate corrosion.

13.5 Pitting corrosion

13.5.1 Introduction

Pitting corrosion **can** be thought of as a form of localised corrosion that occurs on one part of a metal surface at a much higher rate than over the rest of the surface. Pitting corrosion is associated with the breakdown of a surface film and often occurs on completely flat surfaces. If the surface film is cathodic, an area without the film **can** act as a small anode, thus suffering intense corrosion that leads to pitting.

Pits can also be nucleated at points determined not only by faults in the surface film, but also at sites determined by the underlying metal. Such sites **can** arise from alloy heterogeneities in the surface, or be associated with grain or phase boundaries. Solid non-metallic inclusions from processing procedures or from impurities, e.g. sulphides in stainless steels, **can** also provide initiation sites.

13.5.2 Alloy Susceptibility

13.5.2.1 Alloy Steels

Stainless steels possess excellent resistance to pitting corrosion in oxidising atmospheres. However, in the absence of oxygen the protective oxide film can break down and pitting corrosion can occur very rapidly.

13.5.2.2 Aluminium

In most natural environments, aluminium and its alloys give satisfactory resistance to pitting corrosion. However, at high and low pH values, in the absence of oxygen, or in the presence of film destructive ions, the protecting oxide film can breakdown with a resultant pitting attack. In Al-Zn-Mg alloys this can lead to intergranular corrosion and a significant loss of strength.

13.5.2.3 Titanium

This metal and its alloys are extremely resistant to pitting corrosion.

13.5.3 Prevention of Pitting Corrosion

The incidence of pitting corrosion can be reduced by selection of materials that exhibit a high resistance to this form of corrosion.

13.6 References

13.1	T.K Ross	Metal Corrosion, published by the Design Council, the British Standards Institution and the Council of Engineering Institutions by Oxford University Press.
13.2	R.E. Johnson	Apollo Experience Report - The Problem of Stress Corrosion Cracking, NASA TND-711, March 1973.
13.3	MSFC-STD-3029A	Guidelines for the Selection of Metallic Materials for Stress Corrosion Cracking Resistance in Sodium Chloride Environments, 2005
13.4	ECSS-Q-ST-70-36	Space product assurance - Material Selection for Controlling Stress Corrosion Cracking
13.5	A T Bainbridge	Residual Stresses Arising from Machining and Fabrication, AGARD CP No 53, 1970.
13.6	ECSS-Q-ST-70-37	Space product assurance - Determination of the susceptibility of metals to Stress Corrosion Cracking
13.7	R. Wanhill, M. Windisch	Corrosion and Stress Corrosion Testing of Aerospace Vehicle Structural Alloys, Springer Briefs in Applied Sciences and Technology, Springer, 2018,https://doi.org/10.1007/978-3-319-89530-7

14

Lubricants for Space Use

14.1 Introduction

The nearly total absence of air around and within space vehicles has two major implications for tribology. Firstly, oxygen and water vapour are not on hand to repair damaged surfaces, so strong adhesion (welding and galling) between clean degreased materials becomes inevitable if they are unprotected. Secondly, a liquid phase lubricant (e.g. oil or grease) can quickly volatilise or boil away, either directly to space or contaminating the spacecraft, unless the lubricant has sufficiently low vapour pressure and/or is suitably “sealed” to retard molecular effusion. Thus, the space environment impose the use of lubricants that neither volatilise nor creep, and which are not influenced by temperature extremes.

14.2 Lubricant Selection

Reference 14.4 contains guidelines for space materials selection. It deals with lubricants in general and lists lubricants that are suitable for space applications.

Table 14-1 provides a list of recommended lubricants.

Table 14-1 - Recommended Lubricants for Space Applications

Trade Name	Chemical Composition	Type of Product	Manufacturer
FOMBLIN Y VAC 3	Perfluoropolyether	Grease lubricant	Montedison, Milan, Italy
BRAYCO MICRONIC 815Z	Perflourinated poly-ether	Oil	Bray Oil company, California, USA
MoS ₂ Molycote Z, Moly- Paul ITC, Lubri-Bond...	Molybdenum disulphide	Lubricant	Several (Dow Corning Belgium, K.T. Paul Products U.K., Electrofilem Inc. USA. etc.)
BRAYCOTE 3L-38RP	Perflourinated poly-ether	Grease lubricant	Bray Oil company, California, USA
DICRONITE	Modified Tungsten Disulphide (WS ₂)	Lubricant	Rotary Components Inc. California USA
APIEZON L	Hydrocarbon	Grease lubricant	Shell Chemie Den Haag – NL
KINEL 5518	Polymide / PTEE	Thermosetting, self lubricating resin	Rhone – Poulenc – Paris - F
FOMBLIN Z 25	Perflouralkylether	Oil	Montedison, Milan, Italy
P.T.F.E (Teflon, Halon, Fluon, Hostafluon...)	Polytetrafluorethylene	Thermoplastic	Several (Du Pont US, Hoechst D, Montecatini I, etc.)

14.3 Plating and Coatings for Fasteners

Silver coating is primarily a lubricant for high temperature applications on corrosion resistant fasteners in steel and other structures where galvanic corrosion is not a problem.

It is also used because it does not sublime. The specification is usually AMS2410. Other coatings such as Electrofilm are really lubricants and provide minimal corrosion protection. Soft metals like Lead (Pb) can be sheared easily, so that in certain circumstances they can also be used as solid lubricants. However, they **cannot** support heavy loads without deforming, so they are used as thin coatings on stronger metal surfaces. Soft metal films are mainly used as lubricants only in a vacuum.

Fastener qualification data has been generated on the use of Ion Vapour Deposited (IVD) aluminium (IVADISE) as a replacement for cadmium in general engineering use (Reference 14.2).

The conclusions can be summarised as follows:

- a. IVD aluminium does not produce any detrimental effects on the mechanical properties.
- b. The coefficient of friction of aluminium is higher than cadmium, therefore higher installation forces are necessary. These higher values, however, are within the working ranges presently used for cadmium in most cases. A closer attention to the type of lubricants used can be necessary for interference fit fasteners.

With a silver-plated A286 nut, an IVD coated titanium bolt, and using EVERLUBE 812 as a lubricant, a consistently low coefficient of friction can be obtained for multiple installations. Kalgard 2240 (an aluminium rich paint) can be also used instead of the IVADIZE coating (Reference 14.3).

Refer to Reference 14.4 for processing requirements for platings and coatings. Since plating process bears the risk of hydrogen embrittlement sustained tensile load tests can be needed (see references 14.5, 14.6 and 14.7).

Note that the use of bolts with coatings based on chemically deposited lubricants is preferred w.r.t. the implementation of a lubricant during the installation of the fastener. The deposited layer guarantee a more controlled low coefficient of friction also for multiple installation. Typical examples are deposited MOS2 and Dicronite.

Other plating and coatings are cadmium, zinc, nickel, phosphate, chromium, etc. for details see Reference 14.8.

14.4 Liquid Lubricants

Probably the most significant addition to space lubricants is a polyfluoralkylether called Fomblin Z25. The fluid has the very high viscosity index of 345 and a vapour pressure that is suitably low at room temperature.

The Bray Oil Co in the USA have distilled the Italian raw stock (Fomblin Oil) to make Bray 815Z, which has been flown on a number of USA satellites mostly in the form of a PTFE thickened grease, Bray 3L38RP.

14.5 Dry Lubricants

Molybdenum disulphide (MoS_2) in various formulations is the most extensively used lubricant. It possesses excellent anti-galling properties and low friction. In vacuum MoS_2 performs even better than in air because there is no oxidation. Also, MoS_2 can withstand over 1000°C in vacuum before it sublimates.

Application of MoS_2 can be by a number of means;

- a. as a spray-bonded film,
- b. using a polymeric or inorganic carrier,
- c. as a burnished film where the hard-edged platelets are forced into the surface, or as a sputtered film applied by radio frequency (RF).

The RF sputtering method offers a highly reproducible way of obtaining adherent and thin films.

14.6 Codification of Space Lubricant Systems and Processes

The behaviour of any tribological system is governed by a large number of factors, many of which are difficult to control; material properties, both macro and micro, surface condition, presence of micro quantities of contaminants, system geometry, speed, load, duty cycle are only some of the variables. In consequence the rules to be met by any lubrication process to be acceptable for space are as follows:

- a. In order to ensure consistent repeatability of performance, only fully codified and documented lubrication processes are used for space application .
- b. Only lubricants that are approved and validated for space to a recognised specification, and source traceable, are used.
- c. The test programme to determine the performance of the lubrication system reproduces all the operational conditions of the duty cycle, the environment and the life that it can experience in the application.

The use of a commercial system for a space application is acceptable only if it fulfils these three rules.

14.7 References

14.1	Deleted ANON	Guidelines for space materials selection, ESA PSS 07 (QRM 07) Issue 5, July 1979 Deleted
14.2	J. Newnham, B. Hassell, P. Betiam	Evaluation of Titanium bolts and coated with Ivadize Aluminium and Kalgard 2240C in torque tension tests. SPS Technologies, Inc., NAAS Lab, Ref., No. 5254 1979.
14.3	MCAIR M & PD	R & D Report No. 118, 6 th February, 1975.
14.4	ECSS-Q-ST-70-71C Rev.1	Materials, processes and their data selection (15 October 2019)
14.5	ISO-10587	Metallic and other inorganic coatings – Test for residual embrittlement in both metallic-coated and uncoated externally threaded articles and rods – Inclined wedge method
14.6	ISO-15330	Fasteners – Preloading test for the detection of hydrogen embrittlement – Parallel bearing surface method

14.7	ASTM F519-13	Standard Test Method for Mechanical Hydrogen Embrittlement Evaluation of Plating/Coating Processes and Service Environments
14.8	NASA-RP-1228	Fastener Design Manual, 1990

Manufacturing Quality Control

15.1 Introduction

It is essential that quality is 'built-in' at the design stage. If it is not, no amount of subsequent quality activity **can** be entirely satisfactory.

The overall quality of a joint is a function of its design quality and manufacturing quality. The former includes the analytical aspects of joint design and is dealt with in some detail in the earlier this guidelines document. The latter includes performance variations, which occur as a result of production tolerances and is covered in this section.

15.2 Manufacturing and Quality Assurance

Specific overall requirements are imposed by agencies (such as NASA, ESA, CNES and MILITARY). These requirements relate to the need to address such aspects as safety factors for the Space Transportation System. An example of this is the requirement to use materials which have been previously qualified as non-stress corrosive. The information concerning such aspects is to be found in the respective Space Agency supporting documentation, processes, specification or project requirements.

For projects conducted within the European Space Agency a system of ECSS documents exists which are mandatory when called for in the contract requirements. [ECSS-Q-ST-70-46 \(ref 15.4\)](#) is generally found to be a good basis for this. In some cases (mainly in human spaceflight) a 'fastener integrity plan' or 'fastening system control plan' is issued to capture organization-specific processes for ensuring quality and integrity.

Quality Assurance, or as it is more commonly known in space projects, Product Assurance, has the responsibility to ensure that designers have recognised requirements of the type indicated above and that the necessary controls and verification have been conducted to ensure compliance. This ensures the traceability of materials from their source and that the specified testing and inspection is carried out. Testing **can** include hardness, non-destructive tests and preloading of fasteners. Inspection includes all dimensional tolerances. Additionally, all materials used in spacecraft have to be listed and reviewed for acceptability.

The controls imposed to achieve these objectives are primarily associated with the detail of planning, review, inspection and that recording of data that gives final traceability of all the information in the event of any failure.

15.3 Quality of Threaded Fastener Joints

15.3.1 Overview

When designing a threaded fastener joint, **it is important that** the designer considers all production variations that might influence the joint's performance. These variations come under the following broad categories:

- Process Variations
- Material Variations
- Tolerancing

It is important that the designer **specifies** the acceptable variation of the above parameters in the engineering drawings, also citing the relevant company, national or international standards.

Production testing and inspection is an important part of Quality Control and it provides feedback on achievement and limits variations. **It is important that** the designer therefore considers the necessary testing and inspection and facilitate this (as far as possible) within the design.

15.3.2 Process Variations

The performance of the threaded fastener joints is affected by the following:

- a. Dimensional tolerances, e.g. fastener/hole fits, hole positional tolerances.
- b. Surface finish on the mating part of the design.
- c. Preload variations.
- d. Thread profile and dimensional tolerances.
- e. Lubrication conditions.

The above variations are limited by the designer specifying an acceptable level on the drawings or by invoking standards.

15.3.3 Material Variations

Performance of the joint **can** be affected by the following material variations:

- a. Ultimate strength (compressive and tensile)
- b. Proof strength (compressive and tensile)
- c. Moduli of the material
- d. Poisson Ratio
- e. Friction characteristics
- f. Corrosion characteristics

15.3.4 Tolerancing

Tolerances **can** affect the joint characteristics such as its load carrying ability, stiffness and backlash. It is likely that the larger the tolerances, the greater the joint strength variation.

When considering the effect of manufacturing tolerances it is necessary to assume some statistical distribution of the variations. If all tolerances were assumed to be at their worst possible value, then the design **is** far too pessimistic. However, there can be cases where this has been designed in deliberately and so **it is important that it is not** overlooked completely.

When using statistical analysis it is essential to recognise the distribution of the variation. Manufacturing variations can generally be classified as Gaussian. However, Skewed-Gaussian or Rectangular distributions **can** be more suitable for certain manufacturing methods. Inspection and testing **can** affect the distribution by truncating the ends of the distribution.

It is important that the designer obtains information on the variation of important joint characteristics and examine test results in order that he **can** have confidence in his statistical analysis. **It is important that** the tolerances specified take account of the variation in the controlled characteristic. In order to optimise production yield and minimise costs, **it is important that** the tolerances **are** increased to the maximum consistent with the performance to be achieved.

15.4 References

15.1	ECSS-Q-ST-70	Space product assurance - Materials, mechanical parts and processes
15.2	ECSS-Q-ST-70-36	Space product assurance - Material selection for controlling stress-corrosion cracking
15.3	ECSS-Q-ST-70-37	Space product assurance - Determination of the susceptibility of metals to stress-corrosion cracking
15.4	ECSS-Q-ST-70-46	Space product assurance - Requirements for manufacturing and procurement of threaded fasteners
15.5	B.D. Dunn	Materials and Processes for Spacecraft and High Reliability Applications' Springer, 2016 (section 5.2 on Fasteners) ISBN 978-3-319-23361-1

16

Joint Validation by Testing

16.1 Introduction

Successful design is usually achieved through the combination of theoretical analysis and practical testing. The level of confidence in theoretical work alone is limited by the accuracy of the data being used and the accuracy of the theoretical method. Physical testing overcomes this problem but it is usually impossible to explore the limits of all potential variations. Close agreement between theoretical and practical results gives the designer high confidence that the joint's behaviour is understood, that the theory is correct and that a successful design results.

This section aims to give the designer guidelines for the testing of threaded fastener joints. It is not specific since the type of validation depends on the type of joint and the circumstances in which it is being designed.

16.2 Types of Testing

There are two broad categories of testing:

- a. Development testing, and
- b. Production testing.

During development testing an exhaustive set of tests is recommended, dependent on the type of joint and its application. The general aim of development testing is to confirm the understanding of how the joint works (e.g. to confirm the theory applied for its design). Development testing also includes long-term effects such as [creep](#), corrosion and fatigue.

Production testing is much more restrictive and [can](#) include every joint or be limited to testing of samples. The objective is to determine whether the joint has been manufactured and assembled correctly, and made from the correct materials. [It is important that](#) the amount of production testing [is dependent](#) on how great the risk of failure is.

16.3 Development Testing

16.3.1 Overview

Development testing aims to confirm the theoretical analysis carried out on the joint. This also applies to long-term characteristics such as fatigue. All joints show a statistical variation of performance, and it is important to take this into account when obtaining approval based on test results. Development testing can include any or all of the following approaches:

- a. A large number of samples simply tested under normal loading conditions.
- b. A small number of samples simply tested but at loads enhanced in relation to the number of samples.
- c. A small number of samples tested in great detail such that the internal functioning of the joint [can](#) be understood.

[It is important that](#) above [approaches](#) include both static and dynamic tests (if appropriate) and also long-term effects.

16.3.2 The Test Factor

When a test is made on a single specimen or a number of randomly chosen specimens, **it is important that** the results show an extra margin of strength, or 'test factor', over the design value to allow for the possibility that the chosen specimens were stronger than average and also to ensure that the weakest specimen produced has acceptable strength. Past experience has shown that for conventional metallic structures the strength can be expressed as a normal distribution with a specified coefficient of variation (the ratio of standard deviation to the mean). This distribution can be used to deduce the magnitude of the test factor that **is** used for a given number of test specimens, in order to establish with an acceptable probability that the weakest specimen **has** the required strength.

A coefficient of variation of 0,03 has been established for joints made to aircraft standards from the following materials:

- Aluminium Alloy
- Titanium
- Steel

If the coefficient of variation is not known, tests **are** necessary to establish a value.

The probability that the mean strength realised on test divided by the test factor is less than the required design strength given by,

$$P = P \left(\frac{S_{mt}}{F_t} < S_{req} \right) \quad [16.3.1]$$

where P is, S_{mt} is the mean strength found during testing, F_t is the test factor, and S_{req} is the required strength.

Table 15.3.1 shows the test factors to be used to give a range of values of P under for a range of variation coefficients using Equation [16.3.1].

Table 16-1 - Test Factors to be used for Given Probability of Failure

Number of Tests	Probability of Failure (P)	Coefficient of Variation (V)				
		0,03	0,05	0,07	0,10	0,20
1 Test	1 in 10	1,056	1,095	1,136	1,200	1,452
	1 in 100	1,104	1,180	1,262	1,400	2,069
	1 in 1000	1,141	1,247	1,366	1,577	2,890
	1 in 10 000	1,172	1,276	1,461	1,749	4,241
3 Tests	1 in 10	1,046	1,078	1,112	1,167	1,385
	1 in 100	1,086	1,150	1,220	1,339	1,943
	1 in 1000	1,117	1,207	1,310	1,495	2,716
	1 in 10 000	1,143	1,257	1,392	1,650	4,023

Table 16-1 indicates that if only one test can be done on a joint with a coefficient of variation of 0,10 and the probability of joint failure in service is to be better than 1 in 1000 then the test factor to be used is 1,577. However, if three tests were done against the same requirement then the test factor to be used **is** 1,495.

The alternative method to the relatively straightforward tests factors described above is undertaking testing that provides detailed knowledge of how the joint works. In this approach tests are conducted which provide detailed knowledge of the loads, stresses and strains within the joint as a function of the external applied loads. These results are compared to an equally detailed theoretical analysis of the joint using a suitable method (such as the Finite Element Method) to ensure that measurements are being made in the most relevant areas.

16.3.3 Specific Development Tests

16.3.3.1 Overview

It is important to consider very carefully the environment to be withstood by a joint before specifying the development test programme. In general, higher loads are applied to the structure while it is in a benign environment, whereas lower loads are applied whilst there are extremes of temperature and temperature gradient. It is important that the effects of such temperatures and temperature gradients are investigated during the testing, especially if dissimilar materials are involved, and care is taken to ensure that the joint is loaded in a manner compatible with the real application.

The following sections describe the most important categories of benign environment tests.

16.3.3.2 Load - Deflection

A load - deflection curve can provide knowledge on the following:

- Stiffness of the joint
- Hysteresis characteristics
- Backlash
- Load sharing
- Failure mechanism

16.3.3.3 Ultimate Strength

Ultimate strength tests are used to prove the suitability of the joint. After failure, it is important to examine the joint carefully to determine the mode of failure.

16.3.3.4 Fatigue Testing

Fatigue testing is normally only relevant on re-useable space equipment. It provides information in the following areas:

- Fatigue Life
- Vibration Loosening
- Crack growth
- Fretting
- Creep

16.3.3.5 Corrosion Testing

Corrosion can considerably alter the characteristics of a joint both in terms of its strength and life. It is important to consider corrosion testing in accordance with the relevant environmental conditions, and that the effects of the corrosion are observed and measured.

16.3.3.6 High/Low Temperature Testing

One of the objectives of testing at extreme temperature conditions is to reproduce the appropriate material characteristics as well as thermal strains and stress. Hence, not only temperatures be simulated but also thermal gradients. Due to the difficulties and expense, **it is important to minimise** this testing. **It is important** under this condition, **to derive the** information on joint strength and stiffness and variation from similar tests carried out at normal ambient **to be noted**.

16.3.3.7 Creep Testing

Creep of joints can significantly reduce the preload over time. Loss of preload can be caused by creep of materials in the joint interface such as thermal spacers, CFRP, peelable shims, thermal fillers, etc. It is important to consider creep testing in accordance with the relevant environmental conditions, in particular for thermal exposure and thermal cycling.

16.3.3.8 Vibration Loosening

One objective of proto-flight or acceptance dynamic testing (sine, random, acoustic) is to verify, that the bolted junctions are not loosening under vibration loads.

16.4 Production Testing

It is unlikely that individual joints **are** production tested. It is far more likely that the joints **are** tested as part of an overall spacecraft structural test. Obviously, normal quality control procedures aim to ensure that the production joint resembles the joint development tested within expected production tolerances.

When a production test procedure is used, there is no need to use a test factor. It ensures freedom for each part from both proof and ultimate failures up to the level of the production test load. **It is important that** the production test load specified **is** set at the specified proof load where the component is designed by the proof criterion. Where the component is designed by the ultimate criterion the production test level **is** set at a value higher than the specified proof load. **It is important to note that this can** only be done when the proof/ultimate ratio is higher than the ratio of the specified proof and ultimate factors.

It is important that the proposed method of production testing **is** taken into account when designing the joint.

Annex A

Recommended Starting Values for Seating Torque

A.1 Recommended values

Table A-1 - Recommended torques for unlubricated fasteners

Fastener	Nut/Insert	Washer	Size	Recommended Torque (Nm)	Preload (N)
Titanium (3.7164) LN 29950 – ox blank, Ref. 16.1	Steel Nut (1.4944.4) LN 9161 – ox silver- plated	Steel (1.4944.4) ENN 399	M4	2,4	2920
			M5	6,0	6050
			M6	11,0	8799
			M8	30,0	18100
Titanium (3.7164) LN 29950 – ox blank, Ref. 16.1	Steel Insert (1.4301) LN 9499	Steel (1.4944.4) ENN 399	M4	3,0	1950
			M5	7,3	4330
			M6	14,0	6080
			M8	36,0	13700
Titanium (3.7164) LN 29950 – ox blank, Ref. 16.1	Steel Captive Nut (1.4301) LN 9499	Steel (1.4944.4) ENN 399	M4	2,7	1830
			M5	6,0	3850
			M6	11,0	5480
			M8	-	-
Steel (1.4944.6) EN 3328, Ref. 16.2	Steel Insert (1.4301) LN 9499 Silver Plated	Steel (1.4944.4) ENN 399	MJ4	-	-
			MJ5	-	-
			MJ6	12,5	7700
			MJ8	33,5	15900
Steel (A2-70), Ref. 16.3	-	-	M4	1,7	2970
			M5	3,4	4850
			M6	5,9	6850
			M8	12,6	14500
Steel (A2-80), Ref. 16.3	-	-	M4	2,3	3960
			M5	4,6	6470
			M6	8,0	9130
			M8	19,3	16700

Fastener	Nut/Insert	Washer	Size	Recommended Torque (Nm)	Preload (N)
<p>NOTE 1: The appropriate seating torque depends on the requirements of the particular joint.</p> <p>NOTE 2: Table A-1 shows recommended seating torque values (do not consider self-locking torque) for the most frequently used aerospace fastener materials; Ti6Al4V, A286, A2-70/80.</p> <p>NOTE 3: The data cover the most common metric sizes from M4 to M8.</p> <p>NOTE 4: The values in the table are only provided as an initial estimate of the required torques, and are only intended for use at the beginning of the design process. All relevant analyses are still be performed for the final design.</p> <p>NOTE 5: The data show unlubricated fasteners. If lubrication is used, it is important to give attention to the increased preload since often the preload can be too high. In such cases, it is important to reduce the applied torque reduced and all relevant analyses are performed.</p> <p>NOTE 6: It is advised to use the minimum possible torque that can satisfy the critical MoS (for gapping, separation, etc) since this can improve fatigue life of the fastener.</p> <p>NOTE 7: Some specifications limit the maximum pretension for Ti6Al4V fasteners due to creep. When such specifications apply, it is important that the values taken from Table A-1 are adjusted accordingly.</p> <p>NOTE 8: Inconel 718 and MP35N are sometimes used as high strength fasteners but no recommendations are given for initial torque values, rather it is important that the analysis methods are used from the beginning of the design process.</p>					

A.2 References

A.1	MBB ERNO	EURECA Project, Doc: ERC-12124-HB-ER-001, 1986.
A.2	Daimler-Benz Aerospace	COLUMBUS Project, Doc: HB 1213800 002, 1997.

Annex B

Measured Friction Coefficients of Fasteners

Table B-1 - Friction Coefficients of Fasteners used in European Space Industry - Unlubricated Fasteners

Fastener	Type of nut or threaded hole	$\mu_{th,max}$	$\mu_{th,min}$	$\mu_{uh,max}$ [4]	$\mu_{uh,min}$ [4]
M4, LN 29949 (A-286)	Anchor nut (floating), LN 29693	-	-	-	-
	Helicoil, bronze CuSn6, LN 9499 ^[1]	-	-	-	-
	Nut, LN 9161	-	-	-	-
M5, LN 29949 (A-286)	Anchor nut (floating), LN 29693	0,199	0,129	0,294	0,226
	Helicoil, bronze CuSn6, LN 9499 ^[1]	0,176	0,118	0,335	0,222
	Nut, LN 9161	0,112	0,046	0,120	0,081
M6 , LN 29949 (A-286)	Anchor nut (floating), LN 29693	0,176	0,086	0,296	0,179
	Helicoil, bronze CuSn6, LN 9499 ^[1]	0,119	0,062	0,302	0,222
	Nut, LN 9161	0,140	0,074	0,140	0,069
M8, LN 29949 (A-286)	Anchor nut (floating), LN 29693	-	-	-	-
	Helicoil, bronze CuSn6, LN 9499 ^[1]	0,162	0,131	0,335	0,268
	Nut, LN 9161	-	-	-	-
Ti (3.7164) LN 29950, ox blank ^[2]	Steel Nut (1.4944.4), ox silver-plated, LN 9161	0,26	0,10	- ^[3]	-
	Steel Insert (1.4301), LN 9499	0,34	0,18	-	-
	Steel Captive Nut (1.4301), LN 9499	0,34	0,18	-	-
NOTE 1: LN 9499 is only applicable for CRES helicoils. For aerospace joints it is important to use DIN 65536-1					
NOTE 2: Steel (1.4944.4) ENN 399 washer was used with this fastener					
NOTE 3: No data available					
NOTE 4: Flange material AA 7075 T7351					

Annex C

Typical Friction Coefficients for Joint Materials

Table C-1 - Typical thread and Underhead Friction Coefficients

Friction coefficient class	Range for μ_{th} and μ_{uh}	Selection of typical examples	
		Material surfaces	Lubricants
A	0,04 to 0,10	metallicly bright black oxide phosphated galvanic coatings such as Zn, Zn/Fe, Zn/Ni Zinc laminated coatings	solid lubricants, such as MoS ₂ , graphite, PTFE, PA, PE, PI in lubricating varnishes, as top coats or in pastes; liquefied wax wax dispersions
B	0,08 to 0,16	metallicly bright black oxide phosphated galvanic coatings such as Zn, Zn/Fe, Zn/Ni Zinc laminated coatings Al and Mg alloys	solid lubricants, such as MoS ₂ , graphite, PTFE, PA, PE, PI in lubricating varnishes, as top coats or in pastes; LIQUEFIED WAX; wax dispersions, greases; oils; delivery state
		hot-galvanized	MoS ₂ ; graphite; wax dispersions
		organic coatings	with integrated solid lubricant or wax dispersion
		austenitic steel	solid lubricants or waxes; pastes

Friction coefficient class	Range for μ_{th} and μ_{uh}	Selection of typical examples	
		Material surfaces	Lubricants
C	0,14 to 0,24	austenitic steel	wax dispersions, pastes
		metallically bright phosphated	delivery state (lightly oiled)
		galvanic coatings such as Zn, Zn/Fe, Zn/Ni Zinc laminated coatings	none
D	0,20 to 0,35	austenitic steel	oil
		galvanic coatings such as Zn, Zn/Fe; hot-galvanized	none
E	$\geq 0,30$	galvanic coatings such as Zn/Fe, Zn/Ni austenitic steel Al, Mg alloys	none

NOTE: Table taken from Reference VDI

Table C-2 - Friction Coefficients for Common Joint Materials (from Reference 8.3)

Material combination	Static friction coefficient	
	Dry	Lubricated
Steel – steel/cast steel	0,1 to 0,23	0,07 to 0,12
Steel – gray cast iron	0,12 to 0,24	0,06 to 0,1
Gray cast iron – gray cast iron	0,15 to 0,3	0,2
Bronze – steel	0,12 to 0,28	0,18
Gray cast iron – bronze	0,28	0,15 to 0,2
Steel – copper alloy	0,07	-
Steel – aluminum alloy	0,1 to 0,28	0,05 to 0,18
Aluminum – aluminum	0,21	-

NOTE: Table taken from Reference VDI

Annex D

Material Data of Fasteners Typically Used in Aerospace Industry

D.1 Overview

A short compendium of material data needed for bolt analyses of the most common fastener materials in space industry is given in Table D-1 to Table D-7 below.

When defining structural fastener design allowables it is important to exercise some caution when using base material A-basis allowables. According to NASA-STD-6016B: MMPDS design values are not transferrable to fasteners, because raw material used to make fasteners is reprocessed using various metallurgical practices such as hot heading, thread rolling, and heat treating. These processes might change the strength of the metal from the original bar stock.

Therefore, it is important that the derivation of fasteners allowables to be used in the bolt analysis of joints are based on lot tested design strength values of the procured fasteners batches defined in the specific fastener part and corresponding procurement specifications plus on the material A-basis allowables of the original bar stock. It is important that the lot tested values are higher than the A-basis ones to be on the safe side. This additional check can allow to use the material A-basis with confidence.

D.2 Stainless Steel

Table D-1- Stainless steel A 286

Material Specification		A 286					
Alternative notations for this material		1.4944 AISI 660					
Temperature		Room temperature					
Property Reference Source		German Aviation Material Handbook					
Condition		1.4944.4			1.4944.6		
Material Basis		A	B	S	A	B	S
tensile yield strength σ_y	[N/mm ²]	-	-	660	-	-	950
tensile ultimate strength σ_u	[N/mm ²]	-	-	960	-	-	1100
shear yield strength τ_y	[N/mm ²]	-	-	-	-	-	548
shear ultimate strength τ_u	[N/mm ²]	-	-	595	-	-	655
E (Young's modulus)	[N/mm ²]	201000					
ν (Poisson ratio)	[-]	0,31					
ρ (density [g/cm ³])	[g/cm ³]	7,95					
Fastener types made of this material		LN 29 949					

Table D-2 - Stainless steel A2-70 and A2-80

Material Specification		A 2					
Alternative notations for this material		1.4301, 1.4541 AISI301-304, AISI 321					
Temperature		Room temperature					
Property Reference Source		DIN 267 Teil 11					
Condition		A2-70			A2-80		
Material Basis		A	B	S	A	B	S
tensile yield strength σ_y	[N/mm ²]	-	-	450	-	-	600
tensile ultimate strength σ_u	[N/mm ²]	-	-	700	-	-	800
shear ultimate strength τ_u	[N/mm ²]	-	-	420	-	-	480
E (Young's modulus)	[N/mm ²]	193000 – 200000					
ν (Poisson ratio)	[-]	0,29					
ρ (density [g/cm ³])	[g/cm ³]	8,00					
Fastener types made of this material		DIN 912, DIN 7991					

Table D-3 Stainless steel custom 450

Material Specification		custom 450					
Alternative notations for this material		-					
Temperature		Room temperature					
Property Reference Source		MIL-HDBK-5J					
Condition		H1000					
Material Basis		A	B	S	A	B	S
tensile yield strength σ_y	[N/mm ²]	-	-	1034	-	-	-
tensile ultimate strength σ_u	[N/mm ²]	-	-	1103	-	-	-
shear ultimate strength τ_u	[N/mm ²]		-	-	-	-	-
E (Young's modulus)	[N/mm ²]	193000					
ν (Poisson ratio)	[-]	0,30					
ρ (density [g/cm ³])	[g/cm ³]	7,75					
Fastener types made of this material							

Table D-4 - Stainless steel custom 455

Material Specification		custom 455					
Alternative notations for this material		-					
Temperature		Room temperature					
Property Reference Source		MIL-HDBK-5J					
Condition		H1000					
Material Basis		A	B	S	A	B	S
tensile yield strength σ_y	[N/mm ²]	-	-	1275	-	-	-
tensile ultimate strength σ_u	[N/mm ²]	-	-	1379	-	-	-
shear ultimate strength τ_u	[N/mm ²]	-	-	855	-	-	-
E (Young's modulus)	[N/mm ²]	200000					
ν (Poisson ratio)	[-]	0,30					
ρ (density [g/cm ³])	[g/cm ³]	7,76					
Fastener types made of this material							

Table D-5 - Stainless steel PH 13-817-7 Mo

Material Specification		17-7PH Stainless Steel PH 13-8 Mo					
Alternative notations for this material		1.4568 1.4534					
Temperature		Room temperature					
Property Reference Source		ESA TEC-MSP Total Material Dataset MIL-HDBK-5H					
Condition		CH900 H 950			H 1000		
Material Basis		A	B	S	A	B	S
tensile yield strength σ_y	[N/mm ²]	1793	-1413	-	-1310	-1379	-
tensile ultimate strength σ_u	[N/mm ²]	1827	-1524	-	-1386	-1434	-
shear ultimate strength τ_u	[N/mm ²]	-900	-915	-	-807	-841	-
E (Young's modulus)	[N/mm ²]	200000 195000					
ν (Poisson ratio)	[-]	0,28					
ρ (density [g/cm ³])	[g/cm ³]	7,64 7.72					
Fastener types made of this material							

Table D-6 - Stainless steel PH 15-7 Mo

Material Specification		15-7PH Stainless Steel					
Alternative notations for this material							
Temperature		Room temperature					
Property Reference Source		ESA TEC-MSP Total Material Dataset					
Condition		CH900					
Material Basis		A	B	S	A	B	S
tensile yield strength σ_y	[N/mm ²]	1586			-	-	-
tensile ultimate strength σ_u	[N/mm ²]	1694			-	-	-
shear ultimate strength τ_u	[N/mm ²]				-	-	-
E (Young's modulus)	[N/mm ²]	193000					
ν (Poisson ratio)	[-]	0,28					
ρ (density [g/cm ³])	[g/cm ³]	7,67					
Fastener types made of this material							

Table D-7- Stainless steel 15-5 PH

Material Specification		15-5 PH Stainless Steel					
Alternative notations for this material		1.4545					
Temperature		Room temperature					
Property Reference Source		MIL-HDBK-5J					
Condition		H1025					
Material Basis		A	B	S	A	B	S
tensile yield strength σ_y	[N/mm ²]	1000			-	-	-
tensile ultimate strength σ_u	[N/mm ²]	1069			-	-	-
shear ultimate strength τ_u	[N/mm ²]	669			-	-	-
E (Young's modulus)	[N/mm ²]	200000					
ν (Poisson ratio)	[-]	0,28					
ρ (density [g/cm ³])	[g/cm ³]	7,67					
Fastener types made of this material							

D.3 Nickel and Nickel/Cobalt Based Alloys

Table D-8 - Inconel 718

Material Specification		Inconel 718					
Alternative notations for this material		2.4668					
Temperature		Room temperature					
Property Reference Source		German Aviation Material Handbook and MIL-HDBK-5J					
Condition		2.4668.7			2.4668.9		
Material Basis		A	B	S	A	B	S
tensile yield strength σ_y	[N/mm ²]	-	-	1040	-	-	1440
tensile ultimate strength σ_u	[N/mm ²]	-	-	1240	-	-	1550
shear ultimate strength τ_u	[N/mm ²]	-	-	785	-	-	885
E (Young's modulus)	[N/mm ²]	203000					
ν (Poisson ratio)	[-]	0,29					
ρ (density [g/cm ³])	[g/cm ³]	8,19					
Fastener types made of this material							

Table D-9 - MP35N

Material Specification		MP35N					
Temperature		Room temperature					
Property Reference Source		MIL-HDBK-5J					
Condition		Solution treated, cold drawn and aged					
Material Basis		A	B	S	A	B	S
tensile yield strength σ_y	[N/mm ²]	1586	-		-	-	-
tensile ultimate strength σ_u	[N/mm ²]	1793	-		-	-	-
shear ultimate strength τ_u	[N/mm ²]	1000	-		-	-	-
E (Young's modulus)	[N/mm ²]	234500					
ν (Poisson ratio)	[-]						
ρ (density [g/cm ³])	[g/cm ³]	8,26					
Fastener types made of this material		-					

Table D-10 – MP159

Material Specification		MP159					
Temperature		Room temperature					
Property Reference Source		MIL-HDBK-5J					
Condition		Solution treated, cold drawn and aged					
Material Basis		A	B	S	A	B	S
tensile yield strength σ_y	[N/mm ²]	1724	-		-	-	-
tensile ultimate strength σ_u	[N/mm ²]	1793	-		-	-	-
shear ultimate strength τ_u	[N/mm ²]	903	-		-	-	-
E (Young's modulus)	[N/mm ²]	243400					
ν (Poisson ratio)	[-]						
ρ (density [g/cm ³])	[g/cm ³]	8,26					
Fastener types made of this material		-					

D.4 Titanium Alloys

Table D-11 - Ti6Al4V

Material Specification		Ti 6Al 4V		
Alternative notations for this material		3.7164		
Temperature		Room temperature		
Property Reference Source		German Aviation Material Handbook		
Condition		3.7164.1		
Material Basis		A	B	S
tensile yield strength σ_y	[N/mm ²]	830	925	-
tensile ultimate strength σ_u	[N/mm ²]	900	980	-
shear ultimate strength τ_u	[N/mm ²]	570	600	570
E (Young's modulus)	[N/mm ²]	113800		
ν (Poisson ratio)	[-]	0,342		
ρ (density [g/cm ³])	[g/cm ³]	4,43		
Fastener types made of this material		LN 29 950		

D.5 References

D.1	German Aviation Material Handbook	
D.2	DIN 267 Teil 11	
D.3	MIL-HDBK-5J	
D.4	NASA-STD-6016B	Standard Materials and Processes Requirements for Spacecraft, 2020

Other Useful References

The documents listed below are of general interest for the field of threaded fasteners and/or were references by previous versions of this handbook.

- | | |
|----------------------------------------|----------------------------------------------------------------------------------------------------------------------------------------------------------------------------|
| NASA STD-5001 | Structural design and test factors of safety for spaceflight hardware |
| G. Meyer & D. Strelow | Simple Diagrams Aid in Analysing Forces in Bolted Joints, <i>Assembly Engineering</i> Jan. 1972 pp. 28-33 |
| K.H. Illgmer & D. Blume | Schrauben Vademecum, Bauer and Schaurte Karacher Aug. 1983 |
| J.H. Bickford | An Introduction to the Design and Behaviour of Bolted Joints, Marcel Dekker, 1981 |
| G.H. Junker & P.W. Wallace | The Bolted Joint: Economy of Design Through Improved Analysis and Assembly Methods, <i>Proc. Instn. Mech. Engrs.</i> Vol. 198B No. 14., 1984 |
| S.D. Rossides | Behaviour of a Simple Tension Joint with Fasteners Tightened into Yield, <i>British Aerospace Report BT.12065</i> July 1981 |
| D.J. Light | Torque-Tension Literature Surrey, B.A.C. (G.W. Div) Report ST.14857 1975 |
| E.P. Donald | Pretension Diagrams for Bolted Joints, <i>Aeronautical Journal</i> Feb. 1981 |
| J. Cherry | A Finite Element Analysis of the Pressure Distribution in Bolted Joints, <i>British Aerospace report BT21927</i> June 1987.
(Von Mises Criterion) |
| W. Thomala | Zur Brechnung der erforderlichen Mutterhöhe bei Schraubenverbindungen, <i>Konstruktion</i> 47 (1995) |
| JUNKER O.H.
WALLACE P.W. | The Bolted Joint: Economy of Design Through Improved Analysis and Assembly Methods" <i>Proc. I. Mech. E.</i> Vol. 198 B, No. 14., 1984 |
| BROBERG H. | Skrurförband - Dimensionering - Montering" Iuf - resultat 82611, July 1983 |
| HERTEL W, PAUL W,
WAGNER D | Insert Design Handbook. ERN - 3442/77 - 28 Iss A. |
| RAYMOND L. | Infinite Life High Strength Bolts. <i>Assembly Engineering.</i> April 1975. |
| KELLERMAN R | Bolts for light weight construction made of ultra high strength steels and titanium alloys. |
| TURLACH G. | |
| BROEK D. | Elementry Engineering Fracture Mechanics, Norrdhof (Netherlands) 1974. |
| DE KONING A.U., LOF,
C.J., SCHRA, L | Assessment of 3D Stress Intensity Factor Distributions for Nut Supported Threaded Rods and Bolt/Nut Assemblies, NLR CR 96692 L, National Aerospace Laboratory (NLR), 1996. |
| MCIC REPORTS | Cracks at Structural Holes March 1975. |
| MCIC - HB - 01 | Damage Tolerant Design Handbook A compilation of Fracture and Crack-Growth Data for High-Strength Alloys. Metals and Ceramics Information Centre, Battelle. |

ROOKE D.P. & CARTWRIGHT D.J.	Compendium of Stress Intensity Factors, Her Majesty's Stationary Office, 1976. AvP 32, AvP 932, AvP 970 and their successors. Design Criteria for Controlling Stress
NASA	Corrosion Cracking MSFC - SPEC - 522A, November 1977.
NASA-STD-5020	Requirements For Threaded Fastening Systems In Spaceflight Hardware
NASA/TP-2018-219787	Preload Loss in a Spacecraft Fastener via Vibration-Induced Unwinding
Ed Hemminger, Alan Posey and Michael Dube	Torque Tension Testing of Fasteners used for NASA Flight Hardware Applications, Proceedings of the 42nd Aerospace Mechanisms Symposium, NASA Goddard Space Flight Center, May 14-16, 2014
ISO-16047	Fasteners – Torque/clamp force testing
Franck Pichoff, Matthieu Kummel, and Morten Schiff	Dynamic vibration testing of fasteners: fastener self-loosening theory, vibration testing practical applications, comparison of the international standards and recommendations on how to set-up a meaningful testing protocol, Matériaux & Techniques 106, 307 (2018)
DIN 65151: 2002-08	Dynamic testing of the locking characteristics of fasteners under transverse loading conditions (vibration test), Deutsches Institut für Normung e.V., Berlin 2002